Synthesis and characterization of fulvic acids in tre C-H-O, C-H-O-N and C-H-O-N-S systems : UV-visible spectroscopic investigations of uranyl(VI)-fulvate complexation as a function of pH at 25 degrees C and 1 bar

Ambrose Kipchumba Kiprop

Université Henri Poincaré, Faculté des Sciences et Techniques, U.F.R. S.T.M.P.
Ecole doctorale RP2E : Ressources, Procédés, Produits et Environnement
UMR 7566 G2R : Géologie et Gestion des Ressources Minérales et Energétiques

Thèse

présentée pour l'obtention du titre de
Docteur de l'Université Henri Poincaré (Nancy)
en Géosciences

par

Ambrose Kipchumba KIPROP

Synthèse et caractérisation des acides fulviques dans des systèmes C-H-O, C-H-O-N et C-H-O-N-S. Etude spectroscopique UV-visible des complexes uranyle (VI) – fulvate en fonction du pH à 25°C et 1 bar.

Synthesis and characterization of fulvic acids in the C-H-O, C-H-O-N and C-H-O-N-S systems. UV-Visible spectroscopic investigations of uranyl (VI)-fulvate complexation as a function of pH at 25°C and 1 bar.

Date de soutenance : 19 novembre 2009

Membres du Jury :

Rapporteurs :	Mme. C. RICHARD	*Directeur de Recherches, CNRS, Clermont-F[d].*
	M. A. CASTELLAN	*Professeur Emérite, Université de Bordeaux 1*
Examinateurs :	M. P. GERARDIN	*Professeur, Université Henri Poincaré, Nancy*
Directeurs de thèse :	M. C. NGUYEN-TRUNG	*Chargé de Recherches, CNRS, Nancy*
	M. L. RICHARD	*Consultant, Amphos21, Barcelone*

DEDICATION

I dedicate this Ph.D. Thesis to the mother (Monica Chebet) of my dear children Lynn Jepkoech Kipchumba and Stacey Jepkemoi Kipchumba, Hon. Prof. M.J. Kamar, Hon. N.K. Biwott, my beloved mother and to all my family members.

I have fought the good fight. I have finished the course. I have kept the faith.

2 Timothy 4:7

ACKNOWLEDGEMENTS

I wish to express my sincere gratitude to Mr. Chinh NGUYEN-TRUNG of G2R (CNRS), Nancy Université, Université Henri Poincaré, who apart from accepting to supervise me for Ph.D. studies went further to encourage and share his experiences and wide knowledge in Chemistry. He drove me to a point of a “hands-on” chemist. I learnt to have satisfaction in whatever I did in the laboratory. It was a great pleasure for me and I really thank him for his personal involvement and interest in the research work. Many at times, he went out of his way to facilitate my research during the four years of study in Nancy Université.

Many thanks and appreciation go to Mr. Laurent RICHARD of G2R, Nancy Université, Université Henri Poincaré, for his academic guidance, hard work, financial assistance and constant care during my research study. His constructive suggestions and criticisms really made me to achieve this much. My stay and thus my research study was really facilitated by him. He never hesitated to assist and to me he was my elder brother and motivator for hard work. He made me enjoy the holidays while I was in France despite his busy schedule. Thanks most sincerely to my supervisors and Mr. Phillipe Gérardin for the academic advice, support of all kinds and encouragement. They all dedicated their time and energies, tirelessly to read and correct my manuscript to its present form. Their contribution cannot be overemphasized. Thanks too to Anne-Sylvie André, Aurélien Randi, Frédéric Lannuzel, Marie-Camille Caumon, Luc Siebenaller and Emilie Pourtier for the invitations to your dear families, it was a pleasure for me. Thanks to Kirimi Kiriamiti of Moi University - Eldoret, Kenya for all the facilitation during my study.

I would also wish to appreciate Mr. Michel Cathelineau and Mr. Jacques Pironon for the good administrative organization of the laboratory. The constant assistance and all forms of help from Roland Mairet, Patrick Lagrange, Marie-Odile Campadieu, Laurence Moine, Pierre Schuhmacher, Esther Goetz, Olinda Gimello, Gilles Bessaque and Christine Léonard were highly appreciated. I also express my appreciation to Emilie Pourtier and Carolina Sabater for their assistance and encouragement. I wish to extend my thanks to all the entire G2R staff and colleagues; Cédric (Carpentier and Demeurie), Jérôme Sterpenich, Régine Mosser-Ruck, Judith Sausse, Pierre Faure, Cécile Fabre, Pauline Michel, Marc Lespinasse, Erwan Perfetti, Frédéric Lannuzel, Christophe Rozsypal, Marta Berkesi (our “Hungry Hungarian” friend), Stéphane Renard, Antonin Richard, Isabelle Duhamel, David Salze, Rakhim Uteyev, Jeremy Neto, Askar Munara, Michael Franiatte, Laurent Jeanneau (Kipjeannu), Shaahin Zaman, Aimeryc Schuhmacher, Apolline Lefort, Yacouba Coulibaly, Aleyda Traoré, Anne-Laure

Henriot, Vincent Girard, Julien Mercadier and the several Olivier's (Belcourt, Cardon, Pierron and VDH) among many many others, for assisting me in one way or another. Thanks to Aurélien Randi who invited me to sports whenever time permitted and also for sparing his time to see that all was okay with me. I am grateful also to my other friends; Francis Mburu, Thierry Koumbi, Sirmah, Bouddah, Thierry and Steve among others. Thanks to all the staff of LERMAB, LCPME and UMR CNRS-UHP 7565, Equipe Synthèse et Assemblage de Composés Amphiphiles who allowed me to perform the analyical measurements. I don't forget to register my gratitude to Régine Mosser-Ruck, Stéphane Dumarçay, François Dupire and Sandrine Adach for their assistance and/or the analysis of my numerous samples.

Financial assistance from the University, through the much appreciated efforts of L. Richard, and from the French Government, through the French Embassy in Nairobi, is gratefully acknowledged. I sincerely thank Moi University for granting me study leave during my studies. This made it possible to realize my dream of obtaining a Ph.D., which will prove very important for my career development and promotion.

I wish to acknowledge Thérèse Lhomme, who was the first staff member of G2R I met. I can't forget to register my many thanks to Marie-Camille Caumon whose thoughtful suggestions, contributions and comments were of great value to me. Great thanks too to Coralie Biache whose smile and constant willingness to assist was and is really appreciated. I do also register my appreciation to Madame Monique Diter and her family for their care and invitations to be together during holidays. To me she was my mother in France.

I am particularly indebted to my late grandmother, KOKO Magdaline Kong'ato Arusei who encouraged me to work hard and pursue studies though she never lived to enjoy my care, in spite of the great love she had for me. I do and will always miss you KOKO. Last but not the least, I thank my entire family for the trust they bestowed on me during my studies in France. I am grateful to my beloved wife Monica Chebet and my dear children Lynn Jepkoech and Stacey Jepkemoi for their LOVE, patience, support, prayers, kindness and understanding despite my constant absence from home. This allowed me to fulfil my academic endeavours. I sincerely thank all of you. God bless you all.

TABLE OF CONTENTS

LIST OF FIGURES

LIST OF TABLES

INTRODUCTION GÉNÉRALE

Les *Substances Humiques* (désignées par SH) sont largement répandues dans la nature et contribuent de manière significative au cycle géochimique global du carbone (Aiken et al., 1985). Elles constituent une fraction majeure de la matière organique (jusqu'à 80% en masse), et représentent la plus grande partie de la matière organique des systèmes aquatiques (Stevenson, 1994). Par exemple, les SH représentent environ 55-70 % du total de la matière organique dans l'eau de la rivière Amazone (Hedges et al., 1992). Elles se trouvent dans des sédiments terrestres, lacustres et marins où elles pourraient être des précurseurs potentiels de la formation du kérogène (Hatcher et al., 1983), la forme la plus abondante de carbone organique sur la Terre et le matériel source dans la formation du pétrole (Hunt, 1996).

Selon Stevenson (1982), les SH dans les sols sont formées selon quatre voies différentes. Les deux premières résultent de la dégradation de la lignine par des microorganismes qui produisent directement soit des SH soit des aldéhydes phénoliques et des acides. Ces derniers composés sont ensuite oxydés par des enzymes en quinones, lesquels polymérisent ensuite pour donner des SH. La troisième voie fait intervenir la dégradation microbienne de la cellulose en polyphénols. Ceux-ci sont ensuite oxydés en quinones dont la polymérisation conduit à la formation des SH. La quatrième voie, proposée par Maillard dès 1912, correspond à la condensation des sucres et des acides aminés, respectivement des dérivés de la cellulose et des polypeptides, pour former des SH.

La formation des SH dans les milieux aquatiques tels que les cours d'eau, les lacs ou les mers résulte d'autres mécanismes. Thurman (1985) a proposé que les SH se forment selon le ou les processus suivants : lessivage de la matière organique des plantes avec un transfert direct vers les eaux de surface ou après une transformation de cette matière organique dans les différentes couches du sol ; lessivage des SH du sol et transfert ultérieur vers les eaux de surface; dégradation des débris d'algues et de phytoplanctons; oxydation sous l'effet des rayons ultraviolets et polymérisation subséquente des molécules organiques réactives dans les microcouches supérieures des cours d'eau, des lacs et des mers; réactions de polymérisation entre les composés portant des groupements phénols, amines et/ou aldéhydes, lesquels résultant de la dégradation des biomolécules dans les eaux naturelles.

Selon de nombreux auteurs (Senesi, 1993; Wood, 1996 ; Lichtfouse et Lévêque, 1999; Tipping, 2002 et Linnik et al., 2004), les SH jouent un rôle important dans un certain nombre de processus géochimiques tels que la régulation du pH du sol, la dissociation des groupements fonctionnels, la formation des complexes et le transport des polluants organiques

et minéraux dans l'environnement. Bien que l'acidité et le pouvoir complexant des SH intéressent les scientifiques, en particulier les géochimistes, les pédologues et les chimistes environnementaux, ces propriétés ont été rarement décrites en raison de la nature complexe des SH (voir plus loin).

Depuis longtemps, il a été supposé que les SH sont de nature polymérique[1], avec des masses moléculaires (déterminées par la diffusion des rayons X aux petits angles) comprises entre $5x10^2$ et $2x10^3$ Daltons (Da) pour les AF en milieu aquatique et dans les sols. Les masses moléculaires des AF aquatiques peuvent également atteindre des tailles supérieures à 10^4 Da (Thurman et al., 1982; Thurman, 1985). Selon ce modèle, les SH peuvent être classifiées en trois fractions. La classification a été fondée sur les solubilités relatives, lesquelles sont fonction de la masse moléculaire. Ces trois fractions incluent :

- *Les humins*, qui sont insolubles dans tout le domaine de pH;
- *Les acides humiques* (AH), qui sont insolubles en milieu acide fort (pH < 2) mais solubles au-delà de pH 2;
- *Les acides fulviques* (AF), qui sont solubles dans tout le domaine de pH.

Les humins, les AH et les AF contiennent essentiellement les trois éléments C, H, O avec de faibles quantités de N et S. Le tableau 1 montre les compositions élémentaires représentatives des AF et AH des sols, déterminées par Seelink (1985). La lecture du Tableau 1 permet de déduire que les AH des sols ont des teneurs en carbone supérieures et des teneurs en oxygène inférieures à celles des AF des sols. Le Tableau 2 rassemble les données de compositions élémentaires de l'AF marin de l'eau de surface de la mer de Saragosse (Stuermer and Harvey, 1974) et d'AH dans des sédiments marins au large du sud de la Californie (Nissenbaum and Kaplan 1972). Les teneurs en carbone des ces AF et AH marins sont similaires à celles de leurs équivalents continentaux, alors que les teneurs en oxygène (non mesurées mais calculées par différence) sont généralement plus faibles. Des teneurs en azote plus élevées et des teneurs en soufre plus faibles sont observés pour les AF marins par comparaison aux AH marins (Tableau 2). Ceci peut être attribué à des transformations diagénétiques précoces, dénitrogénation et sulfurisation, qui sont des processus couramment observés dans les sédiments marins (cf. par exemple Waples et Sloan, 1980 pour l'azote et François, 1987 pour le soufre).

[1] Comme nous soulignerons dans le texte, le modèle de polymères des substances humiques a été remise en question, avec les progrès qui ont été réalisés par techniques d'analytique au cours de la dernière décennie. Ces avancements sont abouti à la proposition que les substances humiques devrait plutôt être considéré comme supramolécules.

Hedges et al. (1992) ont analysé les compositions élémentaires et moléculaires de SH dans l'eau de mer de l'océan pacifique profond ainsi que dans l'eau douce du système de la rivière Amazone. Ils ont montré que les SH marines sont caractérisées par des rapports N/C plus élevés et des teneurs en carbone aromatiques plus faibles. Ils l'attribuent à une proportion plus importante de matériel protéinique dans le phytoplancton, la matière organique des plantes vasculaires étant majoritairement constituée de lignine et de tanins riches en carbone aromatique[2]. Le spectre RMN du ^{13}C de SH marines dissoutes (Hedges et al. 1992) montrent des carbones alkyliques non substitués et substitués par l'oxygène et des groupes carboxyliques. Au contraire, le spectre de la fraction humique du Rio Negro (affluent de l'Amazone) montre une majorité de carbones insaturés, de groupes méthoxyl et aromatiques oxygénées, compatibles avec une structure dérivée de la lignine.

Tableau 1. Composition élémentaire représentative des substances humiques d'un sol (Steelink, 1985).

	Acides humiques	Acides fulviques
Carbone	53.8 – 58.7 %	40.7 – 50.6 %
Hydrogène	3.2 – 6.2 %	3.8 – 7.0 %
Oxygène	32.8 – 38.3 %	39.7 – 49.8 %
Azote	0.8 – 4.3 %	0.9 – 3.3 %
Soufre	0.1 – 1.5 %	0.1 – 3.6 %

[2] La nature phénolique prédominante des acides fulviques des sols a été remise en question par Farmer et Pisaniello (1985), se fondant sur le fait que les quantités de benzène et d'acides polycarboxyliques hydroxybenzèniques produites par l'oxydation des acides fulviques ne sont pas compatibles avec les spectres RMN du ^{13}C des mêmes acides fulviques. Ces produits pourraient plutôt être le fait d'artefacts ou de contaminations. Farmer et Pisaniello (1985) ont proposés pour les acides fulviques des sols une structure d'acide polycarboxylique insaturé aliphatique, avec des substitutions hydroxyles. Cette conclusion est en contradiction avec celles proposées dans des études plus récentes (par exemple Mycke et Michaelis, 1986; Michaelis et al., 1989; Hedges et al., 1992).

Tableau 2. Composition élémentaire d'acides fulviques marins provenant de la mer des Sargasses et d'un sédiment marin.

	Acide fulvique de la mer des Sargasses [a]	Acide humique de sédiments marins [b]
Carbone	49.98	51-69 – 58.88
Hydrogène	6.76	5.93 – 6.56
Oxygène	36.40	27.16 – 36.69
Azote	6.40	3.88 – 5.17
Soufre	0.46	0.87 – 2.12

[a] Stuermer et Harvey (1974) [b] Nissenbaum et Kaplan (1972) [c] Calculé par différence

Les modèles structuraux des AH et AF proposés dans la littérature depuis 80 ans sont résumés par Stevenson (1985, 1994) et Leenheer (2007) (Figure 1). Le premier modèle (a) a été proposé par Fuchs en 1930. Il est constitué de noyaux aromatiques condensés, de structure similaire à celle du charbon. Flaig (1960) a ensuite proposé un modèle (b) constitué d'éthers polyphénoliques, molécules présentes dans la lignine et les tanins. Ce modèle présente de nombreux alcools aromatiques et des groupes fonctionnels de type quinone, mais relativement peu d'acides carboxyliques. En 1971, Schnitzer (cité par Schnitzer et Khan, 1972) propose un modèle d'AF du sol qui tient compte des données expérimentales disponibles à cette époque. L'AF est alors présenté sous forme d'acides phénoliques et benzoïques liés par liaison hydrogène pour former un réseau polymérique (modèle c). Les espaces vides entre les différentes sous-unités peuvent contenir des composés organiques ou minéraux d'une taille correspondant à celle de l'espace disponible. Harvey et al. (1983, 1984) ont été les premiers à synthétiser en laboratoire des AF et AH marins par auto-oxydation de lipides insaturés planctoniques, qu'ils ont ensuite comparés à ceux extraits d'eau de mer. Harvey et al. ont proposé comme structure pour l'AF marin un modèle riche en carbone aliphatique, de formule $C_{52}H_{83}O_{14}$, avec des rapports H/C et O/C de 1.60 et 0.27 respectivement. On notera que, si le rapport H/C correspond à celui calculé à partir des données du Tableau 2, le rapport O/C est quant à lui deux fois plus petit. Ceci peut être dû au fait que les teneurs en oxygène ne sont pas issues de mesures directes mais calculées par différence. Enfin, plus récemment, Leenheer et al. (1995) ont interprété le caractère acide fort de l'AF de la rivière Suwanee (Géorgie, E.-U.) comme une possible conséquence de la présence d'acides carboxyliques porteurs de groupes fonctionnels éther ou ester en position α à l'intérieur de structures cycliques. Les auteurs ont alors proposé un modèle (Figure 1), de formule $C_{25}H_{28}O_{14}$, avec des rapports H/C et O/C de 1.12 et 0.56 respectivement et une masse moléculaire de 552.481 $g.mol^{-1}$.

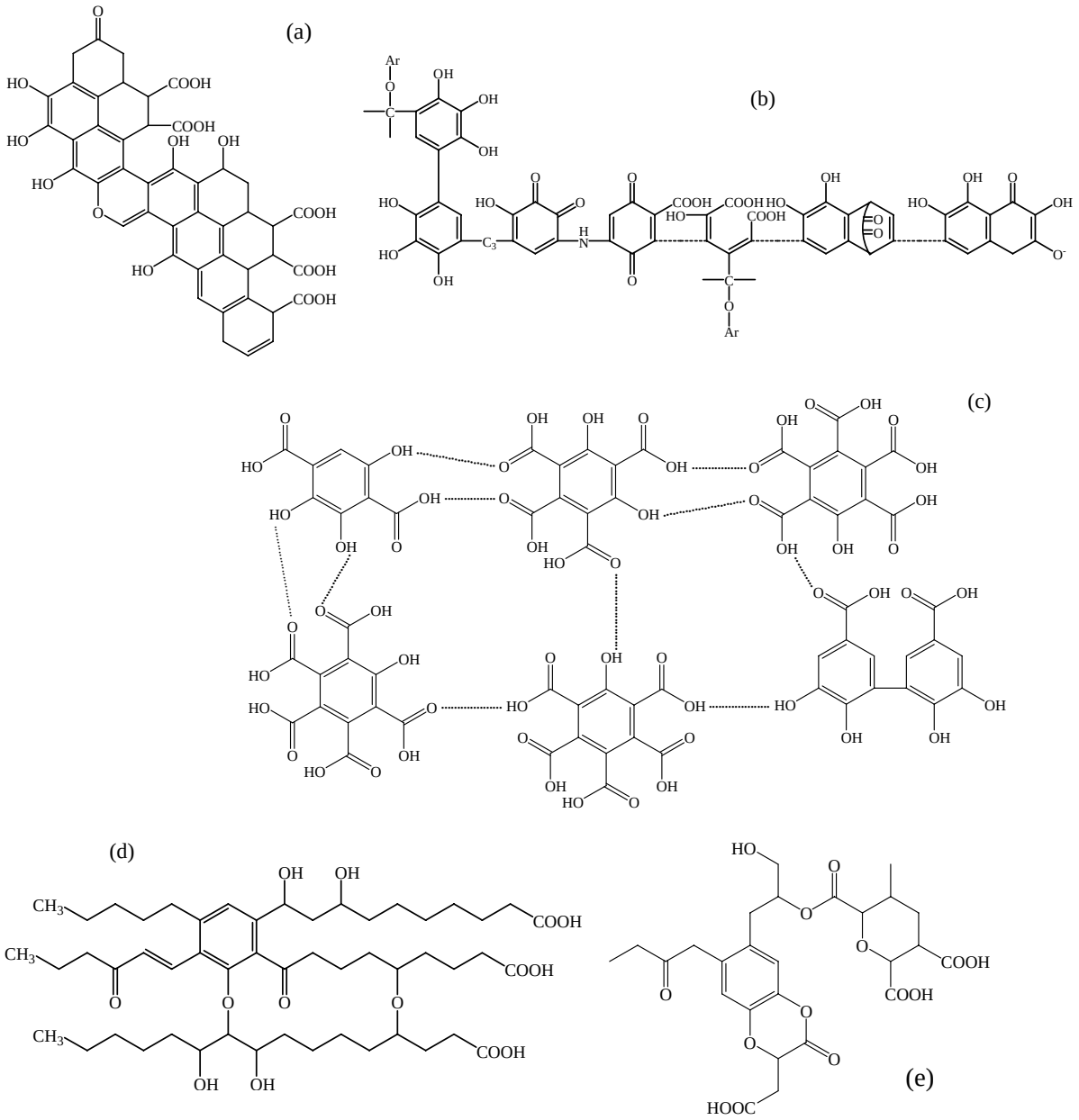

Figure 1. Quelques uns des modèles structuraux d'AF et d'AH proposés dans la littérature.

Les récents développements de techniques analytiques, en particulier la chromatographie haute pression d'exclusion stérique HPSEC et la spectrométrie de masse à ionisation électrospray (ESI-MS), ont fortement changé la perception de la structure moléculaire des SH (Sutton et Sposito, 2005). Brièvement, les études HPSEC de Piccolo et collaborateurs (Piccolo et al., 1996a,b ; Conte et Piccolo, 1999, Piccolo et Conte, 2000; Piccolo, 2001) suggèrent que les SH pourraient être considérées comme des entités supramoléculaires, constituées de composés de faible masse moléculaire assemblés par interactions hydrophobes et liaisons hydrogène. Ces assemblages sont similaires à des

micelles, avec des zones hydrophobes isolées du milieu aqueux par une zone hydrophile extérieure.

Le fait que les SH puissent être considérées comme des micelles a été formulé pour la première fois par Rochus et Sipos (1978). Ces auteurs ont déterminé une concentration micellaire critique en fonction de la température dans des solutions aqueuses de compositions électrolytiques variables. Plus tard, Wershaw (1986) proposa un modèle micellaire de SH en solution aqueuse[3]. Dans ce modèle, les composés de faible masse moléculaire formant les micelles sont des molécules amphiphiles, représentant des fragments partiellement oxydés de lignine ou de biopolymères végétaux plus grands. Ces fragments portent très probablement des fonctions acides carboxyliques ou carboxylates à l'une des extrémités, ce qui constitue la partie hydrophile des molécules amphiphiles. Les parties non oxydées des fragments s'organisent à l'intérieur des régions hydrophobes des micelles (Figure 2). La confirmation de cette structure micellaire a été apportée par Engebreston et von Wandruzka (1994) quelques années plus tard grâce à des mesures de la fluorescence du pyrène. Ces auteurs ont observé que le quenching de la fluorescence du pyrène par le bromure était significativement plus faible en présence d'une faible quantité (2.5-10 ppm) d'AH dans la solution aqueuse. L'AH empêcherait les interactions entre molécules de pyrène et donc le quenching par les ions bromure. De plus, les auteurs ont également observé une augmentation de la fluorescence initiale en présence de cations spécifiques (Cs^+ et Mg^{2+}), due à la favorisation par les ions de microenvironnements micellaires dans lesquels le pyrène pourrait s'insérer.

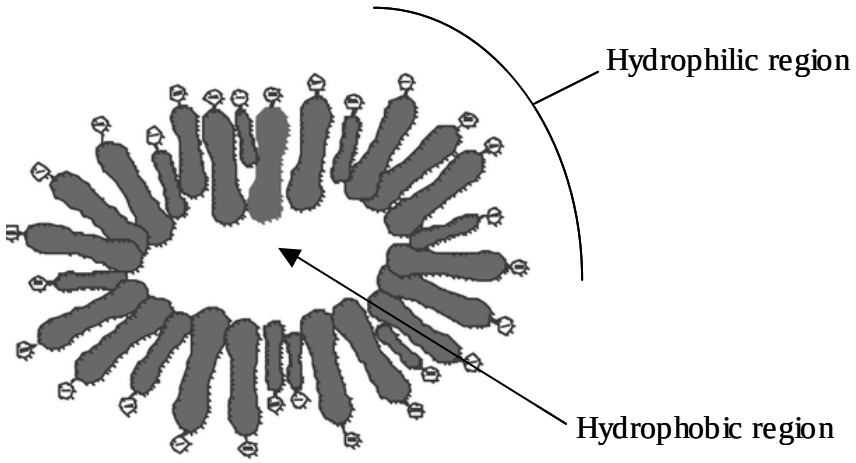

Figure 2. Représentation schématique du modèle micellaire des substances humiques aqueuses (d'après Wershaw, 1986).

[3] Wershaw (1986) propose également un modèle de SH en membrane dans les solides et les sédiments, dans lequel les SH en double couche sont sorbées à la surface de grains minéraux.

Récemment, des progrès importants dans la compréhension de la nature moléculaire des AF et AH ont été faits grâce à l'apport des techniques d'ionisation douce, telles que la désorption laser (LD) ou l'ionisation électrospray (ESI), conjuguées à la spectrométrie de masse (MS). Novody et al. (1995) ont ainsi montré par LD-MS qu'un mélange d'AF provenant d'un aquifère du Dakota du Sud (E.-U.) était dominé par des composés de faible masse moléculaire (en moyenne 418 Da). La première application de l'ESI-MS4[4] à l'étude des SH est due à McIntyre et al. (1997). Ces auteurs ont identifié dans une eau souterraine d'une aquifère sableux (New South Wales, Australie) une série d'AF dans la gamme 200-700 Da avec un maximum autour de 350 Da (ions négatifs monochargés). À partir de la distribution des pics, McIntyre et al. ont suggéré que ces AF étaient majoritairement des acides polycarboxyliques aliphatiques, n'excluant pas cependant la présence d'autres composés ne pouvant pas former d'ions négatifs dans leurs conditions d'analyse ESI-MS. Plancque et al. (2001) ont étudié des AF aquatiques de différentes provenances par spectrométrie de masse avec un détecteur quadrupole en temps de vol (Q-TOF) couplé à une ionisation électrospray. La distribution des pics ainsi obtenus présente un maximum autour de 450 Da. Les auteurs suggèrent que le mélange d'AF isolés de l'aquifère Mol est constitué d'une famille de molécules (Figure 3) associées en entités supramoléculaires.

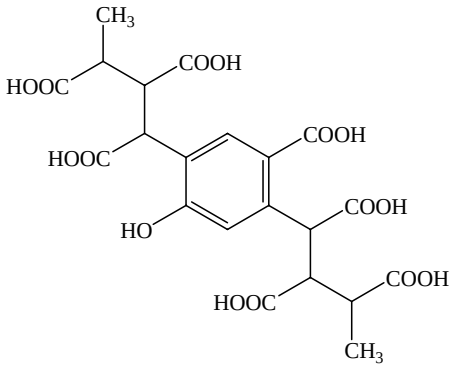

Figure 3. Structure moléculaire possible d'un AF représentatif de ceux isolés dans l'aquifère Mol (Plancque et al., 2001). Formule moléculaire $C_{20}H_{22}O_{15}$ et masse moléculaire 502 Da.

La spectrométrie de masse avec un quadripôle à temps de vol ne permet pas une identification complète et détaillée de tous les AF présents dans un mélange donné d'acide fulvique (McIntyre et al, 2001). En conséquence, Stenson et al. (2003) ont généré des ions produits à partir de l'acide fulvique de référence Suwannee par ionisation électrospray (ESI) et ont déterminé les masses exactes et les formules chimiques de 4626 ions individuels par

[4] Les détails de l'ESI-MS ESI-MS technique d'analytique sont présentées dans le chapitre suivant.

spectrométrie de masse ultra-haute résolution à transformée de Fourier par résonance cyclotron (FTICR-MS). Stenson et al. (2003) ont classé ces 4626 formules en une série de familles homologues, dont les structures moléculaires sont compatibles avec les voies de dégradation de la lignine. Un exemple de structure proposée par Stenson et al. pour un AF de formule chimique $C_{19}H_{22}O_{10}$ (masse moléculaire 410 Da) est montré sur la Figure 4.

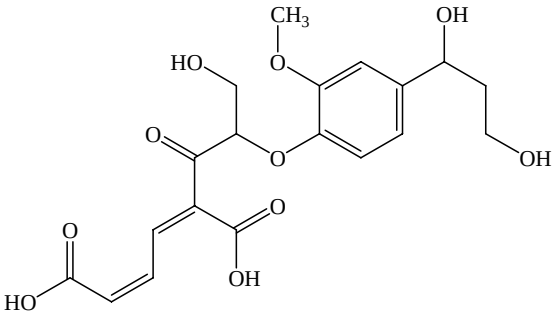

Figure 4. Structure moléculaire d'un AF de Suwannee compatible avec la dégradation de la lignine (Stenson et al., 2003).

Reemtsma et collaborateurs (Reemtsma et These, 2003, 2005; These et al., 2004) ont mis au point une méthode d'analyse alternative permettant aussi de comprendre la structure et la distribution en masse des AF de faible masse moléculaire. Un mélange d'acide fulvique est d'abord séparé en trois fractions par chromatographie d'exclusion stérique (HPSEC). La dernière fraction correspondant aux plus faibles masses moléculaires est analysée par spectrométrie de masse. Les formules moléculaires ont ensuite été obtenues pour plusieurs centaines de composés de faible masse moléculaire. Une analyse comparative sur quatre mélanges d'AF provenant de différentes sources et de lieux ont indiqué que des molécules identiques ont été trouvées dans les quatre mélanges différents. Un exemple de structures moléculaires proposées par Reemstma et These (2005) pour une molécule identifiée $C_{10}H_{12}O_5$ (212.068 Da) est montré dans la Figure 5. Suite à cette observation importante, Reemtsma et These ont conclut que *la structure des molécules d'acide fulvique semblent être largement indépendante de toute matière brute* due à une profonde modification du matériau biologique précurseur. Bien que cela puisse être vrai pour les AF les plus légers, cette conclusion est quelque peu contradictoire avec les précédents rapports sur l'isolement des biomarqueurs dérivés de la lignine à partir d'AH (par exemple Mycke et Michaelis, 1986 ; Michaelis et al., 1989) et avec l'interprétation de Stenson et al. (2003) pour des AF de la rivière Suwannee. Ces biomarqueurs peuvent être présents dans les deux fractions de masses moléculaires les plus élevées qui n'ont pas été analysées par Reemtsma et These (2005).

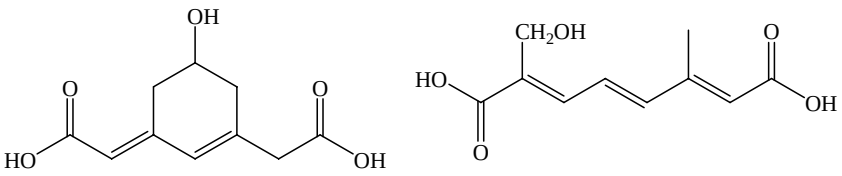

Figure 5. Structures moléculaires possibles pour un AF de faible masse moléculaire (212.068 Da) Acide fulvique séparé par Reemtsma et These (2005).

Outre une description correcte de la structure moléculaire des SH, une connaissance de leurs propriétés physico-chimiques est nécessaire si l'on veut évaluer et quantifier leur rôle dans la complexation et le transport des métaux dans l'environnement, par exemple en utilisant des modèles géochimiques. À cet égard, les valeurs expérimentales des propriétés acido-basiques des SH et des constantes de formation des complexes métal-fulvate ou métal-humate sont d'une importance primordiale. Jusqu'à récemment, de nombreuses études expérimentales ont été consacrées à l'étude des interactions des substances humates et/ou fulvates et un certain nombre de substances métalliques toxiques telles que Ni, Cr, Cu, Cd, Pb, Hg et U. Le dernier élément est particulièrement intéressant dans la gestion des déchets nucléaires. La majorité des expériences a été réalisée avec des acides humiques naturels, dont certains ont été caractérisés (par ex. acide humique de Gorleben (Allemagne) (Czerwinski et al., 1994), de Suwannee River (USA) (Lenhart et al., 2000)). Cependant, les données sont souvent incohérentes et divergentes. Dans le but d'obtenir des données cohérentes et interprétables, quelques auteurs ont développé des synthèses expérimentales des substances humiques (Andreux (1978); Pompe et al. (1996); Bubner et al. (1998); Pompe et al. (1998a, b, c)), d'autres ont étudié le système ternaire U(VI) –Acide Humique synthétisé – H_2O (Pompe et al., 1996; Denecke et al., 1997; Bubner et al., 1998; Pompe et al., 1998; Schuster et al., 1998; Pompe et al., 2000; Schmeide et al., 2003). Toutefois, la grande majorité des acides humiques a été synthétisée dans des conditions fortement oxydées (fO_2 = 0.1 MPa). Par voie de conséquence, les produits obtenus sont différents des acides humiques naturels. Les données sur les masses moléculaires des acides humiques et/ou fulviques ne sont pas connues. Les travaux expérimentaux sur les complexes U(VI)-humate et/ou fulvate ont été limités aux solutions acides ($pH \leq 4$).

Les propriétés acido-basiques des acides fulviques et/ou humiques ont fait l'objet de nombreuses études, mais l'examen de ces dernières est au-delà du cadre d'étude de ce travail. Bien que ces propriétés acido-basiques soient rendues assez complexes en raison de la présence de groupements fonctionnels acides de différente nature présents en quantité relativement variable, Perdue et Lytle (1983) et Perdue et al. (1984) ont suggéré que les

propriétés acides des substances humiques pourraient être décrites par une distribution gaussienne bimodale, se fondant sur le fait que ces propriétés acides sont principalement liées à deux types de groupements fonctionnels, à savoir les groupements carboxyliques et les groupements phénoliques.

Le nombre de fonctions acides carboxyliques dans un acide fulvique du lac de Drummond (Virginie, E.-U.) a été estimé à 9 meq (g C_{org})$^{-1}$ par Cabaniss (1991) en utilisant la potentiométrie couplée à la spectrométrie infrarouge à transformée de Fourier. De rares exceptions comprennent les déterminations potentiométriques des constantes d'ionisation d'un acide fulvique par Ramos et al. (1999).

Compte tenu des inadéquations des données citées ci-dessus, ce travail se propose de développer

(a) une nouvelle procédure de synthèse d'AF comportant trois éléments (C,H,O), quatre éléments (C,H,O,N) ou cinq éléments (C,H,O,N,S) en fonction du pH,

(b) la caractérisation systématique des AF synthétisés,

(c) une étude expérimentale des interactions entre les AF synthétisés et les ions uranyle (VI) en fonction du pH et de la concentration en AF.

La synthèse sera réalisée à partir des composés chimiques purs et de composition chimique bien déterminée en présence de l'air ambiant et sous oxydation atmosphérique. Les produits synthétisés seront ensuite analysés à l'aide d'une combinaison de six techniques de mesure complémentaires : analyse quantitative des éléments CHONS par pyrolyse, microscopie électronique à balayage, diffraction des rayons X, spectroscopies optiques (infrarouge et UV-visible) et spectrométrie de masse (ESI-MS et APCI-MS).

Les spectroscopies optiques fournissent des informations sur la présence ou non de groupements fonctionnels (-OH,-COOH, -NH_2, -SH) des fulvates et humates aqueux ou solides. La spectrométrie de masse complète l'analyse quantitative des AF et AH dissous en fournissant des données précises sur le nombre d'AF et AH et de leurs éventuels complexes aqueux avec l'uranyle (VI), ainsi que leur masse moléculaire. Les formules chimiques des acides fulviques peuvent être déduites à l'aide d'une combinaison des données des spectres de l'ATR FTIR et de l'ESI-MS.

GENERAL INTRODUCTION

Humic substances (designated hereafter by HS) are widely distributed in nature and represent a significant contribution to the global geochemical cycle of carbon (Aiken et al., 1985). They constitute a major fraction of soil organic matter (up to 80% by weight), and represent the largest fraction of natural organic matter in aquatic systems (Stevenson, 1994). For example, HS account for 55-70 % of the total dissolved organic matter in the Amazon riverwater (Hedges et al., 1992). They are also found in terrestrial, lake and marine sediments, where they may constitute potential precursors to the formation of kerogen (Hatcher et al., 1983), the most abundant form of organic carbon on the Earth and the parent material to petroleum accumulations (Hunt, 1996).

According to Stevenson (1982), HS in soils form through four different pathways. Two of these include the degradation of lignin by microorganisms, which produce either directly HS or phenolic aldehydes and acids. The latter compounds are then enzymatically oxidized to quinones, which subsequently polymerize to give HS. A third pathway involves the microbial degradation of cellulose to polyphenols. These polyphenols are again oxidized to quinones, the polymerization of which yields HS. The fourth pathway (proposed as early as 1912 by Maillard), corresponds to the condensation of sugars and amino acids (respectively derived from cellulose and polypeptides) to form HS.

The formation of HS in aquatic environments such as streams, lakes or seawater requires other mechanisms. Thurman (1985) has proposed that aqueous HS form through one or several of the following processes: leaching of plant organic matter with direct transfer to surface waters or following a transformation of this organic matter in soil profiles; leaching of soil HS and subsequent transfer to surface waters; degradation of algal and phytoplanktonic remains; ultraviolet oxidation and subsequent polymerization of reactive organic molecules in the uppermost microlayer of streams, lakes or seawater; polymerization reactions among phenol-, amine-, and/or aldehyde-bearing compounds derived from biomolecules decaying in natural waters.

Humic substances indeniably play an important role in a number of low temperature geochemical processes, including among others soil pH regulation through the dissociation of acidic functional groups, and the complexation and transport or organic and inorganic pollutants in the environment. Recent reviews on these subjects have been published by Senesi (1993), Wood (1996), Lichtfouse and Lévêque (1999), Tipping (2002), and Linnik et al. (2004), among others. Although the acidic and complexation properties of HS are of

primary interest to geochemists, soil scientists, and environmental chemists, these properties have rarely been adequately described due to the complex nature of HS (see below).

It has long been thought that HS were of a polymeric nature[5], with molecular weights determined by small angle X-ray scattering ranging from 500 to 2000 Dalton (Da) for both aquatic and soil fulvic acid, and 1000 to more than 10,000 Da for aquatic humic acid (Thurman et al., 1982; Thurman, 1985, p.305). According to this polymeric model, HS have been operationally classified into three fractions, based on their relative solubilities which were thought to be a function of molecular weight. These three fractions include

- *humin*, which is insoluble in water on the whole pH range;
- *humic acids* (HA), which are insoluble in water below pH 2 but soluble at higher pH values;
- *fulvic acids* (FA), which are soluble at all pH values.

The chemical composition of humin, HA and FA is essentially accounted for by carbon, hydrogen and oxygen, with lesser amounts of nitrogen and sulfur. Representative elemental compositions of soil humic and fulvic acids given by Steelink (1985) are shown in Table 1. It can be deduced from this table that soil humic acids have higher carbon content but lower oxygen content than soil fulvic acids. The elemental compositions of a marine fulvic acid from the surface water in the Sea of Sargasso determined by Stuermer and Harvey (1974) and of humic acids in marine sediments from offshore Southern California determined by Nissenbaum and Kaplan (1972) are presented in Table 2. It can be seen in this table that the carbon content of both marine fulvic and humic acids is similar to that of their continental counterparts, while their oxygen content (although not directly measured but calculated by difference) is usually lower. The decrease in nitrogen content and increase in sulfur content observed in Table 2 between the marine fulvic and humic acids may be attributed to early diagenetic transformations, namely denitrogenation and sulfurization, which are common processes within marine sediments (see for example Waples and Sloan, 1980 for nitrogen, and François, 1987 for sulfur).

Hedges et al. (1992) have analyzed the elemental and molecular compositions of humic substances in the seawater from the deep Pacific Ocean as well as in freshwater from the Amazon River system. These authors found that marine humic substances are characterized by higher N/C atomic ratios but lower aromatic carbon contents, which they

[5] As will be emphasized later in the text, the polymeric model of humic substances has been called into question with the advances which have been made in analytical techniques over the last decade. These advances resulted in the proposition that humic substances should rather be considered as supramolecules.

attributed to the higher proportion of proteinic material in phytoplankton, the organic matter from vascular plants being predominantly constituted by aromatic-rich lignin and tannins.[6] The ^{13}C-NMR spectra obtained by Hedges et al. (1992) for marine dissolved humic substances showed a predominance of unsubstituted alkyl carbons, oxygen-substituted alkyl carbons, and carboxyl carbons. In contrast, the spectrum for a humic acid fraction from the Rio Negro affluent of the Amazon river indicated a majority of unsaturated carbons, methoxyl carbons, and oxygenated aromatic carbons consistent with a lignin-derived structure.

Table 1. Representative elemental compositions of soil humic substances (Steelink, 1985).

	Humic acids	Fulvic acids
Carbon	53.8 – 58.7 %	40.7 – 50.6 %
Hydrogen	3.2 – 6.2 %	3.8 – 7.0 %
Oxygen	32.8 – 38.3 %	39.7 – 49.8 %
Nitrogen	0.8 – 4.3 %	0.9 – 3.3 %
Sulfur	0.1 – 1.5 %	0.1 – 3.6 %

Table 2. Elemental composition of marine fulvic acids from the surface water of the Sea of Sargasso and from a marine sediment.

	Sea of Sargasso fulvic acid [a]	Marine sediment humic acids [b]
Carbon	49.98	51-69 – 58.88
Hydrogen	6.76	5.93 – 6.56
Oxygen [c]	36.40	27.16 – 36.69
Nitrogen	6.40	3.88 – 5.17
Sulfur	0.46	0.87 – 2.12

[a] Stuermer and Harvey (1974) [b] Nissenbaum and Kaplan (1972) [c] Determined by difference

Reviews of structural models proposed in the literature over the last 80 years for humic and fulvic acids have been presented by Stevenson (1985, 1994) and Leenheer (2007). These models are depicted in Figure 1. The first model (a) proposed by Fuchs (1930) essentially consisted of condensed aromatic rings, similar to the structure of coals. Flaig (1960) subsequently proposed a model (b) based on polyphenol ethers which are present in lignin and tannins. The latter model contains abundant aromatic alcohol and quinone

[6] Note that a predominantly phenolic nature of soil fulvic acid has been called into question by Farmer and Pisaniello (1985), who pointed that the amounts of benzene and hydroxybenzene polycarboxylic acids produced by the oxidation of fulvic acids were inconsistent with the ^{13}C-NMR spectra of the same fulvic acids, and that the benzene and hydroxybenzene polycarboxylic acids were in fact artifacts or contaminants. Farmer and Pisaniello (1985) proposed that the structure of soil fulvic acid should instead correspond to a hydroxyl-substituted unsaturated aliphatic polycarboxylic acid. This conclusion appears to be in contradiction with those reached in subsequent studies (e.g. Mycke and Michaelis, 1986; Michaelis et al., 1989; Hedges et al., 1992).

functional groups, but relatively few carboxylic acids. Schnitzer (1971, cited in Schnitzer and Khan, 1972) has proposed a model of soil fulvic acid which accounts for the experimental data gathered by the two authors at that time. This model, which consists of phenolic and benzenecarboxylic (benzoic) acids held together by hydrogen bonds to form a polymeric network, corresponds to stuctural model (c) in which the voids between the different subunits can accommodate organic or inorganic compounds provided that these compounds have the appropriate molecular size. Harvey et al. (1983, 1984) carried out the synthesis in the laboratory of marine humic and fulvic acids by autoxidation of planktonic unsaturated lipids, which they compared to those isolated from seawater. Harvey et al. proposed for marine fulvic acid an aliphatic-rich structural model (d) corresponding to a chemical formula $C_{52}H_{83}O_{14}$ and atomic H/C and O/C ratios respectively equal to 1.60 and 0.27. Note that although this H/C ratio is consistent with the elemental composition listed in Table 2, the O/C ratio is half of that computed from the data in Table 2. The difference may be due to the fact that oxygen was not directly measured by Stuermer and Harvey (1974), but calculated by difference. More recently, on the basis of model compound studies, Leenheer et al. (1995) have interpreted the strong acid character of the Suwannee River (Georgia, USA) fulvic acid as possibly reflecting carboxylic acids with ether or ester functional groups in α position within cyclic structures. Accordingly, they proposed structural models such as model (e) in Figure 1. This model corresponds to a chemical formula $C_{25}H_{28}O_{14}$, atomic H/C and O/C ratios of 1.12 and 0.56, and a molecular weight of 552.481 g mol^{-1}.

Recent developments in analytical techniques, including high pressure size exclusion chromatography (HPSEC) and electrospray ionization mass spectrometry (ESI-MS), have drastically changed the perception of the molecular structure of humic substances. These developments and their implications, which have been reviewed recently by Sutton and Sposito (2005), are briefly summarized below. Comprehensive studies of HS by size exclusion chromatography carried out by Piccolo and co-workers (Piccolo et al., 1996a,b; Conte and Piccolo, 1999) led to the proposition that HS may be considered as supramolecular entities consisting of assemblages of low-molecular-weight compounds held together by hydrophobic interactions and hydrogen bonds (Piccolo and Conte, 2000; Piccolo, 2001). These assemblages are similar to micelles, the arrangement of the low-molecular-weight compounds defining internal hydrophobic regions isolated from aqueous solutions by exterior hydrophilic regions.

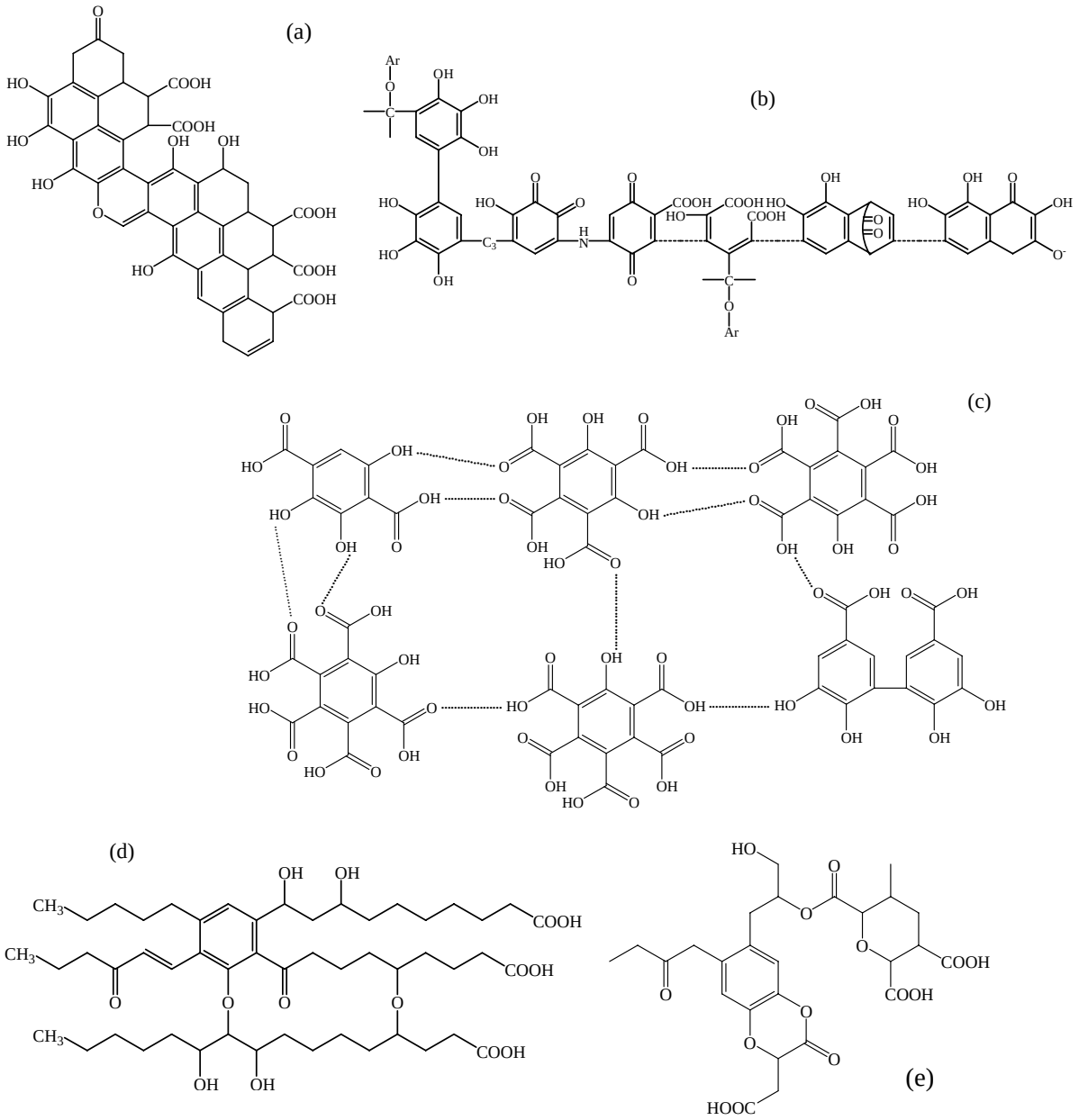

Figure 1. Some structural models proposed in the literature for fulvic and humic acids.

The suggestion that HS could form micelles was first formulated by Rochus and Sipos (1978), who determined critical micelle concentrations as a function of temperature in aqueous solutions of varying electrolyte content. Subsequently, Wershaw (1986) proposed a micellar model for HS in aqueous solutions[7]. In this model, the low-molecular-weight compounds constituting the micelles are amphiphilic molecules which represent partially oxidized fragments of lignin or other higher plant biopolymers. These partially oxidized fragments most probably bear a carboxylic acid (or carboxylate) functional group at one

[7] Wershaw (1986) also proposed a membrane-like model for HS in solid and sediments, in which HS double layers are attached to the surface of mineral grains.

extremity, which constitutes the hydrophilic part of the amphiphilic molecules, while the unoxidized parts of the fragments tend to organize in the hydrophobic interior regions of the micelles (see Figure 2). Independent evidence for a micellar structure of humic substances came a few years later from pyrene fluorescence measurements reported by Engebretson and von Wandruzka (1994). These authors observed that the quenching of pyrene fluorescence by bromide was significantly decreased by the presence of small amounts (2.5-10 ppm) of humic acid in aqueous solution, which suggested that the humic acid was preventing interactions between pyrene and the quenching bromide ions. In addition, they also noted an initial increase of the fluorescence in the presence of specific cations (namely Cs^{+} and Mg^{2+}), which Engebretson and von Wandruzka attributed to a cation-enhanced formation of hydrophobic micellar microenvironments in which pyrene could be protected.

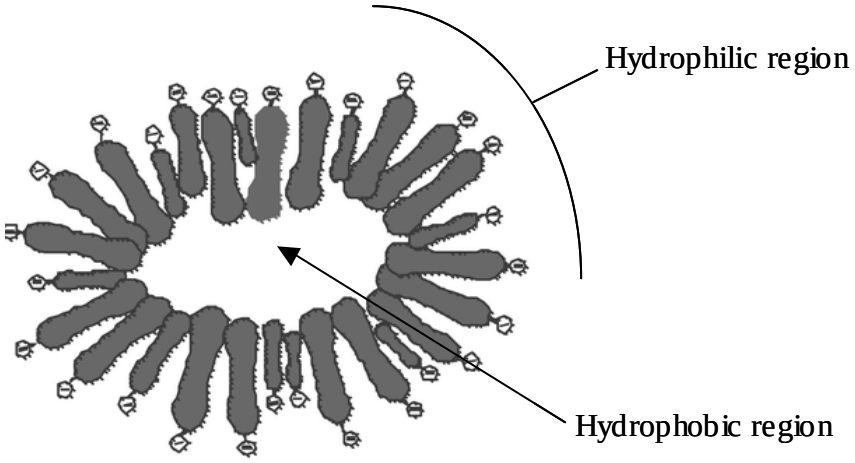

Figure 2. Schematic representation of Wershaw's micellar model of aqueous humic substances (after Wershaw, 1986).

A recent important step towards the understanding of the molecular nature of humic and fulvic acids has been made with the advent of soft ionization techniques such as laser desorption or electrospray ionization (ESI) used in conjunction with mass spectrometry (MS). Using laser desorption mass spectrometry, Novotny et al. (1995) showed that the molecular weight distribution of a fulvic acid mixture from an aquifer in South Dakota, USA, was dominated by low-molecular-weight compounds with an average of 418 Da, while higher molecular weight compounds were only representing a small fraction of the fulvic acid

mixture. The first application of ESI-MS[8] to the study of HS is due to McIntyre et al. (1997), who identified in a groundwater from a sand aquifer in New South Wales, Australia, a series of individual fulvic acids (negative, singly charged ions) in the mass range 200-700 Da, with a maximum at ~ 350 Da. From the distribution of peaks which they obtained, McIntyre et al. (1997) proposed that these fulvic acids were predominantly aliphatic, polycarboxylic acids but they were cautious in recognizing that alternative compounds may not produce negatively charged ions for the conditions under which they obtained their ESI-MS spectra. Plancque et al. (2001) reported an investigation of aquatic fulvic acids from different locations by quadrupole time-of-flight (Q-TOF) mass spectrometry coupled to an ESI device, which resulted in distributions of peaks maximizing at ~ 450 Da. Plancque et al. (2001) performed additional measurements by tandem mass spectrometry (MS-MS) to obtain some information on the molecular structure of these fulvic acids. They proposed that the fulvic acid mixture in a sample isolated from the Mol aquifer was constituted by a family of molecules such as that represented in Figure 3, these molecules being associated in a supramolecular entity.

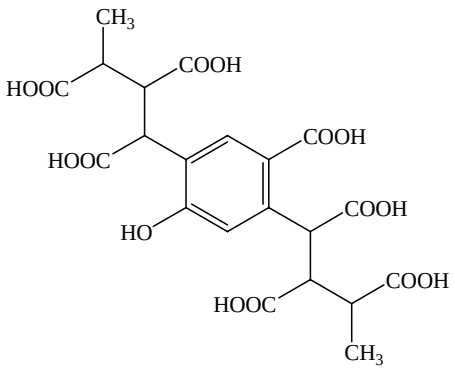

Figure 3. Possible molecular structure for a representative individual fulvic acid identified by Plancque et al. (2001) in a sample isolated from the Mol aquifer. This structure corresponds to a molecular formula $C_{20}H_{22}O_{15}$ and a molecular weight of 502 Da.

Quadrupole time-of-flight mass spectrometry does not permit a complete and detailed identification of all the individual fulvic acid ions present in a given fulvic acid mixture (McIntyre et al., 2001). Accordingly, Stenson et al. (2003) generated ions produced from the reference Suwannee River fulvic acid by electrospray ionization (ESI) and determined the exact masses and chemical formulas of 4626 individual ions by ultrahigh-resolution Fourier transform ion cyclotron resonance mass spectrometry (FTICR-MS). Stenson et al. (2003) sorted these 4626 formulas in a series of homologous families, the molecular structures of which are consistent with lignin degradation pathways. An example of structure proposed by

[8] The details of the ESI-MS analytical technique are presented in the following chapter.

Stenson et al. for an individual fulvic acid with a chemical formula corresponding to $C_{19}H_{22}O_{10}$ (molecular weight 410 Da) is shown in Figure 4.

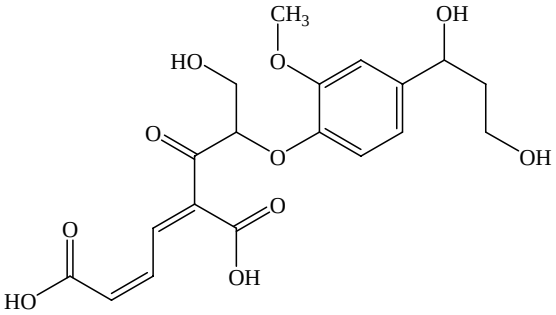

Figure 4. Molecular structure of an individual Suwannee River fulvic acid consistent with a lignin degradation pathway (Stenson et al., 2003).

Reemtsma and coworkers (Reemtsma and These, 2003, 2005; These et al., 2004) have developed an alternative analytical procedure also providing insights into the structure and mass distribution of the lower molecular weight fulvic acids. In this procedure, a fulvic acid mixture is first separated into three fractions by size exclusion chromatography (SEC). The last fraction corresponding to the lowest molecular weight fulvic acids is then analyzed by mass spectrometry. Molecular formulas have then been obtained for several hundred low-molecular-weight single compounds. A comparative analysis on four fulvic acid mixtures originating from different sources and locations indicated that the same exact molecules were found in the four different mixtures. An example of molecular structures proposed by Reemstma and These (2005) for an identified $C_{10}H_{12}O_5$ molecule (212.068 Da) is shown in Figure 5. Following this important observation, Reemtsma and These concluded that the *structure of fulvic acid molecules appear to be largely independent from any source material* due to an intensive reworking of the biological precursor material. Although it may be true for the lighter fulvic acids, this conclusion is somewhat contradictory with earlier reports of the isolation of lignin-derived biomarkers from humic acids (e.g. Mycke and Michaelis, 1986; Michaelis et al., 1989) and the interpretation of Stenson et al. (2003) for the individual Suwannee River fulvic acids. Such biomarkers may well be present in the two higher molecular weight fractions not analyzed by Reemtsma and These (2005).

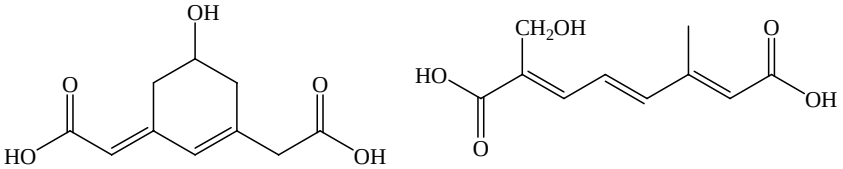

Figure 5. Proposed molecular structures for a low-molecular-weight (212.068 Da) fulvic acid separated by Reemtsma and These (2005).

Besides a correct description of the molecular structure of HS, a knowledge of their physicochemical properties is required if one wants to evaluate and quantify their role in the dissolution, complexation and transport of metals in the environment, for instance by using geochemical models. In that respect, experimental values for the acid-base properties of HS and for the formation constants of metal-fulvate or metal-humate complexes are of primary importance. Until recently, several experimental works have been devoted to the study of interactions of humate and/or fulvate substances and several toxic metal substances such as Ni, Cr, Cu, Cd, Pb, Hg and U. The latter element is particularly interesting in the nuclear waste management. The majority of experiments have been carried out using natural Humic Acids, some of which are characterized (*e.g.* humic acid of Gorleben (Germany) (Czerwinski et al., 1994), of Suwannee River (USA) (Lenhart et al., 2000)). Meanwhile, data often are inconsistent divergent. In order to obtain consistent and interpretable data, some authors have developed experimental synthesis of humic substances (Andreux (1978); Pompe et al (1996); Bubner et al (1998); Pompe et al (1998a, b, c)), some other workers have investigated the ternary system U(VI) – synthesized Humic Acid – H_2O (Pompe et al., 1996; Denecke et al., 1997; Bubner et al., 1998; Pompe et al., 1998; Schuster et al., 1998; Pompe et al., 2000; Schmeide et al., 2003). However, the great majority of humic acids have been synthesized under high oxidation condition (fO_2 = 0.1 MPa). Products obtained are thus different from natural humic acids. Data concerning the molecular mass of synthesized Humic and/or Fulvic Acid appears not to be available. Experimental works on U(VI)-humate and/or fulvate complexes have been limited in acid solutions (pH $\leq$ 4).

The acid-base properties of Humic and/or Fulvic acid also have been the subject of many investigations, the review of which is beyond the scope of the present work. Although these acid-base properties are rendered quite complex due to the presence of acidic functional groups of different nature and which are present in variable relative amounts, it has been suggested by Perdue and Lytle (1983) and Perdue et al. (1984) that the acidic properties of humic substances could be described by a bimodal Gaussian distribution accounting for experimental evidence that these acidic properties were mainly related to two kinds of functional groups, i.e. carboxylic groups and phenolic groups.

The amount of carboxylic acid functional groups in a fulvic acid from Lake Drummond in Virginia (U.S.A.) was tentatively estimated to 9 meq (g C_{org})$^{-1}$ by Cabaniss (1991) using potentiometry coupled to fourier transform infrared spectrometry. Rare

exceptions include the potentiometric determinations of the ionization constants of a fulvic acid by Ramos et al. (1999).

Based on the above mentioned inadequacies of data, the present study develops

(a) a new experimental procedure to synthesize fulvic acids with three elements (C,H,O), four elements (C,H,O,N) and five elements (C,H,O,N,S) as a function of pH,

(b) a systematic characterization of the synthesized fulvic acids

(c) and a systematic experimental study of interactions between the synthesized fulvic acids (ligand) and toxic metal (uranyl(VI) ion as a function of four physico-chemical parameters:

i) pH

ii) metal concentration

iii) ligand concentration and

iv) temperature.

Synthesis will be carried out under atmospheric oxidation and ambient conditions using pure chemical products as initial compounds.

Final products have been analyzed using a combination of measurement techniques: quantitative analysis of CHONS elements by pyrolysis, scanning electron microscope (SEM), X-ray diffraction (XRD), optical spectroscopy (ATR-FTIR (attenuated total reflectance Fourier transform infra red) and UV-Vis) and mass spectroscopy (Electrospray ionization-mass spectroscopy (ESI-MS) and/or Atmospheric pressure chemical ionization (APCI-MS).

ATR-FTIR spectroscopy provides information about the presence of functional groups (-OH, -COOH, $-NH_2$, -SH) of aqueous or solid fulvate and humate substances. ESI-MS and/or APCI-MS allow determining the number of fulvic acids and their molecular weight. Chemical formula of fulvic acids could be deduced using a combination of ATR-FTIR and mass spectrometry data.

References

Aiken G.R., McKnight D.M., Wershaw R.L., and MacCarthy P. (1985) An introduction to humic substances in soil, sediment, and water. In *Humic Substances in Soil, Sediment, and Water* (eds. G.R. Aiken, D.M. McKnight, R.L. Wershaw, and P. MacCarthy), pp. 1-9. Wiley-Interscience.

Andreux F. (1978) Etude des étapes initials de la stabilisation physico-chimique et biologique d'acides humiques modèles. *Thèse d'état à l'Université de Nancy 1* 174 p.

Andreux F., Golebiowska D., and Metche M. (1980) Oxidative polymerization of o-diphenols in presence or absence of amino-acids. Topics on (catechol-glycocolle) and (catechol-diglycylglycine). *Bulletin de Liaison / Groupe Polyphénols* **9**, 178-188.

Bubner M., Pompe S., Jander R., Schuster G., Heise K. H. and Nitsche H. (1998) Synthesis of solid iron and uranyl complexes with natural and synthetic humic acids. *Forschungszentrum Rossendorf e.V., [Bericht] FZR (1998),* **FZR-218**, 44-46.

Cabaniss S.E. (1991) Carboxylic acid content of a fulvic acid determined by potentiometry and aqueous Fourier transform infrared spectrometry. *Analytica Chimica Acta* **255**, 23-30.

Conte P. and Piccolo A. (1999) Conformational arrangement of dissolved humic substances.Influenece of solution composition on association of humic molecules. *Environmental Science and Technology* **33**, 1682-1690.

Czerwinski K.R., Buckau G., Scherbaum F. and Kim J. I. (1994) Complexation of the uranyl ion with aquatic humic acid. *Radiochim. Acta* **65**(2), 111-19.

Denecke, M. A.; Pompe, S.; Reich, T.; Moll, H.; Bubner, M.; Heise, K. H.; Nicolai, R.; Nitsche, H. (1997) Measurements of the structural parameters for the interaction of uranium(VI) with natural and synthetic humic acids using EXAFS. *Radiochim. Acta* 79(3), 151-159.

Engebretson R.R. and von Wandruszka R. (1994) Microorganization in dissolved humic acids. *Environmental Science and Technology* **28**, 1934-1941.

Farmer V.C. and Pisaniello D.L. (1985) Against an aromatic structure for soil fulvic acid. *Nature* **313**, 474-475.

Flaig W. (1960) Chemistry of humus materials. *Suomen Kemistilehti B* **33A**, 229-251.

François R. (1987) A study of sulphur enrichment in the humic fraction of marine sediments during early diagenesis. *Geochimica et Cosmochimica Acta* **51**, 17-27.

Fuchs W. (1930) Humic acids. *Kolloid-Zeitschrift* **52**, 248-251, 350-356 and **53**, 124-126 (in German).

Harvey G.R., Boran D.A., Chesal L.R.A., and Tokar J.M. (1983) The structure of marine fulvic and humic acids. *Marine Chemistry*, **12**, 119-132.

Harvey G.R., Boran D.A., Piotrowicz S.R., and Weisel C.P. (1984) Synthesis of marine humic substances from unsaturated lipids. *Nature* **309**, 244-246.

Hatcher P.G., Spiker E.C., Szevernyi N.M., and Maciel G.E. (1983) Selective preservation and origin of petroleum-forming aquatic kerogen. *Nature* **305**, 498-501.

Hedges J.I., Hatcher P.G., Ertel J.R., and Meyers-Schulte K.J. (1992) A comparison of dissolved humic substances from seawater with Amazon River counterparts by ^{13}C-NMR spectrometry. *Geochimica et Cosmochimica Acta* **56**, 1753-1757.

Hunt J.M. (1996) *Petroleum Geology and Geochemistry* (2nd Edition). Freeman.

Jokic A., Wang M.C., Liu C., Frenkel A.I. and Huang P.M. (2004) Integration of the polyphenol and Maillard reactions into a unified abiotic pathway for humification in nature: the role of δ-MnO_2. *Organic Geochemistry* **35**, 747-762.

Jung A.-V., Frochot C., Parant S., Lartiges B.S., Selve C., Viriot M.-L. and Bersillon J.-L. (2005) Synthesis of amino-phenolic humic-like substances and comparison with natural aquatic humic acids: A multi-analytical techniques approach. *Organic Geochemistry* **36**, 1252-1271.

Leenheer J.A., Wershaw R.L., and Reddy M.M. (1995) Strong-acid, carboxyl-group structures in fulvic acid from the Suwannee River, Georgia. 2. Major structures. *Environmental Science and Technology* **29**, 399-405.

Leenheer J.A. (2007) Progression from model structures to molecular structures of natural organic matter components. *Annals of Environmental Science* **1**, 57-68.

Lenhart J.J., Cabaniss S.E., MacCarthy P. and Honeyman B.D. (2000) Uranium(VI) complexation with citric, humic and fulvic acids. *Radiochim. Acta* **88**(6), 345-353.

Lichtfouse E. and Lévêque J., eds. (1999) Humic substances, a challenging analytical puzzle (semi-special issue). *Analusis* **27**, 383-444.

Linnik P.N., Vasilchuk T.A., and Linnik R.P. (2004) Humic substances of natural waters and their importance for aquatic ecosystems: a review. *Hydrobiological Journal* **40**, 81-107.

Maillard L.C. (1912) Action des acides aminés sur les sucres; formation des mélanoïdine par voir méthodique. *Comptes-Rendus des Séances de l'Académie des Sciences de Paris* **154**, 66-68.

McIntyre C., Jardine D.R., and McRae C. (2001) Electrospray mass spectrometry of aquatic fulvic acids. *Rapid Communications in Mass Spectrometry* **15**, 1974-1975.

McIntyre C., Batts B.D., and Jardine D.R. (1997) Electrospray mass spectrometry of groundwater organic acids. *Journal of Mass Spectrometry* **32**, 328-330.

Michaelis W., Richnow H.H., and Jenisch A. (1989) Structural studies of marine and riverine humic matter by chemical degradation. *The Science of the Total Environment* **81/82**, 41-50.

Mycke B. and Michaelis W. (1986) Lignin-derived molecular fossils from geological materials. *Naturwissenschaften* **73**, 731-734.

Nissenbaum A. and Kaplan I.R. (1972) Chemical and isotopic evidence for the in situ origin of marine humic substances. *Limnology and Oceanography* **17**, 570-582.

Novotny F.J., Rice J.A., and Weil D.A. (1995) Characterization of fulvic acid by laser-desorption mass spectrometry. *Environmental Science and Technology* **29**, 2464-2466.

Perdue E.M. and Lytle C.R. (1983) Distribution model for binding of protons and metal ions by humic substances. *Environmental Science and Technology* **17**, 654-660.

Perdue E.M., Reuter J.H., and Parrish R.S. (1984) A statistical model of proton binding by humus. *Geochimica et Cosmochimica Acta* **48**, 1257-1263.

Piccolo A. (2001) The supramolecular structure of humic substances. *Soil Science* **166**, 810-832.

Piccolo A. and Conte P. (2000) Molecular size of humic substances. Supramolecular associations versus macromolecular polymers. *Advances in Environmental Research* **3**, 508-521.

Piccolo A., Nardi S., and Cancheri G. (1996a) Macromolecular changes of soil humic substances induced by interactions with organic acids. *European Journal of Soil Science* **47**, 319-328.

Piccolo A., Nardi S., and Cancheri G. (1996b) Micelle-like conformation of humic substances as revealed by size-exclusion chromatography. *Chemosphere* **33**, 595-600.

Plancque G., Amekraz B., Moulin V., Toulhoat P., and Moulin C. (2001) Molecular structure of fulvic acids by electrospray with quadrupole time-of-flight mass spectrometry. *Rapid Communications in Mass Spectrometry* **15**, 827-835.

Pompe S., Bubner M., Denecke M.A., Reich T., Brachmann A., Geipel G., Nicolai R., Heise K.H. and Nitsche H. (1996) A comparison of natural humic acids with synthetic humic acid model substances: characterization and interaction with uranium(VI). *Radiochim. Acta* **74**, 135-140.

Pompe S., Brachmann A., Bubner M., Geipel G., Heise K.H. Bernhard G. and Nitsche H. (1998a) Determination and comparison of uranyl complexation constants with natural and model humic acids. *Radiochim. Acta* **82**, 89-95.

Pompe S., Bubner M., Meyer M., Heise K.H., Nicolai R. and Nitsche H. (1998b) Defined model substances for humic acids. Part 1. Synthesis and characterization of nitrogen-free humic acids. *Forschungszentrum Rossendorf e.V., [Bericht] FZR (1998),* **FZR-218**, 29-30.

Pompe S., Bubner M., Jander R., Heise K.H., Nicolai R. and Nitsche H. (1998c) Defined model substances for humic acids. Part 2. Synthesis and characterization of a synthetic humic acid with blocked phenolic hydroxyl groups. *Forschungszentrum Rossendorf e.V., [Bericht] FZR (1998),* **FZR-218**, 30-32.

Pompe S., Schmeide K., Bubner M., Geipel G., Heise K.H., Bernhard G. and Nitsche H. (2000) Investigation of humic acid complexation behavior with uranyl ions using modified synthetic and natural humic acids. *Radiochim. Acta* **88**(9-11), 553-558.

Ramos A., López S., López R., Fiol S., Arce F. and Antelo J.M. (1999) Ionization costants of a soil fulvic acid. *Analusis* **27** No. 5, 418-420.

Reemtsma T. and These A. (2003) On-line coupling of size exclusion chromatography with electrospray ionization-tandem mass spectrometry for the analysis of aquatic fulvic and humic acids. *Analytical Chemistry* **75**, 1500-1507.

Reemtsma T. and These A. (2005) Comparative investigation of low-molecular-weight fulvic acids of different origin by SEC-Q-TOF-MS : New insights into structure and formation. *Environmental Science and Technology* **39**, 3507-3512.

Rochus W. and Sipos S. (1978) Die Micellbildung bei Huminstoffen. *Agrochimica* **22**, 446-454.

Schmeide K., Sachs S., Bubner M. Reich T., Heise K.H. and Bernhard G. (2003) Interaction of uranium(VI) with various modified and unmodified natural and synthetic humic substances studied by EXAFS and FTIR spectroscopy. *Inorganica Chimica Acta* **351**, 133-140.

Schnitzer M. and Khan S.U. (1972) *Humic Substances in the Environment*. Marcel-Dekker.

Schuster G., Bubner M., Jander R., Pompe S., Heise K. H. and Nitsche H. (1998) Thermal analyses of iron and uranyl complexes with natural and synthetic humic acids. *Forschungszentrum Rossendorf e.V., [Bericht] FZR (1998),* **FZR-218**, 54-55.

Senesi N. (1993) Metal-humic substance complexes in the environment. Molecular and mechanistic aspects by multiple spectroscopic approach. In *Biogeochemistry of Trace*

Metals (eds. D.C. Adriano, Z.-S. Chen, S.-S. Yang, and I.K. Iskander), pp. 429-495. Northwood.

Steelink C. (1985) Implications of elemental characteristics of humic substances. In *Humic Substances in Soil, Sediment, and Water* (eds. G.R. Aiken, D.M. McKnight, R.L. Wershaw, and P. MacCarthy), pp. 457-476. Wiley-Interscience.

Stenson A.C., Marshall A.G., and Cooper W.T. (2003) Exact masses and chemical formulas of individual Suwannee River fulvic acids from ultrahigh resolution electrospray ionization Fourier transform ion cyclotron resonance mass spectra. *Analytical Chemistry* **75**, 1275-1284.

Stevenson F.J. (1982) *Humus Chemistry*. Wiley and Sons.

Stevenson F.J. (1985) Geochemistry of soil humic substances. In *Humic Substances in Soil, Sediment, and Water* (eds. G.R. Aiken, D.M. McKnight, R.L. Wershaw, and P. MacCarthy), pp. 13-52. Wiley-Interscience.

Stevenson F.J. (1994) *Humus Chemistry: Genesis, Composition, Reactions*. Wiley and Sons. (2^{nd} Edition).

Stuermer D.H. and Harvey G.R. (1974) Humic substances from seawater. *Nature* **250**, 480-481.

Sutton R. and Sposito G. (2005) Molecular structure in soil humic substances: The new view. *Environmental Science and Technology* **39**, 9009-9015.

These A., Winkler M., Thomas C., and Reemtsma T. (2004) Determination of molecular formulas and structural regularities of low molecular weight fulvic acids by size-exclusion chromatography with electrospray ionization quadrupole time-of-flight mass spectrometry. *Rapid Communications in Mass Spectrometry* **18**, 1777-1786.

Thurman E.M., Wershaw R.L., Malcolm R.L., and Pinckney D.J. (1982) Molecular size of aquatic humic substances. *Organic Geochemistry* **4**, 27-35.

Thurman E.M. (1985) *Organic Geochemistry of Natural Waters*. Martinus Nijhoff/Dr W. Junk Publishers, Dordrecht.

Tipping E. (2002) *Cation Binding by Humic Substances*. Cambridge University Press.

von Wandruszka R. (1998) The micellar model of humic acid: evidence from pyrene measurements. *Soil Science* **163**, 921-930.

Waples D.W. and Sloan J.R. (1980) Carbon and nitrogen diagenesis in deep sea sediments. *Geochim. Cosmochim. Acta* **44**, 1463-1470.

Wershaw R.L. (1986) A new model for humic materials and their interactions with hydrophobic organic chemicals in soil-water or sediment-water systems. *Journal of Contaminant Hydrology* **1**, 29-45.

Wood S.A. (1996) The role of humic substances in the transport and fixation of metals of economic interest (Au, Pt, Pd, U, V). *Ore Geology Reviews* **11**, 1-31.

CHAPTER 1. Materials, experimental methods, and analytical techniques

This chapter describes all materials, chemicals, reagents, methods, and analytical techniques used for the synthesis and characterization of four different types of fulvic acids (which will be designated in the following text by SFA for synthetic fulvic acids), as well as for the study of the complexation reactions between these SFA and toxic metals.

1. Materials

All chemicals and reagents used in the present study were of analytical grade and were used without any further purification.

1.1. Reactants used in the synthesis of fulvic acids

Fulvic acids have been synthesized in three different systems, including the C-H-O system, the C-H-O-N system; and the C-H-O-N-S system. The fulvic acids in these systems were respectively obtained from the auto-polymerization (or self-association – see below) of catechol, as well as co-polymerization of catechol ($C_6H_6O_2$) and acetic acid ($C_2H_4O_2$), catechol and glycine ($C_2H_5NO_2$), and catechol and cysteine ($C_3H_7NO_2S$). The molecular structures of these four reagents are shown in Figure 1.1. Each of these reagents are described in detail in terms of its properties, and then characterized with the same analytical techniques which will be used to characterize the reaction products, i.e. the synthetic fulvic acids.

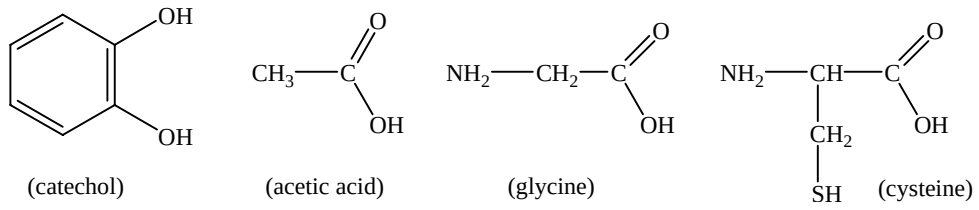

Figure 1.1. Molecular structures of the organic reagents used in the synthesis of fulvic acids.

1.1.1. Catechol – Catechol Reagent Plus (≥ 99 %) was used in the present work and was obtained from *Sigma Aldrich*. Catechol is a white solid with a melting point of 105°C (378 K) (*Handbook of Data on Organic Compounds*, 1989). The liquid has a normal boiling point of 245.5°C at ~ 1 bar (Schleede, 1955). The chemical formula of catechol ($C_6H_6O_2$) corresponds to a molecular weight of 110.11 $g \cdot mol^{-1}$ and the following elemental composition expressed in weight percent: C 65.45%, H 5.49%, O 29.06%. Its aqueous solubility at 25°C is ~ 450 $g \cdot L^{-1}$

(Varhaníčková et al., 1995). The first and second ionization constants of catechol at the same temperature are pK_{a1} = 9.45 and pK_{a2} = 12.82, respectively (Dubey and Mehrotra, 1964).

1.1.2. Acetic acid – Acetic acid (> 99.8 %) was purchased from Riedel–deHaën. Its chemical formula $C_2H_4O_2$ corresponds to a molecular weight of 60.05 g·mol^{-1} and the following elemental composition expressed in weight percent: C 40.00%, H 6.71%, O 53.29%. The ionization constant of acetic acid at 25°C and 1 bar is pK_a = 4.76 (Harned and Ehlers, 1933).

1.1.3. Glycine – Glycine (99+%) was obtained from Aldrich. Its chemical formula $C_2H_5NO_2$ corresponds to a molecular weight of 75.07 g·mol^{-1} and the following elemental composition expressed in weight percent: C 32.00%, H 6.71%, N 18.66%, O 42.63%. Glycine is a white solid with a melting point of 262°C (535 K) (*Handbook of Data on Organic Compounds*, 1989). The aqueous solubility of glycine at 25°C is 251.6 g (kg H_2O)$^{-1}$ (Nozaki and Tanford, 1971). The first and second ionization constants of glycine are pK_{a1} = 2.35 and pK_{a2} = 9.78 (Talukdar et al., 1988).

1.1.4. Cysteine – L-Cysteine (97%) was also obtained from Aldrich. Its chemical formula $C_3H_7NO_2S$ corresponds to a molecular weight of 121.16 g·mol^{-1} and the following elemental composition expressed in weight percent: C 29.74%, H 5.82%, N 11.56%, O 26.41%, S 26.47%. Cysteine appears as white crystals. Its melting point is 240°C (513 K) (*Handbook of Data on Organic Compounds*, 1989). The aqueous solubility of L-cysteine is ~ 280 g (kg H_2O)$^{-1}$ (Wilhoit, 1969). Two ionization constants have been reported for cysteine by Perkins (1953): pK_{a1} = 8.53 and pK_{a2} = 10.53.

1.2. Reactants used in the complexation studies

In order to investigate the complexation of the uranyl (UO_2^{2+}) cation by the SFA prepared in the present study, stock solutions of uranyl perchlorate ($UO_2(ClO_4)_2$; 10^{-3} M) have been prepared. Uranyl perchlorate was prepared in the following manner. Reagent grade uranyl nitrate $UO_2(NO_3)_2 \cdot 6H_2O$ (Merck >98%) was heated to 400°C to yield UO_3, which was subsequently redissolved in pure perchloric acid $HClO_4$.

The complexation experiments were carried out as a function of the concentrations of both the cation and ligand (i.e. the dissociated SFA)and pH. Fixed values of the latter parameter were obtained by using the corresponding acid ($HClO_4$) of the uranyl salt ($UO_2(ClO_4)_2$) chosen for the experiments. For experiments carried out at alkaline pH values, NaOH was used. The origin and purity of these reagents were the following: $HClO_4$ (R.P.

Normapur >70%) was purchased from ProLabo, and NaOH (>98%) were provided by Sigma-Aldrich.

1.3. Dialysis membranes

Dialysis is a separation technique which allows the separation of molecules as a function of their molecular size by the selective diffusion of small molecules through the pores of a semi-permeable membrane (McPhie, 1971). The experimental solution to be dialyzed is introduced in the dialysis membrane – which is pinched at both ends (Figure 1.2) – and the membrane is soaked in distilled (Milli-Q academic) water. The small molecules start to diffuse through the pores of the membrane towards the aqueous solution, in which the concentration of the diffusing molecule progressively increases until it equals the concentration inside the membrane. The aqueous solution must then be replaced with distilled water for further dialysis. The dialysis membranes used in the present study were cellulose acetate Spectra/Por® Biotech membranes, manufactured by Spectrum Laboratories, Rancho Dominguez, CA, USA). Fulvic acid fractions of different molecular sizes were obtained using membranes of different Molecular Weight Cut-Off (MWCO). The membranes used were 500, 1000, 2000, 8000, and 10000 MWCO. The MWCO value of a given membrane is usually determined by using proteins of known molecular weights.

Figure 1.2. Dialysis membranes containing a solution of a mixture of synthetic fulvic acids.

2. Experimental methods

2.1. Synthesis of fulvic acids

This section describes the experimental procedure followed to synthesize four different types of fulvic acids. For all sample preparation and dilutions, ultra pure water (milli-Q water) was obtained from Milli-Q academic (Millipore). The organic reagents and

the synthesized products were all stored at 4°C whenever they were not in use. All syntheses were carried out at room temperature, under atmospheric partial pressure of oxygen, and at a constant pH value equal to 10.0, which is slightly higher than the first dissociation constant of catechol. The duration of each synthesis was 2 months. Fulvic acids have been synthesized in the C-H-O, C-H-O-N, and C-H-O-N-S systems in the manner described below.

2.1.1. Synthesis in the C-H-O system

Fulvic acids have been synthesized in the C-H-O system by two different polymerization reactions, including the autopolymerization of catechol and the polymerization through condensation of catechol and acetic acid. Those substances obtained from the first reaction will be designated below by SFA_1, while those obtained by the second reaction will be referred to as SFA_2.

2.1.1.1. Autopolymerization of catechol

The synthesis procedure to obtain SFA_1 was as follows. Catechol (44.04 g) was first dissolved in 4 liters of ultra pure water to obtain a 0.1 M solution. The pH of the reaction medium was adjusted to pH = 10 by using NaOH 1.0 M. The resulting solution was allowed to stand in the dark at 25°C (± 0.1°C), under constant stirring at 3000 rounds per minute (rpm) for homogenization. Successive samplings indicated that both the viscosity and color intensity of the solution were increasing as a function of reaction progress. The color first turned to light brown, then dark brown, and finally black after approximately three days. The polymerization was carried out for 63 days, and a constant value of pH was maintained by adding NaOH 0.1 M on a daily basis. The synthesis procedure described above differs from that originally proposed by Andreux et al. (1980), who performed the synthesis of their humic-like polymers at pH = 7.9 and under a constant current of pure oxygen while the synthesis was carried out in contact with the atmosphere in the present study. All samples collected over the period of the synthesis have been deep frozen, lyophilized (see below), ground to fine powder, and then stored at 4°C to await analysis.

2.1.1.2. Polymerization through condensation of catechol and acetic acid

A mixture of SFA_2 containing alcohol (—OH) and perhaps carboxylic acid (—COOH) groups has been obtained by dissolving catechol (44.04 g) and acetic acid (24.02 g) in equimolar (0.1 M) proportions in 4.0 L of ultra pure water. The pH of the reaction medium was again adjusted to pH = 10 by using NaOH 1.0 M, and the synthesis was carried out at 25°C, in the dark and under a constant stirring of 3000 rpm for 63 days. The same

observations of increasing viscosity and color intensity were made, with the color of the reaction medium slowly turning into black as a function of the progress of the polymerization reaction. Samples of the solution were withdrawn just after the initiation of the reaction (zeroth day) and every five days for one month. These samples were again deep frozen, lyophilized, ground to powder and stored at 4°C to await analysis.

2.1.2. Synthesis in the C-H-O-N system

Fulvic acids synthesized in the C-H-O-N system will be designated in the following text by SFA_3. These substances which contain alcohol (—OH), amine (—NH_2), and perhaps carboxylic acid (—COOH) groups have been synthesized using a procedure which is identical to that described for SFA_2, except that glycine was used instead of acetic acid. Note that catechol and glycine are the reactants used in the original synthesis of humic acids by Andreux et al. (1980). Catechol (44.04 g) was dissolved with glycine (30.03 g) to obtain an equimolar (0.1 M) mixture in 4.0 L of ultra pure water. NaOH 1.0 M was added daily to adjust the pH of the reaction medium to pH = 10. The synthesis was again carried out at 25°C, in the dark and under a constant stirring of 3000 rpm for 63 days. The same observations of increasing viscosity and color intensity were made, although in this case a pink color was initially observed, which has been attributed by Jung et al. (2005) to the formation of N-substituted quinones. Samples were withdrawn from the solution just after the initiation of the reaction (zeroth day,) and then every five days for one month. These samples were deep frozen, lyophilized, ground to powder and stored at 4°C to await analysis.

2.1.3. Synthesis in the C-H-O-N-S system

Fulvic acids synthesized in the C-H-O-N-S system will be designated in the following text by SFA_4. These substances obtained by reacting catechol with cysteine again contain alcohol (—OH), amine (—NH_2), and perhaps carboxylic acid (—COOH). In addition, the presence of the thiol (—SH) group in cysteine may allow polymerization by cross-linking, resulting in the formation of sulfide or disulfide groups. Catechol (44.04 g) was dissolved with cysteine (48.06 g) to obtain an equimolar (0.1 M) mixture in 4.0 L of ultra pure water. The synthesis was carried out at 25°C, in the dark and under a constant stirring of 3000 rpm for 63 days while the pH of the reaction medium was adjusted to pH = 10 by using NaOH 1.0 M. The solution again showed an increase in darkening with increasing reaction progress. Samples were withdrawn from the solution just after the initiation of the reaction (zeroth day,) and then every five days for one month. These samples were deep frozen, lyophilized, ground to powder and stored at 4°C to await analysis.

2.2. Lyophilisation

Lyophilisation is the process by which water is removed from a sample. It uses that property which water has to undergo sublimation under very low temperatures and pressures. Details about the technique can be found in Everse and Stolzenbach (1971). Various aqueous solutions of SFA have been lyophilized in the present study using a LYOTEC™ lyophilisator at a lyophilisation temperature of -90°C. Pressures as low as 10^{-5} bar, are obtained with a high vacuum pump. The time required to lyophilize a given sample was 2 weeks per liter of solution. Both bulk and dialyzed solutions have been lyophilized, including samples taken at intermediate times during a given synthesis. Typically, between 10 and 30 g of SFA solids were recovered for each liter of lyophilized solution, depending on the type of SFA. It can be seen in Figure 1.3 that the solids obtained in the different systems (i.e. the C-H-O, C-H-O-N, and C-H-O-N-S systems) were of different colors, which also changed as a function of time for a given system. After lyophilisation, these solids have been ground in a mortar and stored at 4°C prior to extraction, detailed characterization and use in complexation experiments.

Figure 1.3. SFA samples obtained at intermediate times of synthesis. SFA_1 is synthesized from catechol alone, SFA_2 from catechol and acetic acid, SFA_3 from catechol and glycine, and SFA_4 from catechol and cysteine. The width of a photograph is approximately 5 cm.

2.3. Extraction

In order to purify the SFA, that is to separate them from a possible fraction of reactants remaining at the end of the synthesis, classical extraction procedures have been performed. Extraction is a physical process in which a solute is transferred from one phase to another, usually from a solid phase to a liquid phase (solid-liquid extraction), or from a liquid phase to another liquid phase (liquid-liquid extraction). Both of these techniques have been used in the present study. The details of the procedures followed for the purification of the SFA are given below.

2.3.1. Solid-liquid extraction

In the solid-liquid extraction technique, a solid sample consisting of a mixture of different components with varying solubilities is sequentially extracted by several solvents. In our case, these different components include the SFA, the remaining reactants, and possibly by-products such as sodium catecholate or sodium acetate. In order to have an extraction procedure which is efficient, the following two requirements must be met:

- the solid sample to be extracted must be ground, milled or rolled in order to increase the surface area of the sample, hence the contact between the sample and the solvent;
- the chosen solvent must be selective for the solute to be extracted at a given temperature.

Purification of the SFA was performed in the present study by Accelerated Solvent Extraction (ASE) using a Dionex ASE 200 extraction system. The procedure, which is depicted in Figure 1.4, was the following. Serial extractions on 2.53 g of samples of each SFA (SFA_1, SFA_2, SFA_3 and SFA_4) were carried out by successively using dichloromethane (DCM), ethyl acetate, methanol, acetonitrile, a 1:1 v/v methanol:DCM mixture, and finally 9:1, 4:1, and 3:2 v/v methanol:water mixtures. The extractions were performed in a 33 mL cell at 100°C and under a pressure of 100 bar, and represented 3 static cycles of 5 minutes each. The fractions collected were evaporated to dryness using a rotatory evaporator. Dichloromethane and ethyl acetate were found to be ineffective solvents to extract raw SFA. The amount of material extracted by acetonitrile (< 3 mg) was also negligible. In contrast, solids were obtained with methanol as well as with the methanol:DCM and methanol:water mixtures. Note that three successive extractions were carried out with methanol since this solvent appeared to be the most efficient. These solids were weighed and stored at 4°C to await analysis.

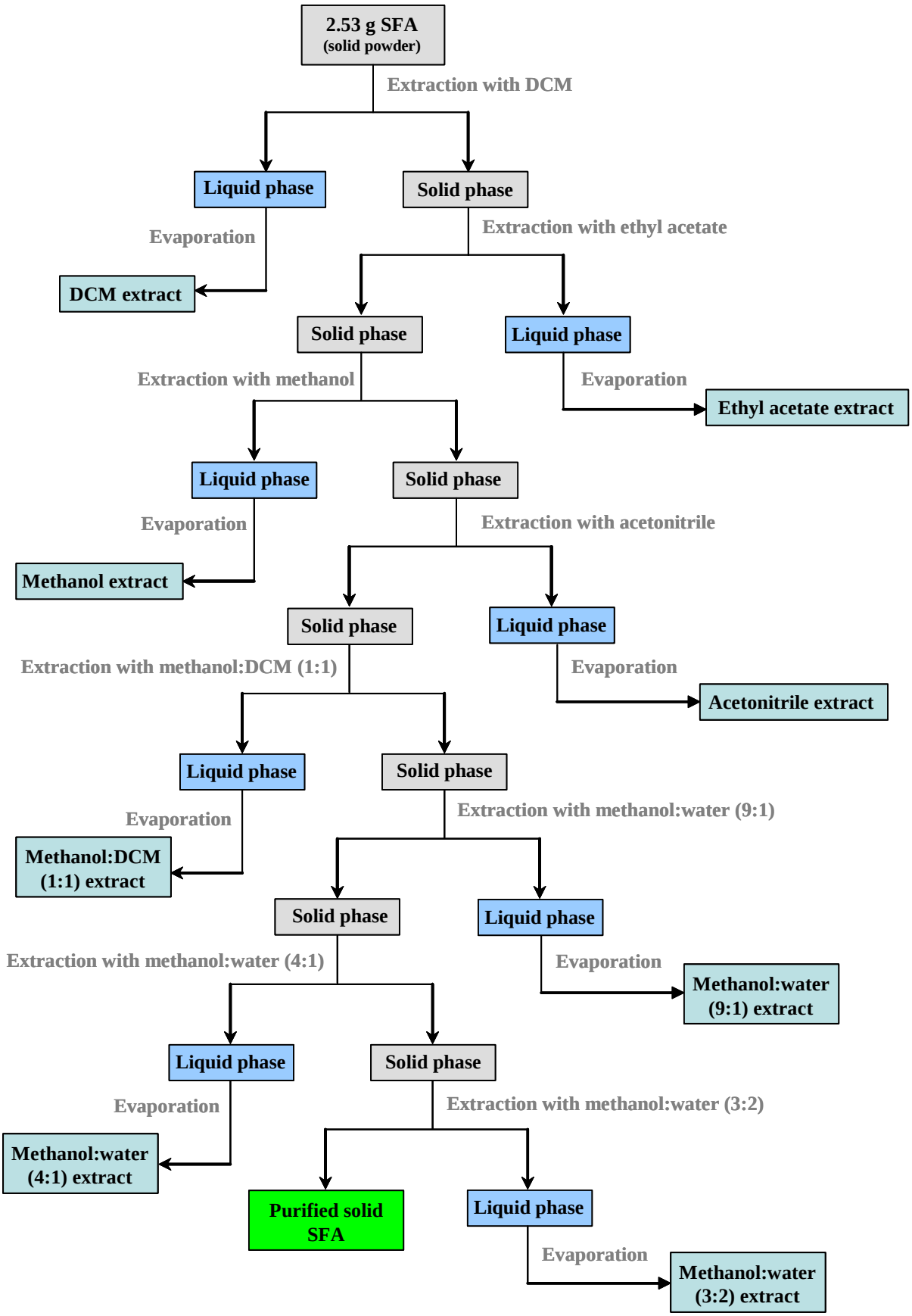

Figure 1.4. Schematic representation of the solid-liquid extraction of raw SFA at 100°C and 100 bar.

2.3.2. Liquid-liquid extraction

In the liquid-liquid extraction procedure, the solute is removed from one liquid phase by adding to that phase an immiscible solvent in which the solute is more soluble. The procedure, which was applied only to SFA_1, is depicted in Figure 1.5 and was the following. A sample of 4.06 g of solid SFA_1 was dissolved in ultra pure water and the pH of the resulting solution was adjusted to 2.052 using 1.0 M HCl. The acidified solution was extracted with ethyl acetate (heated up to ~ 60°C) using a glass liquid-liquid extractor. The extraction was carried out continuously for 63 hours. After separation of the organic phase and aqueous phase, the organic phase was evaporated to dryness and an orange solid was obtained with a 15% yield with respect to the initial mass of SFA_1 (4.06 g). The aqueous phase was deep-frozen and then lyophilized. A black solid was obtained with a 85% yield.

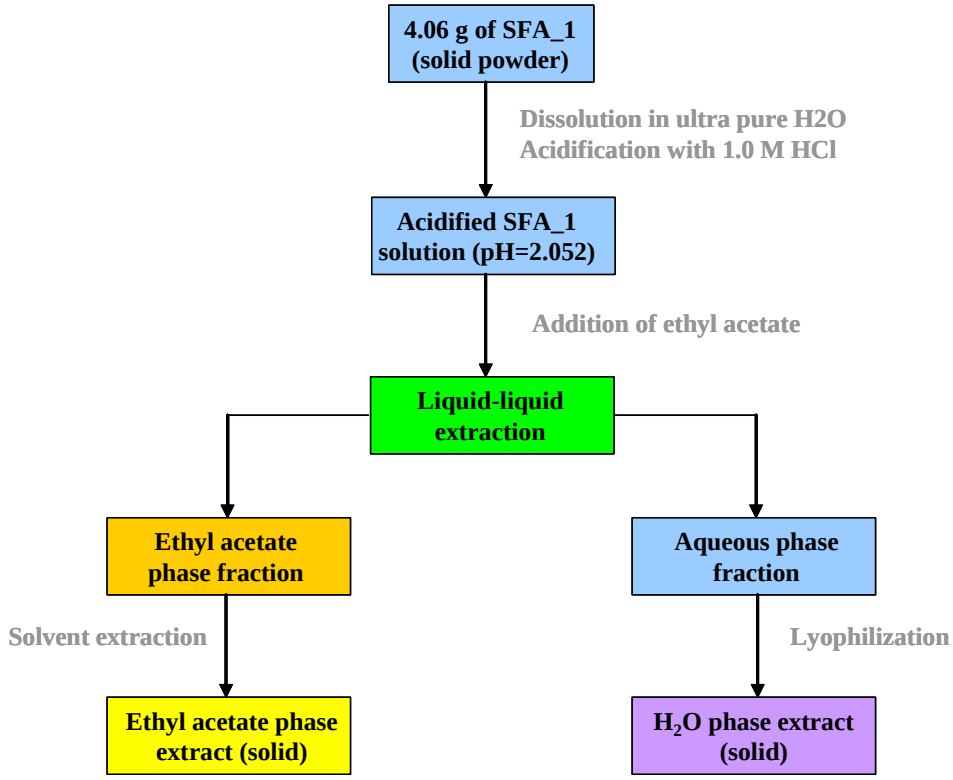

Figure 1.5. Schematic representation of the liquid-liquid extraction of raw SFA_1.

3. Analytical techniques

3.1. Elemental analysis

Elemental analysis has been carried out in the present study to determine the weight percentages of each element (C,H,O,N,S) in the SFA synthesized in the C-H-O, C-H-O-N, and C-H-O-N-S systems. The analyses have been performed with a Thermo Finnigan EA™

1112 elemental analyzer equipped with an automatic sampler. A schematic representation of the apparatus is shown in Figure 1.6. For each measurement, approximately 1.5 mg of sample is required. The sample is inserted in a tin vial, and weighed with an accuracy of 1 μg on a Sartorius M2P microbalance. The sample is subsequently combusted in a reactor at high temperature (940°C) under a current of oxygen for a very short time (15 s) and in the presence of anhydrous tungsten trioxide WO_3 (which is used as a catalyst to facilitate the combustion). The combustion produces carbon dioxide (CO_2), water (H_2O), sulfur dioxide (SO_2) and nitrogen oxides (NO_x), the latter being reduced to nitrogen (N_2) by native copper. For the determination of oxygen, the sample is pyrolyzed at 1060°C in a different reactor under a helium atmosphere, which produces carbon monoxide (CO). Following the combustion, the system is swept with helium and the produced gases are mixed before being separated on a Porapak^{TM} packed column, are finally analyzed by a gas chromatograph equipped with a Chromosorb column and a catharometric detector. The system is completely controlled by the Eager 300 software. The resulting elemental compositions are reported with an absolute accuracy of ± 0.2% on the basis of a minimum of two analyses.

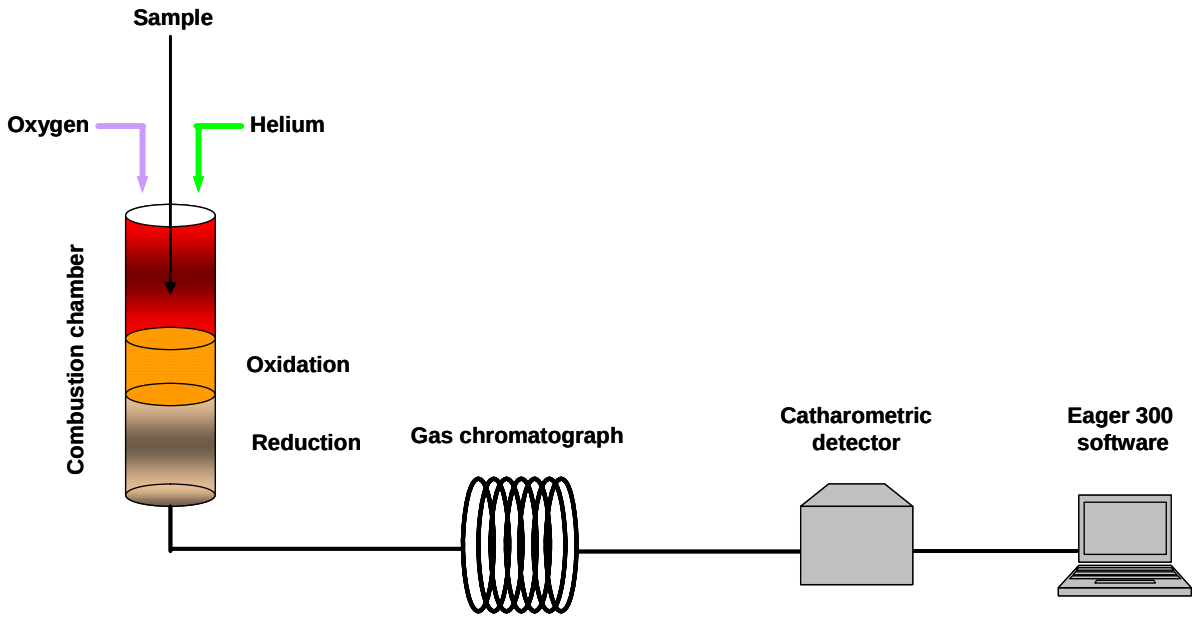

Figure 1.6. Schematic representation of the elemental analyzer used in the present study.

3.2. X-ray diffraction

X-Ray diffraction is a versatile, non destructive analytical technique for the identification and quantitative determination of the various crystalline materials of compounds present in powdered and solid samples. Identification is achieved by comparing the X-ray diffraction pattern obtained from unknown sample with an internationally recognized database (ICDD) containing reference patterns. Solid samples of the synthesized products were investigated by comparing them with their starting materials.

For XRD analysis, the solid samples were collected using a D8 Bruker diffractometer with Co-Kα radiation (λ = 1.7902Å). General operating conditions were 35 kV accelerating voltage, 45 mA intensity, step-scanning at 0.035°(2θ) intervals, 3-sec counting time, and 3-75°(2θ) for disoriented powder.

3.3. Infrared spectroscopy

Infrared (IR) spectroscopy is an extremely reliable and well recognized fingerprinting method. It has long been used for the characterization of humic substances (Schnitzer et al., 1959; Ishiwatari, 1970; Stevenson and Goh, 1971). The technique of Attenuated Total Reflectance (ATR) has in recent years revolutionized solid and liquid sample analyses because it combats the most challenging aspects of infrared analyses, namely sample preparation and spectral reproducibility. ATR is an IR sampling technique that provides excellent quality data in conjunction with the best possible reproducibility of any IR sampling technique. It has revolutionized IR solid and liquid sampling through:

• Faster sampling
• Improving sample-to-sample reproducibility and
• Minimizing user to user spectral variation.

An attenuated total reflection accessory operates by measuring the changes that occur in a totally internally reflected infrared beam when the beam comes into contact with a sample (see Figure 1.7). An infrared beam is directed onto an optically dense crystal with a high refractive index at a certain angle. This internal reflectance creates an evanescent wave that extends beyond the surface of the crystal into the sample held in contact with the crystal. This evanescent wave protrudes only a few microns (0.5 μ - 5 μ) beyond the crystal surface and into the sample. Consequently, there must be good contact between the sample and the crystal surface. In regions of the infrared spectrum where the sample absorbs energy, the evanescent wave will be attenuated or altered. The attenuated energy from each evanescent wave is

passed back to the IR beam, which then exits the opposite end of the crystal and is passed to the detector in the IR spectrometer. The system then generates an infrared spectrum.

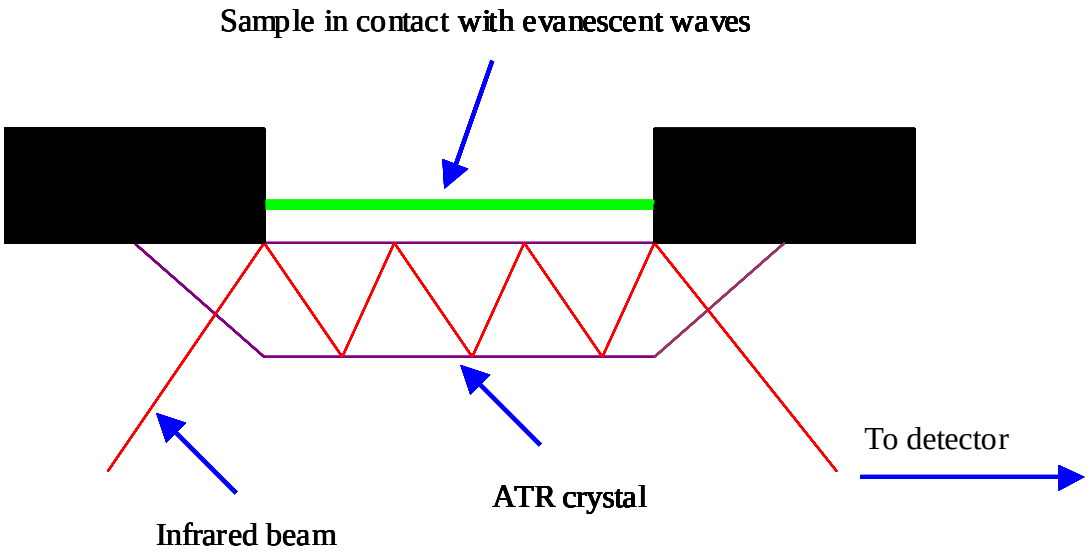

Figure 1.7. A multiple reflection ATR system.

ATR-FTIR spectra in the region between 4000-650 cm^{-1} were obtained using PerkinElmer Instruments, Spectrum One, FT-IR Spectrometer. The scanner velocity was 10 kHz, with the resolutions of 4 cm^{-1}. Reference is atmosphere for solids and pure water for aqueous solutions. ATR spectra are shown with absorbance scale corresponding to log ($R_{reference}/R_{sample}$), where R is the internal reflectance of the device.

3.4. UV-visible spectroscopy

Molecular absorption in the ultraviolet (UV) and visible region of the electromagnetic spectrum is a function of the electronic structures of molecules. The absorption of a UV or visible radiation corresponds to the excitation of outer electrons in these molecules. Three types of so-called electronic transitions can be distinguished:

- transitions involving electrons pertaining to σ, π or *n* (or *p*) orbitals;
- transitions involving charge-transfer electrons;
- transitions involving *d* and *f* electrons.

Only the first type of transitions which is concerned with organic compounds will be discussed below. The second and third types of transition concern organo-metallic complexes and transition metal ions and lanthanide or actinide ions, respectively. The absorption of ultraviolet or visible radiation involving σ, π or *n* (or *p*) electrons in organic molecules is

restricted to particular functional groups (termed *chromophores*) which contain valence electrons of low excitation energy. The spectrum of a molecule containing such functional groups is complex, because of the superposition of rotational and vibrational transitions on the electronic transitions. This results in a combination of overlapping lines which appears as a continuous absorption band.

In general, the absorption of a photon by an organic molecule in the ultraviolet or visible region of the spectrum corresponds to the excitation of one electron pertaining to one bonding (σ or π) or non bonding (*n* or *p*) orbital to the next, higher energy antibonding (σ* or π*) orbital. There are four possibilities for promoting an electron from a bonding or non-bonding orbital to an antibonding orbital. These four possibilities are represented in Figure 1.8, and separately discussed below. In terms of transition energies, a *n* (or *p*) → π* transition requires less energy than *n* (or *p*) → σ*, σ → σ* or π → π* transitions.

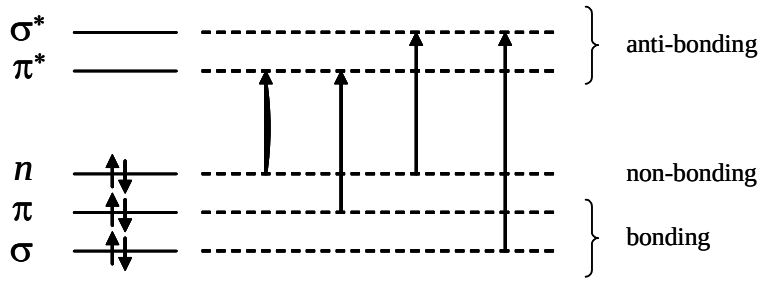

Figure 1.8. Possible electronic transitions in organic molecules.

All organic molecules absorb in the ultraviolet region (~ 135-400 nm), but their absorption characteristics depend on two principal factors which are 1) the type of electronic transition which occurs (σ → σ*, π → π*, *n* → π* or *n* → σ*) and 2) the effect of the atomic environment on the transition. The second factor is mainly due to physico-chemical parameters, including solvent effects, pH, oxidation-reduction reactions, the formation of complexes, polymerization, self-association, and the presence of covalently bonded unsaturated groups or saturated groups with non-bonding electrons. Among these parameters, the covalently unsaturated groups (e.g. alkene, ketone, imine or carboxylic groups) are reponsible for electronic absorption and are called *chromophores*. In contrast, saturated groups with non-bonded electrons (e.g. alcohol, amine, or halogenide groups) are refered to as *auxochromes*. Auxochromic groups do not absorb UV radiation even at wavelengths ≤ 200 nm when they are individually measured. In contrast, when a auxochromic group is bonded to a chromophoric group in a given molecule, the presence of the auxochromic group alters both

the wavelength and the intensity of the absorption of that molecule. Displacements of absorption bands towards higher and lower wavelengths are respectively called *bathochromic* (or red) and *hypsochromic* (or blue) shifts. Increases and decreases in the intensity of absorption are respectively referred to as *hyperchromic* and *hypochromic* effects.

Ultraviolet absorption bands can be designated using different notation systems. The simplest approach to this problem is either to refer to the electronic transitions or to designate the absorption bands with letters. The notation system proposed by Burawoy (1930, 1939) and completed by Braude (1945, 1955) is as follows. Burawoy (1930, 1939) proposed that electronic transitions could be attributed to three main types of absorption bands:

- *R* bands (*R* for Radikalartig) characterizing forbidden $n \rightarrow \pi^*$ transitions
- *K* bands (*K* for Konjugierte) representing $\pi \rightarrow \pi^*$ transitions in conjugated alkenes
- *B* bands (*B* for *Benzenoid*) representing $\pi \rightarrow \pi^*$ transitions in aromatic or heteroaromatic molecules.

Although Burawoy's notation system correctly describes aliphatic compounds containing σ electrons, π electron chromophores and *n* electrons pertaining to heteroatoms (oxygen, nitrogen, sulfur or halogens), this notation does not allow a complete description of the absorption bands of compounds containing benzene rings. For example, the UV spectrum of benzene in *n*-heptane solvent displays three absorption bands at 184 nm, 204 nm and 255 nm (Wojtkowiak and Chabanel, 1977). Only the last two of these bands can be designated as *K* and *B* bands using Burawoy's notation. Braude (1945, 1955) subsequently completed the notation of Buravoy by defining *E* bands (*E* for *Ethylenic*), thereby designating the first two bands of benzene at 184 nm and 204 nm as E_1 and E_2 bands. Both of these bands characterize aromatic $\pi \rightarrow \pi^*$ transitions.

Four important observations must be kept in mind when discussing the absorption characterisitics of aromatic compounds:

- the substitution of auxochromic groups on benzene rings shifts the E_2 and *B* bands to longer wavelengths, with an intensification of the *B* band and a loss of its vibrational fine structure due to the *n*-π conjugation;
- the addition of a carboxylic group on benzene (and by extension phenol – see below) to form benzoic acid (or hydroxybenzoic acid in the case of phenol) is accompanied by a bathochromic effect with an intense absorption;
- the conversion of a hydroxybenzene to its corresponding anion following an increase of pH results in a bathochromic shift of the E_2 and *B* bands and an increase of the

absorption intensity. This is due to the fact that the nonbonding electrons of the oxygen atom are more available for an interaction with the π-electron system of the aromatic ring.

- the association of substituted aromatic rings through C–C bonds (as in biphenyl) or ether bonds (as in diphenyl ether) enhances the π electron conjugation and produces a bathochromic effect.

3.5. Electrospray ionization – mass spectroscopy (ESI-MS)

Mass spectrometry detection with electrospray ionization is nowadays state-of-the art. There are numerous ionization techniques available for mass spectral analysis. ESI, a 'soft' ionization technique shown in Figure 1.9 below, is one such method that is emerging as the optimal method for humic substances. This is because ESI takes place at atmospheric pressure, ionizes a wide range of polar, hydrophilic molecules with both acidic and basic functional groups, and can be operated in the positive or negative ion mode. Since the samples for ESI are prepared in water or made up in a mixture of water and/or simple, low-molecular-weight organic solvents that evaporate during ESI, solvent-generated ions do not interfere with the mass spectral information generated for the substances being analyzed.

Figure 1.9. A diagram of micrOTOF$_Q$ (ESI-MS) instrument.

The mechanism of ESI is based on a high voltage difference between the needle and capillary which causes the sample to burst into many smaller charged droplets, see Figure 1.10. This voltage difference will determine whether positive or negative ions are formed, i.e. the sign of the voltage difference is the opposite of the sign of the ions formed. As the solvent evaporates with the aid of heat or nitrogen gas, the charges on the droplet accumulate and begin to repel each other owing to charge–charge interactions. Once the droplet reaches the Rayleigh limit, where the coulombic repulsions outweigh the solvent surface tension, the droplet will once again explode into many smaller droplets. The remaining solvent completely evaporates, leaving the analyte molecule in the gas phase, with a charge distributed among the polar functional groups present in the analyte, see Figure 1.11 (Gaskell, 1997).

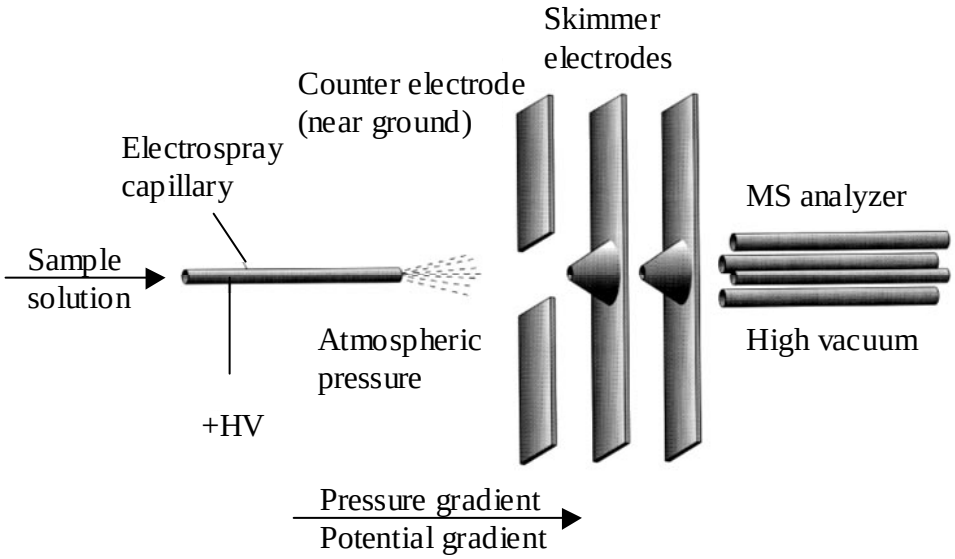

Figure 1.10. Essential features of the electrospray interface, as per Gaskell 1997.

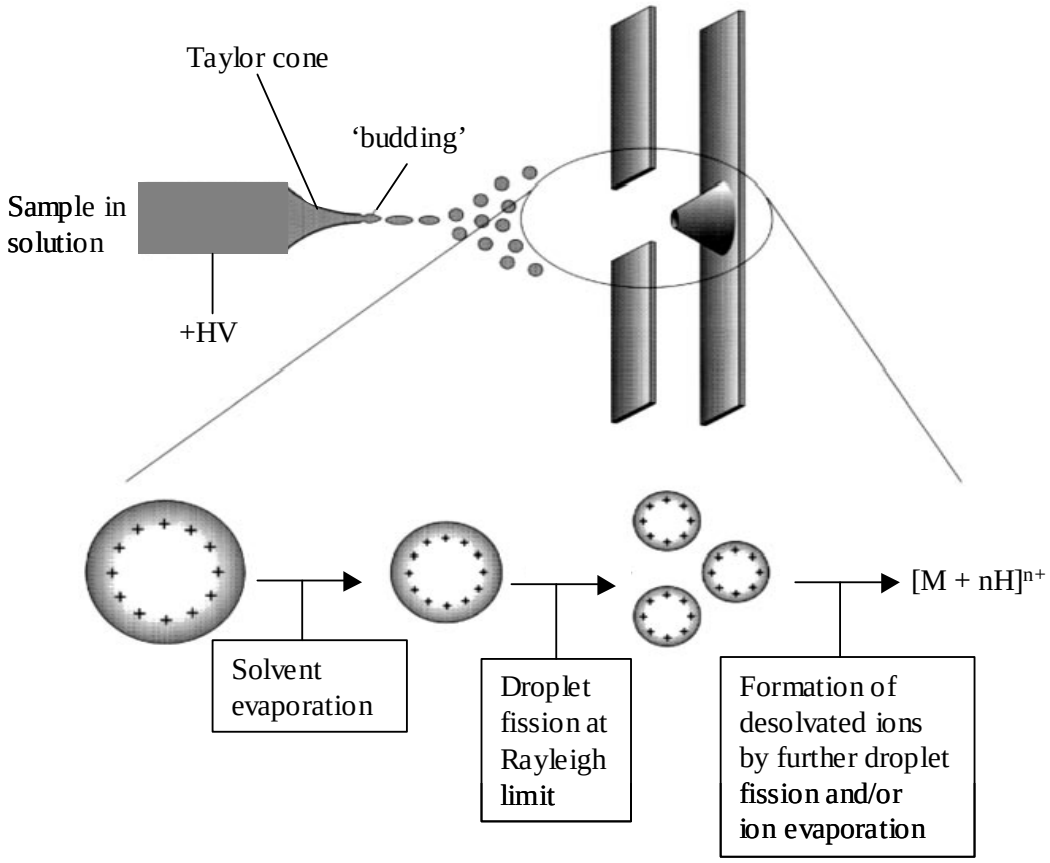

Figure 1.11. Droplet production in the electrospray interface, as per Gaskell 1997.

Positive and negative ion modes

ESI can be operated in both positive and negative ion modes. Depending on the sample, each ionization mode can give very different mass spectra for the same sample, (Brown and Rice, 2000, Rostad and Leenheer, 2004). One must always consider the complexity that evolves from each ionization mode. Of paramount importance are ionization efficiencies, which are determined by the types of functional groups present in the sample and their ability to lose or accept a proton (or other cation) for negative or positive ionization, respectively. For example, a sample with easily ionizable and/or numerous acidic groups, such as carboxylic acids, will readily lose a proton and be negatively ionized very efficiently. In contrast, samples with many basic groups, such as amines, will easily pick up a proton and be positively ionized (Brown and Rice, 2000, Rostad and Leenheer, 2004).

Different mass spectra can be acquired for the same sample from positive and negative ionization modes, indicating that numerous functional groups are present and they are preferentially ionized on the basis of their relative acidity and basicity (Rostad and Leenheer, 2004). Both spectra can be used to give complementary information about the sample, as long

as relative abundances are not compared, because of the different ionization efficiencies of the various molecules. It is very common to add acid or base (for positive or negative ionization, respectively) to samples prior to ESI in order to increase the number of ions formed in the source region (Brown and Rice, 2000).

3.6. Atmospheric pressure chemical ionization – mass spectroscopy (APCI-MS)

APCI (Atmospheric Pressure Chemical Ionization) is one of the two common types of ionization, sometimes referred to as soft-ionization methods. The other one is Electrospray, ESI. The ion source is similar to that of ESI. There are instances where particular analytes do not ionize well with ESI. APCI may often give the needed sensibility. The APCI-source is best used for the analysis of polar and and nonpolar analytes. APCI can be combined with Liquid Chromatograph and Mass Spectrometer (LC/MS), see Figure 1.12 below. The combining of chromatographic and spectroscopic information is well known for the elucidation of structures of a variety of polar natural compounds.

It involves passing LC eluent through a nebulizing needle with temperatures ranging from 250°C to 400°C, creating a fine spray, which is then passed through a heated vaporizer tube, where the eluent droplets are fully vaporized. The resulting gas/vapour mixture is then passed over a corona discharge needle with a current of 4000 nA – 1000 nA, where the solvent vapour and carrier gas are ionized to create reagent gas ions. These reagent ions in turn ionize the eluent sample molecules via a chemical ionization process. This ionization process also requires a counter-current flowing drying gas. To ensure minimal noise level, this is used at a relatively low level.

The sample ions are then introduced into a conductive capillary and through a series of skimmer and lenses before being introduced into the mass spectrometer for analysis. Like Electrospray, APCI has very high ionization efficiency.

The ionization mechanisms in APCI are almost identical with those in conventional chemical ionization. Positive ion formation can be achieved by proton transfer, adduct formation or charge-exchange reactions, whereas in negative mode ions are formed by proton-abstraction, anion-attachment and electron-capture reactions (Niessen and Tinke, 1995 and Herderich et al., 1997).

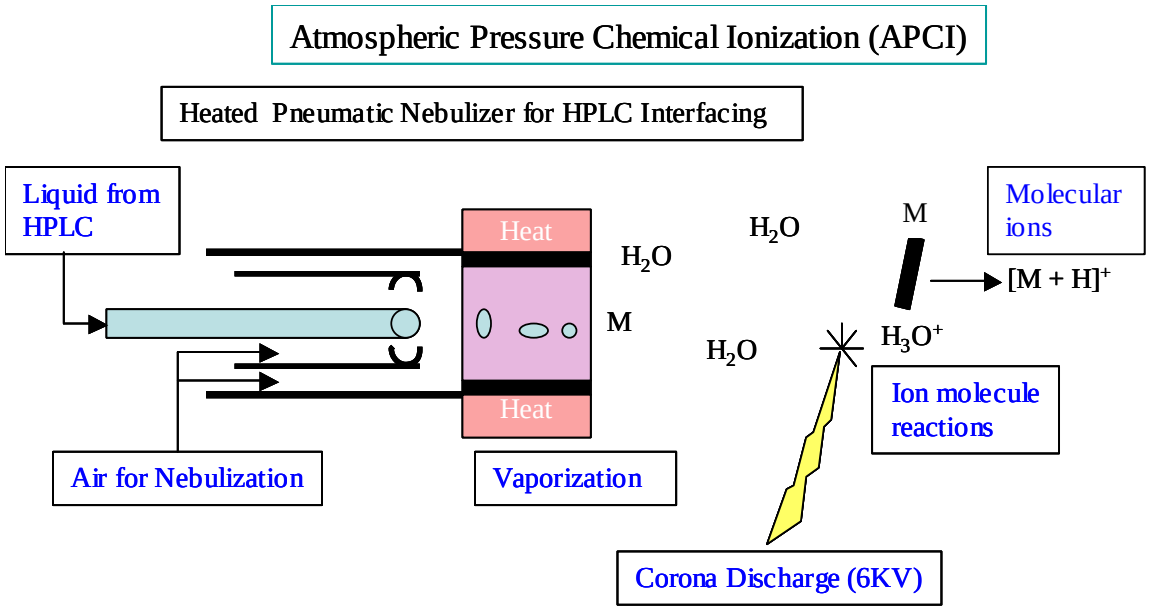

Figure 1.12. Different parts of APCI.

Characteristics of APCI

1. Provides molecular weight information
2. Sensitivity depends strongly upon the analyte
3. Suitable for analyzing less polar compounds compared to ESI
4. Increased fragmentation compared to ESI
5. Enable coupling MS and LC with flow rate up to 1ml/min.

References

Aktaş N., Şahiner N., Kantoğlu Ö, Salih B., and Tanyolaç (2003) Biosynthesis and characterization of laccase catalyzed poly(catechol). *Journal of Polymers and the Environment* **11**, 123-128.

Andreux F., Golebiowska D., and Metche M. (1980) Oxidative polymerization of o-diphenols in presence or absence of amino-acids. Topics on (catechol-glycocolle) and (catechol-diglycylglycine). *Bulletin de Liaison / Groupe Polyphénols* **9**, 178-188.

Burawoy A. (1930) Absorption of light and constitution. I. Homeopolar organic compounds. *Berichte der Deutschen Chemischen Gesellschaft* **63B**, 3155-3172 (in German).

Burawoy A. (1939) The light absorption of organic compounds, and the nature of unsaturated linkages. *Journal of the Chemical Society*, 1177-1188.

Braude E.A. (1945) Ultra-violet light absorption and the structure of organic compounds. *Annual Reports on the Progress of Chemistry* **42**, 105-130.

Braude E.A. (1955) Ultraviolet and visible light absorption. In *Determination of Organic Structures by Physical Methods* (eds. E.A. Braude and F.C. Nachod), pp. 131-194. Academic Press.

Brown T.L. and Rice J.A. (2000) Effect of experimental parameters on the ESI FT-ICR mass spectrum of fulvic acid. *Analytical Chemistry* **72**, 384-390.

Dubey S.N. and Mehrotra R.C. (1964) Study of catechol derivatives of aluminium. *Journal of Inorganic and Nuclear Chemistry* **26**, 1543-1550.

Dubey S., Singh D., and Misra R.A. (1998) Enzymatic synthesis and various properties of poly(catechol). *Enzyme and Microbial Technology* **23**, 432-437.

Everse J. and Stolzenbach F.E. (1971) Lyophilization. *Methods in Enzymology* **22**, 33-39.

Fischer G., Cao X., Cox N., and Francis M. (2005) The FT-IR spectra of glycine and glycylglycine zwitterions isolated in alkali halide matrices. *Chemical Physics* 313, 39-49.

Gaskell S.J. (1997) Electrospray: Principles and practice. *Journal of Mass spectrometry* **32**, 677-688.

Handbook of Data on Organic Compounds (1989) 2nd Edition (eds. R.C. Weast and J.G. Grasselli). CRC Press.

Harned H.S. and Ehlers R.W. (1933) The dissociation constant of acetic acid from 0 to 60° centigrade. *Journal of the Amercian Chemical Society* **55**, 652-656.

Herderich M., Roscher R., Schneider C., Schwab W., Humpf H.-U. and Schreier P. (1997). Application of Atmospheric Pressure Ionization HPLC-MS-MS for the analysis of Natural Products. *Chromatographia* Vol. **45**, 127-132.

Ishiwatari R. (1970) Strucutural characteristics of humic substances in Recent lake sediments. In *Advances in Organic Geochemistry 1966* (eds. G.D. Hobson and G.C. Speers), pp. 283-311. Pergamon Press.

Jung A.-V., Frochot C., Parant S., Lartiges B.S., Selve C.,Viriot M.-L., and Bersillon J.-L. (2005) Synthesis of amino-phenolic humic-like substances and comparison with natural aquatic humic acids: A multi-analytical techniques approach. *Organic Geochemistry* **36**, 1252-1271.

Kumar S., Rai A.K., Singh V.B., and Rai S.B. (2005) Vibrational spectrum of glycine molecule. *Spectrochimica Acta Part A* **61**, 2741-2746.

Little J.L. (1999) "Artifacts in trimethylsilyl derivatization reactions and ways to avoid them." *Journal of Chromatography A* **844**, 1-22.

McPhie P. (1971) Dialysis. *Methods in Enzymology* **22**, 23-32.

MicrOTOF$_Q$ user manual, version 1.0 Bruker Daltonics, September 2006; 3-1 and 3-17.

Niessen W.M.A and Tinke A.P. (1995) Liquid chromatography-mass spectrometry, General principles and instrumentation. *J. Chromatogr. A.* **703**, 37-57.

Nozaki Y. and Tanford C. (1971) The solubility of amino acids and two glycine peptides in aqueous ethanol and dioxane solutions. *The Journal of Biological Chemistry* **246**, 2211-2217.

Pawlukojć A., Leciejewicz J., Ramirez-Cuesta A.J., and Nowicka-Scheibe J. (2005) L-Cysteine: Neutron spectroscopy, Raman, IR and ab initio study. *Spectrochimica Acta Part A* **61**, 2474-2481.

Perkins D.J. (1953) A study of the effect of amino acid structure on the stabilities of the complexes formed with metals of group II of the periodic classification. *Biochemical Journal* **55**, 649-652.

Platt J.R. (1964) *Free-electron theory of conjugated molecules*. University of Chicago.

Rostad C.E. and Leenheer J.A. (2004) Factors that affect molecular weight distribution of Suwannee river fulvic acid as determined by electrospray ionization/mass spectrometry. *Analytica Chimica Acta* **523**, 269–278.

Schleede D. (1955) Separation of simple phenols by paper chromatography. *Brennstoff-Chemie* **36**, 78-79.

Schnitzer M., Sherarer D.A. and Wright J.R. (1959) A study in the infrared of high-molecular weight organic matter extracted with various reagents from a Podzolic B horizon. *Soil Science* **87**, 252-257.

Silverstein R.M., Bassler G.C., and Morrill T.C. (1991) *Spectrometric Identification of Organic Compounds* (5^{th} edition). Wiley.

Stevenson F.J. and Goh K.M. (1971) Infrared spectra of humic acids and related substances. *Geochimica et Cosmochimica Acta* **35**, 471-483.

Talukdar H., Rudra S., and Kundu K.K. (1988) Deprotonation and transfer energetics of glycine in aqueous mixtures of urea and glycerol from emf measurements at different temperatures. *Canadian Journal of Chemistry* **67**, 315-320.

Varhaníčková D., Lee S.C., Shiu W.-Y., and Mackay D. (1995) Aqueous solubilities of chlorocatechols, chlorovanillins, chlorosyringols, and chlorosyringaldehydes at 25°C. *Journal of Chemical and Engineering Data* **40**, 620-622.

Wilhoit R.C. (1969) In (ed. H.D. Brown) *Biochemical Microcalorimetry*. Academic Press.

Wojtkowiak B. and Chabanel M. (1977) *Spectrochimie Moléculaire*. Technique & Documentation.

CHAPTER 2. Characterization of the synthesized fulvic acids

In this chapter, we present a detailed characterization of the four different types of synthesized fulvic acids (SFA) prepared in the present study. Different analytical techniques have been used, including elemental analysis, scanning electron microscopy (SEM), X-ray diffraction (XRD), attenuated total reflectance Fourier transform infrared (ATR-FTIR) spectroscopy, ultraviolet-visible (UV-Vis) spectroscopy, and electrospray ionization coupled to mass spectrometry (ESI-MS). In addition, the weak ionization observed for the SFA in ESI-MS prompted the use of liquid chromatography coupled to atmospheric pressure chemical ionization and tandem mass spectrometry (LC-APCI-MS-MS). The results are discussed in terms of the possible reactions which form SFA, as well as the resulting molecular structures.

1. FULVIC ACID SYNTHESIZED BY POLYMERIZATION OF CATECHOL

1.1. Elemental analysis

Both raw and extracted synthetic fulvic acids (SFA) prepared under atmospheric oxidation and ambient (~25°C) conditions by polymerization of catechol (SFA_1) in the ternary system $C_6H_4(OH)_2$ – NaOH – H_2O in basic solutions (pH = 10) have been analyzed for their elemental compositions. The elemental composition of catechol has also been determined. The results are shown in Table 1. The composition determined for catechol is close to its theoretical value, i.e. C 65.45%, H 5.49%, O 29.06%. The weight percentages determined for carbon, hydrogen and oxygen do not sum up to 100 percent for the raw and extracted SFA_1. We have made the assumption that the difference could be attributed to sodium ions (from NaOH) complexed by phenolate or carboxylate functional groups in the SFA_1. A significant increase of the oxygen content and atomic O/C ratio between catechol and the raw SFA_1 can be deduced from Table 2.1. This increase, which is compensated for by decrease in the carbon and hydrogen content as well as the atomic H/C ratios of the SFA_1, which is most probably due to oxidation of catechol to form quinone, muconic acids and polycatechols among other compounds. Evidence for the rapid formation of such compounds is provided below based on LC-APCI-MS-MS measurements. The elemental composition reported in Table 2.1 for the SFA_1 mixture obtained at the end of the extraction procedure does not show any significant variation with respect to the raw SFA_1, except for a strong decrease of the Na content. The explanation for this decrease is that a major fraction of the Na ions complexed by the phenolate and carboxylate function groups in the raw SFA_1

were removed during the various steps of the extraction procedure, as it can be verified from the Na contents listed on the last four lines of Table 2.1.

Table 2.1. Elemental compositions of the raw and extracted fulvic acid synthesized by polymerization of catechol. No correction for the presence of water has been made.

Sample	% C	% H	% O	(% Na)[a]	H/C	O/C
Catechol	66.28	5.56	28.78	(0.00)	1.000	0.326
SFA_1 ; 0 day (raw)	41.52	2.47	36.18	(19.83)	0.709	0.654
SFA_1 ; 63 days (raw)	33.39	2.29	41.85	(22.47)	0.817	0.941
SFA_1 ; after extraction [b]	39.59	2.32	44.77	(13.32)	0.698	0.849
SFA_1 ; extract 1 [c]	27.09	1.94	52.03	(18.94)	0.853	1.442
SFA_1 ; extract 2 [d]	53.02	7.44	27.49	(12.05)	1.672	0.389
SFA_1 ; extract 3 [e]	55.34	3.69	32.49	(8.48)	0.795	0.441
SFA_1 ; extract 4 [f]	26.56	1.71	25.24	(46.49)	0.767	0.713

[a] Calculated by difference (see text) [b] The SFA on this line corresponds to the purified fulvic acid obtained at the end of the extraction procedure (see chapter 1) [c] First extraction with methanol [d] Second extraction with methanol [e] Liquid-liquid extraction with ethyl acetate (organic phase) [f] Liquid-liquid extraction with ethyl acetate (aqueous phase)

1.2. Scanning electron microscopy

Scanning electron microscope (SEM) observations of samples of SFA_1 obtained by polymerization of catechol in the ternary system $C_6H_4(OH)_2$ – NaOH – H_2O in basic solutions (pH = 10) are shown in Figure 2.1. The observations, which have been made on the raw SFA_1, indicate that the obtained products do not show any particular shape reminiscent of crystals, which suggests that these products are amorphous. This suggestion is confirmed below by the X-ray diffraction results. It should perhaps be noted here that Dubey et al. (1998) also observed irregular shapes for enzymatically synthesized polycatechol, although the textures were different than those shown here. The larger grains in Figure 2.1 most probably correspond to agglomerations of extremely fine (~ 0.1 μm) particles.

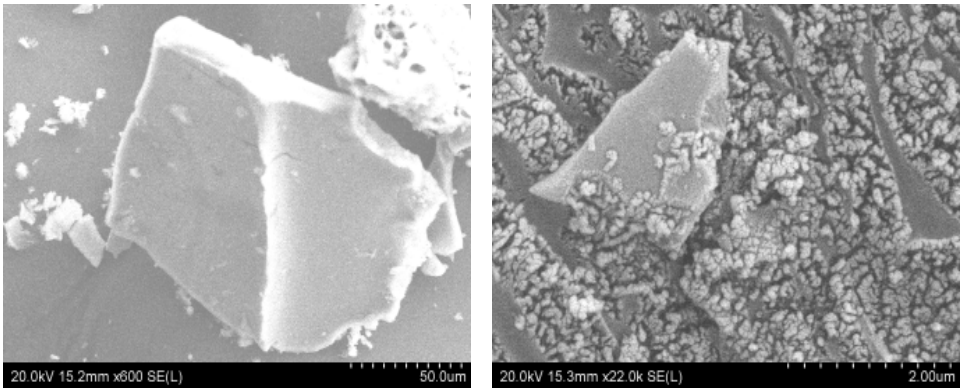

Figure 2.1. SEM photographs of SFA_1. Magnification (left) x 600 (right) x 22,000.

1.3. X-ray diffraction

X-ray diffraction spectra obtained for catechol crystals, raw SFA_1, and purified (extracted) SFA_1 are shown in Figure 2.2 (a), (b) and (c), respectively. The diffractograms have been offset for the sake of clarity. The numbers on the right of each diffractogram refer to scaling factors. The dots over the diffraction peak for pure catechol indicate that this peak has been cut. It can be deduced from Figure 2.2 that the spectra of both the raw and purified SFA_1 are drastically different from that of catechol. Several distinct diffraction peaks are observed for the raw SFA_1 in Figure 2.2 (b). These peaks can be tentatively attributed to crystalline sodium catecholate ($C_6H_5O_2Na$), disodium catecholate ($C_6H_4O_2Na_2$), or to other undetermined crystalline by-products. The virtual absence of peaks in the X-ray diffraction spectrum shown in Figure 2.2 (c) for the SFA_1 after extraction of a possible fraction of unreacted catechol, sodium catecholate and/or other undetermined by-products proves that the solid SFA_1 mixture is composed of amorphous compounds, which is consistent with the SEM observations.

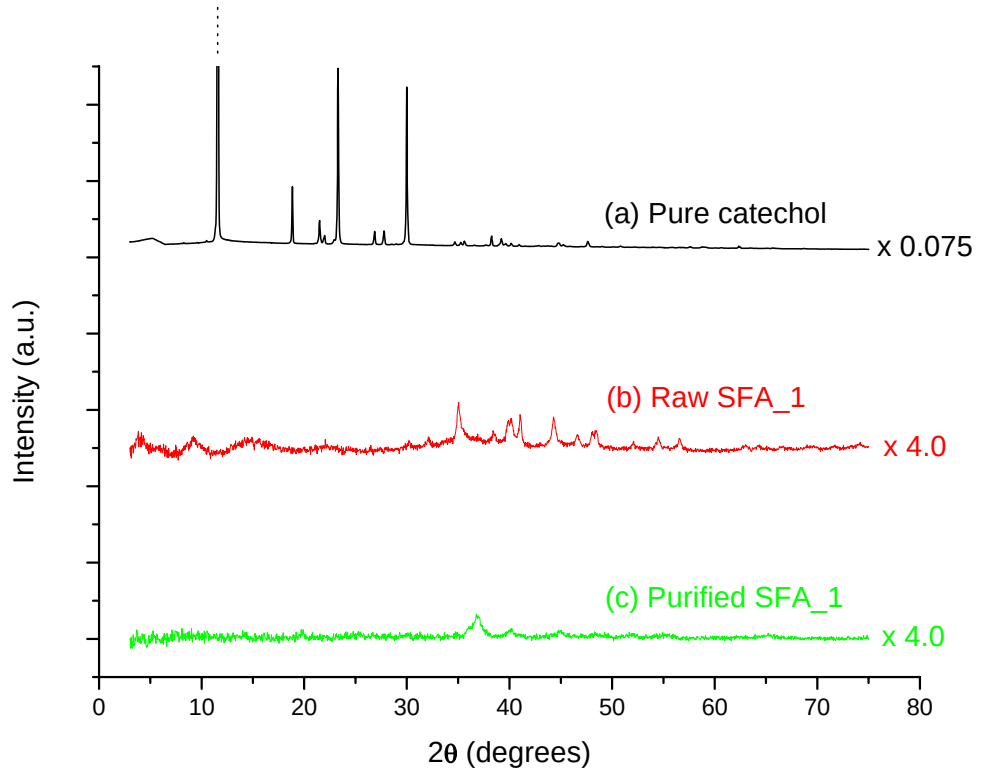

Figure 2.2. X-ray diffraction spectra of crystalline catechol (a), of a raw mixture of SFA_1 and Na-catecholate salts (b), and of amorphous SFA_1 after extraction (c) – see text.

1.4. ATR-FTIR spectroscopy

1.4.1. Catechol

The ATR-FTIR spectrum of catechol recorded at 25°C and 0.1 MPa is shown in Figure 2.3. This spectrum displays the characteristic vibration bands of the two functional groups present in catechol, i.e. aromatic C–H group and alcohol-bearing C–OH phenolic groups. The vibration bands attributable to these two groups are discussed separately below. These attributions are based on the vibrational frequencies listed in Wojtkowiak and Chabanel (1977) and Silverstein et al. (1991).

- ✓ Aromatic C-H group: the infrared absorption characteristics of this group can be classified in three different categories corresponding to two different types of chemical bonds and a combination of the vibrations due to these bonds.
  - *Vibration of aromatic C-H bonds*
    - A stretching mode of aromatic C-H groups (νC-H) occurs at 3052 cm^{-1};
    - Two deformation modes of aromatic C-H groups (δC-H) are observed:

      a) In-plane δC–H of C–H bonds on an aromatic ring at 1039 and 1093 cm^{-1}.

      b) Out-of-plane δC–H of C–H bonds at 848 and 740 cm^{-1} (Dubey et al., 1998; Aktaş et al., 2003). The latter band characterizes δC-H bending of C-H groups in an aromatic substituted at positions 1 and 2. It is perhaps important to note here that the low frequency range between 675 and 900 cm^{-1} represents the most prominent and the most informative portion in the infrared spectra of aromatic compounds.
  - *Vibration of the carbon-carbon bonds in the aromatic ring*

    Three stretching modes at 1469, 1513 and 1619 cm^{-1} are assigned to the C=C bonds (νC=C) in the aromatic ring.
  - *Combination bands*

    Three minor bands at 1760, 1880 and 1923 cm^{-1} represent overtone or combination bands.
- ✓ Phenolic C–OH group: the infrared absorption characteristics of this group correspond to three types of chemical bonding, which correspond to the
  - *O-H bonds of the hydroxyl groups*

- Two distinct stretching modes (νO–H) due to hydroxyl groups bonded to an aromatic ring can be observed at 3326 and 3445 cm^{-1}. The latter band characterizes the stretching νOH of free hydroxyl groups of catechol. The former arises from the vibration of hydrogen bonds between the hydrogen (H) atom at position 1 and the oxygen (O) atom at position 2, or inversely between the H atom at position 2 and the O atom at position 1.
- In-plane δO–H bend deformation of the same hydroxyl groups is measured at 1360 cm^{-1}.

▪ *C-O bonds on the aromatic ring*

Two νC-O stretching bands can be observed at 1279 and 1238 cm^{-1}.

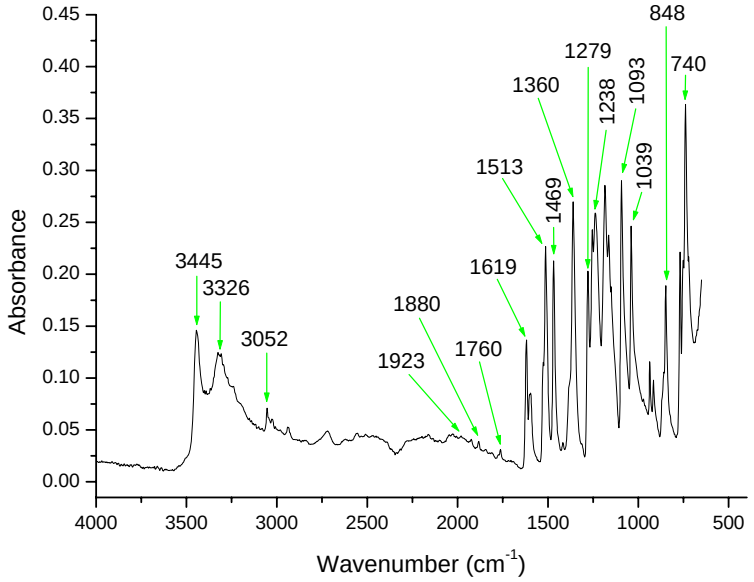

Figure 2.3. ATR-FTIR spectrum of pure solid catechol ($C_6H_4(OH)_2$): T = 25°C, P = 0.1 MPa.

1.4.2. Synthetic fulvic acid SFA_1

The ATR-FTIR spectra of the raw and purified synthetic fulvic acids SFA_1 are presented in Figures 2.4 and 2.5. For the purpose of comparison, the corresponding spectrum for catechol is also shown in Figure 2.4, and the spectrum for the raw SFA_1 is recalled in Figure 2.5. The spectrum of raw SFA_1 contains numerous minor bands which do not seem to appear in the spectrum of purified SFA_1 and this is attributed to the extraction of some compounds during the extraction process. Both spectra are characterized by fourteen distinct absorption bands or broadbands, which are discussed in detail below for the purified SFA_1 only. These characteristic absorption bands and broadbands include:

- a broadband in the region 3700 – 2350 cm^{-1};

- a broadband in the region 2350 – 1800 cm^{-1};
- a broadband in the region 1718 – 1744 cm^{-1};

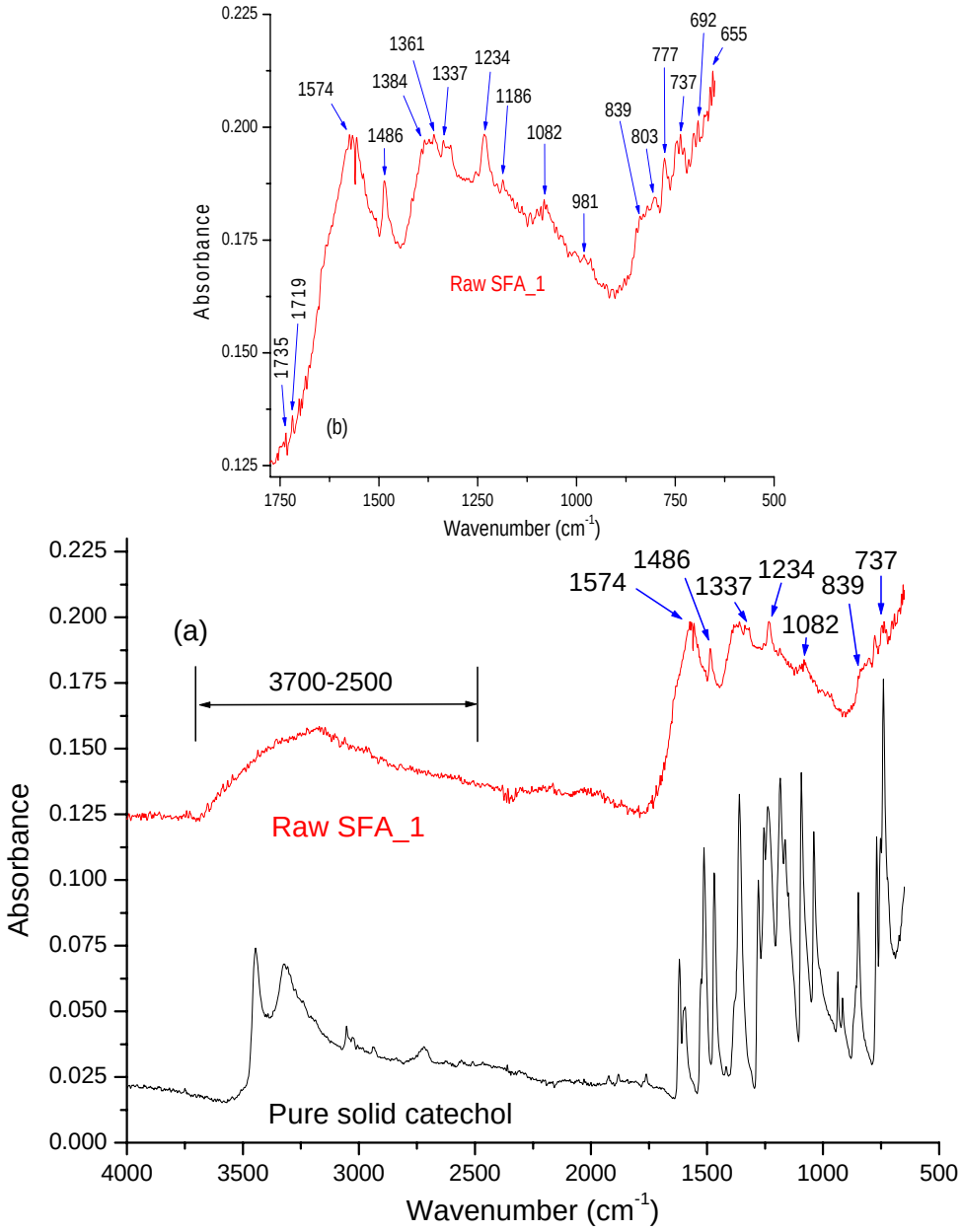

Figure 2.4. ATR-FTIR spectrum of raw SFA_1: T = 25°C, P = 0.1 MPa. (a) complete spectrum; (b) enlargement of the lower wavenumber portion of the spectrum. The corresponding spectrum of pure catechol from which SFA_1 was prepared is shown for comparison.

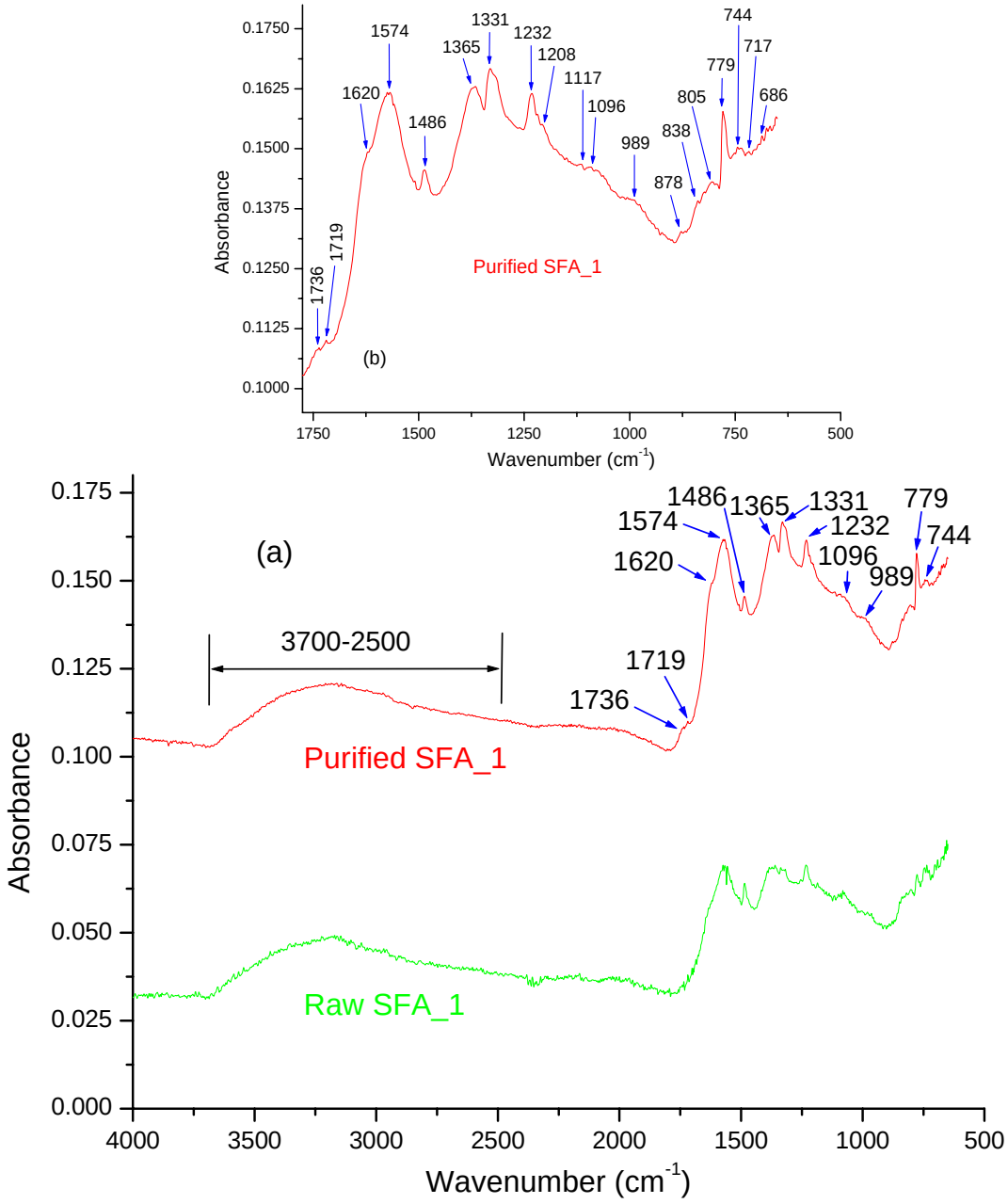

Figure 2.5. ATR-FTIR spectrum of purified SFA_1: T = 25°C, P = 0.1 MPa. (a) complete spectrum; (b) enlargement of the lower wavenumber portion of the spectrum. The corresponding spectrum of raw SFA_1 is recalled for the purpose of comparison.

- one intense band around 1620 cm^{-1};
- one intense and distinct band at 1574 cm^{-1};
- one distinct band at 1486 cm^{-1};
- one distinct band at 1365 cm^{-1};
- one intense broadband in the region 1315 – 1340 cm^{-1};
- one distinct band at 1232 cm^{-1};
- one broadband in the region 1050 – 1120 cm^{-1} with a center near 1096 cm^{-1};
- one broadband in the region 950 – 1017 cm^{-1};
- one broadband in the region 805 – 895 cm^{-1};
- one distinct band at 779 cm^{-1};
- one weak band around 744 cm^{-1}.

The presence of these various absorption bands can be interpreted as follows.

- The broadband in the region 3700 – 2350 cm^{-1} could characterize two vibration modes, including
  - ✓ νO–H stretching mode of
    - o phenol, which is characterized by two types of stretching:
      - ❖ stretching of free hydroxyl groups of phenol (3500 – 3700 cm^{-1})
      - ❖ stretching of both inter- and intramolecular, hydrogen-bonded OH groups (3300 – 3500 cm^{-1})
    - o carboxylic acid: stretching of associated O–H of carboxylate functional group (2500 – 3000 cm^{-1})
  - ✓ νC–H stretching mode of aromatic C-H (3030 – 3075 cm^{-1}).
- The broadband in the region 2350-1800 cm^{-1} corresponds to the strong absorption of diamond used in the ATR-FTIR instrument.
- The broadband in the region 1719 – 1736 cm^{-1} could be assigned to the νC=O stretching mode of four different functional groups: ketones, aldehydes, aliphatic or aromatic esters, or dimers of carboxylic acids (Parker, 1971; Wojtkowiak and Chabanel, 1977).
- The three bands at 1486, 1574 and 1620 cm^{-1} are assigned to the νC=C of the aromatic ring.

- The distinct band at 1365 cm^{-1} corresponds to the in-plane δO–H bend of a hydroxyl group bonded to an aromatic group.
- The intense and distinct band at 1331 cm^{-1} is assigned to the ν_sC–O of an ester functional group linking two aromatic rings together.
- The distinct band at 1232 cm^{-1} and the broadband in the region 1050 – 1120 cm^{-1} with a center near 1096 cm^{-1} are respectively assigned to the asymmetric ν_aC–O–C stretch and the symmetric ν_sC–O–C stretch of an ether functional group linking two aromatic rings together.
- The weak broadband in the 950 – 1017 cm^{-1} region represents the in-plane δC–H bending mode of aromatics.
- Absorption bands in the low frequency region 710 – 895 cm^{-1} result from the out-of-plane δC–H bending of the aromatic ring C–H bonds. Three bands and broadbands can be distinguished:
    - ✓ The first band around 744 cm^{-1} is weak and characterizes two major bending vibrations:
        - o the out-of-plane δC-H bending vibration of an aromatic compound with two substituting groups at positions 1 and 2;
        - o the out-of-plane δC=C bending vibration of an aromatic compound with
            - ❖ three substituting groups at positions (1, 2, 3) or (1, 2, 4);
            - ❖ four substituting groups at positions (1, 2, 3, 4), (1, 2, 3, 5) and (1, 2, 4, 5)
            - ❖ five substituting groups at positions (1, 2, 3, 4, 5).
    - ✓ The second one is the intense and distinct band at 779 cm^{-1}. It is assigned to the out-of-plane δC-H bending vibration of C-H bonds in an aromatic compound containing three substituting groups at positions (1, 2, 3). The strong absorption of this band indicates that SFA_1 mainly consists of aromatic rings which are trisubstituted at positions (1, 2, 3).
    - ✓ The third one is the broadband in the region 805 – 878 cm^{-1}. The interpretation of this broadband is based on the current thinking that the out-of-plane δC-H bending vibrations of an aromatic compound containing
        - o three substituting groups at positions (1, 2, 4);
        - o four substituting groups at positions (1, 2, 3, 4), (1, 2, 3, 5) and (1, 2, 4, 5);
        - o five substituting groups at positions (1, 2, 3, 4, 5)

occur in the wavenumber range 800 – 880 cm^{-1}. Consequently, the broadband at 805 – 878 cm^{-1} observed in the present study suggests that SFA_1 could contain tri-, tetra-, or pentasubstituted aromatic rings.

The ATR-FTIR spectroscopy results described above provide useful information about the molecular structure of the fulvic acid SFA_1 synthesized from the polymerization of catechol. The results suggest that SFA_1 consists of several aromatic rings linked to each other through $C_{Ar} – C_{Ar}$ (aryl-aryl) bonds and $C_{Ar} – O – C_{Ar}$ (ether) bonds. Each aromatic ring may bear up to five substitutional groups.

1.5. UV-Visible absorption spectrophotometry

UV-Visible absorption spectra of purified SFA_1 at two different aqueous concentrations (0.022 and 0.044 $g \cdot L^{-1}$) are presented in Figure 2.6. The purified SFA_1 is characterized by four successive broad bands which are located at approximately 228, 278, 362 and 484 nm. The first broad band can be assigned to aromatic E_2 bands and *K* bands. The second broad band at 278 nm corresponds to the aromatic *B* bands and the bands associated with the $n \rightarrow \pi^*$ forbidden transition. This band at 278 nm could be for an hydrophilic compound such as muconic acid.

The presence of broad bands proves that SFA_1 is a high molecular weight compound with numerous atoms. The multiplicity of their vibrational sublevels and the closeness of their spacing cause the discrete bands to coalesce and to form broad bands.

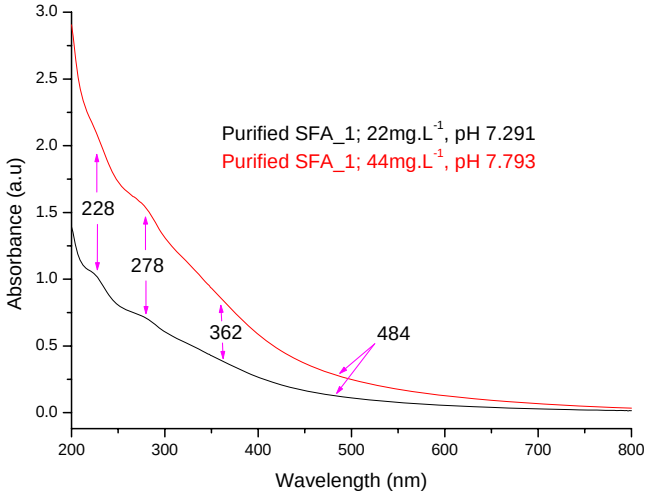

Figure 2.6. UV-Visible spectra of purified SFA_1 at two concentrations and pH ~ 7.5.

From the LC-APCI-MS-MS measurements described below, it is found that one of the predominant SFA_1 single fulvate species has a molecular weight of 434 g·mol^{-1}. Combining this result with the measured absorbance and the cuvette dimension (1 cm) allows to calculate the molar absorptivity coefficient (ε_{max}) for the four above-listed broad bands as a function of the aqueous concentration of SFA_1. The results are presented in Table 2.2.

Table 2.2. Calculated values of the molar absorptivity coefficient ε_{max} for four broad bands as a function of concentration of SFA_1.

Concentration	λ_{max} (nm)	Absorbance	ε_{max}
5.069 x 10^{-5} *M*	228	1.02	20121
	278	0.71	14006
	362	0.37	7300
	484	0.12	2367
1.014 x 10^{-4} *M*	228	2.10	20713
	282	1.51	14894
	362	0.77	7595
	484	0.27	2663

1.6. Electrospray ionization – mass spectrometry (ESI-MS)

A sample of the raw SFA_1 was analyzed by ESI both in positive-ion (PI) and negative-ion (NI) modes. The purified SFA_1 was analyzed by APCI-MS (see below). It has been noted that the spectrum obtained for SFA_1 in NI mode showed much less intense peaks which appeared to be noisy compared to those obtained in PI mode. Consequently, only the spectrum obtained in PI mode is shown in Figure 2.7.

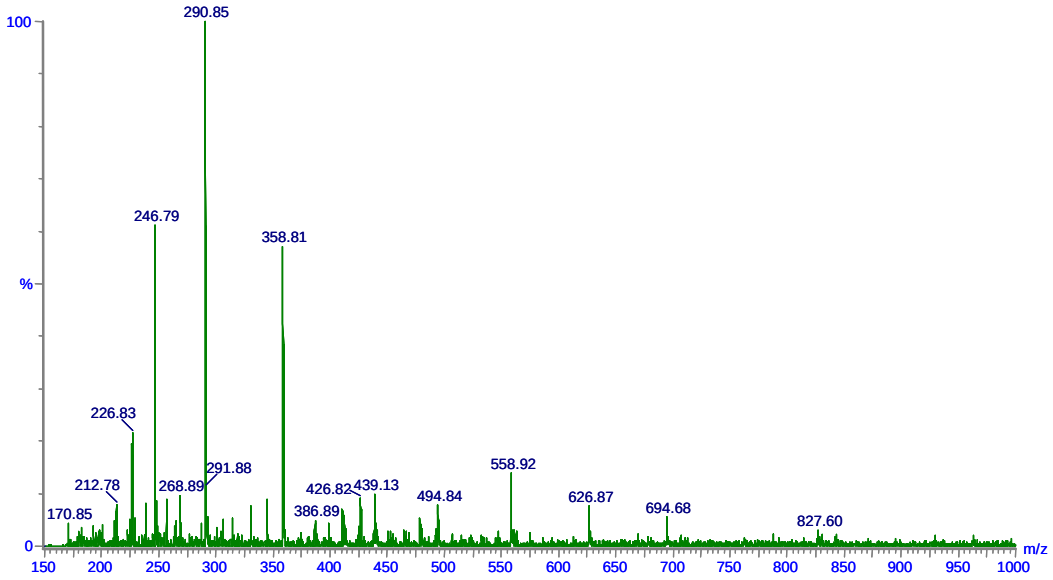

Figure 2.7. ESI-MS spectrum of raw SFA_1 analyzed under positive mode.

Several peaks can be observed over the 150 – 1000 m/z range. These peaks are identified in Table 2.3 with their m/z values, except for the peaks with m/z equal to 291.88 and 827.60 for which no interpretation could be given. Also listed in Table 2.3 are possible chemical formulas coinciding with (or rather approaching) these m/z values. The chemical formulas were established by considering the possibility that Na^+ or H^+ ions used to create positively charged fulvic acid ions or H_2O molecules could be complexed to these fulvic acid ions. The Na^+ or H^+ ions and H_2O molecules are indicated in grey in Table 2.3, as are the molecular weights corresponding to the sum of the actual single fulvic acid molecules and their associated Na^+ or H^+ ions, or H_2O molecules. Tentative molecular structures corresponding to these chemical formulas and m/z ratios are shown in Figure 2.8. Basing on the IR data, the proposed molecular structures have only –OH functional groups and this doesn't suggest that there were no SFA with –COOH. In fact the proposed SFA structures are just among the few, as the list is inexhaustible. The Na atoms appearing in some of the structures result from the NaOH which is used to buffer the pH during the synthesis. Note that in some cases, different structures with different formulas may correspond to the same m/z ratio. The molecular structures depicted in Figure 2.8 represent monomers (a-d), dimers (e-i), trimers (j-l and o), a tetramer (m), pentamers (n and p), and a hexamer (q) of substituted aromatic rings. These rings are linked to each other mainly through aromatic ether (—O—) bonds, with minor C_{aro} — C_{aro} linkages. Three m/z values corresponding to structures (b), (e) and (h) are quinones which are highly substituted. The three proposed structures are characterized by upto four substitutions. Possible reaction mechanisms leading to the formation of the structures shown

in Figure 2.8 will be presented in the discussion following the results of the LC-APCI-MS-MS analyses.

Table 2.3. Summary of m/z ratios obtained in the ESI-MS analysis (PI mode) of the raw SFA_1, together with their corresponding molecular weights and possible chemical formulas for individual compounds in the SFA_1 mixture.

m/z	Chemical Formula	Molecular weight		Structure in Figure 2.8
170.85	$[C_6H_5O_3Na$ (+ Na)$]^+$	148.09	(171.08)	(a)
212.78	$[C_6H_4O_4$ (+ 4 H_2O + H)$]^+$	140.01	(213.06)	(b)
226.83	$[C_6H_3O_4Na_3$ (+ H_2O + H)$]^+$	207.97	(226.99)	(c)
246.79	$[C_6H_3O_3Na_3$ (+ 3 H_2O + H)$]^+$	192.06	(247.11)	(d)
	$[C_{12}H_6O_6$ (+ H)$]^+$	246.22	(247.02)	(e)
268.89	$[C_{12}H_6O_6$ (+ Na)$]^+$	246.22	(269.21)	(e)
	$[C_{12}H_{10}O_6$ (+ H_2O + H)$]^+$	250.20	(269.23)	(f)
290.85	$[C_{12}H_9O_6Na$ (+ H_2O + H)$]^+$	272.19	(291.21)	(g)
	$[C_{12}H_7O_5Na$ (+ 2 H_2O + H)$]^+$	268.20	(291.05)	(h)
358.81	$[C_{12}H_6O_5Na_4$ (+ 2 H_2O + H)$]^+$	322.13	(359.17)	(i)
386.89	$[C_{18}H_{12}O_7Na_2$ (+ H)$]^+$	386.26	(387.27)	(j)
426.82	$[C_{18}H_{11}O_7Na_3$ (+ H_2O + H)$]^+$	408.25	(427.27)	(k)
439.13	$[C_{18}H_{13}O_5Na$ (+ 5 H_2O + H)$]^+$	331.27	(422.36)	(l)
494.84	$[C_{24}H_{16}O_9Na_2$ (+ H)$]^+$	494.36	(495.37)	(m)
558.92	$[C_{30}H_{22}O_{11}$ (+ H)$]^+$	558.49	(559.50)	(n)
	$[C_{18}H_8O_{10}Na_6$ (+ 2 H_2O + H)$]^+$	522.19	(559.23)	(o)
626.87	$[C_{30}H_{19}O_{10}Na_3$ (+ H_2O + H)$]^+$	608.44	(627.46)	(p)
694.68	$[C_{36}H_{24}O_{12}Na_2$ (+H)$]^+$	694.55	(695.56)	(q)

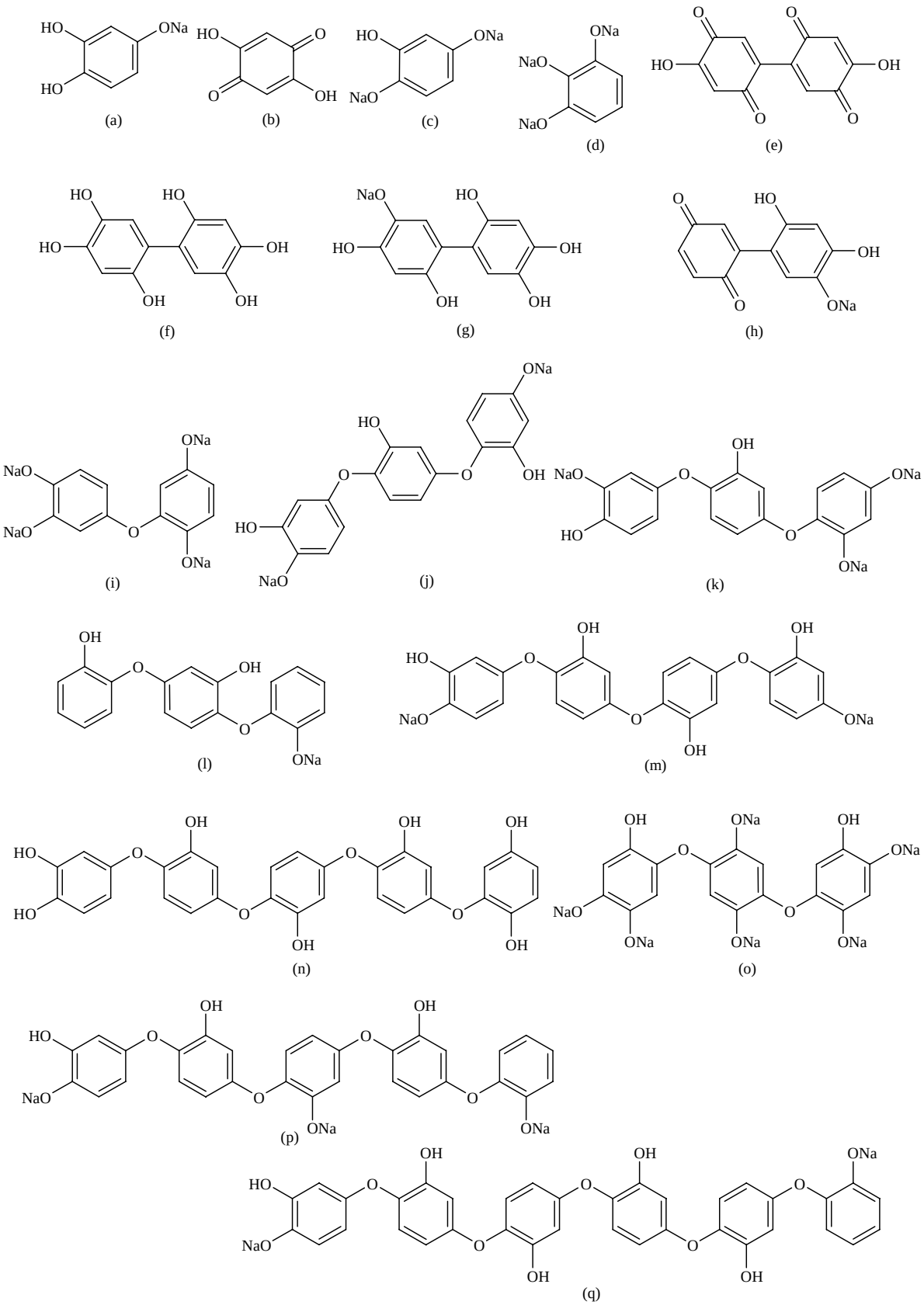

Figure 2.8. Possible molecular structures for individual fulvic acids in the raw SFA_1 mixture deduced from the ESI-MS analysis.

1.7. Atmospheric pressure chemical ionisation mass spectrometry (APCI-MS)

It was observed that the synthetic fulvic acid did not ionize significantly during the ESI-MS analysis described above. This observation prompted us to analyze the raw and purified SFA_1 mixtures as well as the ethyl acetate extract obtained by liquid-liquid extraction of the raw SFA_1 by atmospheric pressure chemical ionization mass spectrometry (APCI-MS). We have found that APCI was best suited to the analysis of synthetic fulvic acids. The protocols and results obtained for each of these samples are discussed separately below.

1.7.1. Analysis of raw SFA_1 by LC-APCI-MS-MS

The analysis of the raw SFA_1 mixture was performed by tandem mass spectrometry (MS/MS) after first separating the components of the mixture by liquid chromatography (LC) using a U3000 Dionex liquid chromatograph interfaced with a Bruker micro Q-ToF mass spectrometer. A saturated solution of raw SFA_1 was prepared by dissolving lyophilized solid SFA_1 in milli-Q water containing 0.2 % by volume of formic acid to favor ionization of the fulvic acid components during the analysis. The resulting solution was filtered through a 0.45 μm millex®-HA filter unit. The pH of the solution was lowered to pH ~ 5-8 using formic acid prior to injecting the sample on the LC column. The different parameters used in the LC-ACPI-MS-MS analysis of raw SFA_1 are summarized in Table 2.4.

Table 2.4. Parameters used in the LC-APCI-MS-MS analysis.

Liquid phase chromatography	
Injection	
Injection solvent	Water at neutral pH
Injected volume	20 μL
Mode of injection	Partial loops
Auto sampler temperature	4°C
Column	Uptisphere Strategy™ RP-C18 7.5 cm x 4.6 mm ID, 5 μm particle size
Mobile phase	
Mobile phase A [a]	Water + 0.2 % vol. formic acid
Mobile phase B	Acetonitrile + 0.2 % vol. formic acid
Flow rate	1 mL/min
Elution gradient (% vol. of phase B)	0 min: 0 %; 1 min 0 %; 31 min 100%; 36 min 100%; 38 min: 0%; 43 min: 0%
High resolution mass spectrometry	
Mass range	300 – 1000 Da
Type of source	Chemical ionisation (APCI)
Temperature at the source	450°C
Temperature of drying gas	200°C
Flow rate of drying gas	8 L/min
Nebulization pressure	1.6 bar
Corona discharge	Negative mode: 1000 nA Positive mode: 4000 nA
Capillary voltage	Negative mode: 2500 V Positive mode: - 4000 V
Endplast	- 500 V

[a] Column cleaning

The tandem mass spectrometry analysis was performed in an automatic mode. Peaks showing intensity higher than 5000 (in arbitrary units) were selected for the fragmentation in collision cells with the following parameters:

m/z	isolation width	collision energy
300	8 Da	10 V
500	10 Da	15 V
1000	10 Da	20 V

Under positive mode, blank chromatograms display wide peaks corresponding to acetonitrile for retention times greater than 30 minutes. Consequently, total ion chromatograms (TIC) are presented below for retention times ranging between 0 and 30 minutes. It can be deduced from the base peak chromatograms shown in Figure 2.9 that all the compounds present in the raw SFA_1 mixture were eluted before 15 minutes in both positive and negative modes. Each peak probably corresponds to a series of compounds with similar elution times. The retention times corresponding to selected chromatographic peaks identified by numbers in Figure 2.9 are listed in Table 2.5 along with the results of the mass spectrometry analysis. The selection of peaks was rendered necessary for clarity reasons in the discussion which is presented below. Also listed in Table 2.5 are possible chemical formulas and molecular weights corresponding to the m/z values. The molecular structures corresponding to the proposed chemical formulas are shown in Figure 2.10. The difference between the molecular weights and m/z values is usually within 0.1 Da, and in some cases ~ 2 mDa.

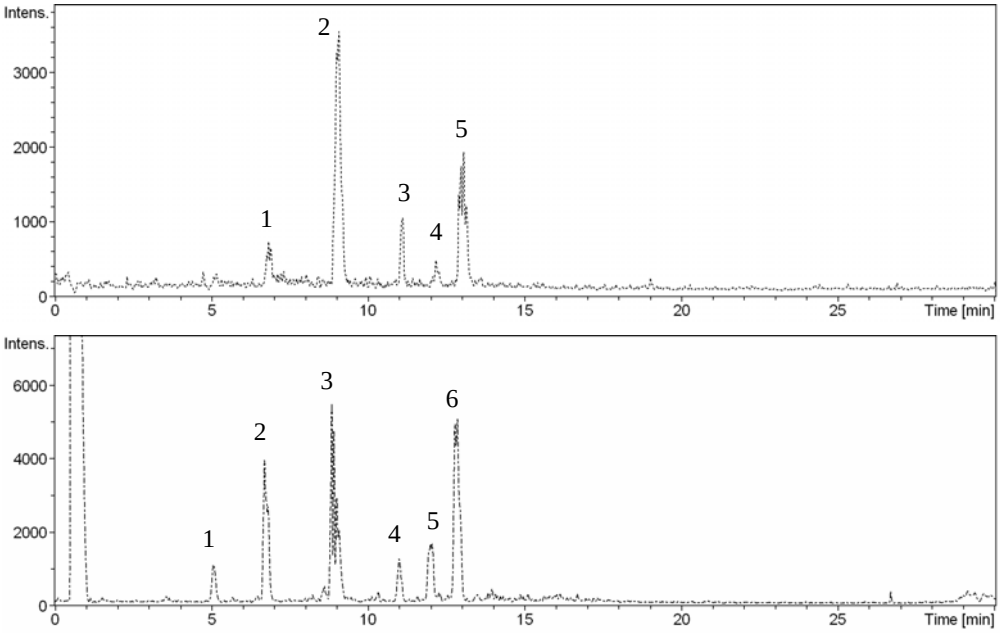

Figure 2.9. Base peak chromatograms (BPC) obtained in the LC-APCI-MS-MS of the raw SFA_1 mixture in positive mode (top) and negative mode (bottom). Peaks have been numbered to facilitate discussion.

Table 2.5. Summary of the LC retention times (RT) corresponding to the peaks identified by numbers in Figure 2.9 and of the m/z ratios obtained in the LC-APCI-MS-MS analysis (positive and negative modes) of the raw SFA_1 mixture, as well as of possible chemical formulas and corresponding molecular weights for individual fulvic acids in the raw SFA_1 mixture.

Peak number (Fig. 2.9)	RT (min)	m/z	Chemical formula	Molecular weight	Structure (Fig. 2.10)
Positive mode					
2	9	493.0101	$[C_{18}H_{11}O_{10}Na_3 + 2\ H_2O + H]^+$	493.033	(o)
		515.01373	$[C_{18}H_{10}O_{10}Na_4 + 2\ H_2O + H]^+$	515.015	(q)
		536.9991	$[C_{18}H_9O_{10}Na_5 + 2\ H_2O + H]^+$	536.997	(s)
	9.4	453.3439	$[C_{18}H_{12}O_{10}Na_2 + H_2O + H]^+$	453.041	(l)
		453.3439	$[C_{24}H_{18}O_8 + H_2O + H]^+$	453.119	(m)
4	13	389.0254	$[C_{18}H_{13}O_6Na + H_2O + Na]^+$	389.061	(g)
		389.0254	$[C_{12}H_5O_5Na_3 + HCOONa + Na]^+$	388.960	(h)
		411.0045	$[C_{18}H_{11}O_6Na_3 + H_2O + H]^+$	411.043	(j)
Negative mode					
3	6.7	459.0102	$[C_{18}H_{12}O_6Na_2 + 5\ H_2O - H]^-$	459.088	(n)
		559.0332	$[C_{30}H_{22}O_{10} + H_2O - H]^-$	559.124	(t)
4	8.9	403.0606	$[C_{18}H_{12}O_7Na_2 + H_2O - H]^-$	403.041	(k)
		469.0386	$[C_{18}H_{12}O_{10}Na_2 + 2\ H_2O - H]^-$	469.036	(l)
		513.0102	$[C_{18}H_{10}O_{10}Na_4 + 2\ H_2O - H]^-$	513.000	(q)
		528.9833	$[C_{24}H_{16}O_9Na_2 + 2\ H_2O - H]^-$	529.072	(r)
	9.4	451.3426	$[C_{18}H_{12}O_{10}Na_2 + H_2O - H]^-$	451.025	(l)
		451.3426	$[C_{24}H_{18}O_8 + H_2O - H]^-$	451.103	(m)
6	12	399.0754	$[C_{18}H_{13}O_7Na + 2\ H_2O - H]^-$	399.069	(i)
		579.0189	$[C_{18}H_7O_{10}Na_7 + 2\ H_2O - H]^-$	578.946	(u)
		579.0189	$[C_{30}H_{21}O_{11}Na - H]^-$	579.090	(v)
7	12.8	321.0677	$[C_{12}H_{10}O_6 + 4\ H_2O - H]^-$	321.082	(a)
		321.0677	$[C_{18}H_{10}O_6 - H]^-$	321.040	(b)
		343.07347	$[C_{12}H_9O_6Na + 4\ H_2O - H]^-$	343.064	(d)
		343.07347	$[C_{18}H_{14}O_6 + H_2O - H]^-$	343.082	(e)
		365.05174	$[C_{12}H_8O_6Na_2 + 4\ H_2O - H]^-$	365.046	(f)
		365.05174	$[C_{18}H_{13}O_6Na + H_2O - H]^-$	365.064	(g)
		433.0313	$[C_{18}H_{12}O_{10}Na_2 - H]^-$	433.015	(l)
		501.0116	$[C_{24}H_{14}O_8 + 4\ H_2O - H]^-$	501.103	(p)
	13	330.9767	$[C_{12}H_7O_7Na_3 - H]^-$	330.981	(c)
		411.0045	$[C_{18}H_{14}O_6 + H_2O + HCOONa - H]^-$	411.069	(e)

For example, let us consider the compound eluted at 9.4 minutes (Figure 2.9, peak 2 of top BPC) which has been analyzed in positive mode. The corresponding mass spectrum is shown in Figure 2.11 A. Two molecular structures have been proposed for this compound. These structures correspond to the highly substituted trimer (l) and the tetramer (m) shown in Figure 2.10. They correspond to a molecular weight of 434 Da. They have been considered as probable structures based on the tandem (MS/MS) mass spectrum shown in Figure 2.11 C. It can be deduced from Table 2.5 that each of the postulated molecules is associated to a water molecule, which for the analysis in positive mode yields a m/z value of 453. Further evidence for the proposed structures comes from similar retention times (9.4 minutes) for the analyses

in positive and negative modes and similar m/z values at 453 (i.e. 434 + 18 + 1) in positive mode and 451 (i.e. 434 + 18 -1) in negative mode (compare Figure 2.11 A and Figure 2.11 B).

For the elution time of 12.8 minutes corresponding to peak 7 in the bottom BPC of Figure 2.9, several structures are possible. The m/z values of 321, 343, 365, 433 and 501 listed in Table 2.5 and corresponding to the peaks identified in the APCI-MS spectrum of Figure 2.12 have been interpreted as representing compounds with molecular weights of either (250 or 322), (272 or 326), (294 or 348), (434) and 430 Da and corresponding molecular structures (a or b), (d or e), (f or g), (l) and (p) in Figure 2.10.

It can be deduced from the top and bottom BPCs of Figure 2.9 that other fractions than those discussed above have been eluted at 6.7, 9.0, 9.4, 11.0, 12.9 and 13.0 minutes and at 5.1, 6.7, 8.9, 9.1, 9.4, 11.0 and 12.0 minutes, respectively. From the LC-APCI-MS and LC-APCI-MS-MS analyses discussed above and the molecular structures proposed in Figure 2.10, it appears that different oligomers have been synthesized by polymerization of catechol: dimers (a-d and f), trimers (e, g-l, n-q, s and u), tetramers (m and r) and pentamers (t and v). It should be pointed out that in the case of structures corresponding to a lower number of aromatic rings (e.g. trimers), these rings appear to be highly substituted. Also, as suggested above from the results of the ESI-MS analysis, it appears that the polymerization of catechol mainly proceeds through the formation of ether (—O—) linkages. Carbon-carbon (e.g. Figure 2.10d) linkages appear to be less frequent as compared to the ether (—O—) linkages. Some of the compounds shown in Figure 2.10 (e.g. Figure 2.10b) are quinones which are characterized by ketonic functional groups, which is in agreement with the observations of infra-red analysis of SFA_1 (see above).

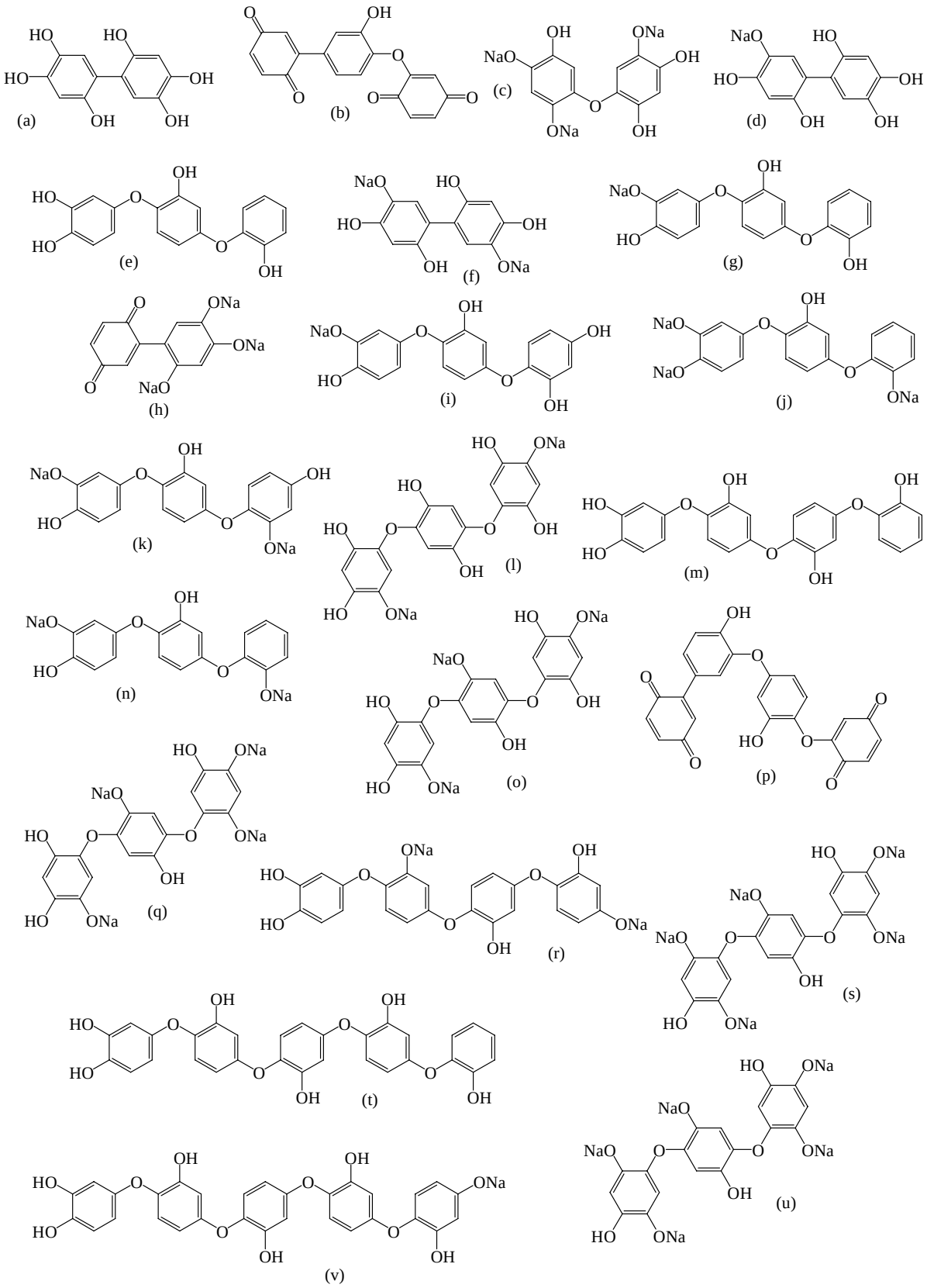

Figure 2.10. Possible molecular structures of individual fulvic acids in the raw SFA_1 mixture deduced from the LC-APCI-MS-MS analysis.

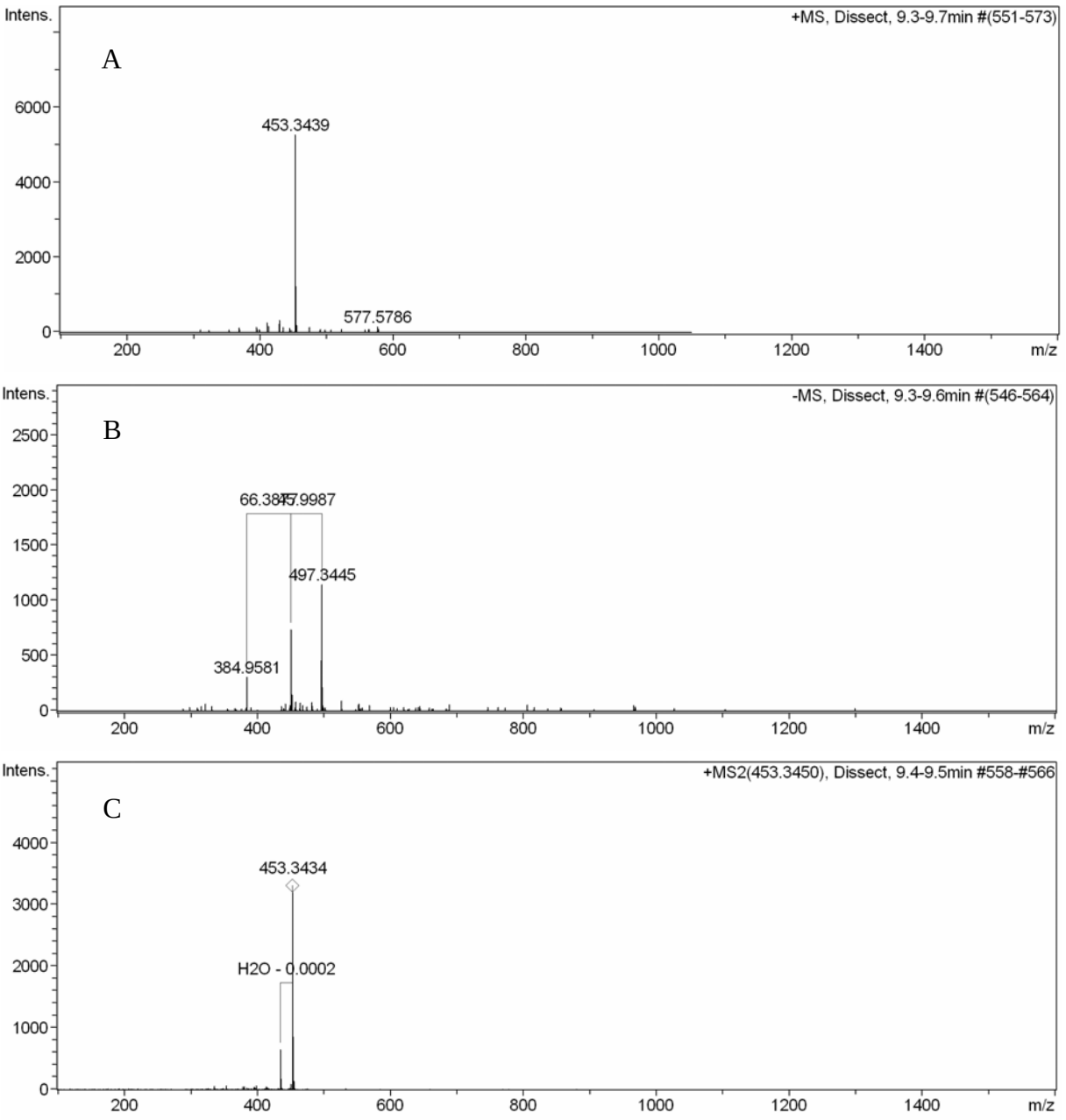

Figure 2.11. APCI-MS spectra of the raw SFA_1 fraction eluted at 9.4 minutes and analyzed in positive (A) and negative (B) modes, and APCI-MS-MS spectrum corresponding to the fragmentation of the compound corresponding to the peak with m/z equal to 453.3439 in Figure 2.11 A.

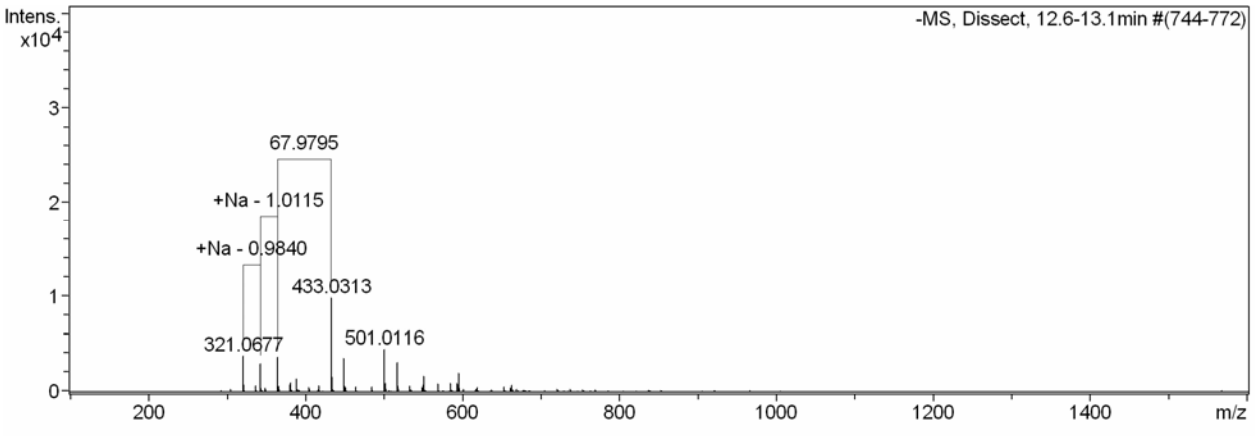

Figure 2.12. APCI-MS spectrum of the raw SFA_1 fraction eluted at 12.8 minutes and analyzed in negative mode.

1.7.2. Analysis of purified SFA_1 by APCI-MS

A saturated solution of purified SFA_1 was prepared by dissolving lyophilized solid purified SFA_1 in milli-Q water. The resulting solution was filtered through a 0.45 μm millex®-HA filter unit. The pH of the solution was not adjusted prior to the APCI-MS analysis, which was performed in both positive-ion and negative-ion modes. The obtained spectra are shown in Figure 2.13. It can be deduced from this figure that a better ionization was obtained in positive-ion mode (spectra B and C in Figure 2.13) compared to negative-ion mode (spectrum A in Figure 2.13). The m/z values corresponding to the two peaks identified in Figure 2.13 A and ten of the fourteen peaks identified in Figure 2.13 B and C are listed in Table 2.6 along with possible corresponding chemical formulas. The molecular structures corresponding to these chemical formulas are either shown in Figure 2.14 or have already been proposed in Figure 2.8 on the basis of the ESI-MS results. The prime notation refers to compounds with identical m/z values (i.e. molecular weights) and identical chemical formulas. Again, most of the proposed structures correspond to monomers (a-c and Figure 2.8, structures c and j) dimers (d and d', e, f, f' and Figure 2.8, structure f), trimers (Figure 2.8, structure o), and pentamers (g, h, i and Figure 2.8, structure n), with the aromatic rings mainly linked to each other through ether bonds. Although no tetramers have been listed in Table 2.5, this does not mean that they are absent from the purified SFA_1 mixture.

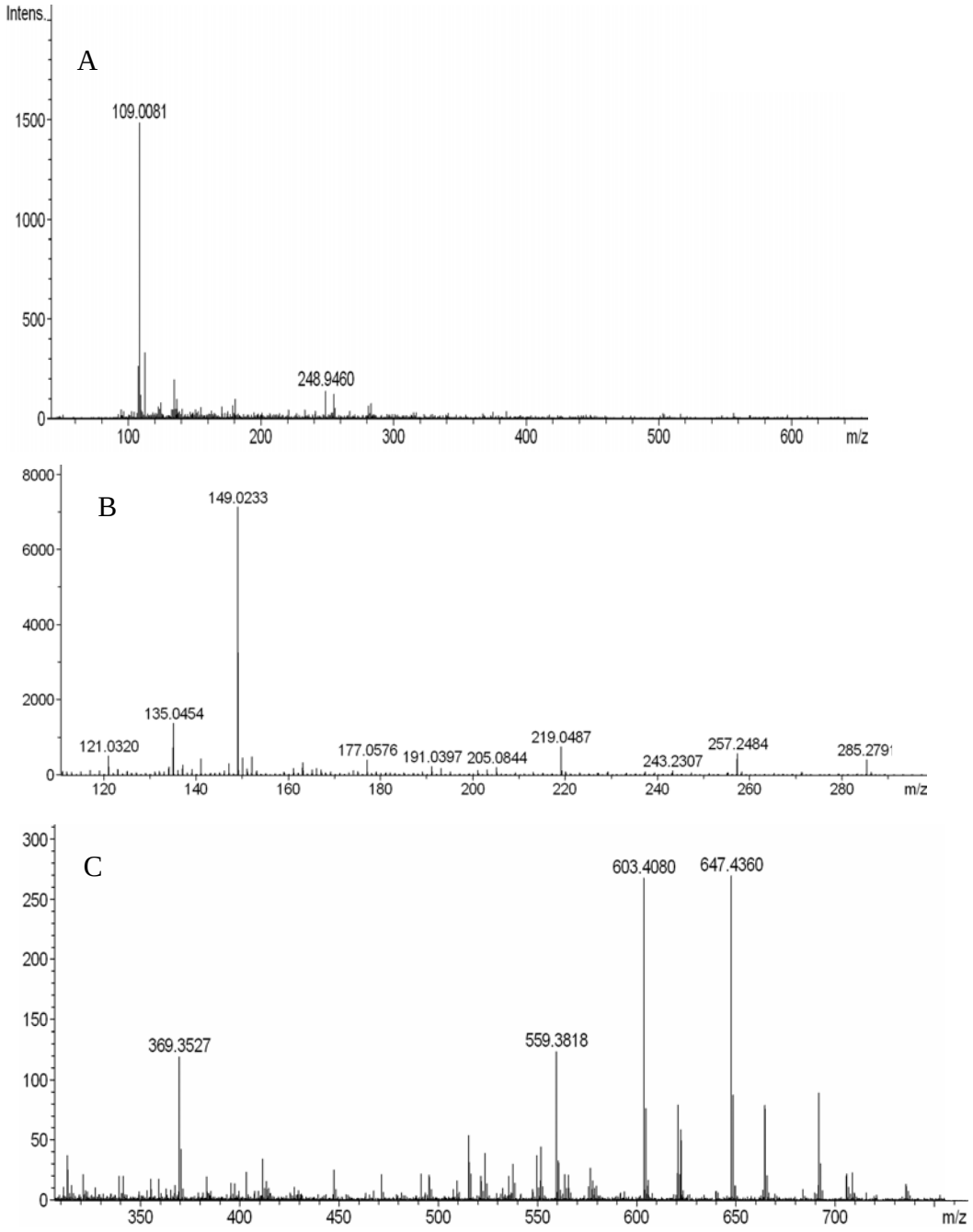

Figure 2.13. APCI-MS spectra of the purified SFA_1 mixture analyzed by ACPI-MS in (A) negative mode and (B and C) positive mode.

Table 2.6. Summary of the m/z ratios obtained in the APCI-MS analysis (positive and negative modes) of the purified SFA_1 mixture, as well as of possible chemical formulas and corresponding molecular weights for individual fulvic acids in the purified SFA_1 mixture.

m/z	Chemical formula	Molecular weight	Structure (Fig. 2.14) [a]
Positive mode			
149.0233	$[C_6H_6O_3 + Na]^+$	149.021	(b)
149.0233	$[C_6H_6O_3Na + H]^+$	149.021	(c)
177.0576	$[C_6H_4O_4 + 2\ H_2O + H]^+$	177.040	(Fig. 2.8 b)
191.0397	$[C_6H_4O_2Na_2 + 2\ H_2O + H]^+$	191.030	(j)
219.0487	$[C_{12}H_{10}O_4 + H]^+$	219.066	(d and d')
285.2791	$[C_{12}H_{10}O_7 + H_2O + H]^+$	285.061	(e)
285.2791	$[C_{12}H_7O_4Na_3 + H]^+$	285.012	(f')
369.3527	$[C_{12}H_7O_7Na_3 + 2\ H_2O + H]^+$	369.017	(f)
559.3818	$[C_{30}H_{22}O_{11} + H]^+$	559.124	(Fig. 2.8 n)
559.3818	$[C_{18}H_8O_{10}Na_6 + 2\ H_2O + H]^+$	558.979	(Fig. 2.8 o)
603.4080	$[C_{30}H_{20}O_{11}Na_2 + H]^+$	603.088	(g)
647.4360	$[C_{30}H_{18}O_{11}Na_4 + H]^+$	647.052	(h)
691.4518	$[C_{30}H_{16}O_{11}Na_6 + H]^+$	691.016	(i)
Negative mode			
109.0081	$[C_6H_6O_2 - H]^-$	109.029	(a)
248.9460	$[C_{12}H_{10}O_6 - H]^-$	249.040	(Fig. 2.8 f)

[a] Unless indicated otherwise.

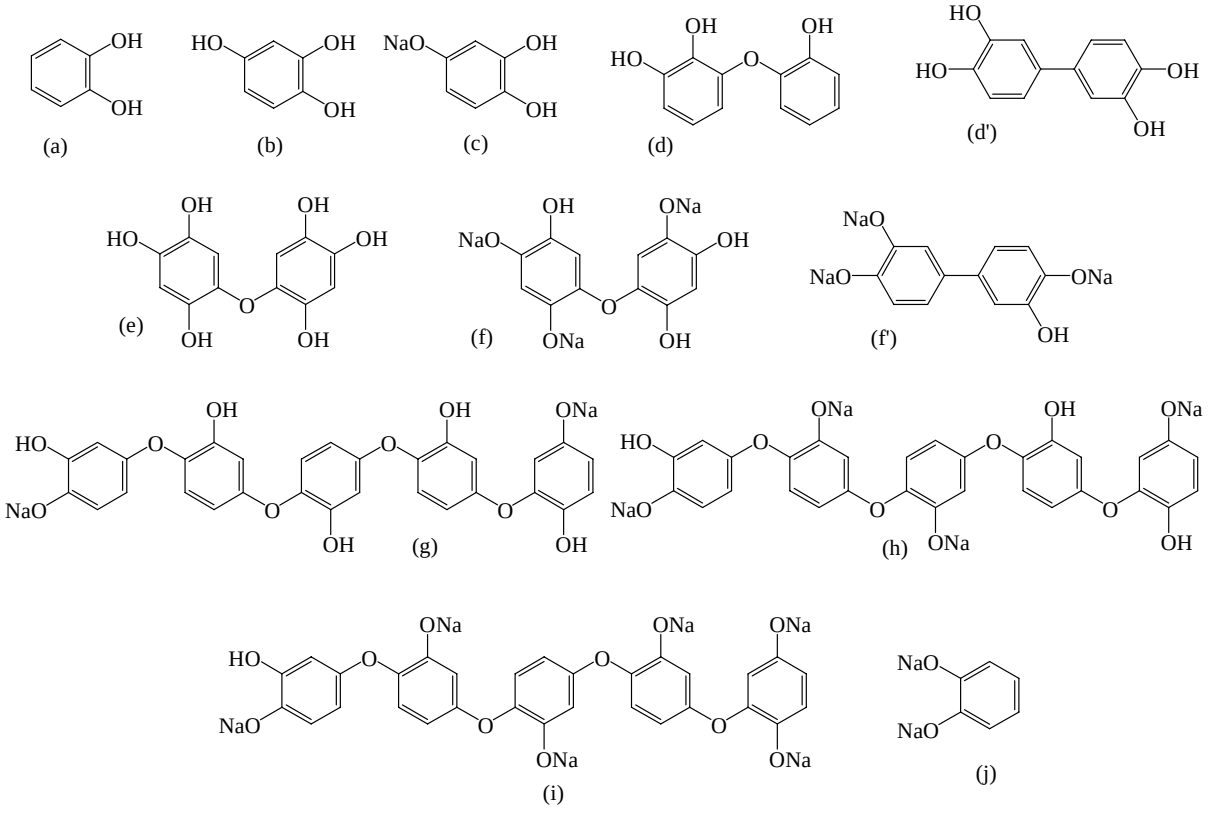

Figure 2.14. Possible molecular structures of individual fulvic acids in the purified SFA_1 mixture deduced from the APCI-MS analysis. Primes are used to designate compounds with identical chemical formulas.

1.7.3. Analysis by APCI-MS of the ethyl acetate extract obtained by liquid-liquid extraction of raw SFA_1

The liquid-liquid extraction was carried out to demonstrate that catechol had indeed reacted to form a variety of reaction products. A saturated solution of the ethyl acetate extract SFA_1 was prepared by dissolving the solid extract in milli-Q water. The resulting solution was filtered through a 0.45 μm millex®-HA filter unit. The pH of the solution was not adjusted prior to the APCI-MS analysis, which was again performed in both positive-ion and negative-ion modes. A good ionization was observed in both modes. The obtained spectra are shown in Figure 2.15. With the exception of four peaks, the m/z values identified in Figure 2.15 are listed in Table 2.7 along with possible corresponding chemical formulas. The molecular structures corresponding to these chemical formulas are shown in Figure 2.16. In contrast to the previous APCI-MS measurements, it can be deduced from this figure that the compounds with the highest number of rings which are recovered during the ethyl acetate extraction correspond to trimers of catechol. Also identified in the extract is a series of catechol derivatives substituted by phenol (—OH) and Na-phenolate (—ONa). A quinone dimer (Figure 2.16h) is among the compounds that have been proposed in the analysis of ethyl acetate extract. The prime notation in Figure 2.16 is again used to designate compounds with identical molecular weights and chemical formulas, which represent equivalent possible molecular structures for a given m/z value. Although it may seem from Figure 2.16 that ether linkages between the aromatic rings in dimers and trimers of catechol are less abundant than in the analysis of the raw and purified SFA_1, this may only be apparent as alternative structures are possible which have not been drawn in Figure 2.16.

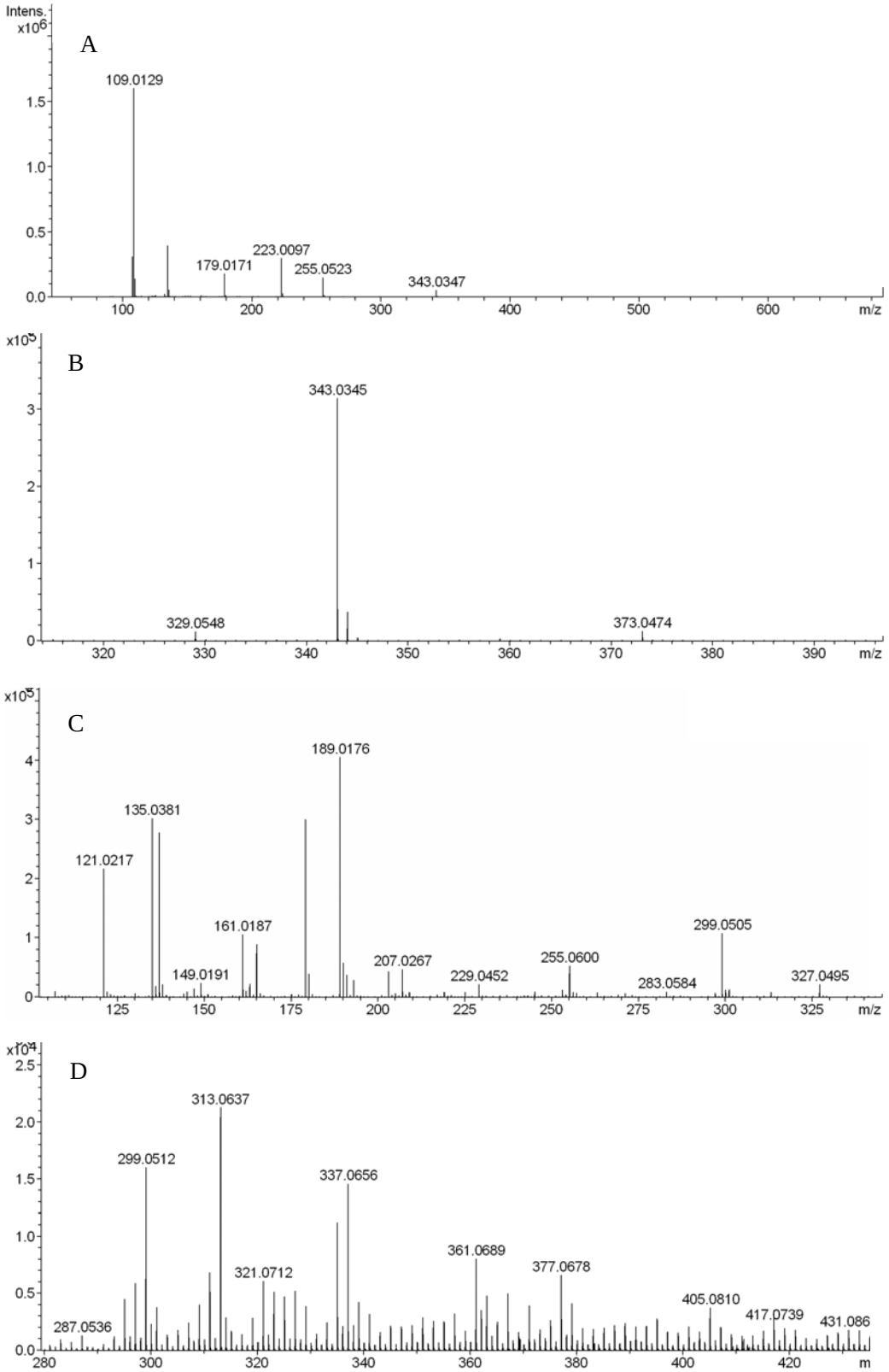

Figure 2.15. APCI-MS spectra of the ethyl acetate extract of SFA_1 analyzed by ACPI-MS in (A and B) negative mode and (C and D) positive mode.

Table 2.7. Summary of the m/z ratios obtained in the APCI-MS analysis (positive and negative modes) of the ethyl acetate extract of SFA_1, as well as of possible chemical formulas and corresponding molecular weights for individual fulvic acids in the ethyl acetate extract of SFA_1.

m/z	Chemical formula	Molecular weight	Structure (Fig. 2.16)
Positive mode			
149.0191	$[C_6H_6O_3 + Na]^+$	149.021	(b)
149.0191	$[C_6H_5O_3Na + H]^+$	149.021	(c)
189.0176	$[C_6H_5O_3Na + H_2O + Na]^+$	189.014	(c)
207.0267	$[C_6H_5O_3Na + 2\ H_2O + Na]^+$	207.025	(c)
229.0452	$[C_6H_6O_4 + HCOONa + H_2O + H]^+$	229.032	(e)
255.0600	$[C_{12}H_{10}O_4 + 2\ H_2O + H]^+$	255.087	(f)
283.0584	$[C_{12}H_6O_4 + HCOONa + H]^+$	283.022	(h)
287.0536	$[C_{12}H_{10}O_6 + 2\ H_2O + H]^+$	287.077	(i)
299.0512	$[C_{12}H_8O_4Na_2 + 2\ H_2O + H]^+$	299.051	(j)
313.0637	$[C_{12}H_8O_6Na_2 + H_2O + H]^+$	313.030	(k)
321.0712	$[C_{12}H_7O_4Na_3 + 2\ H_2O + H]^+$	321.033	(l)
327.0495	$[C_{12}H_9O_6Na + 3\ H_2O + H]^+$	327.069	(m)
327.0495	$[C_{18}H_{14}O_6 + H]^+$	327.089	(n)
337.0656	$[C_{12}H_7O_5Na_3 + 2\ H_2O + H]^+$	337.028	(o)
361.0689	$[C_{18}H_{14}O_7 + H_2O + H]^+$	361.092	(p)
405.0810	$[C_{18}H_{13}O_7Na + H_2O + Na]^+$	405.056	(r)
417.0739	$[C_{18}H_{14}O_6 + 5\ H_2O + H]^+$	417.140	(n)
431.0865	$[C_{18}H_{11}O_7Na_3 + Na]^+$	431.010	(s)
Negative mode			
109.0129	$[C_6H_6O_2 - H]^-$	109.029	(a)
179.0171	$[C_6H_6O_3 + 3\ H_2O - H]^-$	179.056	(b)
223.0097	$[C_6H_4O_3Na_2 + 3\ H_2O - H]^-$	223.019	(d)
255.0523	$[C_{12}H_9O_5Na - H]^-$	255.027	(g)
329.0548	$[C_{12}H_8O_6Na_2 + 2\ H_2O - H]^-$	329.025	(k)
343.0347	$[C_{12}H_9O_6Na + 4\ H_2O - H]^-$	343.064	(m)
343.0347	$[C_{18}H_{14}O_6 + H_2O - H]^-$	343.082	(n)
373.0494	$[C_{12}H_6O_6Na_4 + 2\ H_2O - H]^-$	372.989	(q)

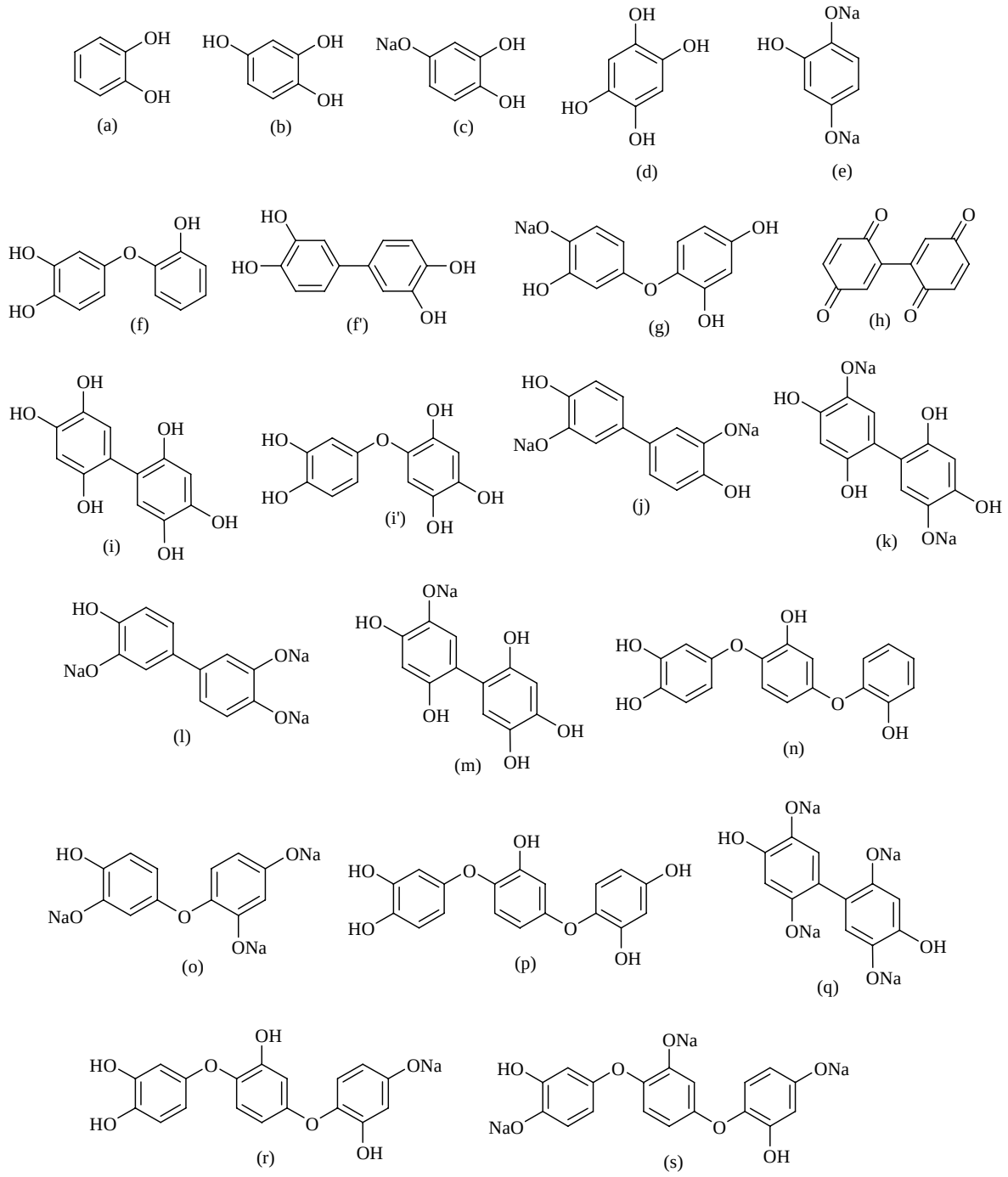

Figure 2.16. Possible molecular structures of individual fulvic acids in the ethyl acetate extract of SFA_1 deduced from the APCI-MS analysis. Primes are used to designate compounds with identical chemical formulas but different molecular structures.

1.8. Discussion

From the results and observations summarized above concerning the nature of the products obtained by polymerization of catechol, several reactions appear to be of major interest for explaining the obtention of these products from a reaction mechanism point of

view. These reactions have been put into two categories. The first of these categories will be referred to as *oxidative coupling* in the discussion to follow. This comprises the most important reactions and leads to the formation of the catechol oligomers. The second category is referred to as *quinone formation and its reactions*.

1.8.1. Oxidative coupling

Oxidative coupling designates to a reaction in which two molecular entities are coupled through an oxidative process, usually (but not necessarily) catalyzed by a transition metal compound and involving dioxygen (O_2) as the oxidant (McNaught and Wilkinson, 1997). The oxidative coupling of substituted phenols is involved in a number of biological reactions. In particular, lignin (one of the most important biopolymers on Earth) is considered to be formed through the oxidative polymerization of coniferyl alcohol (e.g. Freudenberg, 1965; Higuchi, 1990). The structures of coniferyl alcohol and one of its polymerization products are represented in Figure 2.17. A number of experimental studies have been reported on the formation of oligomers by the oxidative coupling of phenols. Most of these studies, a review of which has been presented by Kobayashi and Higashimura (2003), have used a variety of catalysts, including compounds of transition metals (Kim et al., 1983; Sánchez-Cortés et al., 2001; Eickhoff et al., 2001; Šmejkalová et al., 2006), alkaline-earth metal cations (Lebedev et al., 2007), or enzymes (Jackson, 1939; Dubey et al., 1998; Eickhoff et al., 2001; Aktaş et al., 2003). However, the results reported above are also consistent with the fact that the formation of oligomers of catechol by an autoxidation process is also possible in the absence of catalysts. The first step of the reaction mechanism in the autoxidation of catechol is shown in Figure 2.18. It involves the formation of two reactive radical species, including a semiquinone radical and a hydroperoxyl radical, and is the rate-determining step in the autoxidation reaction (Lebedev et al., 2007).

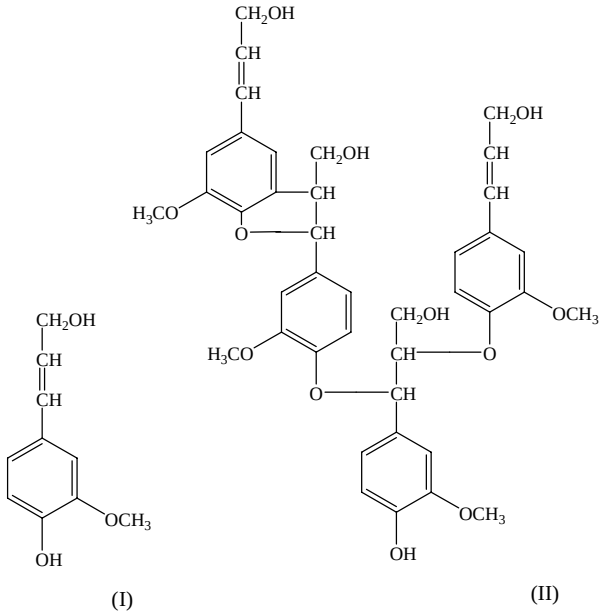

Figure 2.17. Molecular structures of coniferyl alcohol (I), the constitutive monomer of lignin, and of tetralignol (II), an oligomer formed by polymerization of (I) – Fengel and Wegener, 1983.

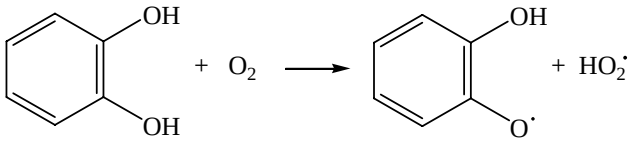

Figure 2.18. Mechanism of catechol autoxidation (modified after Lebedev et al., 2007).

As shown in Figure 2.19, different resonance structures may be drawn for the semiquinone radical, with the possibility of free radicals at various positions on the catechol ring. These free radicals may subsequently undergo different combinations, resulting in a range of coupling products. Coupling may proceed through the formation of C–C or C–O bonds. The possibilities of coupling between semiquinone free radicals are detailed in Table 2.7, in which a different notation than that adopted by Glasser (1980) has been used. Note that resonance structure (IV) cannot yield coupling products because this structure is sterically hindered and the formation of products is therefore thermodynamically unfavorable (Glasser, 1980). From the coupling modes listed in Table 2.8, six different dimers can be obtained. These six dimer products corresponds to the structures labelled (a)-(f) in Figure 2.20. The compound corresponding to structure (a) is an unstable peroxide (2,2'-dioxydiphenol) and will not be further discussed. In compounds (b) and (c), 3-(2-hydroxyphenoxy)benzene-1,2-diol and 4-(2-hydroxyphenoxy)- benzene-1,2-diol, the catechol rings are linked through an ether (—O—) bond. In contrast, in compounds (d)-(f) which correspond respectively to biphenyl-2,3,5',6'-tetrol, biphenyl-2,3,4',5'-tetrol and biphenyl-3,4,4',5'-tetrol, the catechol

rings are linked through a carbon-carbon bond. Note that the formation of compounds (b)-(f) involves a rearomatization step.

The dimers (b)-(f) can further be oxidized to dimer free radicals, which may again be coupled either with monomeric semiquinone free radicals or other dimer free radicals, leading to the formation of higher oligomers. In addition, dimer free radicals may possibly react with hydroxyl radicals, resulting in the addition of a third OH group on the catechol ring such as in compounds (a) in Figure 2.10, (e) in Figure 2.14 or (i) in Figure 2.16.

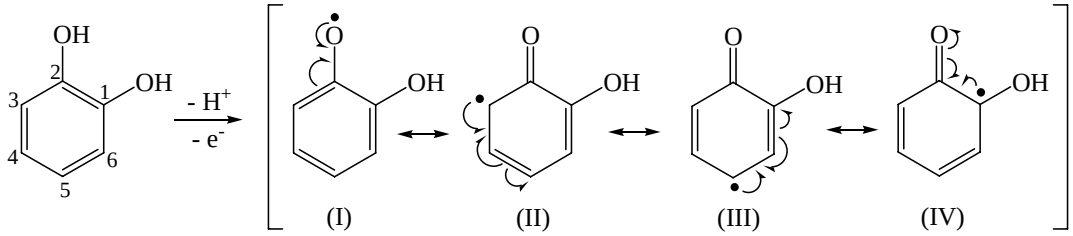

Figure 2.19. Resonance structures of the intermediate semiquinone free radical generated by oxidation of catechol.

Table 2.8. Coupling modes of semiquinone free radicals (after Glasser, 1980). The C(x) and O(x) notation refers to the position of the carbon atom as indicated on the catechol molecule in Figure 2.19, or in the case of oxygen atoms, to the position of the carbon atom to which the oxygen atom is attached.

	(I)	(II)	(III)
(I)	O(2)-O(2)	O(2)-C(3)	O(2)-C(5)
(II)	C(3)-O(2)	C(3)-C(3)	C(3)-C(5)
(III)	C(5)-O(2)	C(5)-C(3)	C(5)-C(5)

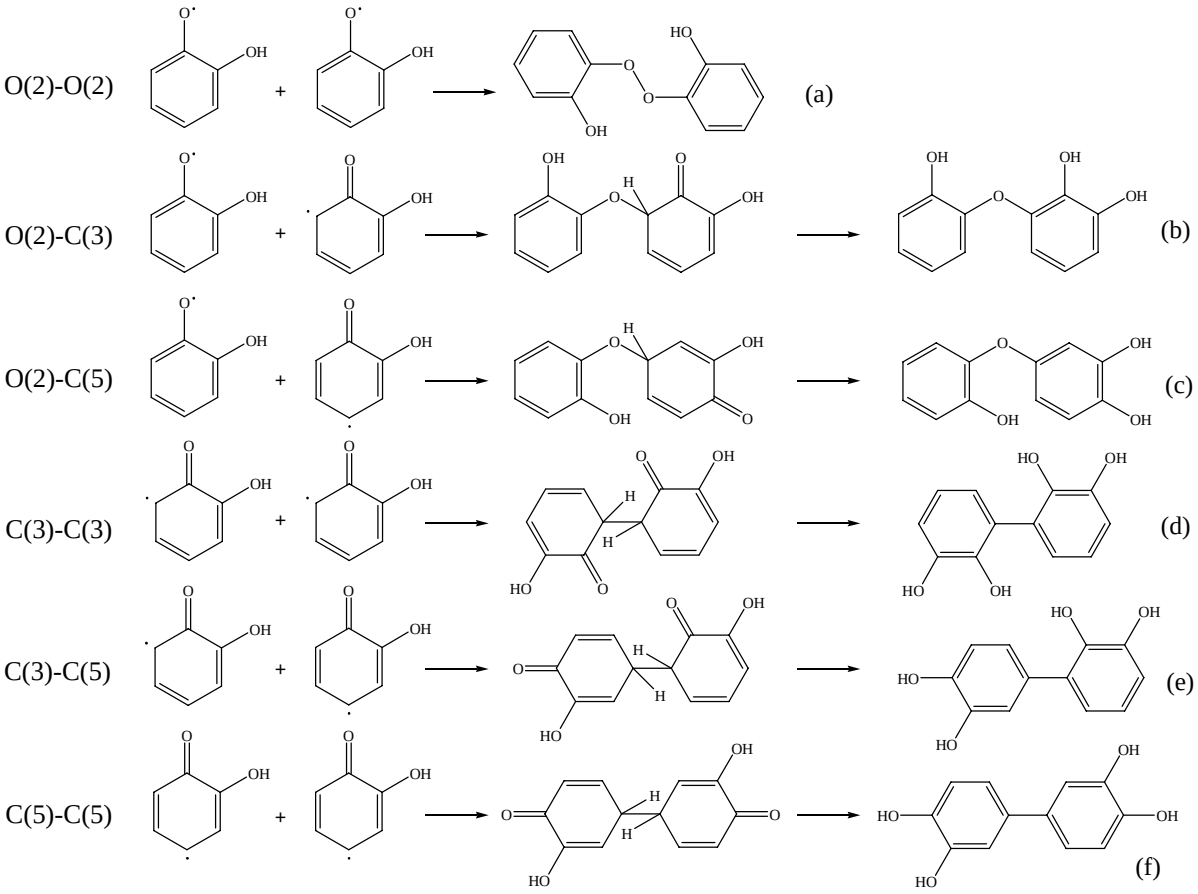

Figure 2.20. Oxidative coupling reactions involving the semiquinone free radical and leading to six possible dimers.

Let us first consider biphenyl-3,4,4',5'-tetrol (compound f in Figure 2.20) in order to illustrate the formation of radicals from a biphenyl structure. It can be deduced from Figure 2.21 that this dimer can produce eight different radical resonance structures (V-XII), three of which (VII, VIII and XII) cannot yield coupling products because they are sterically hindered. The possibilities of coupling between the remaining five free radical dimers are summarized in Table 2.9. It can be deduced from this table that fifteen different tetramers can be obtained by coupling the five dimer free radicals (V), (VI), (IX), (X) and (XI). These fifteen tetramers correspond to structures (g)-(u) in Figure 2.22 and the names summarized in Table 2.10. Among these fifteen compounds, three (compounds g, i and p) are again unstable peroxides. Compounds h, j, k, m, q and r correspond to dibiphenyl ethers bearing seven hydroxy functional groups, whereas compounds l, n, o, s, t and u correspond to quaterphenyls bearing eight hydroxy functional groups. Among these quaterphenyls, compounds s and t are probably highly unstable due to hindered rotation around the C–C bonds between the two biphenyls.

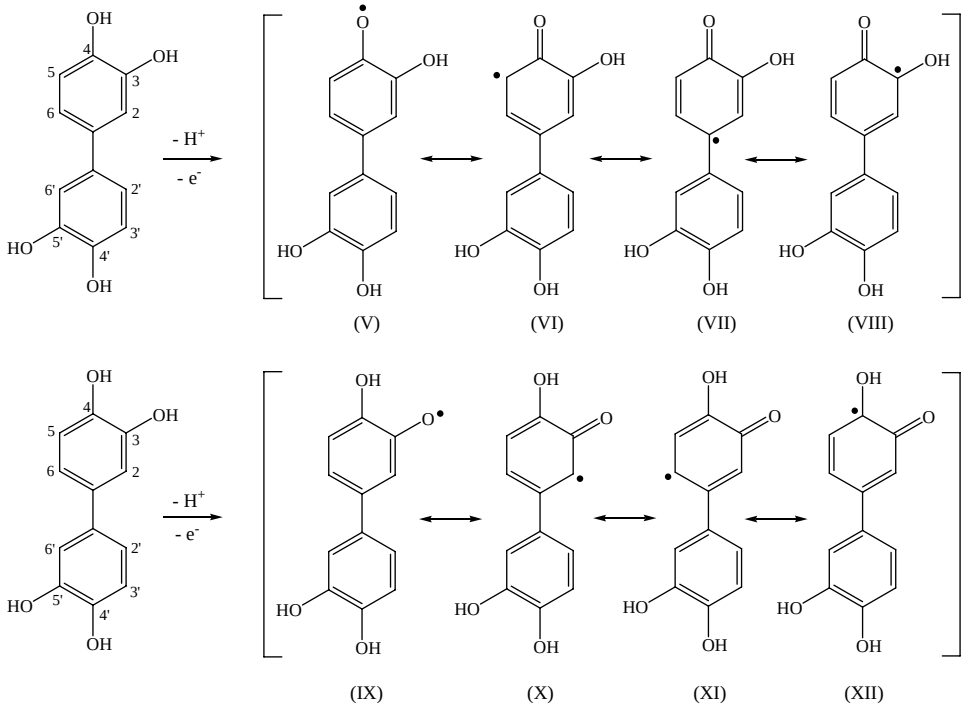

Figure 2.21. Dimer radical resonance structures generated by oxidation of biphenyl-3,4,4',5'-tetrol (compound f in Figure 2.20).

Table 2.9. Coupling modes of dimer free radicals from the oxidation of biphenyl-3,4,4',5'-tetrol. The C(x) and O(x) notation refers to the position of the carbon atom as indicated on the biphenyltetrol molecule in Figure 2.21, or in the case of oxygen atoms, to the position of the carbon atom to which the oxygen atom is attached.

	(V)	(VI)	(IX)	(X)	(XI)
(V)	O(4)-O(4)	O(4)-C(5)	O(4)-O(3)	O(4)-C(2)	O(4)-C(6)
(VI)	C(5)-O(4)	C(5)-C(5)	C(5)-O(3)	C(5)-C(2)	C(5)-C(6)
(IX)	O(3)-O(4)	O(3)-C(5)	O(3)-O(3)	O(3)-C(2)	O(3)-C(6)
(X)	C(2)-O(4)	C(2)-C(5)	C(2)-O(3)	C(2)-C(2)	C(2)-C(6)
(XI)	C(6)-O(4)	C(6)-C(5)	C(6)-O(3)	C(6)-C(2)	C(6)-C(6)

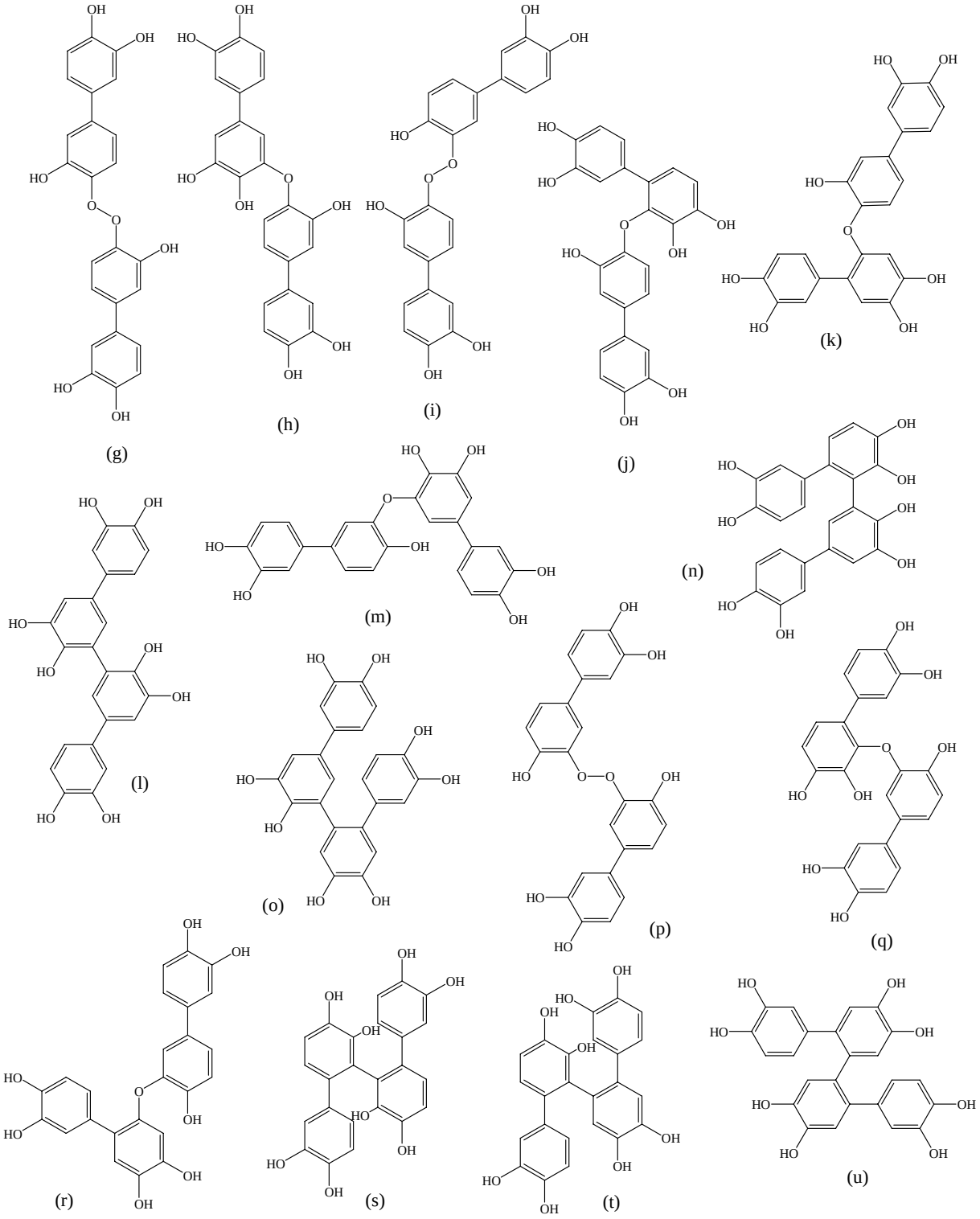

Figure 2.22. Fifteen tetrameric reaction products obtained from the oxidative coupling of five dimer free radicals.

In order to relate the molecular structures obtained above on the basis of reaction mechanisms to peaks identified in the APCI-MS analysis, let us consider the peak at m/z equal to 219 shown in Figure 2.13 B. We have assigned this peak to a compound with a formula $C_{12}H_{10}O_4$ which possible molecular structures such as structures d or d' in Figure

2.14. The mass of 218 Da $[+ H]^+$ could in fact also be assigned to any of the five stable structures denoted by (b)-(f) in Figure 2.20, which are obtained by the oxidative coupling of two catechol free radicals. In the case of the peaks at m/z equal to 453 and 451 obtained from the APCI-MS analysis in positive and negative ion modes, respectively (see Figure 2.11 A and B), we had assigned these peaks to compounds with the structures (l) and (m) in Figure 2.10. The mass of 434 Da corresponding to $[434 + H_2O - H]^-$ and $[434 + H_2O + H]^+$ for m/z equal to 451 and 453, respectively, can in fact be assigned to any of the twelve stable tetrameric structures denoted by (h), (j)-(o) and (q)-(u) in Figure 2.22, which are obtained either from the coupling of two dimer free radicals or by the coupling of a trimer free radical with a catechol free radical.

Let us now consider 2,4',5'-trihydroxydiphenyl ether (compound c in Figure 2.20) as a second example to illustrate the formation of radicals from a diphenyl ether structure. From the three initial possibilities of oxidation on one of the three oxygen atoms, a total of twelve different total resonance structures are obtained for this compound. These resonance structures are depicted in Figure 2.23. Four of these resonance structures (XIV, XVI, XIX and XXIII) cannot yield coupling products for steric hindrance reasons. The possibilities of coupling between the remaining eight free radical dimers are summarized in Table 2.9, from which the thirty-six tetrameric reaction products corresponding to structures (v)-(be) in Figure 2.24 can be obtained.

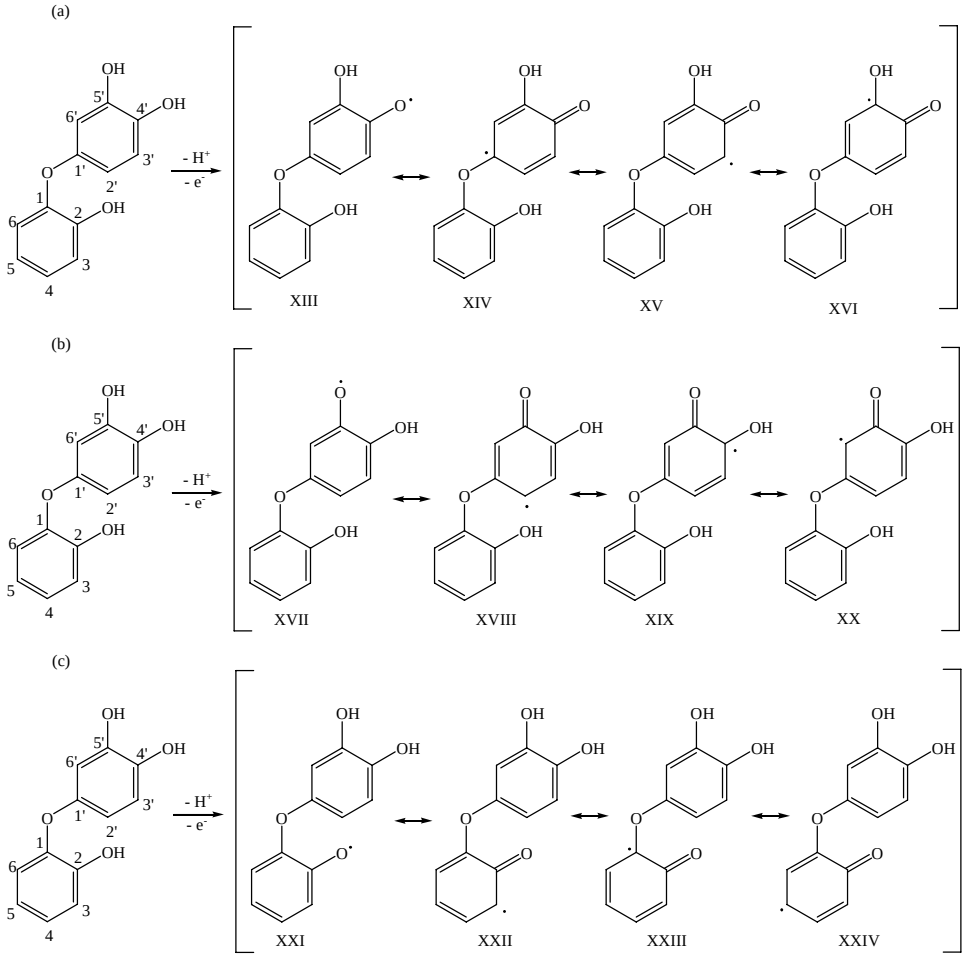

Figure 2.23. Dimer radical resonance structures generated by oxidation of 2,4',5'-trihydroxydiphenyl ether (compound c in Figure 2.20).

Table 2.10. Coupling modes of dimer free radicals obtained from the oxidation of 2,4',5'-trihydroxy-diphenyl ether. The C(x) and O(x) notation refers to the position of the carbon atom as indicated on the trihydroxydiphenyl ether molecule in Figure 2.22, or in the case of oxygen atoms, to the position of the carbon atom to which the oxygen atom is attached.

	(XIII)	(XV)	(XVII)	(XVIII)	(XX)	(XXI)	(XXII)	(XXIV)
(XIII)	O(4)-O(4)	C(5)-O(4)	O(3)-O(4)	C(6)-O(4)	C(2)-O(4)	O(6')-O(4')	C(5')-O(4)	C(3')-O(4)
(XV)	O(4)-C(5)	C(5)-C(5)	O(3)-C(5)	C(6)-C(5)	C(2)-C(5)	O(6')-C(5)	C(5')-C(5)	C(3')-C(5)
(XVII)	O(4)-O(3)	C(5)-O(3)	O(3)-O(3)	C(6)-O(3)	C(2)-O(3)	O(6')-O(3)	C(5')-O(3)	C(3')-O(3)
(XVIII)	O(4)-C(6)	C(5)-C(6)	O(3)-C(6)	C(6)-C(6)	C(2)-C(6)	O(6')-C(6)	C(5')-C(6)	C(3')-C(6)
(XX)	O(4)-C(2)	C(5)-C(2)	O(3)-C(2)	C(6)-C(2)	C(2)-C(2)	O(6')-C(2)	C(5')-C(2)	C(3')-C(2)
(XXI)	O(4)-O(6')	C(5)-O(6')	O(3)-O(6')	C(6)-O(6')	C(2)-O(6')	O(6')-O(6')	C(5')-O(6')	C(3')-O(6')
(XXII)	O(4)-C(5')	C(5)-C(5')	O(3)-C(5')	C(6)-C(5')	C(2)-C(5')	O(6')-C(5')	C(5')-C(5')	C(3')-C(5')
(XXIV)	O(4)-C(3')	C(5)-C(3')	O(3)-C(3')	C(6)-C(3')	C(2)-C(3')	O(6')-C(3')	C(5')-C(3')	C(3')-C(3')

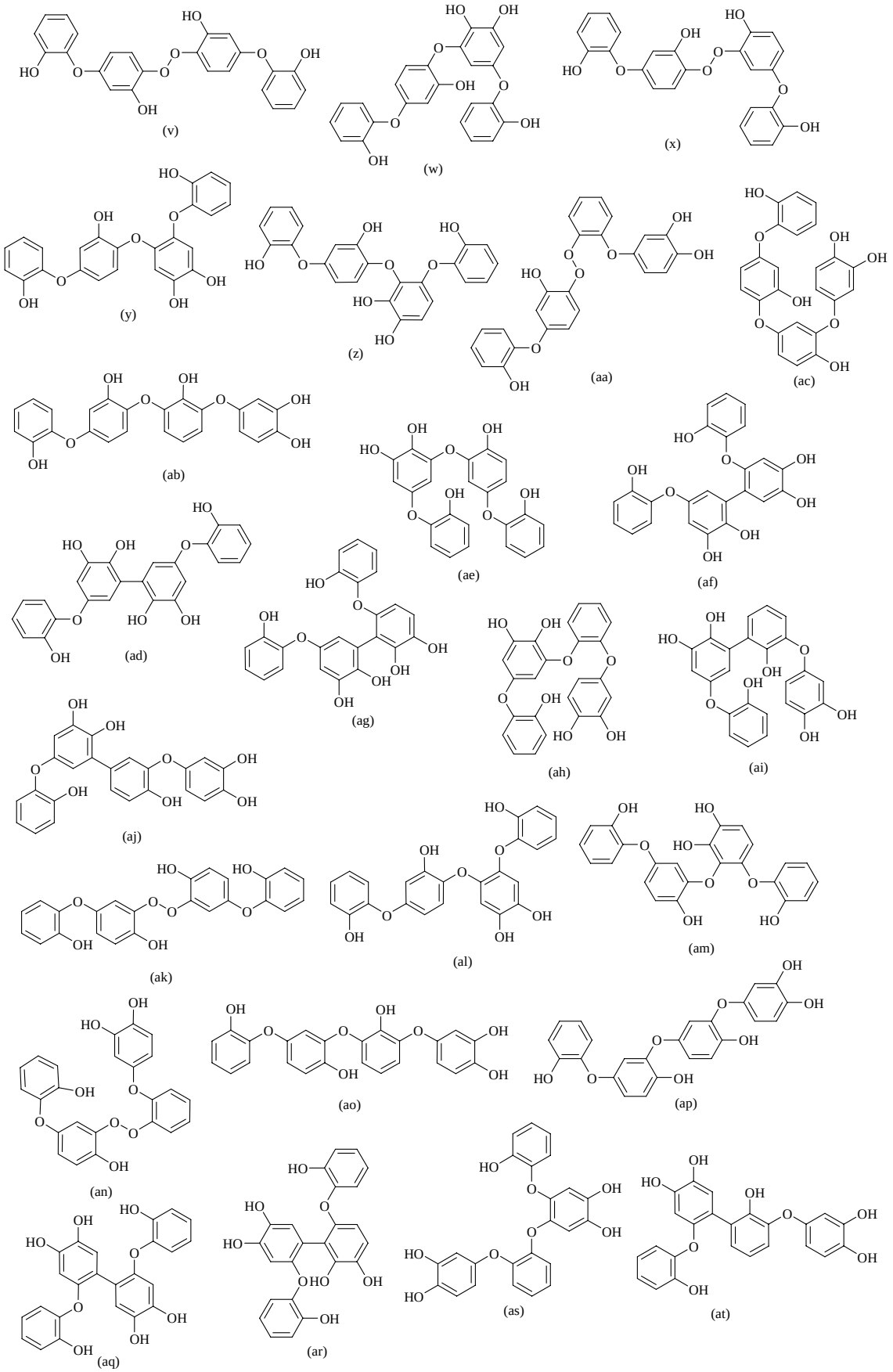

Figure 2.24. Thirty-six tetrameric reaction products obtained from the oxidative coupling of eight ether-linked dimer free radicals.

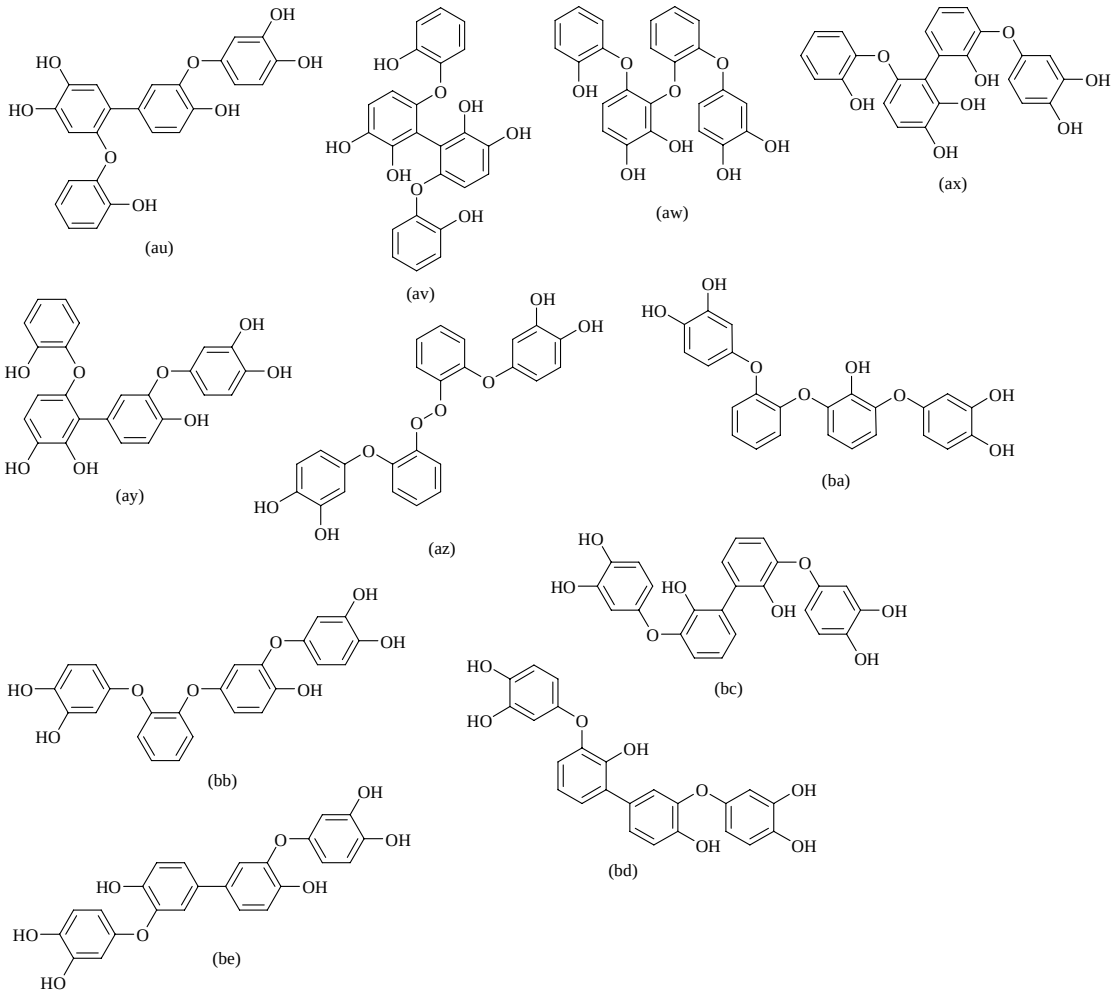

Figure 2.24. Continued.

1.8.2. Quinone formation and its reactions

Quinones are known to be present in aqueous environment either in para or ortho form. Ortho-quinones when fully reduced yields catechol; QH_2, while when fully oxidized or in intermediate oxidation state yields o-quinone; Q and ortho-semiquinone radical; $QH^{\cdot}$ respectively, Figure 2.25 (Uchimiya and Stone, 2009). Catechol, ortho-semiquinone and quinone are linked to one other through single electron-transfer steps, Figure 2.26. Quinones can undergo addition reactions with nucleophiles such as hydroxide ion, amine, thiol, hydrogen silfide and sulfite (Thomson, 1951; Perlinger et al., 2002; Uchimiya and Stone, 2006; Uchimiya and Stone, 2009). Figure 2.27 below shows the o-quinone addition reaction with hydroxide ion.

The formation of cis, cis-5-carboxy-2,4-pentadienoic acid (a.k.a cis, cis-muconic acid) and 2-hydroxy-6-oxo-2,4-hexadienoic acid from catechol has been reported by several researchers (Fujiwara et al., 1975; Lin et al., 2000; Gonçalves et al., 2008; Sundaravel et al.,

2008). Figure 2.28 below shows their formation. It should be noted that in the reported work, they used enzymes (dioxygenase) and catalysts. Under these conditions cleavage can occur in two different positions; the first one being the cleavage of carbon-carbon bond between the two catechol oxygens while the second one is the cleavage of the carbon-carbon bond adjacent to the catechol oxygen atoms. Its certain that we also formed muconic acid and 2-hydroxy-6-oxo-2,4-hexadienoic acid, even though our experimental conditions is not exactly the same. The formation of these compounds accounts for the bands observed at 1719 and 1735 cm^{-1}.

Quinone can also react with the free radicals generated under section 1.8.1. to yield compounds with higher molecular masses.

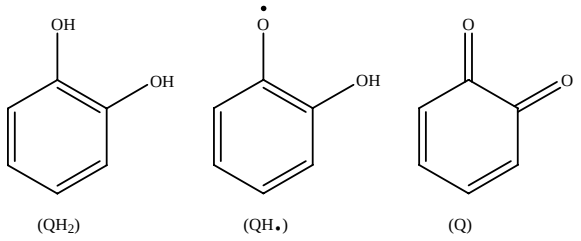

Figure 2.25. The different oxidation states of ortho-quinones (Uchimiya and Stone, 2009).

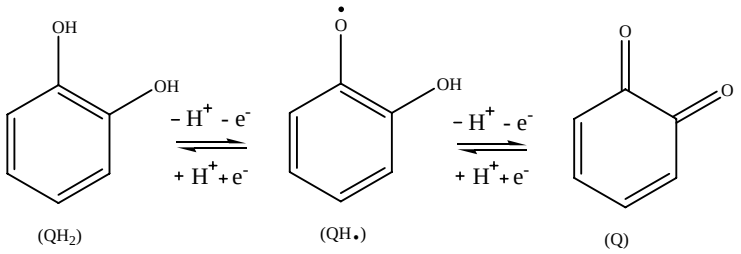

Figure 2.26. Formation of quinones from catechol (Uchimiya and Stone, 2006).

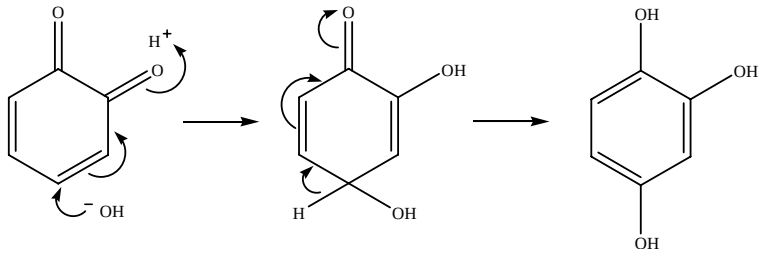

Figure 2.27. *o*-quinone addition reaction with hydroxide ion.

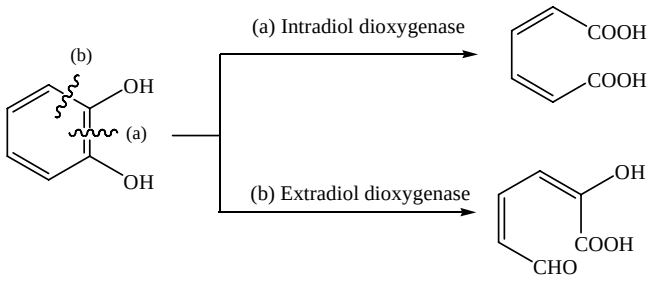

Figure 2.28. Mode of the intradiol and extradiol dioxygenases (Sundaravel et al., 2008).

2. FULVIC ACID SYNTHESIZED BY CONDENSATION OF CATECHOL AND ACETIC ACID

2.1. Elemental analysis

Both raw and extracted synthetic fulvic acid (SFA) obtained through the condensation of catechol and acetic acid (SFA_2) in the quaternary system $C_6H_4(OH)_2$-CH_3COOH-NaOH-H_2O at ~ 25°C, under atmospheric oxidizing conditions and at pH = 10 have been analyzed for their elemental compositions. The results are shown in Table 2.10. The composition listed in this table for catechol corresponds to the determination already shown in Table 2.1, but the composition listed for acetic acid is the theoretical value calculated from the formula and the atomic weights of the elements. This theoretical composition is only shown for the purpose of comparison. As was the case with the SFA_1 analysis, the weight percentages determined for carbon, hydrogen and oxygen do not sum up to 100 percent for both the raw and extracted SFA_2. We have again made the assumption that the difference could be attributed to sodium ions (from NaOH) complexed by phenolate or carboxylate functional groups in the SFA_2. It can be deduced from Table 2.11 that the proportion of oxygen in the raw SFA_2 increases at the expense of carbon between 0 and 63 days. Since the Na content in the two raw SFA_2 samples stays relatively constant, this increase in oxygen content may reflect an increase in carboxylic functional groups with respect to phenolic groups in the SFA_2 structure. However, the inverse observation applies to the final SFA_2 obtained after the extraction procedure, the extracted SFA_2 containing more carbon but less oxygen than the extracted SFA_1. The atomic H/C ratios of the two extracted SFA are similar, but the O/C ratio of SFA_2 is lower than that of SFA_1.

Table 2.11. Elemental compositions of the raw and extracted fulvic acid synthesized by condensation of catechol and acetic acid. No correction for the presence of water has been made.

Sample	% C	% H	% O	(% Na)[a]	H/C	O/C
Catechol	66.28	5.56	28.78	(0.00)	1.000	0.326
Acetic acid [b]	40.00	6.71	53.29	(0.00)	2.000	1.000
SFA_2 ; 0 day (raw)	38.93	3.65	35.80	(21.62)	1.117	0.690
SFA_2 ; 63 days (raw)	31.08	3.13	42.09	(23.70)	1.200	1.017
SFA_2 ; after extraction [c]	42.88	2.55	39.28	(15.29)	0.709	0.688
SFA_2 ; extract 1 [d]	28.51	3.58	33.54	(34.37)	1.496	0.883
SFA_2 ; extract 2 [d]	32.06	3.00	35.38	(29.56)	1.115	0.828
SFA_2 ; extract 3 [d]	27.96	2.85	33.95	(35.24)	1.215	0.912
SFA_2 ; extract 4 [d]	28.08	2.37	35.67	(33.88)	1.006	0.954
SFA_2 ; extract 5 [d]	23.87	1.87	35.03	(39.23)	0.934	1.102

[a] Calculated by difference (see text) [b] The composition shown for this compound is the theoretical one [c] The SFA_2 composition on this line corresponds to the purified fulvic acid obtained at the end of the extraction procedure (see chapter 1) [d] The composition given on this line corresponds to one of five successive extractions with methanol

Additional structural considerations on the various SFA will be provided later based on the results of the spectroscopic measurements and mass spectrometry analyses.

2.2. Scanning electron microscopy

Scanning electron microscope (SEM) observations of samples of the raw SFA_2 obtained by condensation of catechol and acetic acid at 25°C and at pH = 10 are shown in Figure 2.29. As was the case with the observations on SFA_1, the reaction products appear to be amorphous agglomerations of extremely fine, submicrometric particles.

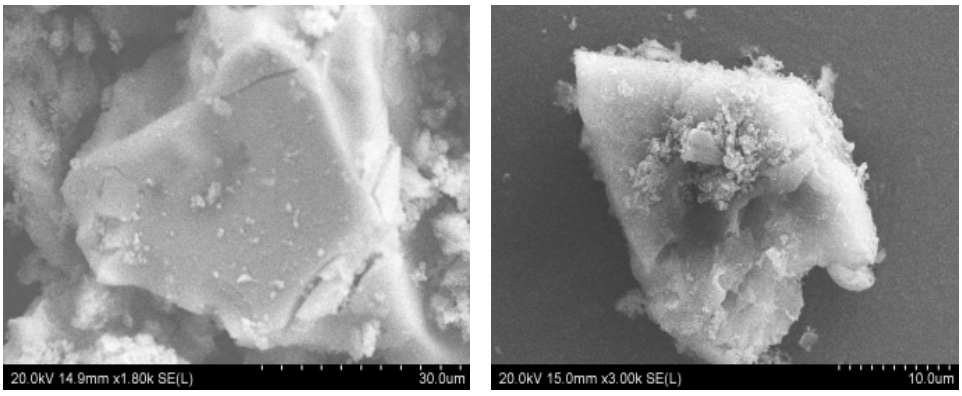

Figure 2.29. SEM photographs of SFA_2. Magnification (left) x 1800 (right) x 3000.

2.3. X-ray diffraction

X-ray diffraction spectra obtained for catechol crystals, sodium acetate crystals, raw SFA_2, and purified (extracted) SFA_2 are shown in Figure 2.30 (a), (b), (c) and (d), respectively. The diffractograms have been offset for the sake of clarity. The difference between the diffractograms of initial catechol and of SFA_2 after solvent extraction clearly indicates that new products have been formed as a result of complex and multiple reactions between five main reacting species, including catecholate anions, catechol free radicals, acetate anions, dissolved CO_2, and hydroxide OH^- anions, the latter being present in relatively high concentrations since the synthesis was carried at pH = 10 (see discussion below). The different peaks observed in the diffractogram of raw SFA_2 can be assigned to crystalline solid compounds such as sodium acetate CH_3COONa, sodium catecholate $C_6H_4(OH)(ONa)$, or other unidentified by-products. The absence of diffraction peaks in the X-ray diffractogram of SFA_2 after the extraction of most of the reacting catechol, Na-acetate, Na-catecholate and other by-products indicates that SFA_2 is mainly constituted by a mixture of amorphous solid compounds.

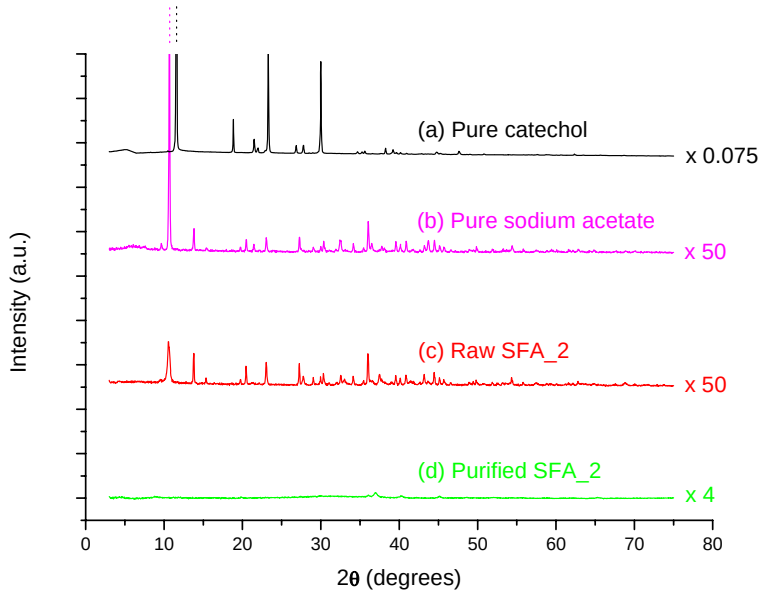

Figure 2.30. X-Ray diffraction spectra of crystalline catechol (a), crystalline sodium acetate (b), raw SFA_2 prior to extraction (c), and purified (extracted) SFA_2.

2.4. ATR-FTIR spectroscopy

The ATR-FTIR spectrum of catechol has been discussed in section *1.4.1* and will not be presented again.

2.4.1. Acetic acid

The ATR-FTIR spectrum of pure acetic acid recorded at 25°C and 0.1 MPa is shown in Figure 2.31. This spectrum has been measured using water as a reference. The ATR-FTIR spectrum of acetic acid is composed of five groups of absorption bands corresponding to the following wavenumber ranges:

- ✓ 3700 – 3000 cm^{-1}: a broadband in the range 3700 – 3000 cm^{-1} corresponding to stretching modes of OH groups (νO–H), with three major bands at 3600 cm^{-1}, 3407 cm^{-1} and 3125 cm^{-1} which are characteristic of carboxylic functional groups.
- ✓ 3000 – 2800 cm^{-1}: three vibration bands due to C–H bonds can be observed, with an antisymmetric stretching mode ν_aCH_3 at 2986 cm^{-1} and a symmetric mode ν_sCH_3 at 2852 cm^{-1}. The band at 2937 cm^{-1} is probably an overtone of the νC–H stretching mode.
- ✓ 1800 – 1600 cm^{-1}: the distinct band at 1716 cm^{-1} is assigned to the νC=O stretch due to the dimerisation of two acetic acid molecules.
- ✓ 1500 – 1200 cm^{-1}: the small broad band near 1470-1450 cm^{-1} represents two bending modes: the antisymmetric bending of the methyl group (δ_aCH_3 at 1475-1450 cm^{-1}) and the symmetric bending of the carboxylate group ($\delta_sO–C–O$ at 1460 – 1400 cm^{-1}). The distinct bands at 1243 cm^{-1}, 1295 cm^{-1} and 1412 cm^{-1} corresponds to the νC–O stretching mode coupled to the δO–H bending mode of the carboxylate group.
- ✓ 1100 – 800 cm^{-1}: in the broad region corresponding that wave number range, four stretching bands νC–C appear at 1052, 1015, 937 and 891 cm^{-1}.

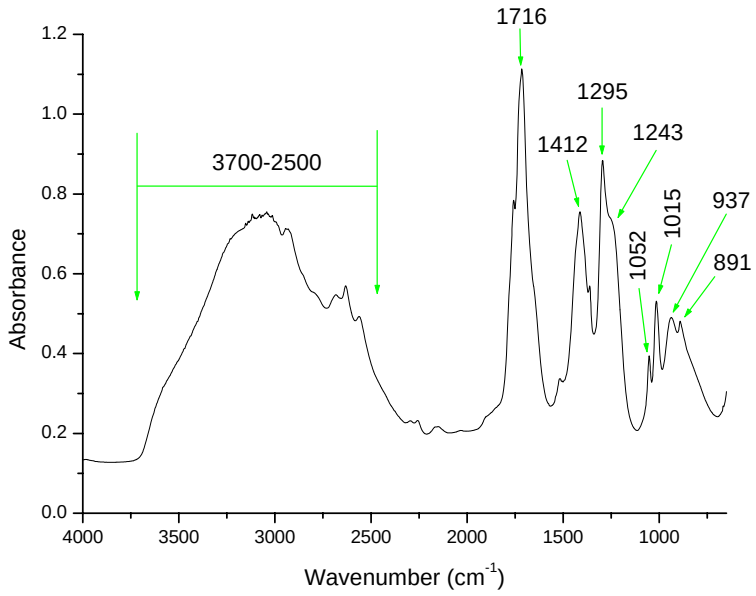

Figure 2.31. ATR-FTIR spectrum of pure liquid acetic acid (CH_3COOH): T = 25°C, P = 0.1 MPa.

2.4.2. Sodium acetate, hydrated

Sodium acetate has been identified as a by-product of the SFA_2 synthesis by ESI-MS (see below). Therefore, the ATR-FTIR spectrum of pure sodium acetate trihydrate $CH_3CO_2Na{\cdot}3H_2O$ (Aldrich, 99+%) has also been recorded at 25°C and 0.1 MPa. This spectrum, which is presented in Figure 2.32, is composed of four groups of absorption bands :

- ✓ 3700 – 3000 cm^{-1}: the two broad bands at 3145 cm^{-1} and 3420 cm^{-1} characterize the νO–H stretching mode of constitutional water.
- ✓ 3000 – 2800 cm^{-1}: three vibration bands due to C–H bonds can be observed, with an antisymmetric stretching mode ν_aCH_3 at 2976 cm^{-1} and a symmetric mode ν_sCH_3 at 2879 cm^{-1}. The band at 2934 cm^{-1} is probably an overtone of the νC–H stretching mode.
- ✓ 1750 – 1400 cm^{-1}: the vibration bands observed at 1716 cm^{-1} (νC=O stretching) and at 1243 – 1412 cm^{-1} (νC–O stretching) in Figure 2.31 for pure liquid acetic acid are replaced in Figure 32 by two equivalent C–O bonds which are intermediate in force constant between C=O and C–O bonds. These two “bond and a half” oscillators are strongly coupled and are characterized by two distinct bands, including a strong antisymmetric stretching band ν_aCO_2 at 1568 cm^{-1} and a weaker symmetric stretching

band $\nu_s CO_2$ at 1409 cm^{-1}. The latter two bands overlap with the antisymmetic deformation $\delta_a CH_3$ band.

- ✓ 1100 – 800 cm^{-1}: in the broad region corresponding to that wave number range, four stretching bands νC–C appear at 1044, 1011, 924 and 811 cm^{-1}.

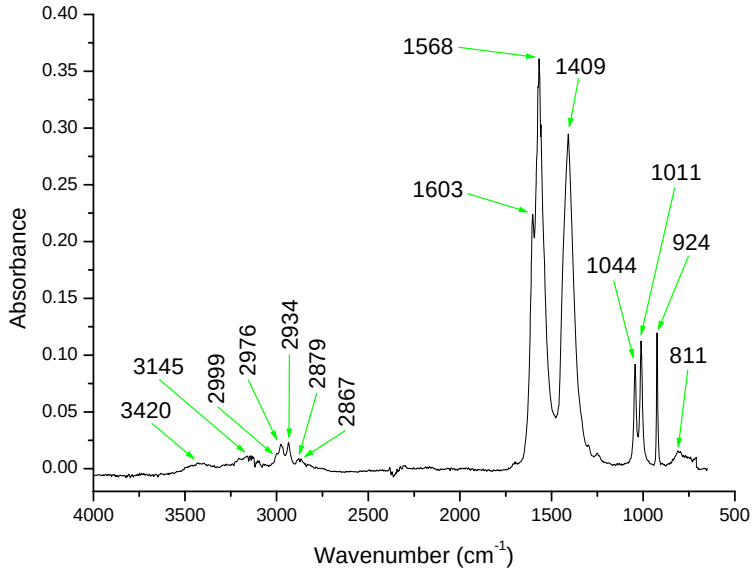

Figure 2.32. ATR-FTIR spectrum of pure solid sodium acetate trihydrate ($CH_3CO_2Na \cdot 3H_2O$): T = 25°C, P = 0.1 MPa.

2.4.3. Synthetic fulvic acid SFA_2

The ATR-FTIR spectra of the raw and purified synthetic fulvic acids SFA_2 are presented in Figure 2.33. These spectra are characterized by four groups of absorption bands, which are discussed in detail below.

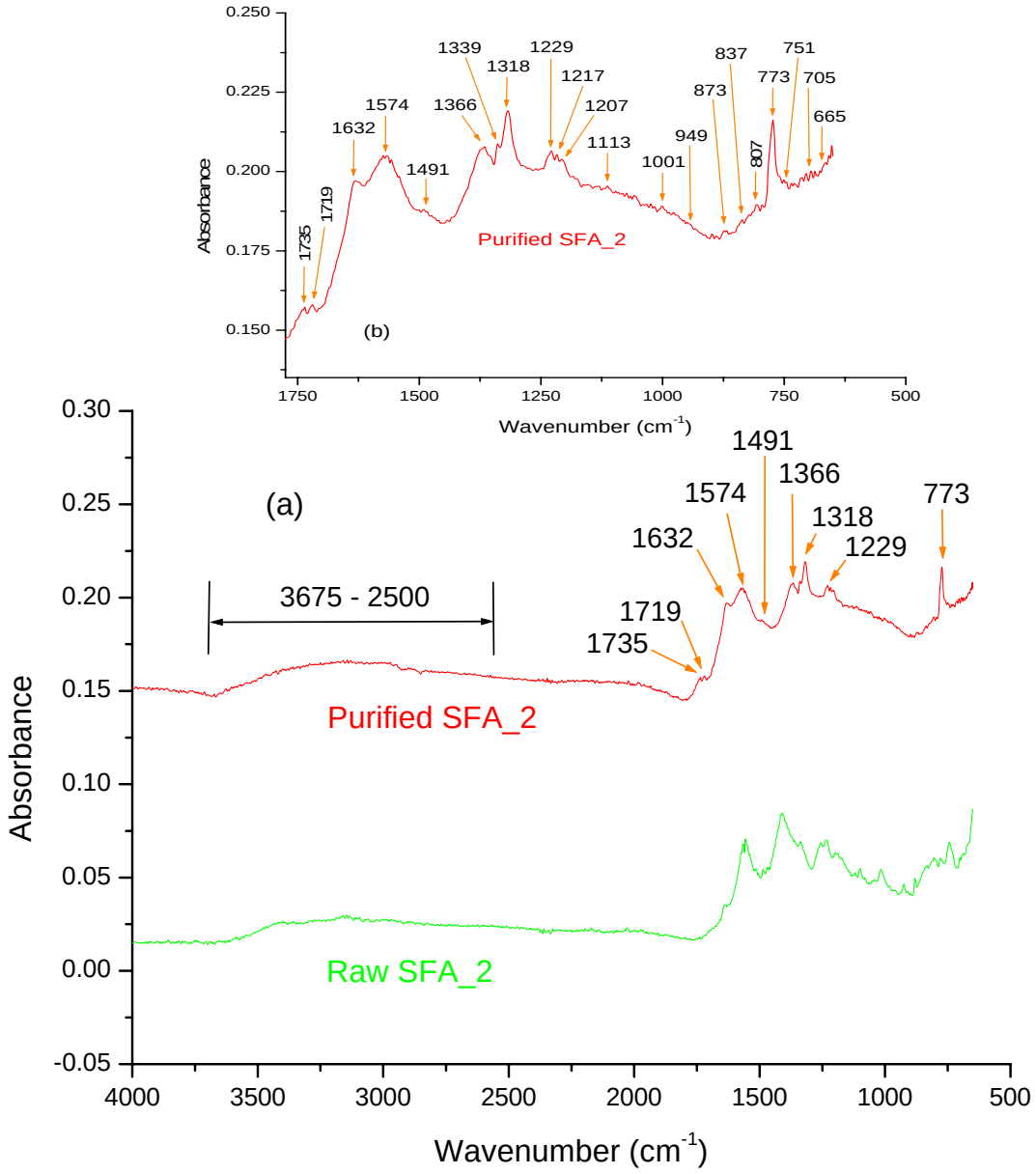

Figure 2.33. ATR-FTIR spectrum of raw and purified SFA_2. T = 25°C, P = 0.1 MPa. (a) complete spectrum; (b) enlargement of the lower wavenumber portion of the spectrum.

- ✓ 3700 – 2500 cm^{-1}: this first group results from five distinct absorption bands, including
  - ❖ a νO–H stretching mode of alcohol O–H functional groups (3700 – 3300 cm^{-1})
  - ❖ a νO–H stretching mode of associated O–H of carboxylate functional groups (3000 – 2500 cm^{-1})
  - ❖ a νC–H stretching mode of aromatic C–H groups (3075 – 3030 cm^{-1})

- ❖ antisymmetric ν_aCH_3 and ν_aCH_2 stretching modes of *n*-alkanes (2970 – 2915 cm^{-1})
- ❖ symmetric ν_sCH_3 and ν_sCH_2 stretching modes of *n*-alkanes (2880 – 2845 cm^{-1})

✓ 1750 – 1400 cm^{-1}: the second group of absorption bands is characterized by the presence of two small but distinct bands at 1719 and 1735 cm^{-1}. These two bands could correspond to the νC=O stretching mode of four different functional groups: ketones, aldehydes, aliphatic or aromatic esters, or dimers of carboxylic acids (Parker, 1971; Wojtkowiak and Chabanel, 1977).

The distinct band at 1632 cm^{-1} probably corresponds to the νC=C stretching mode of a C=C bond in an aromatic ring conjugated with another C=C bond in another aromatic ring (such as in the case of biphenyl), or with a C=O bond.

The absorption band at 1574 cm^{-1} is assigned to the antisymmetric ν_aOCO^- stretching mode of the carboxylate functional group.

The small but distinct band at 1491 cm^{-1} characterizes the νC=C stretch of aromatic rings.

✓ 1400 – 900 cm^{-1}: the presence of a broadband near 1380 – 1360 cm^{-1} corresponds to the symmetric δ_sCH_3 bending of the acetate species.

The two bands at 1318 and 1339 cm^{-1} probably correspond to the νC–O stretching mode of the acetate ion in two different environments.

The broadband near 1229 cm^{-1} could represent two different vibration modes (Wojtkowiak and Chabanel, 1977):

- ❖ the νC–O stretching mode of carboxylic acids (1320 – 1210 cm^{-1})
- ❖ the antisymmetric $\nu_aC–O–C$ stretching mode of aromatic ethers Ar–O–Ar (1270 – 1230 cm^{-1}).

The two distinct bands at 1207 and 1217 cm^{-1} as well as a broadband in the range 1200 – 900 cm^{-1} corresponds to the δCH in-plane bending mode of aromatic rings (1225 – 950 cm^{-1}) in different environments. Note that the 1200 – 900 cm^{-1} broadband could also represent two different vibration modes:

- ❖ the νC–O stretching mode of alcohol functional groups (1200 – 1000 cm^{-1})
- ❖ the symmetric $\nu_sC–O–C$ stretching mode of ether (1150 – 1100 cm^{-1}).

✓ 900 – 650 cm^{-1}: the fourth group of absorption bands includes a major and distinct band at 773 cm^{-1}, three minor bands at 807, 837 and 873 cm^{-1}, as well as one group of

minor bands in the range 730 – 700 cm^{-1}. These bands can be assigned as follows (Wojtkowiak and Chabanel, 1977):

- ❖ the major band at 773 cm^{-1} characterizes the δC-H out-of-plane bending mode of aromatic derivatives with three substitutions at positions 1, 2, and 3 (810 – 750 cm^{-1})
- ❖ the minor band at 873 cm^{-1} can be assigned to the δC-H out-of-plane bending mode of aromatic derivatives with either four substitutions at positions 1,2,3,5 or 1,2,4,5, or five substitutions (880 – 840 cm^{-1}). The two minor bands at 807 and 837 cm^{-1} can be assigned to the δC-H out-of-plane bending mode of aromatic derivatives with either three substitutions at positions 1,2,4 (860 – 800 cm^{-1}), or four substitutions at positions 1,2,3,4 (860 – 800 cm^{-1}).
- ❖ the group of minor bands in the range 730 – 700 cm^{-1} corresponds to the δC-C out-of-plane bending mode of aromatic derivatives with three substitutions at positions 1,2,3 or 1,2,4 (730 – 685 cm^{-1}).

2.5. UV-Visible absorption spectrophotometry

The UV-visible absorption spectra of the raw SFA_2 (0.022 $g \cdot L^{-1}$; pH = 10.240), purified SFA_2 (0.022 $g \cdot L^{-1}$; pH = 10.654), as well as of catechol (0.022 $g \cdot L^{-1}$; pH = 10.478) are presented in Figure 2.34. The measurements were made with a 10 mm path length quartz cuvette. The absorption spectrum of acetic acid is not shown since this compound only absorbs at 204 nm. Catechol at pH = 10.478 is characterized by an intense absorption band at 275 nm and a minor and broad absorption band with a maximum near 327 nm.

The UV-visible absorption spectrum of an aqueous solution of the raw SFA_2 at pH = 10.240 displays a shape similar to that of pure catechol at a similar pH value, but with much less absorption intensity than pure catechol.

Unlike raw SFA_2, the UV-visible absorption spectrum of an aqueous solution of the purified SFA_2 at pH = 10.654 is characterized by a strong absorption in the range 200 – 800 nm. The compounds which constitute the purified SFA_2 mixture are characterized by three broadbands near 230, 280, and 350 nm which can be interpreted as follows:

- ✓ the first broadband around 230 nm could result from two types of bands, including aromatic E_2 bands and conjugated *K* bands
- ✓ the second broadband around 280 nm corresponds either to benzenoid *B* bands or to forbidden $n \rightarrow \pi^*$ transitions. The latter bands originate from *n*-*p* conjugation between

nonbonded *n* or *p* electrons from oxygen atoms attached to two aromatic rings, such as in diphenyl ether

- ✓ the last broadband in the 350 nm region probably results from the hyperconjugation of π electrons of aromatic rings which are bonded to one another by two types of chemical bonds, including $C_{aromatic} - C_{aromatic}$ bonds between two aromatic rings such as in biphenyl, and aromatic ether bonds $C_{aromatic} - O - C_{aromatic}$ such as in diphenyl ether.

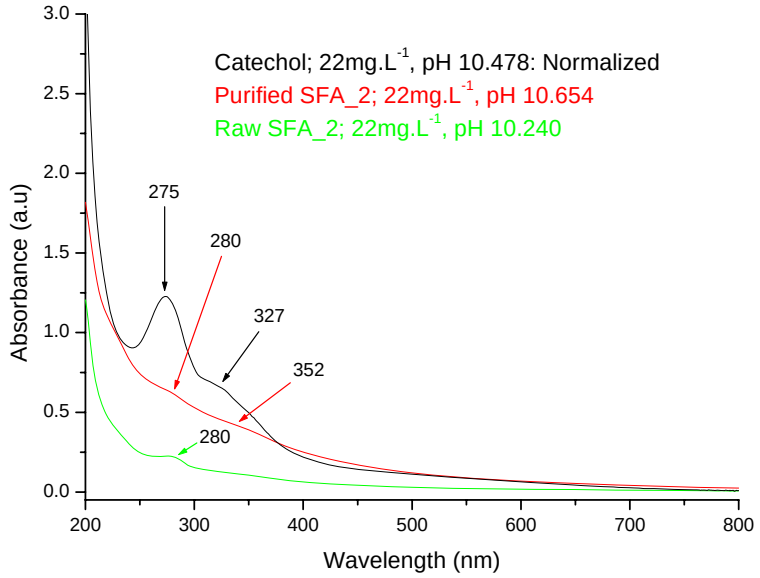

Figure 2.34. UV-Visible spectra of raw SFA_2 (green spectrum), purified SFA_2 (red spectrum), and catechol (black spectrum).

The presence of broadbands in the spectrum of the purified SFA_2 indicates that SFA_2 consists of a mixture of species of relatively high molecular mass with numerous atoms. The effect of the concentration on the absorption intensity can be evaluated from Figure 2.35, where the absorption spectra of purified SFA_2 are shown for two different concentrations at pH ~ 7. The absorption intensity appears to be multiplied by a factor of 2 in the wavelength range 250 – 600 nm with increasing concentration from 0.022 to 0.044 $g \cdot L^{-1}$. However, the effect of the concentration on the absorption intensity does not appear to be respected in the ultraviolet region (< 250 nm) of the spectrum. No reasonable interpretation can be given for this anomaly at the present time.

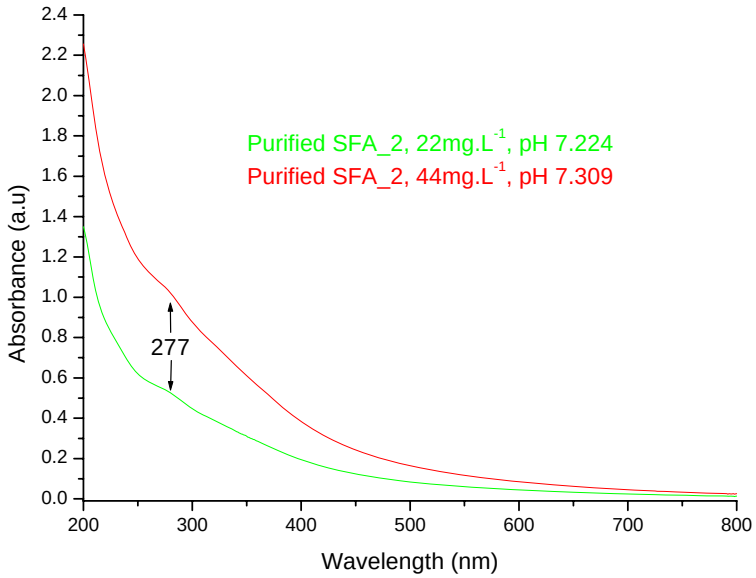

Figure 2.35. UV-Visible spectra of purified SFA_2 as a function of concentration at pH ~ 7.

The effect of pH on the absorption intensity of purified SFA_2 is shown in Figure 2.36. It can be deduced from this figure that increasing pH by three units and a half between 7.2 and 10.7 leads to an increase of approximately 1.2 units of the absorption intensity without modifying the shape of the absorption spectra. The hyperchromic effect is also accompanied by a slight bathochromic shift. The bathochromic effect observed in the basic pH solution probably results from the ionization of a majority of alcohol functional groups in the SFA_2 molecules, which increases the number of nonbonded electrons on the oxygen atoms of the alcohol functional groups and consequently of the $n \rightarrow \pi^*$ transitions under UV-visible excitation. As a result, the ionized alcohol species is colored and absorbs more with a bathochromic shift.

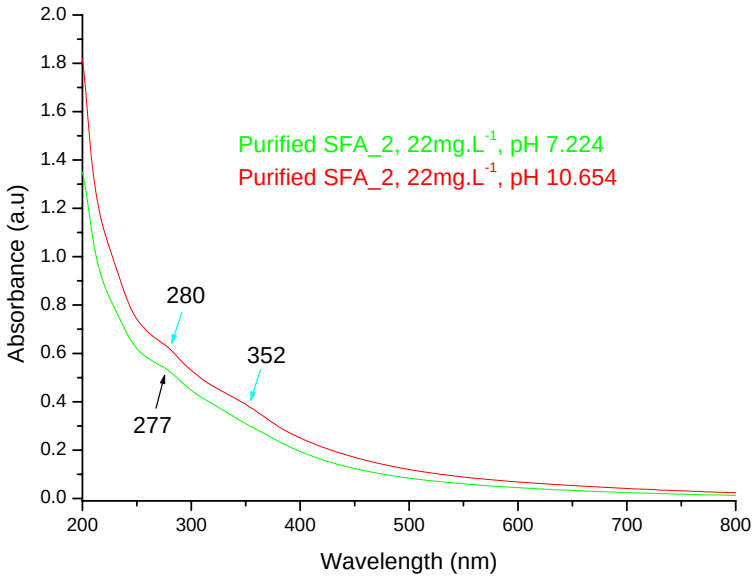

Figure 2.36. UV-Visible spectra of purified SFA_2 as a function of pH at a concentration of 0.022 $g \cdot L^{-1}$.

2.6. Electrospray ionization – mass spectrometry (ESI-MS)

A solution of the lyophilized, raw SFA_2 was prepared by dissolving a small amount of the sample in milli-Q water. This sample was subsequently analyzed by ESI-MS both in positive-ion (PI) and negative-ion (NI) modes. The purified SFA_2 was analyzed along with the raw SFA_2 by LC-APCI-MS-MS and APCI-MS, which will be discussed in the next section. It has been noted that the ionization was much better under the PI mode, which prompted us to add formic acid to the solution of raw SFA_2 to increase the ionization in the NI mode. The spectra obtained under the PI and NI modes are shown in Figures 2.37 and 2.38, respectively.

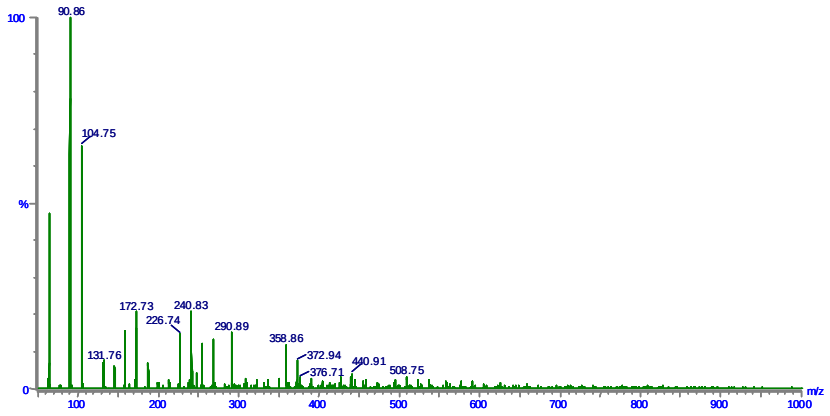

Figure 2.37. ESI-MS spectrum of raw SFA_2 analyzed under positive ion mode.

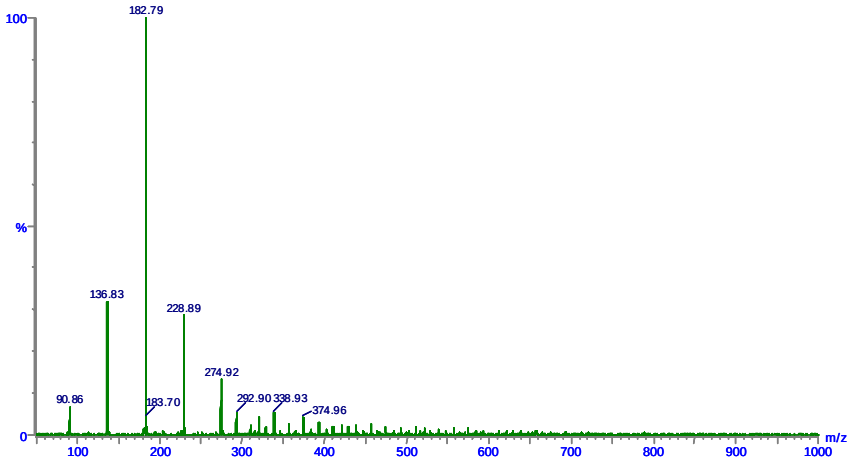

Figure 2.38. ESI-MS spectrum of raw SFA_2 analyzed under negative ion mode.

Several peaks can be observed over the 0 – 600 m/z range in both spectra. These peaks are identified in Table 2.12 with their m/z values and possible chemical formulas approaching or coinciding with these m/z values. Not listed however in Table 2.12 are the peaks with m/z equal to 90.86 and 131.76 for the analysis in PI mode, and 90.86 and 136.83 for the analysis in NI mode. No chemical formulas were found coinciding with these m/z values. The chemical formulas shown in Table 2.12 were established by considering the possibility that Na^+ or H^+ ions formed during the ionization process, or in some cases H_2O molecules, could be attached to the synthetic fulvic acid ions. These Na^+ or H^+ ions and H_2O molecules are indicated in grey in Table 2.12, as are the molecular weights corresponding to the sum of the actual single fulvic acid molecules and their associated Na^+ or H^+ ions, or H_2O molecules. Tentative molecular structures corresponding to the m/z ratios and chemical formulas listed in Table 2.12 are shown in Figure 2.39. The Na atoms appearing in some of the structures results from the NaOH which is used to buffer the pH of the solution during the synthesis. Note that in some cases, different structures with different chemical formulas may correspond to the same m/z ratio. This is the case in Table 2.12 for the m/z values equal to 291 and 359 (PI mode). In contrast, the peaks at m/z equal to 377 under PI mode and at m/z equal to 375 under NI mode coincide with the same molecule which has a molecular weight of 358 and is associated with one molecule of water. The molecular structures depicted in Figure 2.39 represent (a) sodium acetate; (g) a monomer; (b), (e) and (f) are dimers; (c) a trimer and (d) a tetramer. As was the case for SFA_1, the aromatic rings show a high degree of substitution, and are linked to one another through aromatic C–C or aromatic ether bonds. Structures (d) and (e) in Figure 2.39 are a tetramer and a dimer of quinone respectively. It can be noted in

Table 2.12 that many of the proposed chemical formulas and molecular structures are the same as those proposed for SFA_1.

Table 2.12. Summary of m/z ratios obtained in the ESI-MS analysis (PI and NI modes) of the raw SFA_2, together with their corresponding molecular weights and possible chemical formulas for individual compounds in the SFA_2 mixture.

m/z	Chemical Formula	Molecular weight		Structure in Figure 2.39
Positive ion mode				
104.75	$[C_2H_3O_2Na\ (+ Na)]^+$	82.00	(104.99)	(a)
172.73	$[C_6H_4O_2Na_2\ (+ H_2O + H)]^+$	154.00	(173.02)	(g)
226.74	$[C_6H_3O_4Na_3\ (+ H_2O + H)]^+$	207.97	(226.99)	Structure (c) in Figure 2.8
240.83	$[C_{12}H_9O_4Na\ (+ H)]^+$	240.03	(241.05)	(b)
290.89	$[C_{12}H_9O_6Na\ (+ H_2O + H)]^+$	272.19	(291.21)	Structure (g) in Figure 2.8
	$[C_{12}H_7O_5Na\ (+ 2\ H_2O + H)]^+$	268.20	(291.05)	Structure (h) in Figure 2.8
358.86	$[C_{12}H_6O_5Na_4\ (+ 2\ H_2O + H)]^+$	322.13	(359.17)	Structure (i) in Figure 2.8
	$[C_{18}H_{14}O_8\ (+ H)]^+$	358.07	(359.08)	(c)
372.94	$[C_{12}H_7O_5Na_3\ (+ 4\ H_2O + H)]^+$	300.00	(373.05)	Structure (o) in Figure 2.16
376.71	$[C_{18}H_{14}O_8\ (+ H_2O + H)]^+$	376.08	(377.09)	(c)
440.91	$[C_{18}H_{12}O_7Na_2\ (+ 3\ H_2O + H)]^+$	386.26	(441.08)	Structure (j) in Figure 2.8
508.75	$[C_{24}H_{12}O_9Na_2\ (+ H_2O + H)]^+$	490.03	(509.05)	(d)
Negative ion mode				
182.79	$[C_6H_5O_3Na\ (+ 2\ H_2O - H)]^-$	154.12	(183.03)	Structure (c) in Figure 2.8
228.89	$[C_{12}H_6O_5\ (- H)]^-$	230.02	(229.01)	(e)
274.92	$[C_{12}H_9O_4\ (+ 2\ H_2O - H)]^-$	276.06	(275.05)	(b)
292.90	$[C_{12}H_8O_6Na_2\ (- H)]^-$	293.00	(293.00)	(f)
338.93	$[C_{18}H_{10}O_6\ (+ H_2O - H)]^-$	322.05	(339.05)	Structure (b) in Figure 2.10
374.96	$[C_{18}H_{14}O_8\ (+ H_2O - H)]^-$	376.08	(375.07)	(c)

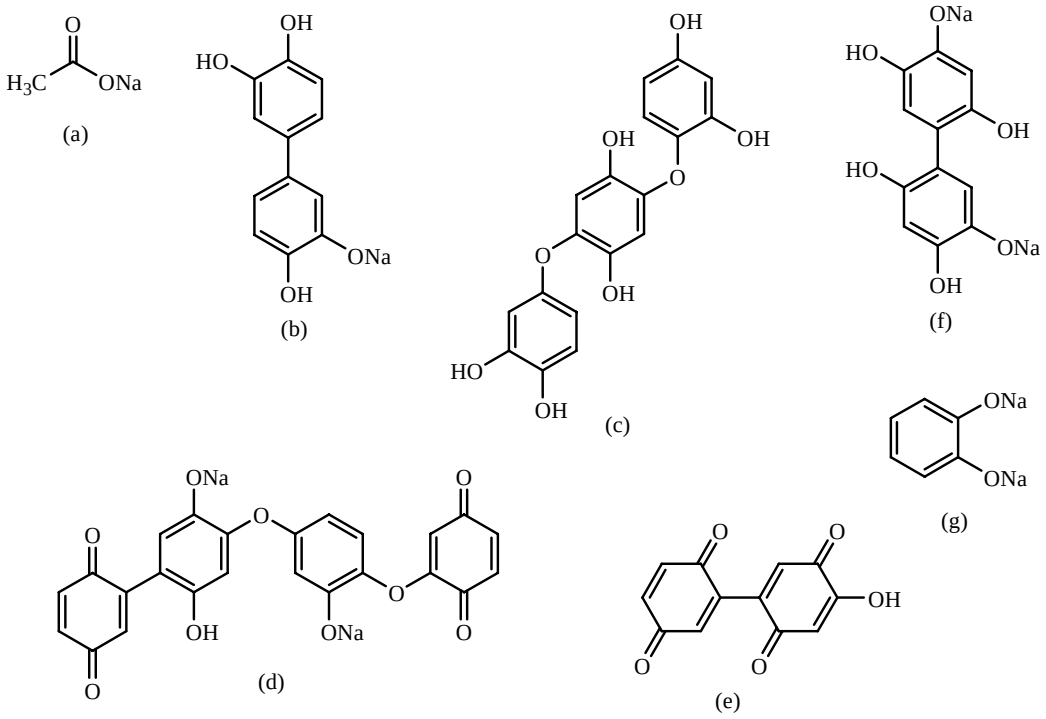

Figure 2.39. Possible molecular structures of individual fulvic acids in the raw SFA_2 mixture derived from the ESI-MS analysis.

2.7. Atmospheric pressure chemical ionisation mass spectrometry (APCI-MS)

Despite the identification of several compounds, it appears that the SFA_2 did not ionize significantly during the ESI-MS analysis reported above. This may have been due either to a low concentration of the compounds present in the SFA_2 mixture, or to the lack of separation before the analysis. This prompted us to further analyze both the raw and purified SFA_2 mixtures by atmospheric pressure chemical ionization mass spectrometry (APCI-MS), coupled to liquid chromatography and using tandem mass spectrometry (LC-APCI-MS-MS) in the case of the raw SFA_2. In addition, the methanol extract of the raw SFA_2 was also analyzed by APCI-MS. We found again this technique to give better results for the characterization of our SFA_2 mixtures. The protocols and results obtained for each of the samples are discussed separately below.

2.7.1. Analysis of raw SFA_2 by LC-APCI-MS-MS

The analysis of the raw SFA_2 mixture was performed by tandem mass spectrometry (MS/MS) after first separating the components of the mixture by liquid chromatography (LC) using a U3000 Dionex liquid chromatograph interfaced with a Bruker micro Q-ToF mass spectrometer. A saturated solution of raw SFA_2 was prepared by dissolving lyophilized solid SFA_2 in milli-Q water containing 0.2 % by volume of formic acid to favor ionization of the

fulvic acid components during the analysis. The resulting solution was filtered through a 0.45 μm millex®-HA filter unit. The pH of the solution was lowered to pH ~ 5-8 using formic acid prior to injecting the sample on the LC column. The different parameters used in the LC-ACPI-MS-MS analysis of raw SFA_2 are the same as those given in Table 2.4, section 1.7.1.

The tandem mass spectrometry analysis was performed in an automatic mode. Again, peaks showing intensity higher than 5000 (in arbitrary units) were those selected for the fragmentation in collision cells using the following parameters:

m/z	isolation width	collision energy
300	8 Da	10 V
500	10 Da	15 V
1000	10 Da	20 V

As was previously done in the case of SFA_1, the base peak chromatograms (BPC) shown in Figure 2.40 are for retention times ranging between 0 and 30 minutes. With the exception of a wide peak appearing between 27 and 28 minutes in negative mode, it can be deduced from Figure 2.40 that all the compounds present in the SFA_2 mixture were eluted before 15 minutes in both positive and negative modes. Each peak probably corresponds to a series of compounds with similar elution times rather than a single compound.

The peaks appearing after 1.1 minute of elution in Figure 2.40 in both PI and NI modes correspond to clusters of sodium formate (HCOONa). Under NI mode, the clusters of sodium formate are represented by $[(HCOONa)_n - Na]^-$ where n designates the number of sodium formate molecules in a given cluster. The APCI-MS peaks with m/z values equal to 317, 385, 453, 521, 589, 657 and 725 in Figure 2.41 A correspond to sodium formate clusters with n = 5, 6, 7, 8, 9, 10 and 11. We could however not assign any n value for the peaks at m/z equal to 809, 877 and 966. Under PI mode, the clusters of sodium formate are represented by $[(HCOONa)_n + Na]^+$. The APCI-MS peaks with m/z values equal to 363, 431, 499 and 1043 in Figure 2.41 B correspond to sodium formate clusters with n = 5, 6, 7 and 15.

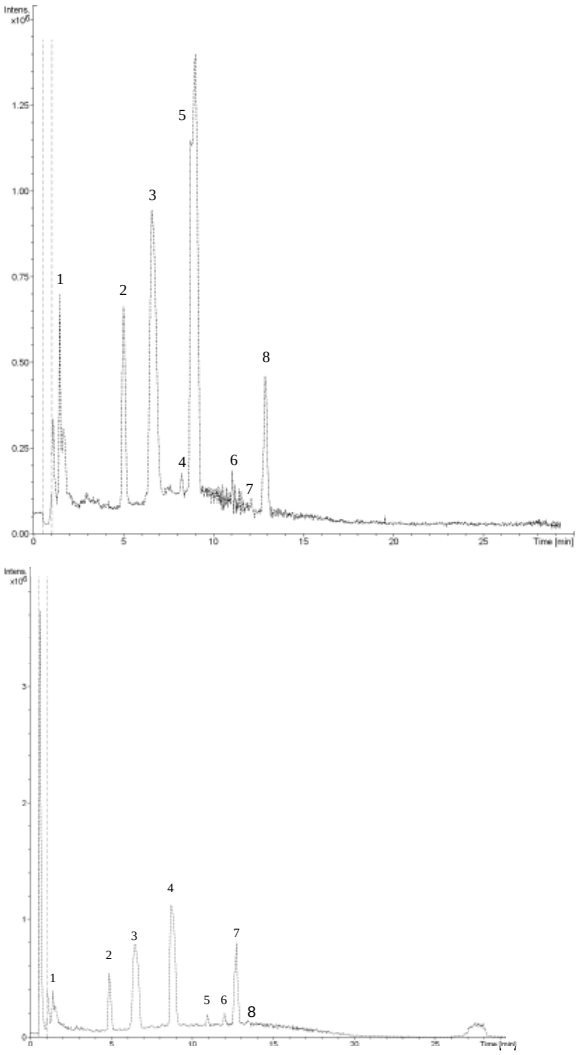

Figure 2.40. Base peak chromatograms (BPC) obtained in the LC-APCI-MS-MS of the raw SFA_2 mixture in positive mode (top) and negative mode (bottom). Peaks have been numbered to facilitate discussion.

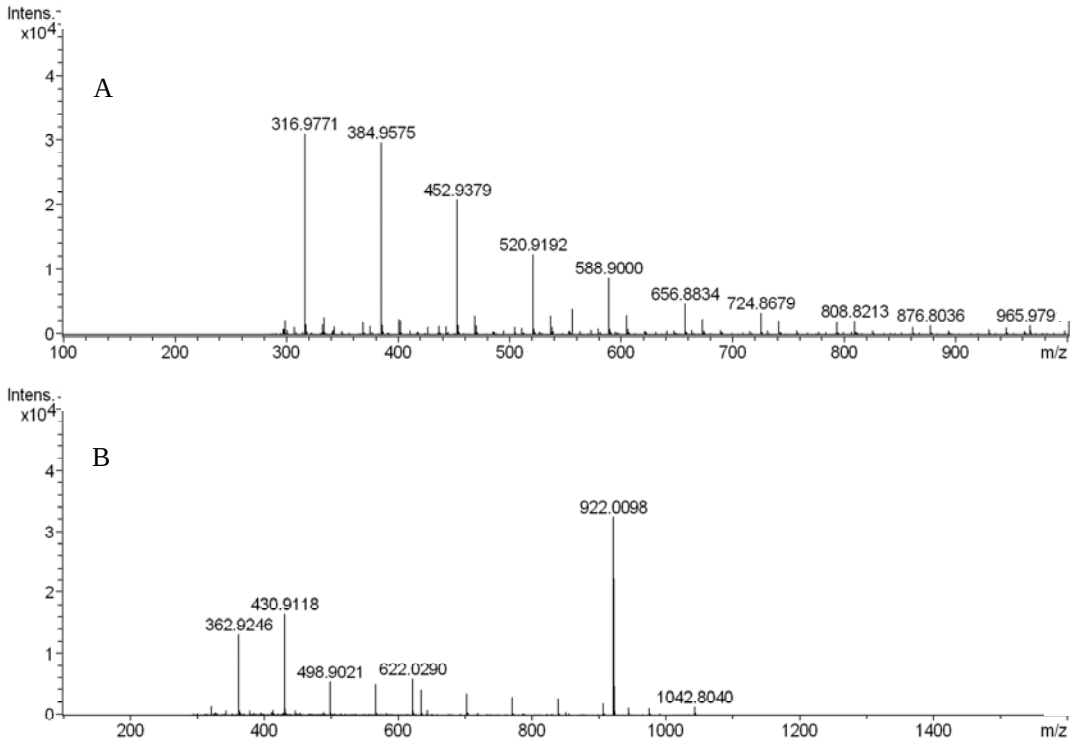

Figure 2.41. APCI-MS spectra of the raw SFA_2 fraction eluted at 1.1 minutes and analyzed in negative (A) and positive (B) modes.

The retention times corresponding to selected chromatographic peaks identified in Figure 2.40 are listed in Table 2.13 along with the results of the mass spectrometry analysis. The selection of peaks was rendered necessary for clarity reasons in the discussion which is presented below. Also listed in Table 2.13 are possible chemical formulas and molecular weights corresponding to the m/z values. The difference between these molecular weights and the m/z values is usually within 0.3 Da, and in some instances 3 mDa. The mass spectra corresponding to retention times of 8.9 minutes (both positive and negative ion mode) and 12.4 minutes (negative ion mode) are shown in Figures 2.42 and 2.43, respectively. The molecular structures corresponding to the chemical formulas proposed in Table 2.13 are depicted in Figure 2.44.

Table 2.13. Summary of the LC retention times (RT) corresponding to the peaks identified by numbers in Figure 2.40 and of the m/z ratios obtained in the LC-APCI-MS-MS analysis (positive and negative modes) of the raw SFA_2 mixture, as well as of possible chemical formulas and corresponding molecular weights for individual fulvic acids in the raw SFA_2 mixture.

Peak number (Fig. 2.40)	RT (min)	m/z	Chemical formula	Molecular weight	Structure (Fig. 2.44)
Positive mode					
4	8.9	330.9757	$[C_{12}H_6O_5Na_2 + 3\ H_2O + H]^+$	331.041	(a)
		449.0185	$[C_{18}H_{13}O_{10}Na + 2\ H_2O + H]^+$	449.070	(b)
		493.0062	$[C_{18}H_{11}O_{10}Na_3 + 2\ H_2O + H]^+$	493.033	Structure (o) in Fig. 2.10
		514.9965	$[C_{18}H_{10}O_{10}Na_4 + 2\ H_2O + H]^+$	515.015	Structure (q) in Fig. 2.10
		537.0072	$[C_{18}H_9O_{10}Na_5 + 2\ H_2O + H]^+$	536.997	Structure (s) in Fig. 2.10
		598.9726	$[C_{30}H_{21}O_{11}Na + H_2O + H]^+$	599.117	(c)
		804.9951	$[C_{42}H_{28}O_{17} + H]^+$	805.151	(d)
5	9.4	453.3431	$[C_{18}H_{12}O_{10}Na_2 + H_2O + H]^+$	453.041	Structure (l) in Fig. 2.10
		453.3431	$[C_{24}H_{18}O_8 + H_2O + H]^+$	453.119	Structure (m) in Fig.2.10
7	12.1	401.0228	$[C_{18}H_{13}O_7Na + 2\ H_2O + H]^+$	401.085	Structure (i) in Fig. 2.10
		419.0325	$[C_{18}H_{13}O_7Na + 3\ H_2O + H]^+$	419.095	Structure (i) in Fig. 2.10
		441.0152	$[C_{18}H_{12}O_7Na_2 + 3\ H_2O + H]^+$	441.077	Structure (k) in Fig. 2.10
8	12.9	389.0216	$[C_{18}H_{12}O_6Na_2 + H_2O + H]^+$	389.061	(e)
		411.0034	$[C_{18}H_{11}O_6Na_3 + H_2O + H]^+$	411.043	(g)
		478.9921	$[C_{24}H_{16}O_8Na_2 + H]^+$	479.072	(h)
		777.0431	$[C_{42}H_{30}O_{14} + H_2O + H]^+$	777.182	(i)
Negative mode					
3	6.7	301.0473	$[C_{12}H_6O_5 + 4\ H_2O - H]^-$	301.056	(j)
		343.0316	$[C_{18}H_{14}O_6 + H_2O - H]^-$	343.082	Structure (e) in Fig. 2.10
		349.0778	$[C_{12}H_7O_7Na_3 + H_2O - H]^-$	348.991	Structure (e) in Fig. 2.10
		393.0623	$[C_{18}H_{14}O_6 + HCOONa - H]^-$	393.059	Structure (e) in Fig. 2.10
		411.0118	$[C_{18}H_{14}O_6 + H_2O + HCOONa - H]^-$	411.069	Structure (e) in Fig. 2.10
		478.9926	$[C_{24}H_{16}O_{11} - H]^-$	479.061	(k)
		627.0120	$[C_{30}H_{17}O_{10}Na + HCOONa - H]^-$	627.052	(l)
		694.9962	$[C_{36}H_{22}O_{14} + H_2O - H]^-$	695.104	(m)

Table 2.13. *(Continued)*.

Peak number (Fig. 2.40)	RT (min)	m/z	Chemical formula	Molecular weight	Structure (Fig. 2.44)
Negative mode					
4	8.9	285.0488	$[C_{12}H_{10}O_6 + 2\ H_2O - H]^-$	285.061	Structure (a) in Fig. 2.10
		355.0442	$[C_{18}H_{10}O_7 + H_2O - H]^-$	355.045	(f)
		425.0413	$[C_{18}H_{10}O_8 + 4\ H_2O - H]^-$	425.072	(n)
		403.0605	$[C_{18}H_{12}O_7Na_2 + H_2O - H]^-$	403.041	Structure (k) in Fig. 2.10
		513.0101	$[C_{18}H_{10}O_{10}Na_4 + 2\ H_2O - H]^-$	513.000	Structure (q) in Fig. 2.10
		580.9928	$[C_{30}H_{21}O_{10}Na + H_2O - H]^-$	581.106	(o)
		698.9927	$[C_{36}H_{26}O_{14} + H_2O - H]^-$	699.135	(p)
		758.9998	$[C_{36}H_{19}O_{15}Na_3 - H]^-$	759.034	(q)
		942.9735	$[C_{48}H_{30}O_{16}Na_2 + 2\ H_2O - H]^-$	943.146	(r)
6	12.4	316.9801	$[C_{12}H_{10}O_6 + HCO2Na - H]^-$	317.027	Structure (a) in Fig. 2.10
		400.9326	$[C_{18}H_{10}O_7Na_2 + H_2O - H]^-$	401.025	(s)
		449.0210	$[C_{24}H_{18}O_9 - H]^-$	449.087	(t)
		565.0097	$[C_{24}H_{16}O_9Na_2 + 4\ H_2O - H]^-$	565.093	(u)
		821.0167	$[C_{42}H_{28}O_{17} + H_2O - H]^-$	821.135	(v)
7	12.7	321.0674	$[C_{12}H_{10}O_6 + 4\ H_2O - H]^-$	321.082	Structure (a) in Fig. 2.10
			$[C_{18}H_{10}O_6 - H]^-$	321.040	Structure (b) in Fig. 2.10
		433.0313	$[C_{18}H_{12}O_{10}Na_2 - H]^-$	433.015	Structure (l) in Fig. 2.10
		501.0120	$[C_{24}H_{14}O_8 + 4\ H_2O - H]^-$	501.103	Structure (p) in Fig. 2.10
		595.0166	$[C_{30}H_{21}O_{12}Na - H]^-$	595.085	(w)
		753.0350	$[C_{36}H_{22}O_{13}Na_4 - H]^-$	753.057	(x)
		821.0174	$[C_{42}H_{28}O_{17} + H_2O - H]^-$	821.135	(v)
8	13.4	363.1124	$[C_{18}H_{13}O_7Na - H]^-$	363.048	Structure (i) in Fig. 2.10
		433.1089	$[C_{18}H_{12}O_{10}Na_2 - H]^-$	433.015	Structure (l) in Fig. 2.10
		565.0532	$[C_{24}H_{16}O_9Na_2 + 4\ H_2O - H]^-$	565.093	(u)
		633.0287	$[C_{30}H_{21}O_{11}Na + 3\ H_2O - H]^-$	633.122	(c)
		701.0107	$[C_{36}H_{26}O_{13} + 2\ H_2O - H]^-$	701.151	(y)
		784.9642	$[C_{36}H_{23}O_{13}Na_3 + 3\ H_2O - H]^-$	785.107	(z)

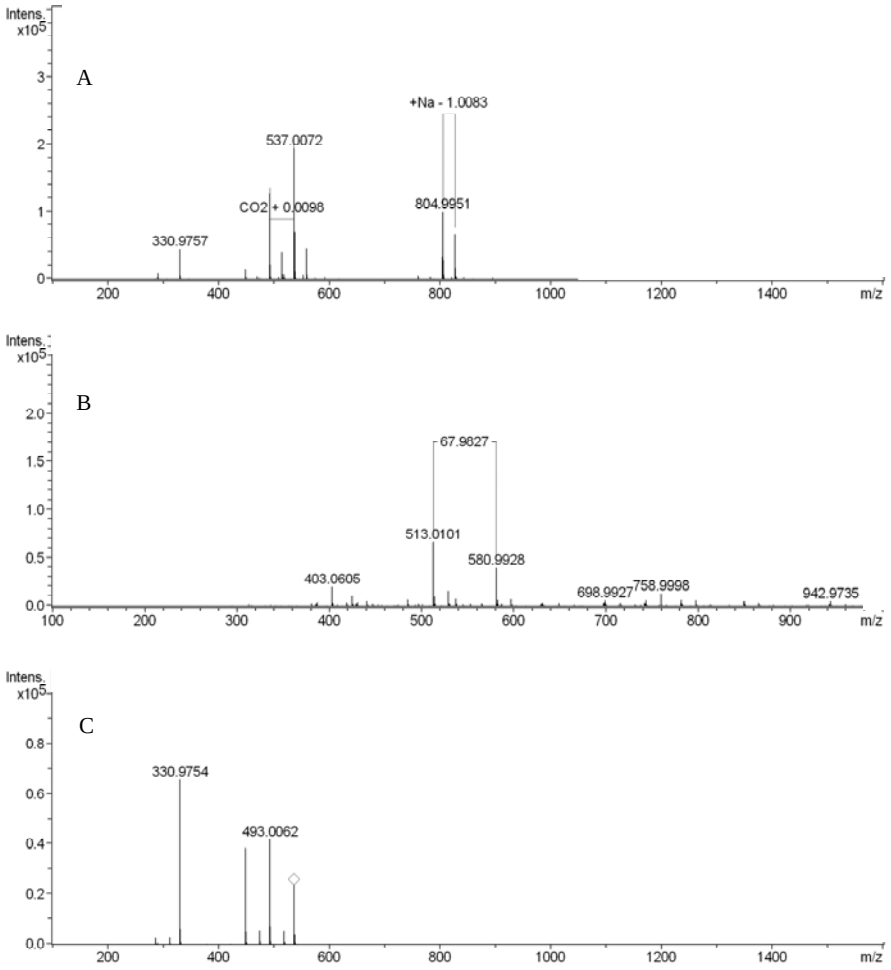

Figure 2.42. APCI-MS spectra of the raw SFA_2 fraction eluted at 8.9 minutes and analyzed in (A) positive and (B) negative modes, and (C) APCI-MS-MS spectrum obtained by fragmentation of the compound corresponding to the peak with m/z equal to 537 in (A).

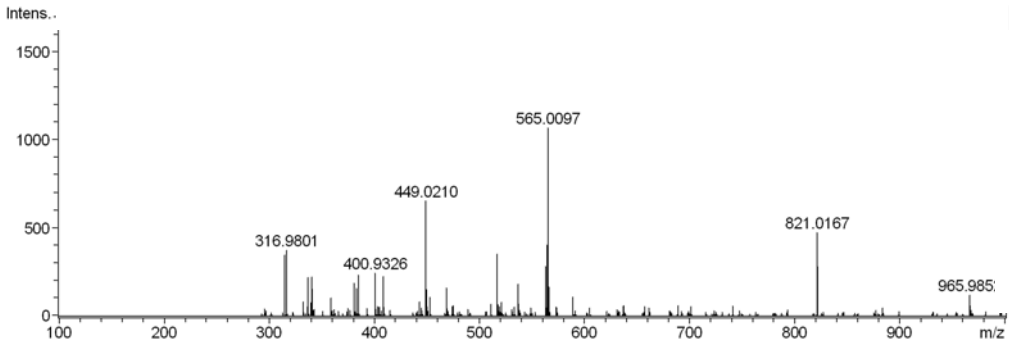

Figure 2.43. APCI-MS spectrum of the raw SFA_2 fraction eluted at 12.4 minutes and analyzed in negative mode.

In the case of the analysis carried out in positive ion mode, there appears to be similarities with the analysis carried out previously for SFA_1 when considering the retention times at 8.9 minutes (SFA_2) and 9.0 minutes (SFA_1 – see Table 2.5 above). Both synthetic

fulvic acid mixtures have m/z values of 493, 515, 537, 599 and 805 in common. The m/z values at 331, 449, 599 and 805 listed in Table 2.13 have been assigned to compounds with molecular structures identified by (a)-(d) in Figure 2.44 and corresponding successively to a dimer, a trimer, a pentamer, and a hexamer. Structures (a) and (d) are both quinones among other quinones; (f, j-n, and q-s) which have been presented in Figure 2.44. Again, all the proposed molecular structures are highly substituted on the aromatic rings. On the basis of a comparison between the APCI-MS analysis in both positive and negative ion mode for the chromatographic peak corresponding to the retention time of 8.9 minutes, the m/z values of 515 (PI mode) and 513 (NI mode) correspond to the same compound already identified in SFA_1. This compound has a molecular weight of 478 Da and corresponds to structure (q) in Figure 2.10. The tandem mass spectrometry analysis of the mass peak m/z equal to 537, which is common to both SFA_1 and SFA_2, is shown in Figure 2.42 C. This analysis yielded ions at m/z values of 331, 449 and 493, thereby confirming the ions observed earlier. It can be deduced from Table 2.13 that the postulated molecule for m/z = 537 is associated to two water molecules for analysis in both positive and negative ion modes.

Also shown in Figure 2.44 are proposed molecular structures for the ACPI-MS analysis of the chromatographic peak corresponding to the retention time of 12.4 minutes (peak 7 in Figure 2.40, bottom). The peaks with m/z values of 317, 401, 449, 565 and 821 in Figure 2.43 have been assigned to compounds with molecular structures corresponding to structure (a) in Figure 2.10 and structures (s), (t), (u) and (d) in Figure 2.44.

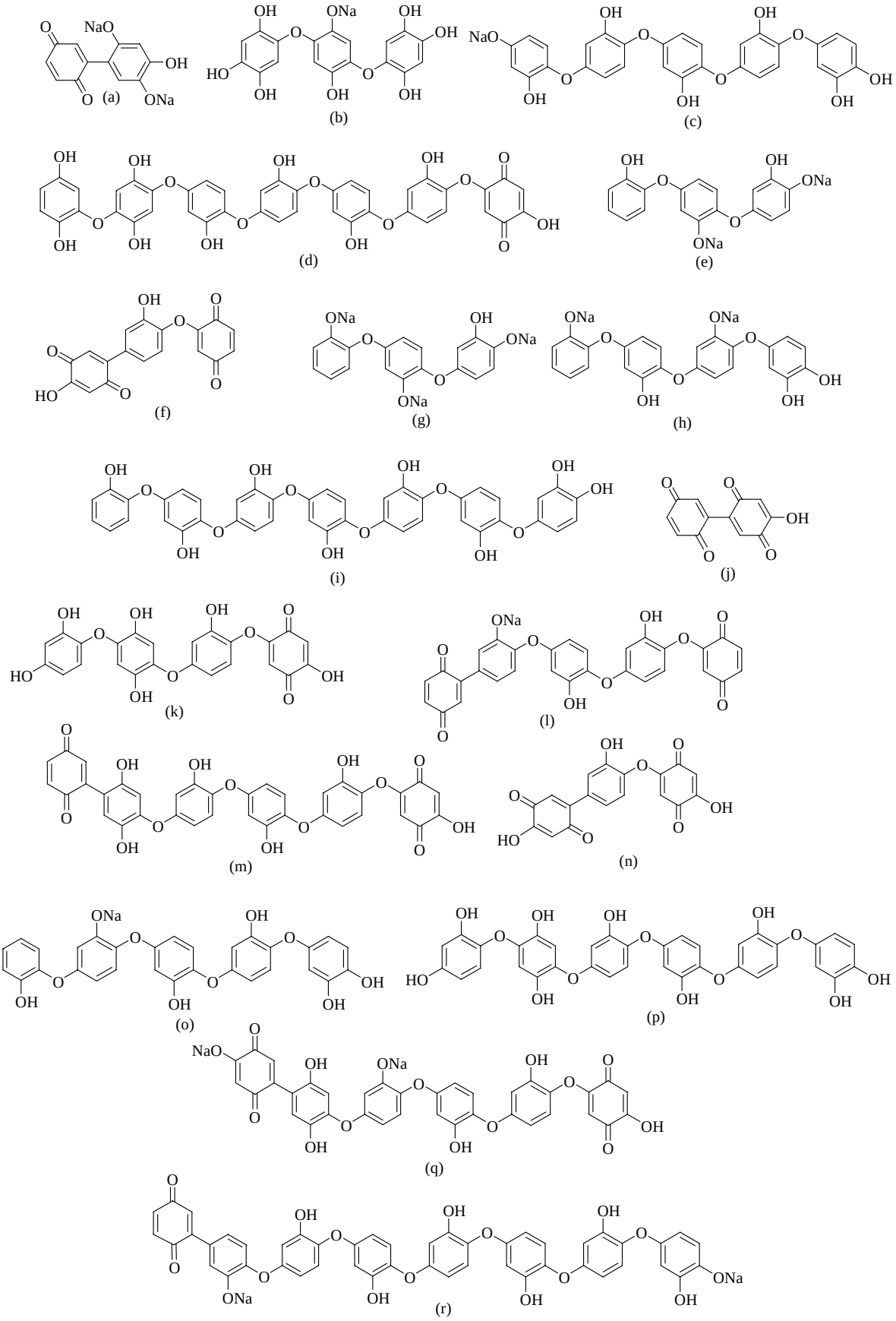

Figure 2.44. Possible molecular structures of individual fulvic acids in the raw SFA_2 mixture deduced from the LC-APCI-MS-MS analysis.

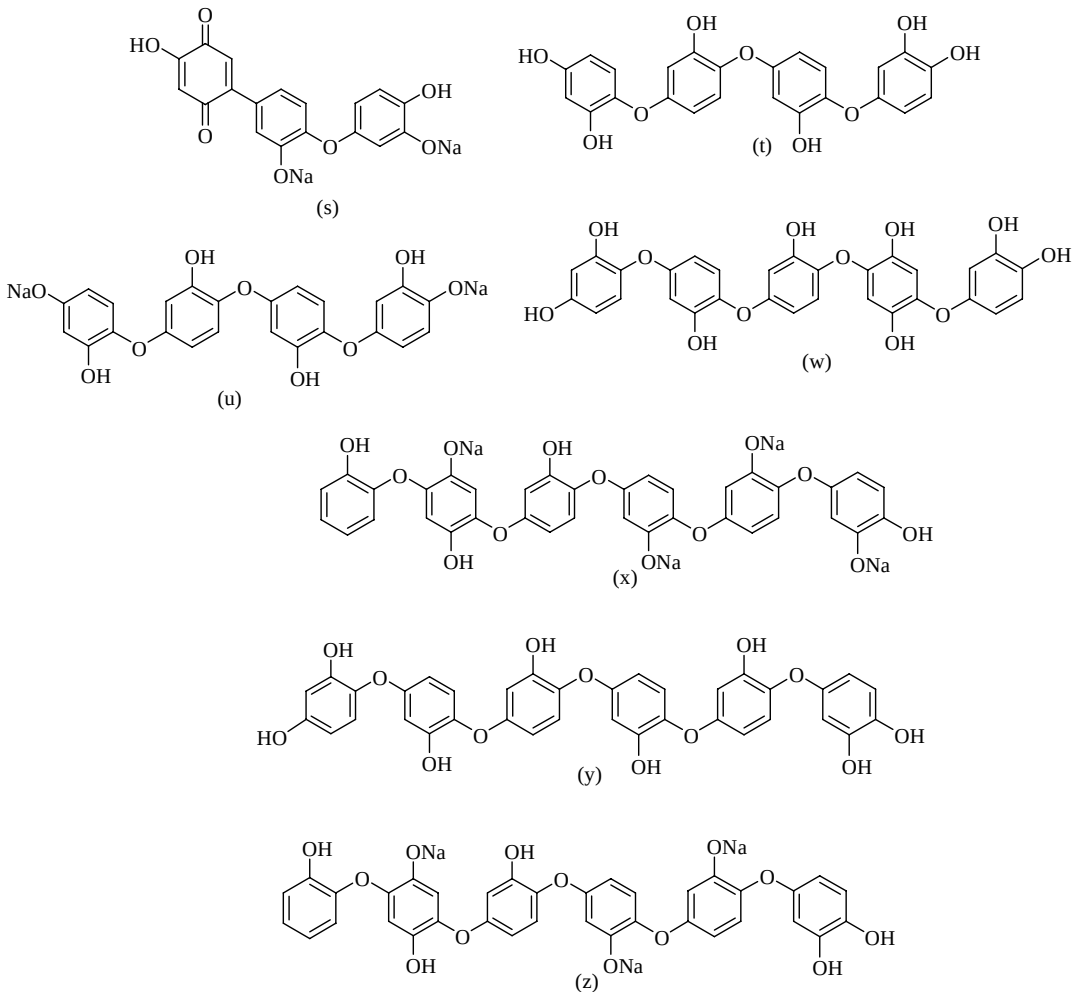

Figure 2.44. *(Continued).*

From the LC-APCI-MS and LC-APCI-MS-MS analyses discussed above and the molecular structures proposed in Figure 2.44, it appears that different oligomers have been synthesized by the polymerization of catechol and acetic acid; these are oligomers ranging from dimers to octamers. It should be pointed out that in the case of the oligomers with lower numbers of aromatic rings (e.g. trimers), these rings are highly substituted. Even though these rings are always linked to one another through ether linkages in the structures shown in Figure 44, it does not necessary imply that these aromatic rings may not be linked through aromatic carbon – carbon bonds.

2.7.2. Analysis of purified SFA_2 by APCI-MS

A saturated solution of purified SFA_2 was prepared by dissolving lyophilized solid purified SFA_2 in milli-Q water. The resulting solution was filtered through a 0.45 μm millex®-HA filter unit. The pH of the solution was not adjusted prior to the APCI-MS analysis, which was performed in both positive-ion and negative-ion modes. The obtained spectra are shown in Figure 2.45. The m/z ratio of 113 observed in Figure 2.45 A has not been assigned to any compound. The other m/z ratios identified in Figure 2.45 A-C have been listed in Table 2.14 along with possible corresponding formulas. The molecular structures corresponding to these chemical formulas either are shown in Figure 2.46 or have been previously discussed.

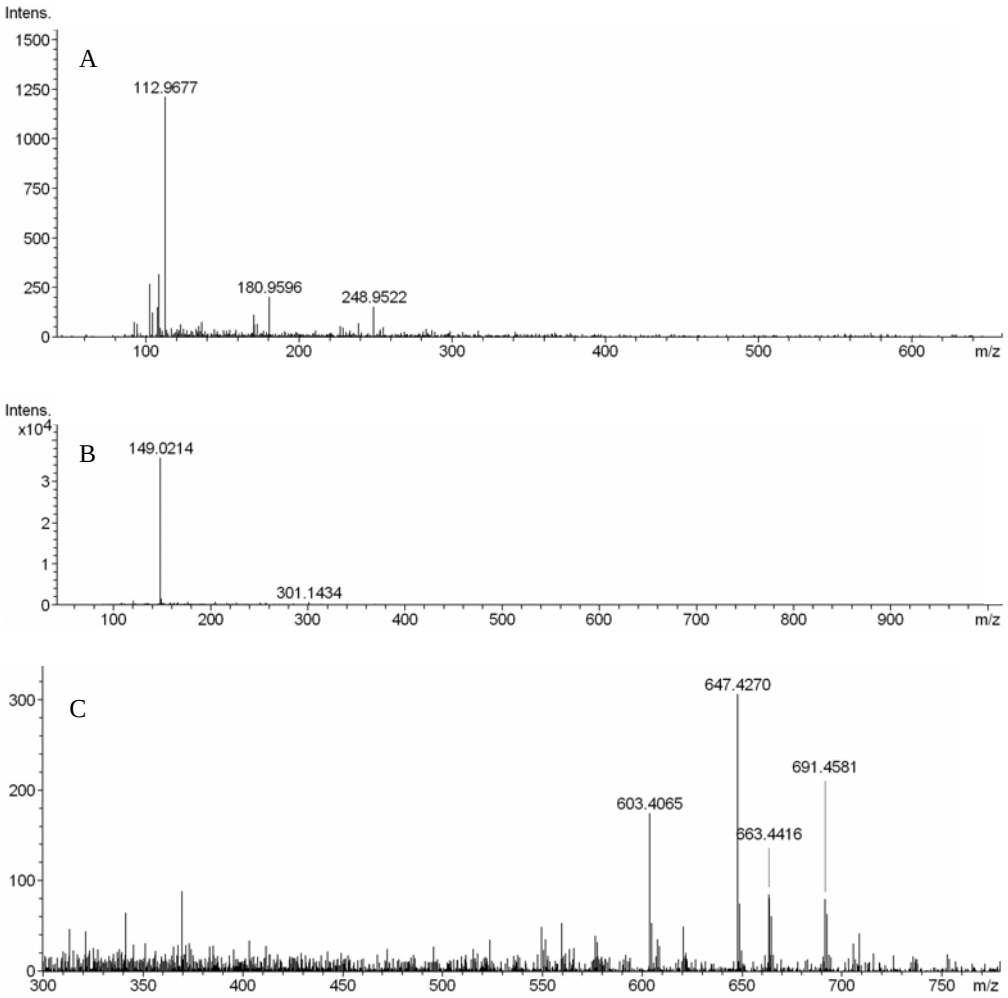

Figure 2.45. APCI-MS spectra of the purified SFA_2 mixture analyzed by ACPI-MS in (A) negative ion mode and (B and C) positive ion mode.

Table 2.14. Summary of the m/z ratios obtained in the APCI-MS analysis (positive and negative ion modes) of the purified SFA_2 mixture, as well as of possible chemical formulas and corresponding molecular weights for individual fulvic acids in the purified SFA_2 mixture.

m/z	Chemical formula	Molecular weight	Structure (Fig. 2.46) [a]
Positive mode			
149.0214	$[C_6H_6O_3 + Na]^+$	149.021	Structure (b) in Fig. 2.14
149.0214	$[C_6H_6O_3Na + H]^+$	149.021	Structure (c) in Fig. 2.14
301.1434	$[C_{12}H_6O_6 + 3\ H_2O + H]^+$	301.056	Structure (e) in Fig.2. 8
301.1434	$[C_{12}H_7O_5Na_3 + H]^+$	301.006	(a)
341.3048	$[C_{12}H_6O_5Na_4 + H_2O + H]^+$	340.999	Structure (i) in Fig. 2.8
369.3583	$[C_{18}H_{10}O_6Na_2 + H]^+$	369.035	(b)
369.3583	$[C_{12}H_7O_7Na_3 + 2\ H_2O + H]^+$	369.017	Structure (f) in Fig. 2.14
603.4065	$[C_{30}H_{20}O_{11}Na_2 + H]^+$	603.088	Structure (g) in Fig. 2.14
647.4270	$[C_{30}H_{18}O_{11}Na_4 + H]^+$	647.052	Structure (h) in Fig. 2.14
663.4416	$[C_{36}H_{22}O_{13} + H]^+$	663.114	(c)
691.4581	$[C_{30}H_{16}O_{11}Na_6 + H]^+$	691.016	Structure (i) in Fig. 2.14
Negative mode			
180.9596	$[C_6H_6O_2 + 4\ H_2O - H]^-$	181.071	Structure (a) in Fig. 2.14
248.9522	$[C_{12}H_{10}O_6 - H]^-$	249.040	Structure (f) in Fig. 2.8

[a] Unless indicated otherwise.

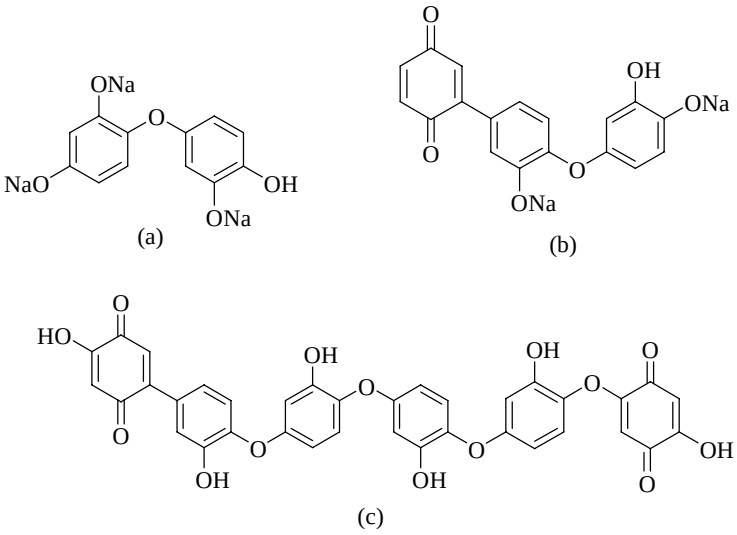

Figure 2.46. Possible molecular structures of individual fulvic acids in the purified SFA_2 mixture deduced from the APCI-MS analysis.

Only three new structures are shown in Figure 2.46, which have the same characteristics as before, i.e. highly substituted aromatic rings linked to one another by either aromatic ether or carbon – carbon bonds or both of them as in the case of structures (b and c). Quinonic structures are exhibited in structures (b) and (c).

2.7.3. Analysis by APCI-MS of the methanol extract obtained by solid-liquid extraction of raw SFA_2

A saturated solution of the methanol extract of SFA_2 was prepared by dissolving a small amount of the lyophilized, solid extract in milli-Q water. The resulting solution was filtered through a 0.45 μm millex®-HA filter unit. The pH of the solution was not adjusted prior to the APCI-MS analysis, which was again performed in both positive-ion and negative-ion modes. A good ionization was observed in both modes. The obtained spectra are shown in Figure 2.47. The m/z values observed in Figure 2.47 have been listed in Table 2.15, along with corresponding molecular weights and possible chemical formulas. The molecular structures corresponding to these formulas are shown in Figure 2.48.

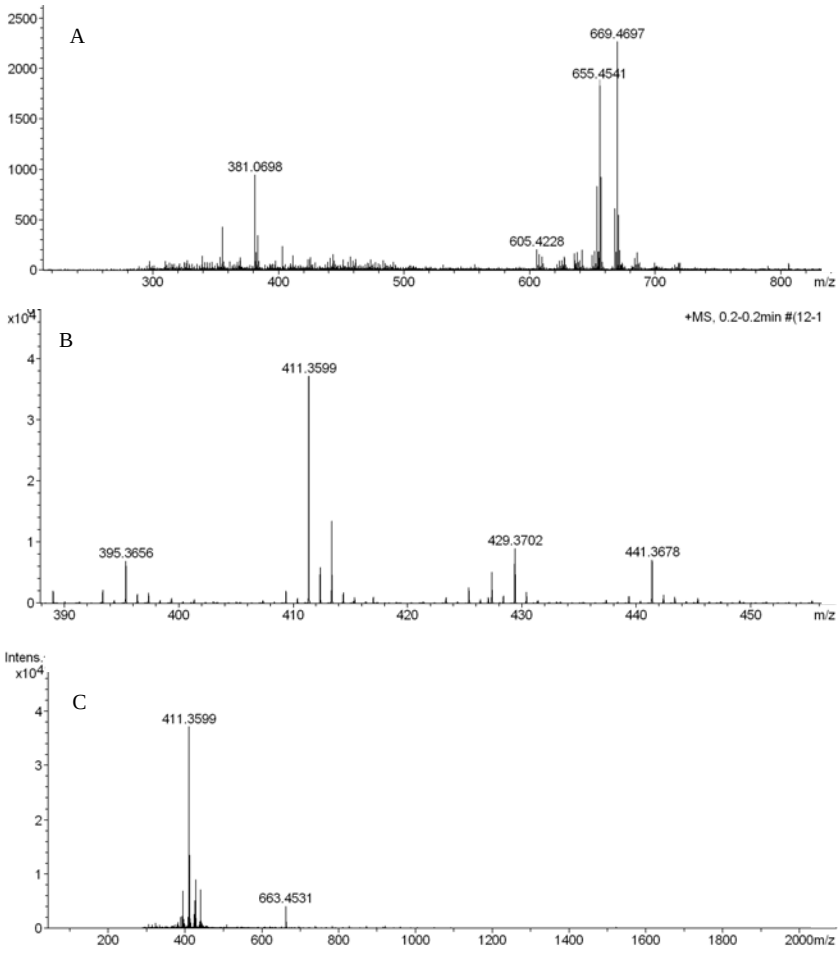

Figure 2.47. APCI-MS spectra of the methanol extract of SFA_2 analyzed by ACPI-MS in (A and B) negative ion mode and (C) positive ion mode.

Table 2.15. Summary of the m/z ratios obtained in the APCI-MS analysis (positive and negative modes) of the methanol extract of SFA_2, as well as of corresponding molecular weights and possible chemical formulas for individual fulvic acids in the methanol extract of SFA_2.

m/z	Chemical formula	Molecular weight	Structure
Positive mode			
395.3656	$[C_{18}H_{14}O_8 + 2\ H_2O + H]^+$	395.098	Structure (c) in Fig. 2.39
411.3599	$[C_{18}H_{11}O_6Na_3 + H_2O + H]^+$	411.043	Structure (g) in Fig. 2.44
429.3702	$[C_{18}H_{11}O_6Na_3 + 2\ H_2O + H]^+$	429.054	Structure (g) in Fig. 2.44
441.3678	$[C_{18}H_{12}O_7Na_2 + 3\ H_2O + H]^+$	441.077	Structure (k) in Fig. 2.10
Negative mode			
355.3321	$[C_{16}H_{14}O_6 + 3\ H_2O - H]^-$	355.103	Structure (f) in Fig. 2.44
381.0698	$[C_{18}H_{13}O_7Na + H_2O - H]^-$	381.059	Structure (i) in Fig. 2.10
605.4228	$[C_{30}H_{17}O_{10}Na_3 - H]^-$	605.044	Structure (a) in Fig. 2.48
655.4541	$[C_{30}H_{20}O_{11}Na_2 + 3\ H_2O - H]^-$	655.104	Structure (g) in Fig. 2.14
669.4697	$[C_{36}H_{23}O_{12}Na - H]^-$	669.101	Structure (b) in Fig. 2.48

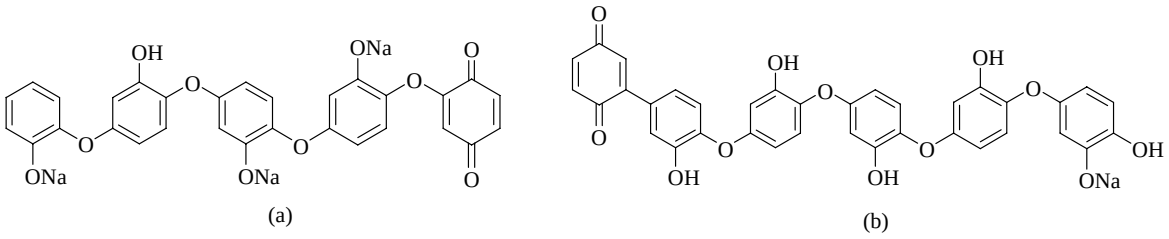

Figure 2.48. Possible molecular structure for a previously unidentified individual fulvic acid. This structure has been established from a chemical formula deduced from the APCI-MS analysis of the methanol extract of SFA_2.

All apart from two of the m/z values listed in Table 2.15 have already been assigned to compounds with possible molecular structures shown in Figures 2.10, 2.14, 2.39 and 2.44. The m/z values equal to 605 and 669 (negative modes) have been assigned to a pentamer and hexamer compounds respectively. They are both quinones. Again, it is not necessarily the case that all benzene rings are actually linked to each other through ether bonds, and there may be alternative structures for the chemical formula corresponding to $C_{34}H_{24}O_{12}Na_2$.

2.8. Discussion

From the results and observations summarized above concerning the nature of the products obtained by polymerization of catechol and acetic acid, there is no much difference from the formation of SFA_1. Analysis of SFA_2 reveals more of quinonic structures as

compared to SFA_1. We conclude that the formaton of SFA_2 followed the same reaction pathway as SFA_1. The reations leading to the formation of SFA_1 has been discussed earlier in section 1.8.2 and hence will not be discussed any further.

3. FULVIC ACID SYNTHESIZED BY CONDENSATION OF CATECHOL AND GLYCINE

3.1. Elemental analysis

Both raw and extracted synthetic fulvic acid (SFA) obtained through the condensation of catechol and glycine (SFA_3) in the quaternary system $C_6H_4(OH)_2$-NH_2CH_2COOH-NaOH-H_2O at ~ 25°C, under atmospheric oxidizing conditions and at pH = 10 have been analyzed for their elemental compositions. The results are given in Table 2.16. The composition listed in this table for catechol is identical to that already listed for SFA_1 and SFA_2. The composition given for glycine has been determined in the present study and is consistent with the theoretical composition calculated from the chemical formula and the atomic weights of the elements. As was the case with the elemental analyses of SFA_1 and SFA_2, the weight percentages of carbon, hydrogen, oxygen and in this case nitrogen do not sum up to 100 percent for both the raw and dialyzed SFA_3, the extracted (purified) SFA_3, and all the SFA_3 extracts. We have again made the assumption that the difference could be attributed to sodium ions (from NaOH) complexed by phenolate or carboxylate functional groups in the SFA_3. It can be deduced from Table 2.16 that the proportion of oxygen in the raw SFA_3 remains constant while that of carbon between 0 and 63 days decreases significantly. The significant decrease in the hydrogen content is attributed to the increase in the sodium content. The sodium content in the dialyzed fraction is the lowest, indicating that most of the Na that was present after the synthesis (raw SFA_3 after 63 days) had been eliminated through dialysis. It can be observed that there is a gradual increase in carbon and oxygen content but decrease in sodium content with increasing extraction. The atomic H/C ratio of the extracted SFA_3 is similar to those in SFA_1 and SFA_2, but the O/C ratio of SFA_3 is lower than that of SFA_1 but greater than that of SFA_2. The atomic N/C ratio is the lowest for the extracted SFA_3, indicating that the nitrogen content in the purified (extracted) SFA_3 is low with an atomic N/C ratio equal to 0.016.

3.2. Scanning electron microscopy

Scanning electron microscopy (SEM) observations of samples of the raw SFA_3 obtained by condensation of catechol and glycine at 25°C and at pH = 10 are shown in Figure 2.49. Again, the reaction products appear as amorphous agglomerations of fine, submicrometric particles.

Table 2.16. Elemental compositions of the raw and extracted fulvic acid synthesized by polymerization condensation of catechol and glycine. No correction for the presence of water has been made.

Sample	% C	% H	% O	% N	(% Na)[a]	H/C	O/C	N/C
Catechol	66.28	5.56	28.78	-	(0.00)	1.000	0.326	-
Glycine	31.98	6.75	39.35	18.84	(0.00)	2.533	0.923	0.504
SFA_3 ; 0 day (raw)	39.65	3.55	35.55	6.01	(15.24)	1.074	0.672	0.130
SFA_3 ; 63 days (raw)	29.55	2.31	35.58	3.42	(29.14)	0.938	0.903	0.099
SFA_3 ; > 500 Da [b]	47.95	2.67	33.28	1.46	(14.64)	0.668	0.521	0.026
SFA_3 ; after extraction [c]	39.17	2.25	42.14	0.72	(15.72)	0.689	0.807	0.016
SFA_3 ; extract 1 [d]	18.51	1.64	33.27	0.58	(46.00)	1.063	1.348	0.027
SFA_3 ; extract 2 [e]	18.50	1.58	34.73	0.42	(44.77)	1.025	1.408	0.019
SFA_3 ; extract 3 [f]	21.10	1.78	33.32	1.10	(42.70)	1.012	1.184	0.045
SFA_3 ; extract 4 [g]	22.37	1.74	34.08	1.39	(40.42)	0.933	1.143	0.053
SFA_3 ; extract 5 [h]	23.91	1.95	40.94	1.73	(31.47)	0.979	1.284	0.062
SFA_3 ; extract 6 [i]	27.34	2.30	44.46	1.32	(24.58)	1.010	1.220	0.041

[a] Calculated by difference (see text) [b] The SFA on this line corresponds to the dialyzed fulvic acid greater than 500 Da [c] The SFA on this line corresponds to the purified fulvic acid obtained at the end of the extraction procedure (see chapter 1) [d] First extraction with methanol [e] Second extraction with methanol [f] Third extraction with methanol [g] Fourth extraction with methanol [h] Fifth extraction with methanol [i] Extraction with methanol-water solvent system (4:1)

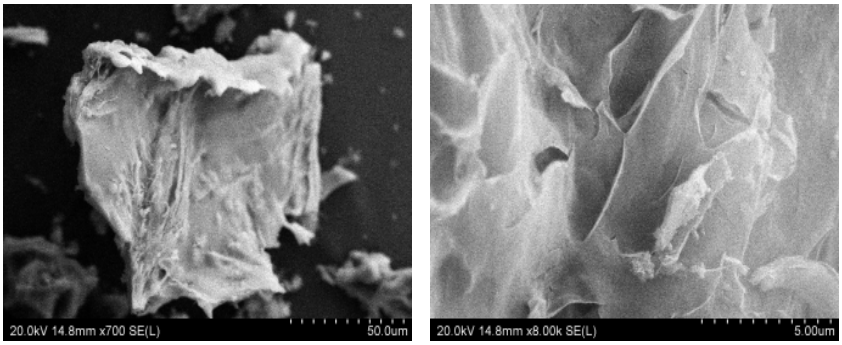

Figure 2.49. SEM photographs of SFA_3. Magnification (left) x 700 (right) x 8000.

3.3. X-ray diffraction

X-ray diffraction spectra obtained for catechol crystals, glycine crystals, raw SFA_3 and purified (extracted) SFA_3 are shown in Figure 2.50 (a), (b), (c) and (d), respectively. The diffractograms have been offset for the sake of clarity. The diffractograms of both raw and purified SFA_3 differ significantly from those of the reactants, which indicates that SFA_3 was formed as a result of the reaction between catecholate anions and radicals, glycine ions, dissolved CO_2 and hydroxide OH^- anions. The distinct peaks observed in the diffractogram (c) of the raw SFA_3 are assigned to unreacted catechol and glycine, or other crystalline undetermined by-products. The absence of peaks in the X-ray diffractogram (d) of purified SFA_3 proves that SFA_3 is composed of amorphous solid compounds.

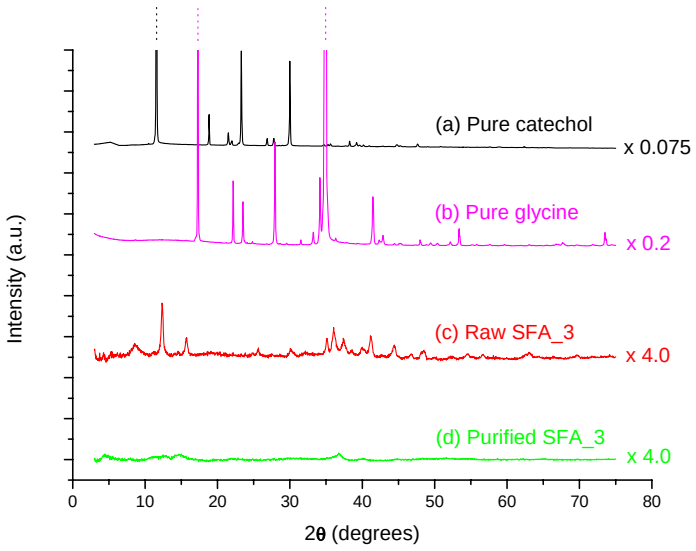

Figure 2.50. X-ray diffraction spectra of crystalline catechol (a), crystalline glycine (b), raw SFA_3 prior to extraction (c), and purified (extracted) SFA_3.

3.4. ATR-FTIR spectroscopy

The ATR-FTIR spectrum of catechol has already been discussed in section 1.4.1 and will not be presented again.

3.4.1. Glycine

Glycine (NH_2CH_2COOH) consists of three functional groups, including an aliphatic methylene $–CH_2–$group, a carboxylic acid –COOH group, and a primary amine $–NH_2$ group.

The ATR-FTIR spectrum of pure glycine recorded at 25°C and 0.1 MPa is shown in Figure 2.51. According to Fischer et al. (2005), the spectrum of glycine is composed of four groups of absorption bands corresponding to the following wavenumber ranges:

- ✓ 3250 – 2400 cm^{-1}: this wavenumber range comprises two broadbands:
  - ❖ one broadband in the range 3250 – 3100 cm^{-1} characterizing the two stretching modes of the N–H bonds, the first one near 3158 cm^{-1} and the second one around 3000 cm^{-1};
  - ❖ a second weak broadband in the range 3000 – 2400 cm^{-1} due to the overlapping of two vibration modes:
  - the stretching mode of the C–H bonds characterized by two distinct $\nu_a CH_2$ and $\nu_s CH_2$ bands around 2955 and 2820 cm^{-1}, respectively. The broadband in the range 2700 – 2400 cm^{-1} is assigned to the overtone of the νC–H stretching.
  - the stretching mode of the O–H bond of the carboxylic group which is responsible for the weak broadband appearing in the region 3000 – 2500 cm^{-1}.
- ✓ 1700 – 1200 cm^{-1}: this wavenumber range includes vibration modes of the three functional groups of glycine:
  - ❖ the carboxylate group, which is characterized by three vibration modes:
  - the δO–H bending mode of the O–H bond, which appears as a weak band around 1443 cm^{-1}. Note that this band overlaps with the δ_sN–H scissoring mode of the primary amine group;
  - the stretching mode of the carboxylate anion. Due to the fact that the C=O and C–O bonds of the carboxylate anion are strongly coupled, this stretching mode is characterized by two distinct bands: an antisymmetric $\nu_a COO$ stretching band at 1582 cm^{-1} and a weak symmetric $\nu_s COO$ stretching band at 1408 cm^{-1};
  - the bending mode of the C–O bond, which appears in the 1330 – 1210 cm^{-1} region. Note that this band overlaps with the $\delta_w CH_2$ out-of-plane wagging mode of the methylene group at 1332 cm^{-1}.

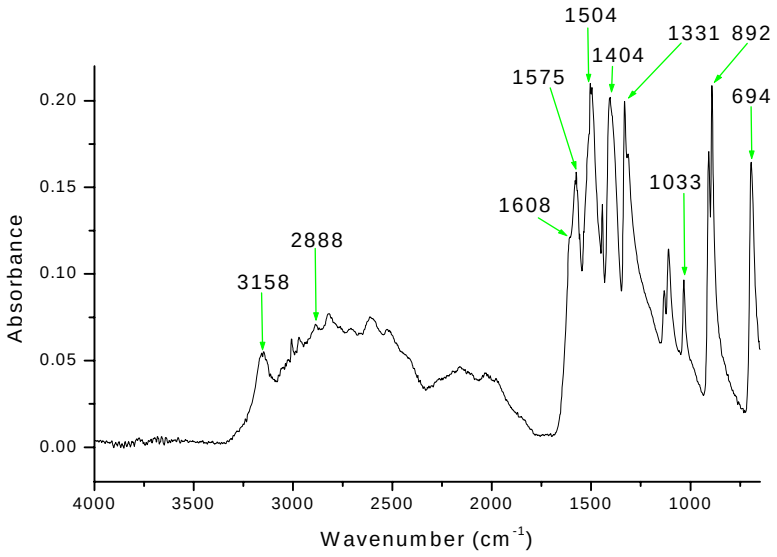

Figure 2.51. ATR-FTIR spectrum of pure glycine (NH_2CH_2COOH): T = 25°C, P = 0.1 MPa.

- ❖ the methylene group: absorption due to the methylene twisting $\delta_t CH_2$ and out-of-plane wagging $\delta_w CH_2$ vibrations is observed in the 1350 – 1150 cm^{-1} region.
- ❖ the primary amine group: this group is characterized by two vibration modes, including the δ_bN–H bending mode near 1609 cm^{-1} and the δ_sN–H scissoring mode with a minor band around 1443 cm^{-1}.

✓ 1200 – 1000 cm^{-1}: this wavenumber range includes vibration bands of:

- ❖ the primary amine group: three medium to weak distinct bands νC–N of the unconjugated C–N linkage in aliphatic primary amines appear at 1131, 1110 and 1033 cm^{-1}. These bands overlap with two νC–C stretching bands of the methylene group.
- ❖ the C–C bond: the aliphatic νC–C stretching vibrations of this bond appear as weak bands in the 1200 – 800 cm^{-1} region.

✓ < 1000 cm^{-1}: in the energy region below 1000 cm^{-1}, the δ_wN–H wagging vibrations of the primary amine group appear in three medium to strong bands at 910, 892 and 694 cm^{-1}. It is important to note that the in-plane δ_rC–H rocking vibrations of the methylene group could absorb near 720 cm^{-1}.

3.4.2. Synthetic fulvic acid SFA_3

The ATR-FTIR spectra of the raw and purified synthetic fulvic acids SFA_3 are presented in Figure 2.52. These spectra are characterized by four groups of absorption bands corresponding to the following wavenumber ranges: 3700 – 2500 cm^{-1}, 1800 – 1400 cm^{-1}, 1400 – 900 cm^{-1}, and 900 – 650 cm^{-1}.

- ✓ 3700 – 2500 cm^{-1}: this wavenumber range comprises seven distinct bands:
  - ❖ a $\nu_a CH_2$ antisymmetric stretching band of a primary amine group (3400 – 3380 cm^{-1})
  - ❖ a $\nu_a CH_2$ symmetric stretching band of a primary amine group (3344 – 3324 cm^{-1})
  - ❖ a νOH stretching band of an alcohol O–H functional group (3700 – 3300 cm^{-1})
  - ❖ a νOH stretching band of the associated O–H group in a carboxylate functional group (3000 – 2500 cm^{-1})
  - ❖ a νCH stretching band of an aromatic C–H bond (3075 – 3030 cm^{-1})
  - ❖ $\nu_a CH_3$ and $\nu_a CH_2$ antisymmetric stretching bands of alkanes (2970 – 2915 cm^{-1})
  - ❖ $\nu_s CH_3$ and $\nu_s CH_2$ symmetric stretching bands of alkanes (2880 – 2845 cm^{-1})

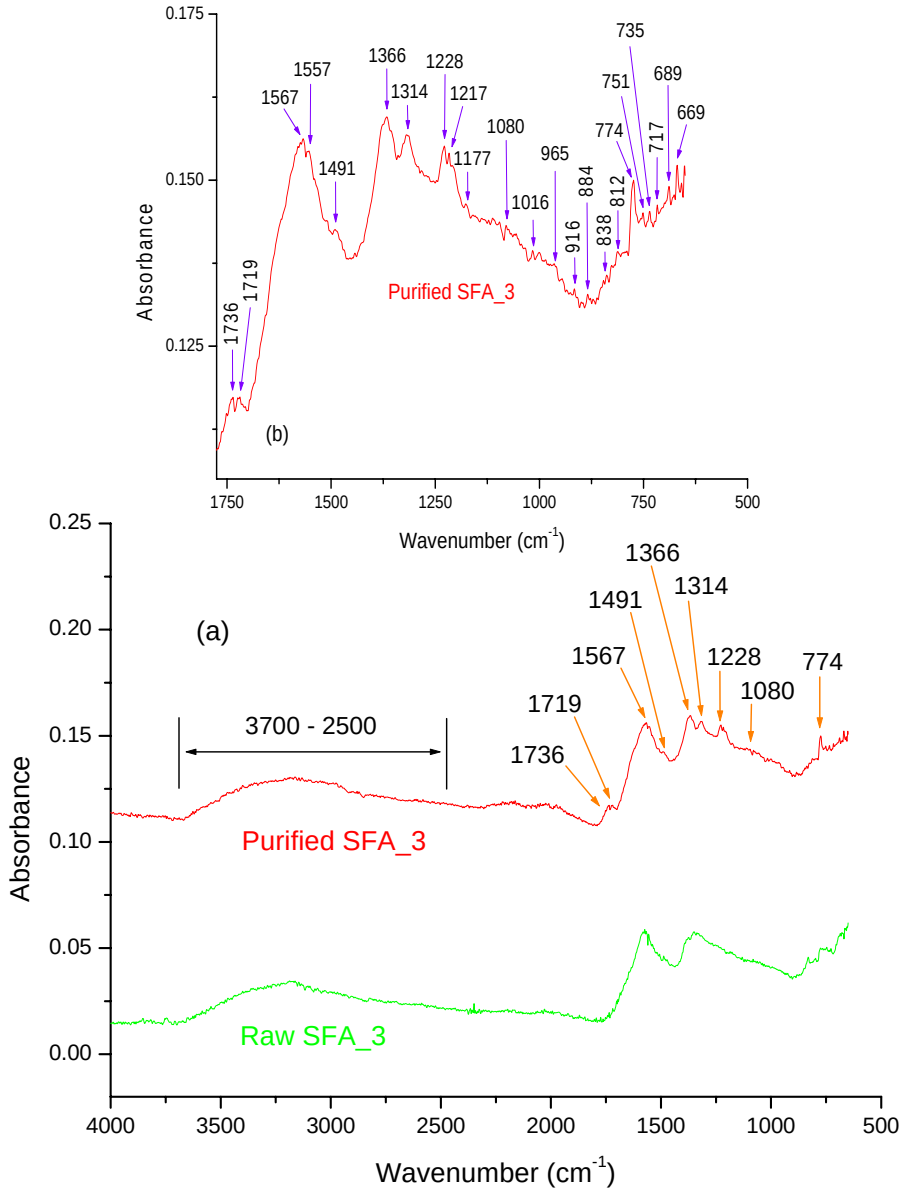

Figure 2.52. ATR-FTIR spectrum of raw and purified SFA_3. T = 25°C, P = 0.1 MPa. (a) complete spectrum; (b) enlargement of the lower wavenumber portion of the spectrum.

- ✓ 1800 – 1400 cm^{-1}: the group of vibration bands corresponding to this wavenumber range is characterized by the presence of two small distinct bands at 1736 and 1719 cm^{-1}. According to Parker (1971), these two bands correspond to the νC=O stretch of four different functional groups: ketones, aldehydes, esters of aliphatic or aromatic acids, and dimers of carboxylic acids. Given the fact that SFA_3 is most probably composed of aromatic rings bonded with glycinate anions (pK_{a1} = 2.4 ; pK_{a2} = 9.8), it

is reasonable to assign these two small bands to esters formed by condensation of the amino acid and catechol.

The band corresponding to the shoulder near 1620 cm^{-1} probably represents the sum of two vibrations modes, including

- ❖ the δN–H bending mode of the primary amine group
- ❖ the νC=C stretching mode of an aromatic C=C bond conjugated either with another aromatic C=C bond in another aromatic ring (such as for example in biphenyl), or with a C=O bond.

The two absorption bands at 1557 cm^{-1} and 1567 cm^{-1} are assigned to the antisymmetric stretching mode $\nu_a OCO^-$ of the carboxylate functional group in two different environments.

The small but distinct band at 1491 cm^{-1} characterizes the νC=C stretching mode of aromatic rings.

- ✓ 1400 – 900 cm^{-1}: in this third group of vibration bands, the presence of a broadband near 1366 cm^{-1} indicates the presence of the $\nu_s OCO^-$ symmetric stretching of the ester group in aminoacetate moieties.

The band at 1314 cm^{-1} corresponds to the δCH_2 stretching mode of the methylene group in aminoacetate moieties.

The broadband near 1228 cm^{-1} may represent two different vibration modes (Wojtkowiak and Chabanel, 1977)

- ❖ the νC–O stretching mode of the ester group in aminoacetate moieties (1320 – 1210 cm^{-1})
- ❖ the ν_aC–O–C antisymmetric stretching mode of aromatic ethers (1270 – 1230 cm^{-1})

The distinct band at 1217 cm^{-1} as well as the broadband appearing in the 1200 – 900 cm^{-1} range correspond to the in-plane δC–H bending of aromatic rings (1225 – 950 cm^{-1}) in different environments. Note that the 1200 – 900 cm^{-1} broadband could also represent two other vibration modes:

- ❖ the νC–O stretching band of alcohol functional groups (1200 – 1000 cm^{-1})
- ❖ the ν_sC–O–C symmetric stretching band of ethers (1150 – 1100 cm^{-1})

Finally, the medium band around 916 cm^{-1} can be assigned to the δ_wN–H wagging vibrations of primary amine groups.

- ✓ 900 – 650 cm^{-1}: this last group of vibration bands includes:
  - ❖ one major and distinct band at 774 cm^{-1}, which is characteristic of the out-of-plane δC–H bending of C–H bonds of aromatic derivatives with three substitutions at positions 1, 2 and 3 (810 – 750 cm^{-1}).
  - ❖ one medium and distinct band at 669 cm^{-1} characteristic to the out-of-plane δC–C bending mode of C=C bonds in aromatic derivatives.
  - ❖ three minor bands near 812 cm^{-1}, 838 cm^{-1} and 884 cm^{-1}. The band at 884 cm^{-1} is assigned to the out-of-plane δC–H bending mode of C–H bonds in aromatic derivatives either with four substitutions at positions 1, 2, 3 and 4 or at positions 1, 2, 4 and 5, or with five substitutions (880 – 840 cm^{-1}). The two minor bands around 812 cm^{-1} and 838 cm^{-1} are assigned to the out-of-plane δC–H bending mode of C–H bonds in aromatic derivatives either with three substitutions at positions 1, 2 and 4 (860 – 800 cm^{-1}) or with four substitutions at positions 1, 2, 3 and 4 (also 860 – 800 cm^{-1}).
  - ❖ a group of four minor and distinct bands at 689 cm^{-1}, 717 cm^{-1}, 735 cm^{-1} and 751 cm^{-1} corresponding to the out-of-plane δC–C bending mode of C=C bonds in aromatic derivatives with three substitutions either at positions 1, 2 and 3 or at positions 1, 2 and 4 (730 – 685 cm^{-1}).

Note that two of the bands described above may overlap with two medium bands near 694 cm^{-1} and 892 cm^{-1}, which correspond to the δ_wN–H wagging vibrations of the primary amine groups of glycine. The interpretations made above are based on the monograph by Wojtkowiak and Chabanel (1977).

3.5. UV-Visible absorption spectrophotometry

The UV-visible absorption spectra of the raw SFA_3 (0.022 $g \cdot L^{-1}$; pH = 10.550), purified SFA_3 (0.022 $g \cdot L^{-1}$; pH = 10.487), and catechol (0.022 $g \cdot L^{-1}$; pH = 10.478) are shown in Figure 2.53. The absorption spectrum of glycine is not shown in this figure because this species does not absorb in the range 200 – 800 nm. Catechol in solution at pH = 10.478 is characterized by an intense absorption band at 275 nm and a minor and broad absorption band with a maximum near 327 nm.

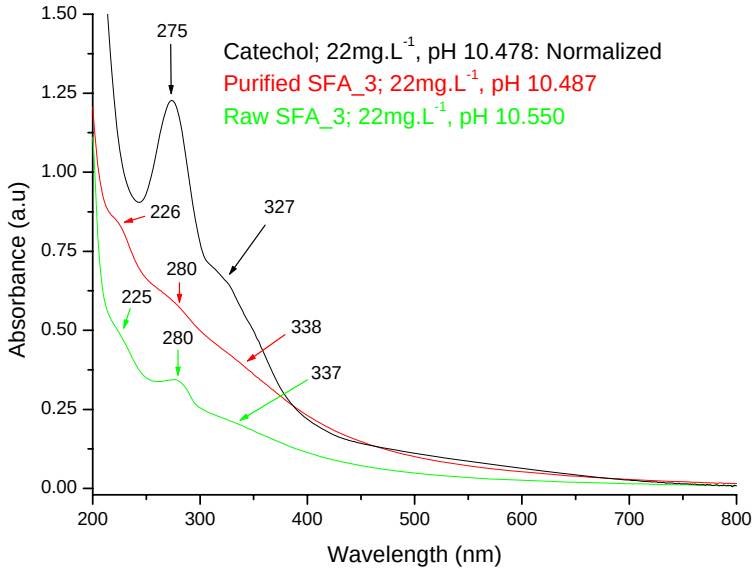

Figure 2.53. UV-Visible spectra of raw SFA_3 (green spectrum), purified SFA_3 (red spectrum), and catechol (black spectrum). Measurements were made with a 10 mm path length quartz cuvette.

The purified SFA_3 is characterized by three broadbands near 226, 280 and 338 nm. The first broadband around 228 nm could result from two bands which may be either characteristic aromatic E_2 bands, or conjugated *K* bands. The second broadband around 280 nm corresponds to the benzenoid *B* bands and the $n \rightarrow \pi^*$ forbidden transition. The latter bands originate from n-π conjugation between nonbonded *n* or *p* electrons of an oxygen atom bonded to two aromatic rings (i.e. diphenyl ether). The last broadband around 338 nm probably results from the hyperconjugation of π electrons of aromatic rings which are bonded to one another by two types of linkages, either $C_{aromatic} - C_{aromatic}$ bonds or ether bonds. The presence of broadbands indicates that the SFA_3 is a mixture of compounds of high molecular weight with numerous atoms. The comparison between the UV-visible absorption spectrum of catechol and that of purified SFA_3 at pH = 10.487 indicates a weak absorption of SFA_3 in the UV region (200 – 400 nm), while the absorption of catechol becomes almost similar to that of purified SFA_3 in the visible region (400 – 800 nm). Apparently, the formation of SFA_3 from catechol and glycine at pH ~ 10 is accompanied by a hypochromic shift in the ultraviolet region.

The effect of the concentration of purified SFA_3 on the absorption intensity at pH = 7.1 is shown in Figure 2.54 for two different concentrations. It can be seen in this figure that the absorption intensity is multiplied by a factor of 2 with increasing concentration of SFA_3

from 0.022 to 0.044 g·L^{-1} in the wavelength range 250 – 600 nm. The proportionality between the absorption and the concentration of SFA_3 proves that the sample is homogeneous.

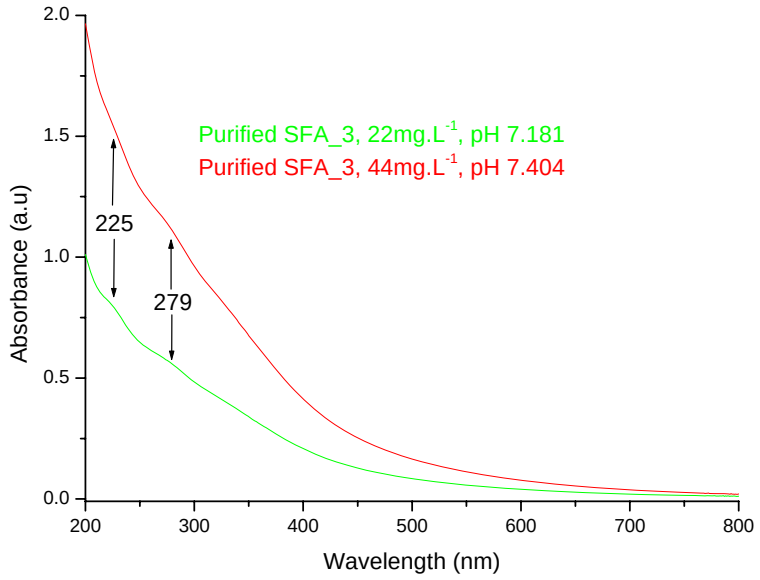

Figure 2.54. UV-Visible spectra of purified SFA_3 as a function of concentration at pH ~ 7. Measurements were made with a 10 mm path length quartz cuvette.

The effect of pH on the absorption intensity of purified SFA_3 is shown in Figure 2.55. It can be seen in this figure that increasing the pH of the solution from 7.18 to 10.49 results in a slight hyperchromic effect (approximately +5%) of the absorption intensity without modifying the shape of the absorption spectrum. The hyperchromic effect observed in basic solution probably results from the ionization of the majority of alcohol functional groups of the molecules which constitute the SFA_3 mixture. The ionization of an alcohol increases the number of nonbonded electrons on the oxygen atoms of the alcohol functional groups and the $n \rightarrow \pi^*$ forbidden transition under UV-visible excitation. Consequently, the ionized alcohol species is colored and produces a hyperchromic shift.

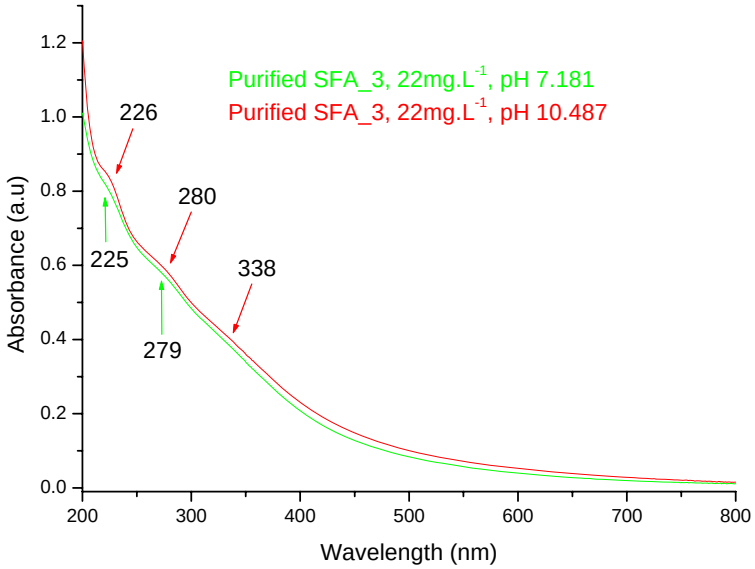

Figure 2.55. UV-Visible spectra of purified SFA_3 as a function of pH at a concentration of 0.022 g·L^{-1}. Measurements were made with a 10 mm path length quartz cuvette.

3.6. Electrospray ionization – mass spectrometry (ESI-MS)

A small amount of the lyophilized, raw SFA_3 was dissolved in milli-Q water and subsequently analyzed by ESI-MS, both in positive-ion (PI) and negative-ion (NI) modes. The spectra obtained are shown in Figure 2.56 for both the PI (A) and NI (B) modes. It can be seen in this figure that ionization was poor in both cases, which prompted us to LC-APCI-MS-MS in search of better results. No attempt has been made to interpret the ESI-MS spectra since the peaks in Figure 2.56 do not appear to be much different from the background and hence some of them could just be due to noise.

It has already been observed in the analysis of both SFA_1 and SFA_2 that significant improvement is obtained when a separation procedure (either LC or one of the extraction procedures already described) is used in conjunction with mass spectrometry in order to eliminate any remaining reactants or other by-products. Both LC-APCI-MS-MS and APCI-MS analyses have been carried out for the raw and purified (extracted) SFA_3, which is discussed below.

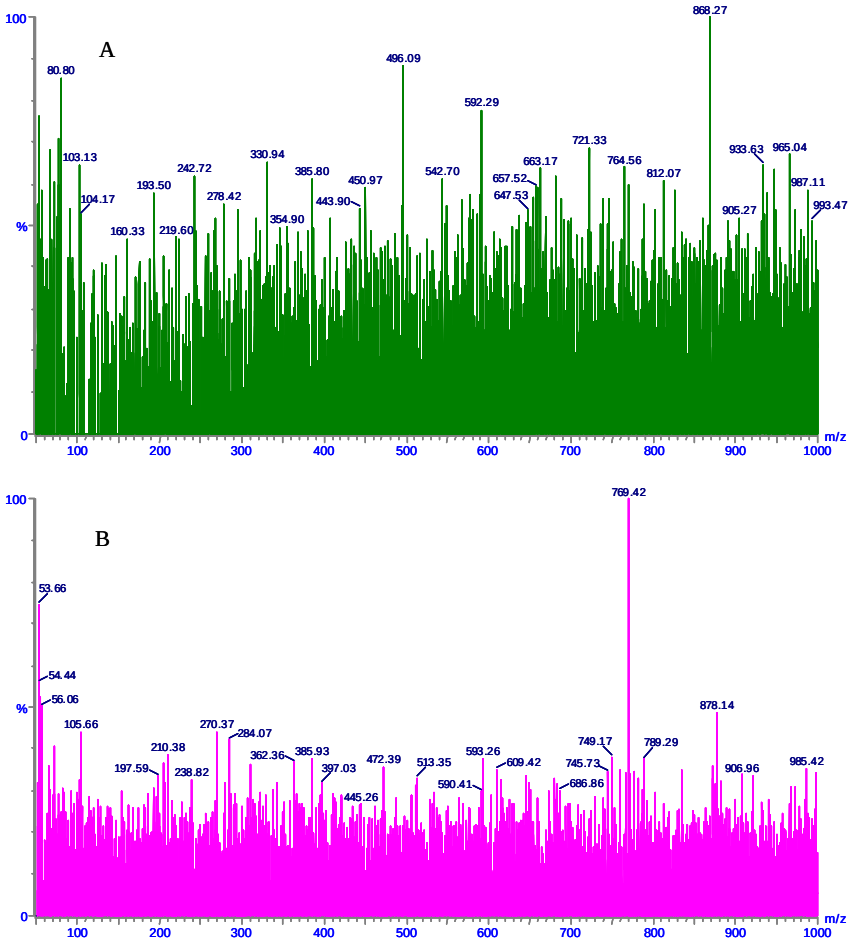

Figure 2.56. ESI-MS spectrum of raw SFA_3 analyzed under positive (A) and negative (B) ion mode.

3.7. Atmospheric pressure chemical ionization mass spectrometry (APCI-MS)

Since the SFA_3 synthetic fulvic acid did not ionize significantly during the ESI-MS analysis, which was already the case for SFA_1 and SFA_2 and as mentioned above may have been due either to a low concentration of the compounds present in the SFA_3 mixture, or to the lack of separation before analysis, both raw and purified SFA_3 have further been analyzed by atmospheric pressure chemical ionization mass spectrometry (APCI-MS), which has been used in conjunction with liquid chromatography and tandem mass spectrometry (LC-APCI-MS-MS) in the case of raw SFA_3. The protocols followed and results obtained for raw and purified SFA_3 are discussed separately below.

3.7.1. Analysis of raw SFA_3 by LC-APCI-MS-MS

The analysis of the raw SFA_3 mixture was performed by tandem mass spectrometry (MS/MS) after first separating the components of the mixture by liquid chromatography (LC) using a U3000 Dionex liquid chromatograph interfaced with a Bruker micro Q-ToF mass

spectrometer. A saturated solution of raw SFA_3 was prepared by dissolving lyophilized solid SFA_3 in milli-Q water containing 0.2 % by volume of formic acid to favor ionization of the fulvic acid components during the analysis. The resulting solution was filtered through a 0.45 μm millex®-HA filter unit. The pH of the solution was lowered to pH ~ 5-8 using formic acid prior to injecting the sample on the LC column. The different parameters used in the LC-ACPI-MS-MS analysis of raw SFA_3 are the same as those given in Table 4, section 1.7.1.

The tandem mass spectrometry analysis was performed in an automatic mode. Peaks showing intensity higher than 5000 (in arbitrary units) were selected for the fragmentation in collision cells with the following parameters:

m/z	isolation width	collision energy
300	8 Da	10 V
500	10 Da	15 V
1000	10 Da	20 V

As in the case of SFA_1 and SFA_2, the base peak chromatograms (BPC) shown in Figure 2.57 are observed for retention times ranging between 0 and 30 minutes. It can be deduced from the base peak chromatograms that all the compounds present in the raw SFA_3 mixture were eluted before 15 minutes in both positive and negative modes, though under negative mode there is again a wide peak between 27 and 30 minutes. Each peak probably corresponds to a series of compounds with similar elution times rather than a single compound.

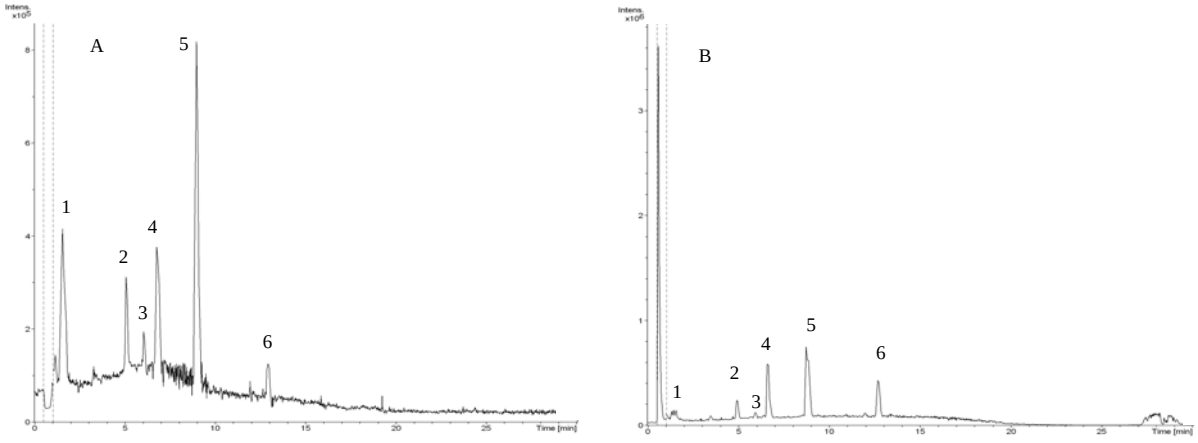

Figure 2.57. Base peak chromatograms (BPC) obtained in the LC-APCI-MS-MS of the raw SFA_3 mixture in positive mode (left) and negative mode (right). Peaks have been numbered to facilitate discussion.

The peaks appearing after 1.1 and 1.2 minutes of elution in Figure 2.57 in both NI and PI modes correspond to clusters of sodium formate (HCOONa). Under NI mode, the clusters

of sodium formate are represented by $[(HCOONa)_n – Na]^-$ where *n* designates the number of sodium formate molecules in a given cluster. The APCI-MS peaks with m/z values equal to 317, 385, 453, 521, 589, 657, 793 and 861 in Figure 2.58 B correspond to sodium formate clusters with *n* = 5, 6, 7, 8, 9, 10, 12 and 13. Under PI mode, the clusters of sodium formate are represented by $[(HCOONa)_n + Na]^+$. The APCI-MS peaks with m/z values equal to 363, 431, 703, 839 and 1043 in Figure 2.58 A correspond to sodium formate clusters with *n* = 5, 6, 10, 12 and 15. We could however not assign any *n* value for the peaks at m/z equal to 622, 922 and 966.

The retention times corresponding to selected chromatographic peaks identified by numbers in Figure 2.57 are listed in Table 2.17 along with the results of the mass spectrometry analysis. The selection of peaks was rendered necessary for clarity reasons in the discussion which is presented below. Also listed in Table 2.17 are possible chemical formulas and molecular weights corresponding to the m/z values. The mass spectra corresponding to retention times of 9.0 (both negative and positive ion modes), 12.7 (negative ion mode) and 6.8 minutes (negative ion mode) are shown in Figures 2.59-2.61 respectively. The molecular structures corresponding to the chemical formulas proposed in Table 16 are depicted in Figure 2.62. Differences between molecular weights and m/z values are usually within 0.3 Da, and in some cases within ~ 3 mDa.

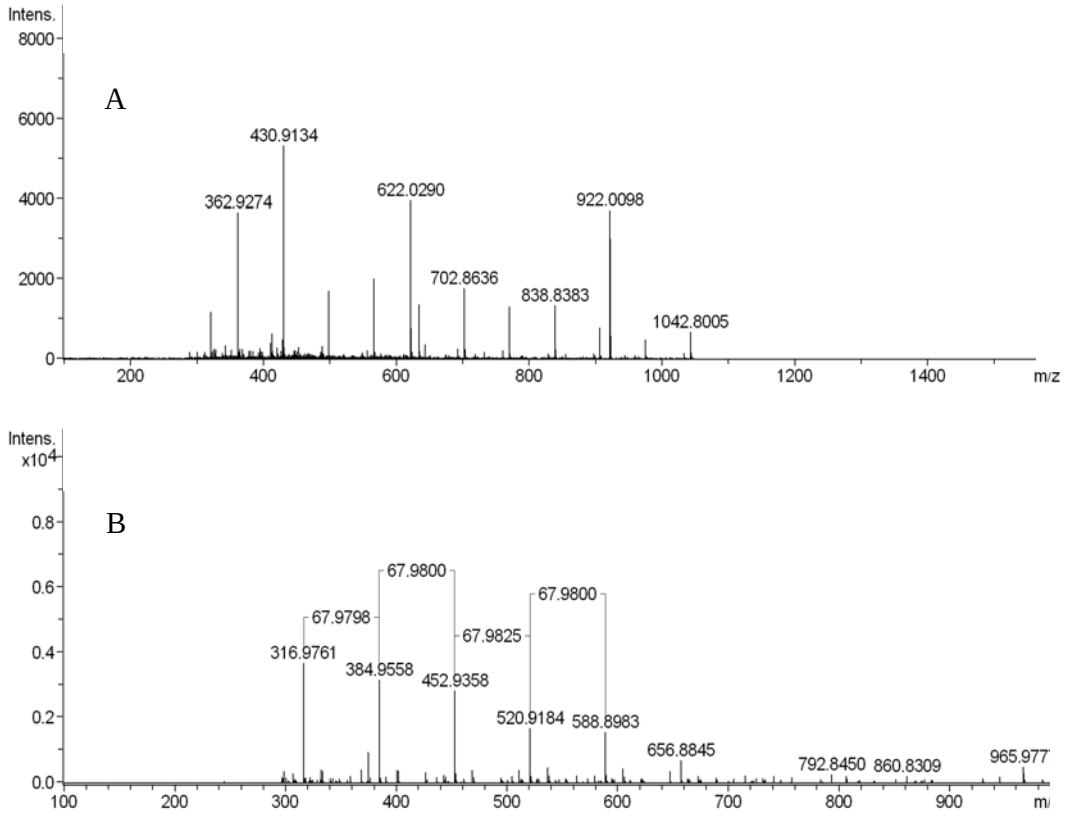

Figure 2.58. APCI-MS spectra of the raw SFA_3 fraction eluted at 1.2 and 1.1 minutes and analyzed in positive (A) and negative (B) modes, respectively.

Table 2.17. Summary of the LC retention times (RT) corresponding to the peaks identified by numbers in Figure 2.57 and of the m/z ratios obtained in the LC-APCI-MS-MS analysis (positive and negative modes) of the raw SFA_3 mixture, as well as of possible chemical formulas and corresponding molecular weights for individual fulvic acids in the raw SFA_3 mixture.

Peak number (Fig. 2.57)	RT (min)	m/z	Chemical formula	Molecular weight	Structure
Positive mode					
5	9.0	330.9773	$[C_{12}H_8O_4Na_2 + HCOONa + H]^+$	331.017	Structure (j) in Fig. 2.16
		493.0079	$[C_{18}H_{11}O_{10}Na_3 + 2\ H_2O + H]^+$	493.033	Structure (o) in Fig. 2.10
		514.9991	$[C_{18}H_{10}O_{10}Na_4 + 2\ H_2O + H]^+$	515.015	Structure (q) in Fig. 2.10
		537.0006	$[C_{18}H_9O_{10}Na_5 + 2\ H_2O + H]^+$	536.997	Structure (s) in Fig. 2.10
		804.9933	$[C_{36}H_{26}O_{14} + HCOONa + 3\ H_2O + H]^+$	805.159	Structure (a) in Fig. 2.62
		826.9761	$[C_{42}H_{27}O_{17}Na + H]^+$	827.122	Structure (p) in Fig. 2.62
6	12.1	441.0182	$[C_{18}H_{12}O_7Na_2 + 3\ H_2O + H]^+$	441.077	Structure (k) in Fig. 2.10
6	12.9	367.0183	$[C_{18}H_{13}O_6Na + H_2O + H]^+$	367.079	Structure (g) in Fig. 2.10
		389.0245	$[C_{18}H_{12}O_6Na_2 + H_2O + H]^+$	389.061	Structure (e) in Fig. 2.44
		411.0049	$[C_{18}H_{11}O_6Na_3 + H_2O + H]^+$	411.043	Structure (j) in Fig. 2.10
		478.9936	$[C_{24}H_{16}O_8Na_2 + H]^+$	479.072	Structure (h) in Fig. 2.44
			$[C_{18}H_{10}O_{10}Na_4 + H]^-$	478.994	Structure (q) in Fig. 2.10
		777.0409	$[C_{42}H_{30}O_{14} + H_2O + H]^+$	777.182	Structure (i) in Fig. 2.44
Negative mode					
4	6.6	301.0426	$[C_{12}H_{10}O_5 + HCOONa - H]^-$	301.032	Structure (b) in Fig. 2.62
		343.0280	$[C_{18}H_{14}O_6 + H_2O - H]^-$	343.082	Structure (e) in Fig. 2.10
		411.0082	$[C_{18}H_{14}O_6 + H_2O + HCOONa - H]^-$	411.069	Structure (e) in Fig. 2.10
		459.0088	$[C_{18}H_{12}O_6Na_2 + 5\ H_2O - H]^-$	459.088	Structure (n) in Fig. 2.10
		559.0268	$[C_{30}H_{22}O_{10} + H_2O - H]^-$	559.124	Structure (t) in Fig. 2.10
		627.0092	$[C_{30}H_{22}O_{12} - H]^-$	627.135	Structure (c) in Fig. 2.62
		857.0121	$[C_{42}H_{30}O_{16} + HCOONa - H]^-$	857.133	Structure (d) in Fig. 2.62
		924.9968	$[C_{48}H_{32}O_{17}Na_2 - H]^-$	925.136	Structure (e) in Fig. 2.62
	6.8	302.0570	$[C_{14}H_9NO_7 - H]^-$	302.030	Structure (f) in Fig. 2.62
		370.0363	$[C_{14}H_9NO_5Na_2 + 3\ H_2O - H]^-$	370.051	Structure (g) in Fig. 2.62
		438.0176	$[C_{20}H_{11}NO_8Na_2 - H]^-$	438.020	Structure (h) in Fig. 2.62
		600.0280	$[C_{26}H_{15}NO_{10}Na_2 + 3\ H_2O - H]^-$	600.073	Structure (i) in Fig. 2.62
		668.0185	$[C_{32}H_{20}NO_{12}Na + 2\ H_2O - H]^-$	668.102	Structure (j) in Fig. 2.62

Table 2.17. *(Continued)*.

Peak number (Fig. 2.57)	RT (min)	m/z	Chemical formula	Molecular weight	Structure
5	8.8	403.0562	$[C_{18}H_{12}O_7Na_2 + H_2O - H]^-$	403.041	Structure (k) in Fig. 2.10
		468.9380	$[C_{18}H_{12}O_{10}Na_2 + 2\ H_2O - H]^-$	469.036	Structure (l) in Fig. 2.10
		513.0062	$[C_{18}H_{10}O_{10}Na_4 + 2\ H_2O - H]^-$	513.000	Structure (q) in Fig. 2.10
		580.9891	$[C_{30}H_{21}O_{10}Na + H_2O - H]^-$	581.106	Structure (o) in Fig. 2.44
		698.9918	$[C_{36}H_{26}O_{14} + H_2O - H]^-$	699.135	Structure (p) in Fig. 2.44
		758.9992	$[C_{36}H_{25}O_{13}Na + 4\ H_2O - H]^-$	759.154	Structure (k) in Fig. 2.62
		920.9898	$[C_{48}H_{33}O_{17}Na + H_2O - H]^-$	921.164	Structure (l) in Fig. 2.62
	9.0	381.0012	$[C_{18}H_{13}O_7Na + H_2O - H]^-$	381.059	Structure (i) in Fig. 2.10
		469.0294	$[C_{18}H_{12}O_{10}Na_2 + 2\ H_2O - H]^-$	469.036	Structure (l) in Fig. 2.10
		513.0068	$[C_{18}H_{10}O_{10}Na_4 + 2\ H_2O - H]^-$	513.000	Structure (q) in Fig. 2.10
		580.9894	$[C_{30}H_{21}O_{10}Na + H_2O - H]^-$	581.106	Structure (o) in Fig. 2.44
		716.9567	$[C_{36}H_{26}O_{14} + 2\ H_2O - H]^-$	717.146	Structure (p) in Fig. 2.44
		810.9547	$[C_{42}H_{30}O_{14} + 3\ H_2O - H]^-$	811.187	Structure (i) in Fig. 2.44
	9.4	316.9772	$[C_{12}H_{10}O_6 + HCOONa - H]^-$	317.027	Structure (i) in Fig. 2.16
		384.9560	$[C_{18}H_{12}O_7Na_2 - H]^-$	385.030	Structure (j) in Fig. 2.8
		451.3414	$[C_{18}H_{12}O_{10}Na_2 + H_2O - H]^-$	451.025	Structure (l) in Fig. 2.10
			$[C_{24}H_{18}O_8 + H_2O - H]^-$	451.103	Structure (m) in Fig. 2.10
		497.3423	$[C_{18}H_{10}O_7Na_4 + HCOONa - H]^-$	496.981	Structure (m) in Fig. 2.62
		620.8442	$[C_{30}H_{20}O_{10}Na_2 + 2\ H_2O - H]^-$	621.098	Structure (n) in Fig. 2.62
6	12.7	321.0629	$[C_{12}H_{10}O_6 + 4\ H_2O - H]^-$	321.082	Structure (a) in Fig. 2.10
			$[C_{18}H_{10}O_6 - H]^-$	321.059	Structure (b) in Fig. 2.10
		365.0483	$[C_{12}H_8O_6Na_2 + 4\ H_2O - H]^-$	365.072	Structure (f) in Fig. 2.10
			$[C_{18}H_{13}O_6Na + H_2O - H]^-$	365.064	Structure (g) in Fig. 2.10
		389.0436	$[C_{12}H_{10}O_6 + HCOONa + 4\ H_2O - H]^-$	389.070	Structure (a) in Fig. 2.10
		501.0085	$[C_{24}H_{14}O_8 + 4\ H_2O - H]^-$	501.002	Structure (p) in Fig. 2.10
		595.0128	$[C_{30}H_{22}O_{10} + 3\ H_2O - H]^-$	595.145	Structure (t) in Fig. 2.10
		753.0334	$[C_{36}H_{22}O_{13}Na_4 - H]^-$	753.057	Structure (x) in Fig. 2.44
		821.0138	$[C_{36}H_{22}O_{13}Na_4 + HCOONa - H]^-$	821.148	Structure (o) in Fig. 2.62
6	13.4	363.1082	$[C_{18}H_{13}O_7Na - H]^-$	363.048	Structure (i) in Fig. 2.10
		433.1052	$[C_{18}H_{12}O_{10}Na_2 - H]^-$	433.015	Structure (l) in Fig. 2.10
		477.0917	$[C_{24}H_{16}O_8Na_2 - H]^-$	477.056	Structure (h) in Fig. 2.44
			$[C_{18}H_{10}O_{10}Na_4 - H]^-$	476.979	Structure (q) in Fig. 2.10
		565.0535	$[C_{24}H_{16}O_9Na_2 + 4\ H_2O - H]^-$	565.093	Structure (m) in Fig. 2.8
		633.0235	$[C_{30}H_{21}O_{11}Na + 3\ H_2O - H]^-$	633.122	Structure (c) in Fig. 2.44
		701.0055	$[C_{36}H_{26}O_{13} + 2\ H_2O - H]^-$	701.151	Structure (y) in Fig. 2.44

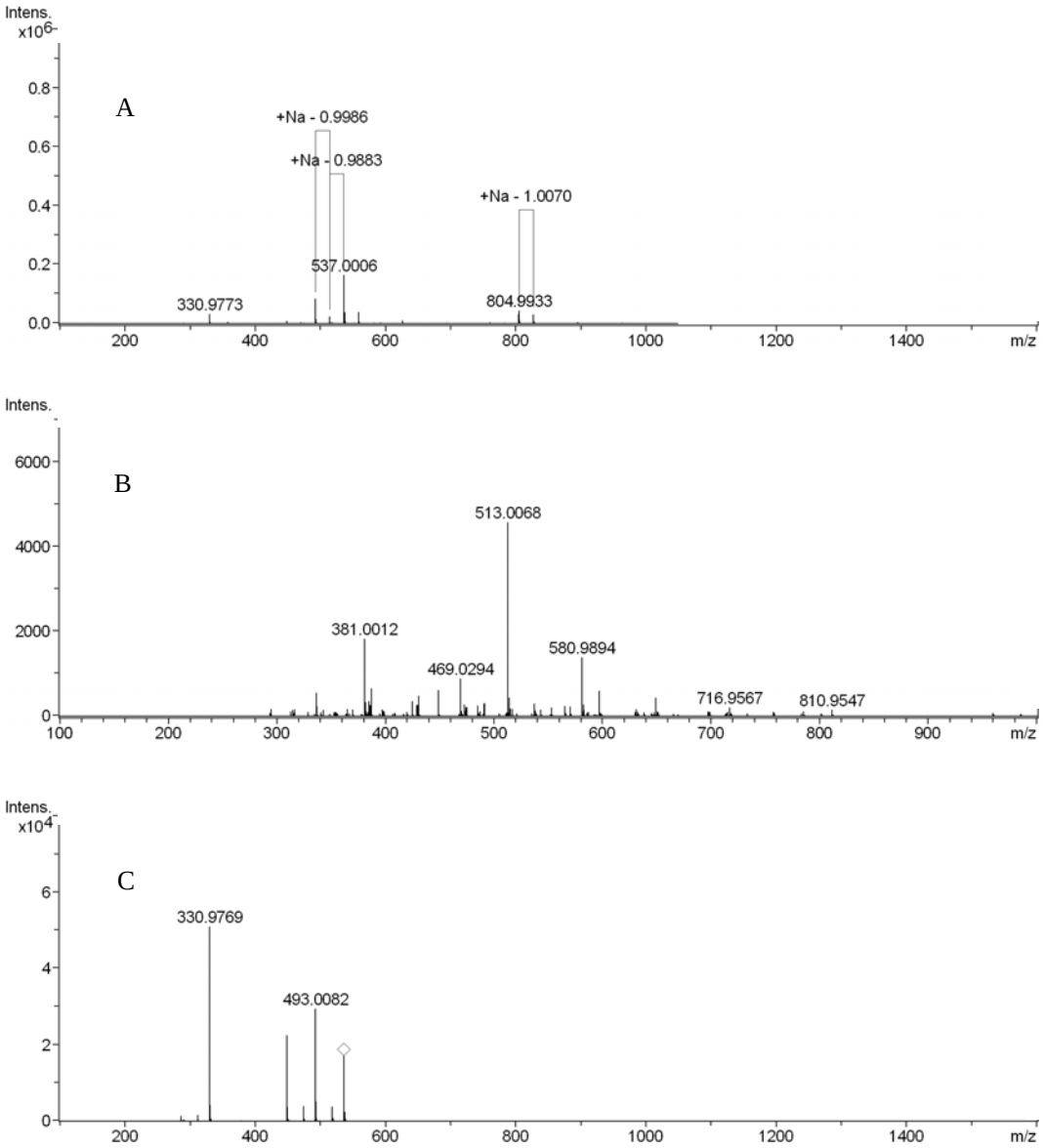

Figure 2.59. APCI-MS spectra of the raw SFA_3 fraction eluted at 9.0 minutes and analyzed in positive (A) and negative (B) modes, and (C) APCI-MS-MS spectrum corresponding to the fragmentation of the compound corresponding to the peak with m/z equal to 537 in Figure 2.59 A.

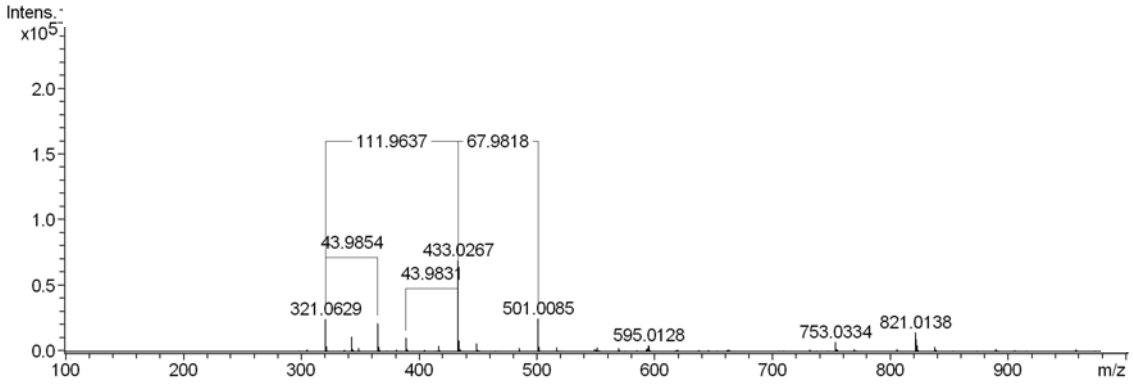

Figure 2.60. APCI-MS spectrum of the raw SFA_3 fraction eluted at 12.7 minutes and analyzed in negative mode.

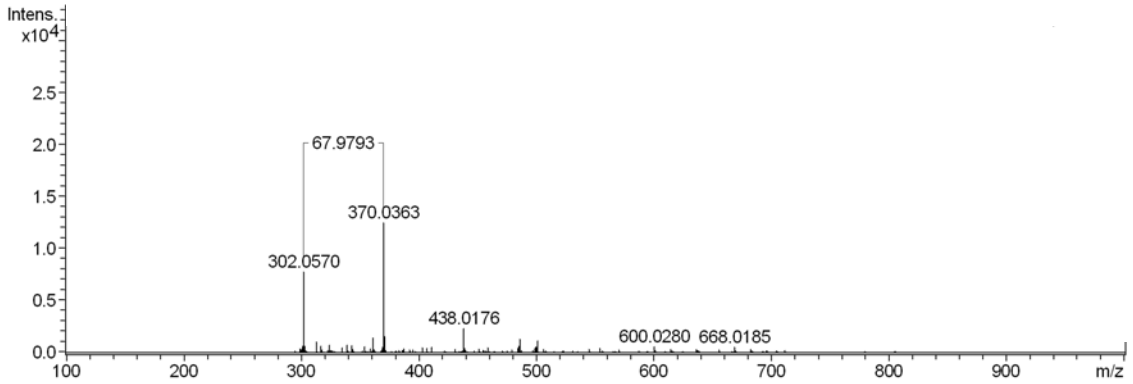

Figure 2.61. APCI-MS spectrum of the raw SFA_3 fraction eluted at 6.8 minutes and analyzed in negative mode.

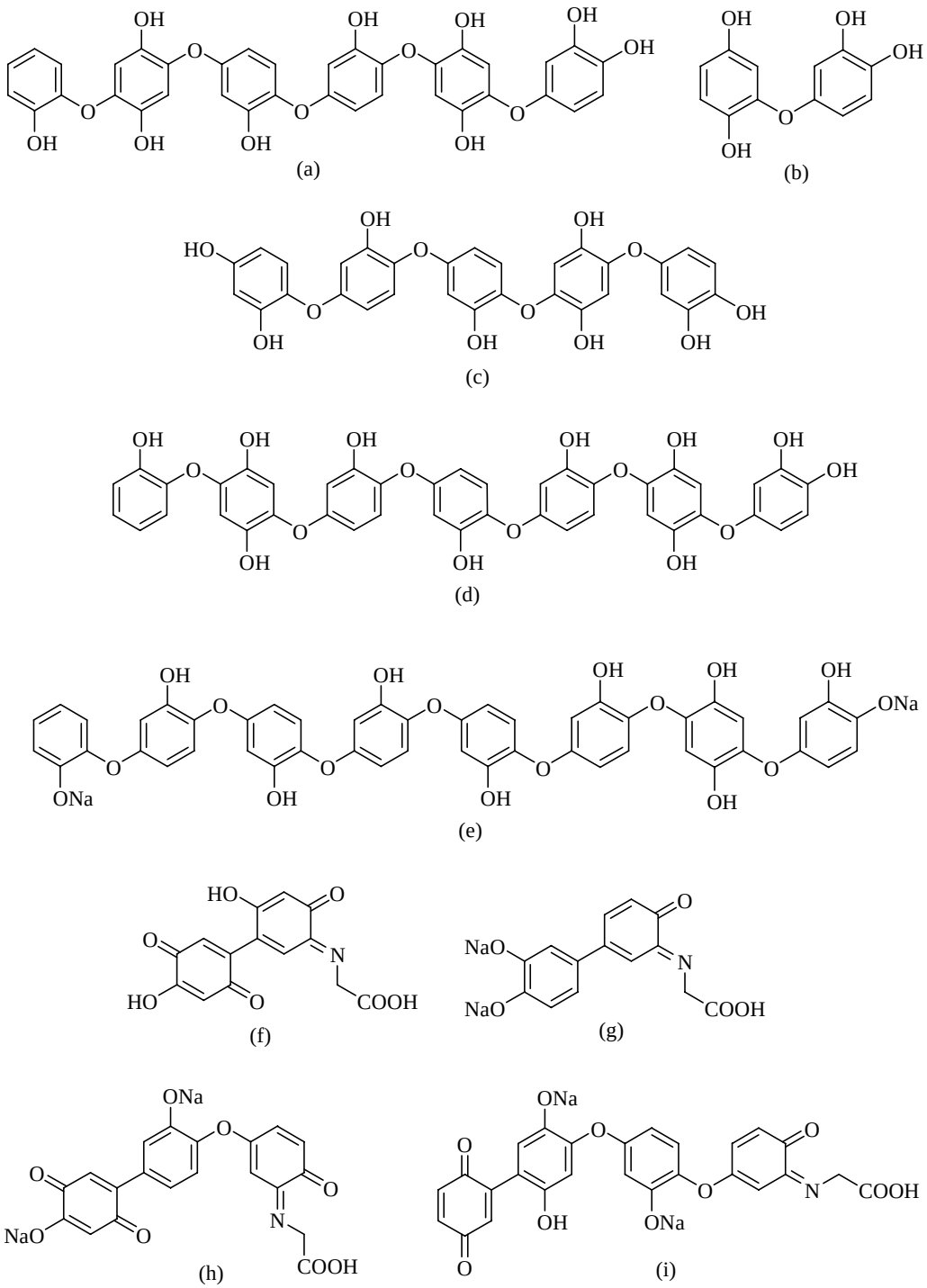

Figure 2.62. Possible molecular structures of individual fulvic acids in the raw SFA_3 mixture deduced from the LC-APCI-MS-MS analysis, to continue in next page.

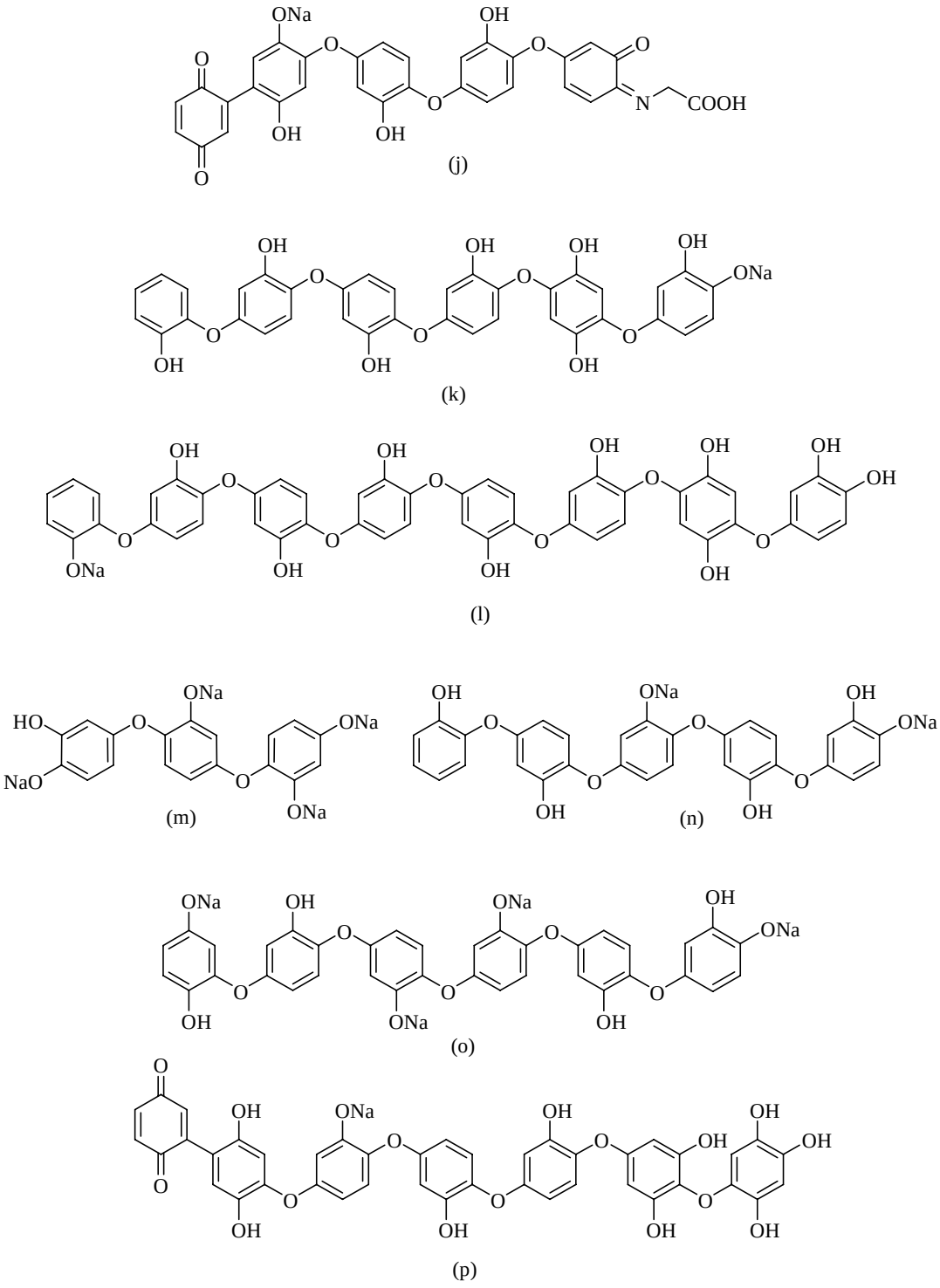

Figure 2.62. *(Continued)*.

In the case of the analysis carried out in PI mode for SFA_3, there appears to be similarities with the analyses carried out previously for SFA_1 and SFA_2. This is particularly evident when considering the retention time at 9.0 minutes for SFA_3 (see Table 2.17) and those at 8.9 (SFA_2, see Table 2.13) and 9.0 minutes (SFA_1, see Table 2.5). The three SFA have m/z values equal to 493, 515, 537 and 805 in common (for SFA_3, see Figure

2.59 A). The m/z value equal to 805 has been assigned molecular structure (a) in Figure 2.62, which corresponds to a hexamer with highly substituted aromatic rings. Still on the basis of a comparison between the APCI-MS analysis in both PI and NI modes for the chromatographic peak corresponding to a retention time of 9.0 minutes, the m/z values at 515 (PI mode, Figure 2.59 A) and 513 (NI mode, Figure 2.59 B) correspond to a compound already identified in both SFA_1 and SFA_2, which has a molecular weight of 478 Da and corresponds to structure (q) in Figure 2.10. Tandem mass spectrometry analysis of the mass peak at m/z equal to 537 shown in Figure 2.59 C displays a pattern which is similar to those already observed for both SFA_1 and SFA_2 – see Figure 2.42 C above (no APCI-MS-MS spectrum has been shown in the case of SFA_1).

Also shown in Figure 2.62 are proposed molecular structures for the APCI-MS analysis of the chromatographic peaks corresponding to the retention times of 6.8 and 12.7 minutes (peaks 3 and 6 of the right BPC in Figure 2.57). The peaks corresponding to m/z values of 321, 365, 389, 501, 595 and 753 in Figure 2.60 have already been assigned to compounds (e.g. see structures (a), (b), (f), (g), (h) and (p) in Figure 2.10 and structure (x) in Figure 2.44. The m/z value equal to 821 in Figure 2.60 has here been reassigned to a compound with molecular structure (o) in Figure 2.62, which corresponds to a hexamer with highly substituted aromatic rings and in which four hydrogen atoms of alcohol functional groups have been substituted by sodium atoms. It is interesting to note that the m/z values observed at the retention time of 6.8 minutes under negative ion mode (Figure 2.61) are even. The peaks corresponding to m/z values equal to 302, 370, 438, 600 and 668 in Figure 2.61 have been assigned to compounds with possible molecular structures corresponding respectively to structures (f), (g), (h), (i) and (j) in Figure 2.62. Structures (f-j) and (p) in Figure 2.62 are quinonoid structures.

Some of the molecular structures proposed in Figure 2.62 contain both aromatic and aliphatic subunits originating from catechol and glycine, respectively. Structures (f-j) are characterized by amine linkage. The size of the fulvic acids formed by the condensation reactions between catechol and glycine again range from dimers (f and g) to octamers (e and l), although these octamers do not contain glycine subunits. The fulvic acids in the SFA_3 mixture contain phenolic, amine, as well as aromatic ether and ester functional groups. Although most of the aromatic rings in these fulvic acids are again linked to each other through aromatic ether (diphenyl oxide) bonds, carbon–carbon bonds between aromatic rings

cannot be excluded on the basis of the present results. The relative importance of the formation of secondary amine *versus* ester linkages will be treated in the discussion below.

3.7.2. Analysis of purified SFA_3 by APCI-MS

A saturated solution of purified SFA_3 was prepared by dissolving lyophilized solid purified SFA_3 in milli-Q water. The resulting solution was filtered through a 0.45 μm millex®-HA filter unit. The pH of the solution was not adjusted prior to the APCI-MS analysis, which was performed in both positive-ion and negative-ion modes. The obtained spectra are shown in Figure 2.63. The peaks corresponding to m/z values equal to 113 in Figure 2.63A and equal to 91 and 121 in Figure 2.63C could not be assigned to any compound. The remaining m/z values shown in Figure 2.63 have been listed in Table 2.18 along with corresponding chemical formulas. Possible molecular structures corresponding to these chemical formulas are either shown in Figure 2.64, or have been presented before.

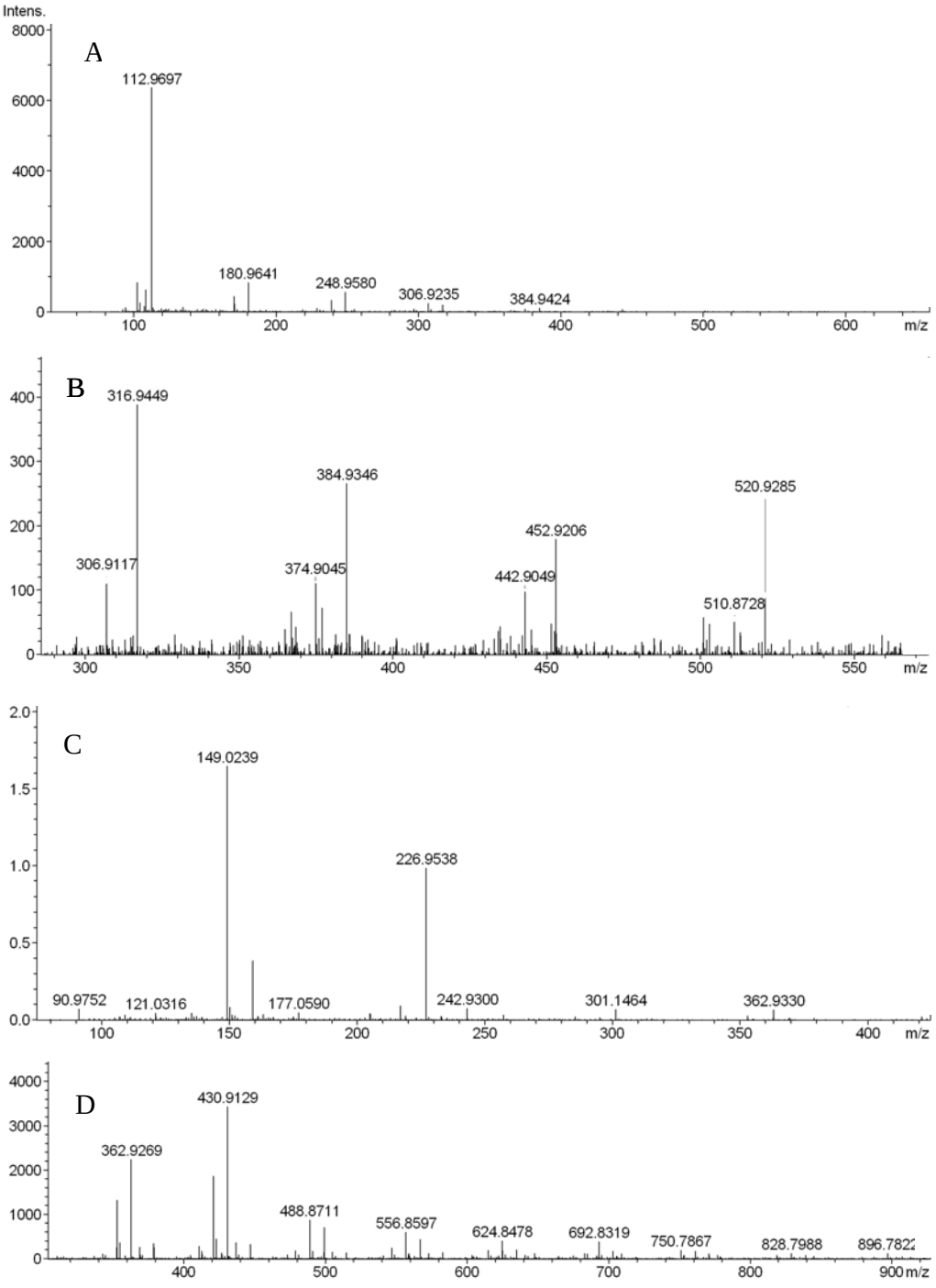

Figure 2.63. APCI-MS spectra of the purified SFA_3 mixture analyzed by APCI-MS in negative mode (A and B) and positive mode (C and D).

Table 2.18. Summary of the m/z ratios obtained in the APCI-MS analysis (positive and negative modes) of the purified SFA_3 mixture, as well as of possible chemical formulas and corresponding molecular weights for individual fulvic acids in the purified SFA_3 mixture.

m/z	Chemical formula	Molecular weight	Structure
Positive mode			
149.0214	$[C_6H_6O_3 + Na]^+$	149.021	Structure (b) in Fig. 2.14
149.0214	$[C_6H_6O_3Na + H]^+$	149.021	Structure (c) in Fig. 2.14
177.0592	$[C_6H_4O_4 + 2H_2O + H]^+$	177.040	Structure (b) in Fig. 2.8
226.9538	$[C_6H_3O_4Na_3 + H_2O + H]^+$	227.077	Structure (c) in Fig. 2.8
242.9300	$[C_6H_4O_3Na_2 + 4\ H_2O + H]^+$	243.046	Structure (a) in Fig. 2.64
301.1434	$[C_{12}H_6O_6 + 3\ H_2O + H]^+$	301.092	Structure (e) in Fig. 2.8
301.1434	$[C_{12}H_7O_5Na_3 + H]^+$	301.006	Structure (o) in Fig. 2.16
362.9330	$[C_{18}H_{14}O_6 + 2\ H_2O + H]^+$	363.108	Structure (e) in Fig. 2.10
430.9129	$[C_{18}H_{10}O_7Na_4 + H]^+$	431.010	Structure (b) in Fig. 2.64
488.8711	$[C_{24}H_{17}O_{10}Na + H]^+$	489.080	Structure (c) in Fig. 2.64
556.8597	$[C_{24}H_{14}O_9Na_4 + H_2O + H]^+$	557.041	Structure (d) in Fig. 2.64
624.8478	$[C_{30}H_{19}O_{11}Na_3 + H]^+$	625.070	Structure (e) in Fig. 2.64
692.8319	$[C_{30}H_{20}O_{11}Na_2 + 5\ H_2O + H]^+$	693.141	Structure (g) in Fig. 2.14
750.7867	$[C_{36}H_{23}O_{13}Na_3 + H_2O + H]^+$	751.102	Structure (f) in Fig. 2.64
828.7988	$[C_{42}H_{30}O_{15} + 3\ H_2O + H]^+$	829.198	Structure (g) in Fig. 2.64
Negative mode			
180.9641	$[C_6H_6O_2 + 4\ H_2O - H]^-$	181.071	Structure (a) in Fig. 2.14
248.9580	$[C_{12}H_{10}O_6 - H]^-$	249.040	Structure (f) in Fig. 2.8
306.9235	$[C_{12}H_9O_6Na + 2\ H_2O - H]^-$	307.043	Structure (d) in Fig. 2.10
316.9449	$[C_{12}H_7O_5Na_3 + H_2O - H]^-$	317.001	Structure (o) in Fig. 2.16
374.9045	$[C_{18}H_{14}O_8 + H_2O - H]^-$	375.072	Structure (c) in Fig. 2.39
384.9424	$[C_{18}H_{12}O_7Na_2 - H]^-$	385.030	Structure (j) in Fig. 2.8
442.9094	$[C_{18}H_{11}O_7Na_3 + 2\ H_2O - H]^-$	443.033	Structure (s) in Fig. 2.16
452.9206	$[C_{18}H_{13}O_7Na + 5\ H_2O - H]^-$	453.101	Structure (i) in Fig. 2.10
510.8728	$[C_{24}H_{16}O_9Na_2 + H_2O - H]^-$	511.062	Structure (m) in Fig. 2.8
520.9285	$[C_{24}H_{18}O_9 + 4\ H_2O - H]^-$	521.130	Structure (h) in Fig. 2.64

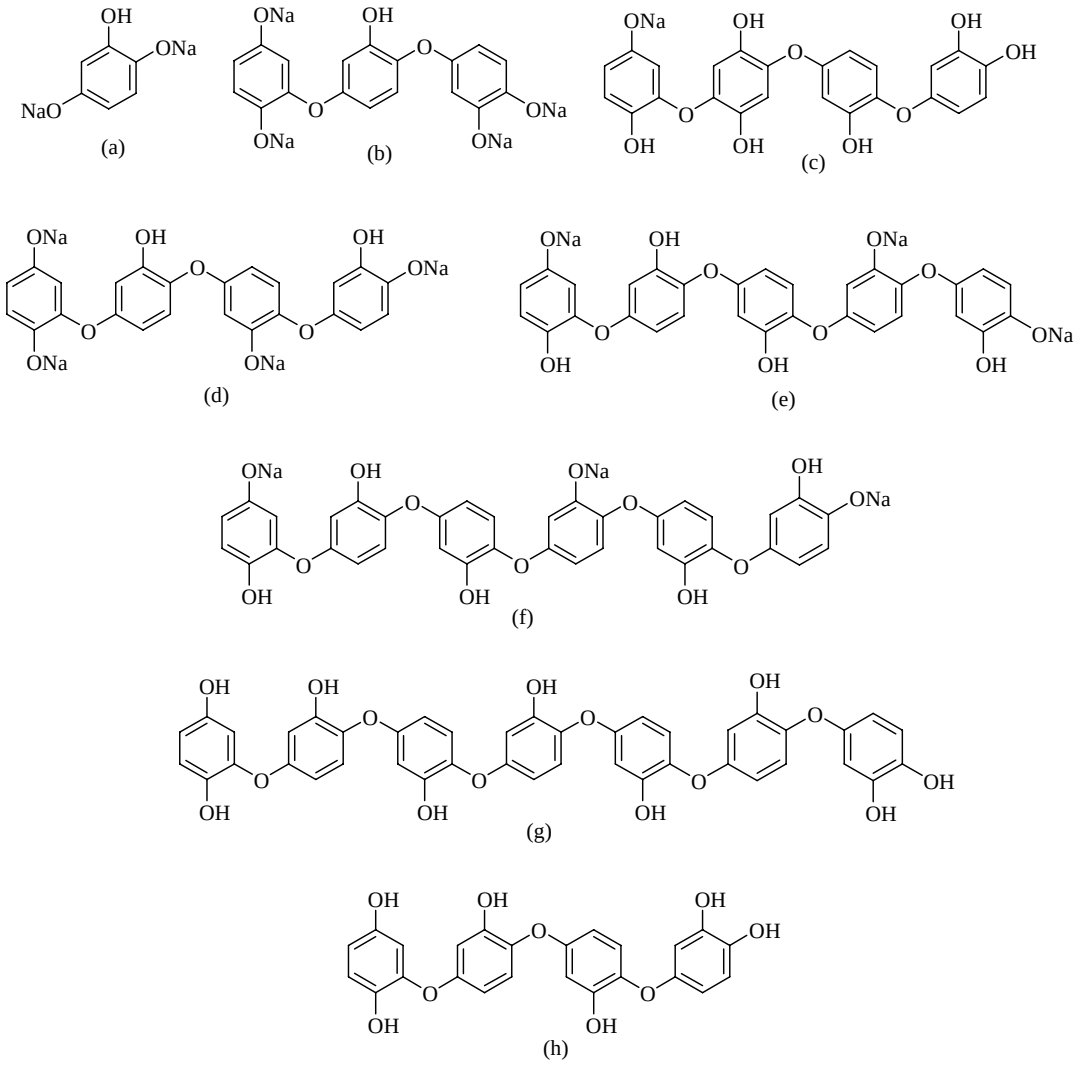

Figure 2.64. Possible molecular structures of individual fulvic acids in the purified SFA_3 mixture deduced from the APCI-MS analysis.

3.8. Discussion

From the results and observations summarized above concerning the nature of the products obtained by polycondensation of catechol and glycine, three reactions appear to be of major interest for explaining the obtention of these products from a reaction mechanism point of view. The first of these reactions is the *oxidative coupling* which has already been discussed under SFA_1, section 1.8.1 and will not be discussed any further. This reaction leads to the formation of the catechol oligomers. The second reaction is the formation of quinones. This was also covered under SFA_1, section 1.8.2. The third one is the reaction of quinone with glycine. Glycine is characterized by two reactive sites (carboxylic and amine functional groups) and hence can react with other elements/compounds either through the carboxylic or the amine group. However, we think that the compounds formed through the

polycondensation of quinone and glycine must have resulted through the amine group, -NH_2). Ketones are known to react with amine; a general reaction is given as

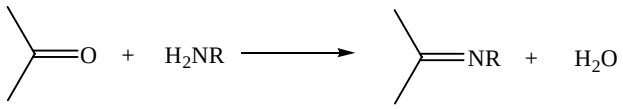

Following this general equation, we then propose

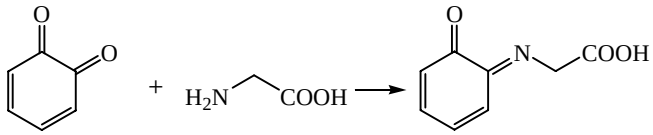

The structures showing compounds comprising both the aromatic and aliphatic parts from quinone and glycine respectively are presented in Figure 2.62 structures (f-j).

4. FULVIC ACID SYNTHESIZED BY CONDENSATION OF CATECHOL AND CYSTEINE

4.1. Elemental analysis

Both raw and extracted synthetic fulvic acid (SFA) obtained through the condensation of catechol and cysteine (SFA_4) in the quaternary system $C_6H_4(OH)_2$-$NH_2CH(CH_2SH)COOH$-NaOH-H_2O at ~ 25°C, under atmospheric oxidizing conditions and at pH = 10 have been analyzed for their elemental compositions. The results are given in Table 2.19. The composition listed in this table for catechol is identical to that already listed for SFA_1, SFA_2 and SFA_3. The composition given for cysteine has been determined in the present study and is consistent with the theoretical composition calculated from the chemical formula and the atomic weights of the elements. As was the case with the elemental analyses of SFA_1, SFA_2 and SFA_3, the weight percentages of carbon, hydrogen, oxygen, nitrogen and in this case sulfur do not sum up to 100 percent for both the raw and dialyzed SFA_4, the extracted (purified) SFA_4, and all the SFA_4 extracts. We have again made the assumption that the difference could be attributed to sodium ions (from NaOH) complexed by phenolate or carboxylate functional groups pertaining to compounds present in the SFA_4 mixture.

It appears from Table 2.19 that the proportions of all elements are constant for the dialyzed SFA_4 fraction (> 500 Da) and the extracted (purified) SFA_4. It can also be deduced from this table that the proportion of oxygen in the raw SFA_4 increased while that of carbon decreased between 0 and 63 days of synthesis. The significant decrease in the

hydrogen content can be related to the increase in the sodium content while the increased oxygen content is probably due to oxidation. It can also be noted that there is a gradual increase in the carbon and oxygen contents but a decrease in sodium content with increasing extraction. The atomic H/C ratio of the extracted SFA_4 is higher than those in SFA_1, SFA_2 and SFA_3. However, its O/C ratio is lower than those of SFA_1 and SFA_3 and greater than that of SFA_2. The nitrogen content and atomic N/C ratio of the extracted SFA_4 are significantly higher than those measured for the extracted SFA_3 (see Table 2.16 above). In contrast, no sulfur has been detected neither in the dialyzed or extracted SFA_4, nor in the various extracts. If we assume that cysteine has indeed reacted with catechol, which is suggested by the nitrogen content of the extracted SFA_4, we must then conclude that the thiol functional group of cysteine was unstable and may have been volatilized under the conditions of the experiments, hence the absence of sulfur in the reaction products.

Table 2.19. Elemental compositions of the raw and extracted fulvic acid synthesized by polymerization of catechol and cysteine. No correction for the presence of water has been made.

Sample	% C	% H	% O	% N	% S	(% Na)[a]	H/C	O/C	N/C
Catechol	66.28	5.56	28.78	-	-	(0.00)	1.000	0.326	-
Cysteine	29.53	5.87	28.19	11.63	25.35	(0.00)	2.385	0.716	0.338
SFA_4 ; 0 day (raw)	32.55	3.26	31.77	4.35	9.71	(18.36)	1.202	0.732	0.115
SFA_4 ; 63 days (raw)	28.50	2.16	35.59	3.82	10.32	(19.61)	0.909	0.937	0.115
SFA_4 ; > 500 Da [b]	32.92	2.52	34.99	4.02	0.00	(25.55)	0.919	0.797	0.105
SFA_4 ; after extraction [c]	32.93	2.39	34.68	3.99	0.00	(26.01)	0.871	0.790	0.104
SFA_4 ; extract 1 [d]	20.60	1.12	39.69	0.00	0.00	(38.59)	0.652	1.445	0.00
SFA_4 ; extract 2 [e]	20.70	1.40	39.76	0.00	0.00	(38.14)	0.812	1.441	0.00
SFA_4 ; extract 3 [f]	22.72	1.42	40.41	0.00	0.00	(35.45)	0.750	1.334	0.00
SFA_4 ; extract 4 [g]	23.64	2.26	40.57	0.00	0.00	(33.53)	1.147	1.287	0.00
SFA_4 ; extract 5 [h]	26.16	1.59	39.79	0.00	0.00	(32.46)	0.729	1.141	0.00
SFA_4 ; extract 6 [i]	26.06	1.96	46.58	0.00	0.00	(25.40)	0.903	1.341	0.00

[a] Calculated by difference (see text) [b] The SFA on this line corresponds to the dialyzed fulvic acid greater than 500 Da [c] The SFA on this line corresponds to the purified fulvic acid obtained at the end of the extraction procedure (see chapter 1) [d] First extraction with methanol [e] Second extraction with methanol [f] Third extraction with methanol [g] Fourth extraction with methanol [h] Fifth extraction with methanol [i] Extraction with methanol-water solvent system (3:2)

4.2. Scanning electron microscopy

Scanning electron microscopy (SEM) observations of samples of the raw SFA_4 obtained by condensation of catechol and cysteine at 25°C and at pH = 10 are shown in Figure 65. As for the three previous SFA, the reaction products appear as amorphous agglomerations of fine, submicrometric particles.

4.3. X-ray diffraction

X-ray diffraction spectra obtained for catechol crystals, cysteine crystals, raw SFA_4 and purified (extracted) SFA_4 are shown in Figure 2.66 (a), (b), (c) and (d), respectively. The diffractograms have been offset for the sake of clarity. The diffractograms of both raw and purified SFA_4 are again significantly different from those of catechol and cysteine, which suggests that SFA_4 may have formed as a result of reactions between catecholate anions and radicals, cysteine ions, dissolved CO_2 and hydroxide OH^- anions. The absence of peaks in the X-ray diffractograms (c) and (d) of both raw and purified SFA_4 proves that they are composed of amorphous solid compounds, and that both SFA_4 mixtures contain less than 5% of crystalline compounds (i.e. unreacted catechol and cysteine or other unidentified crystalline by-products).

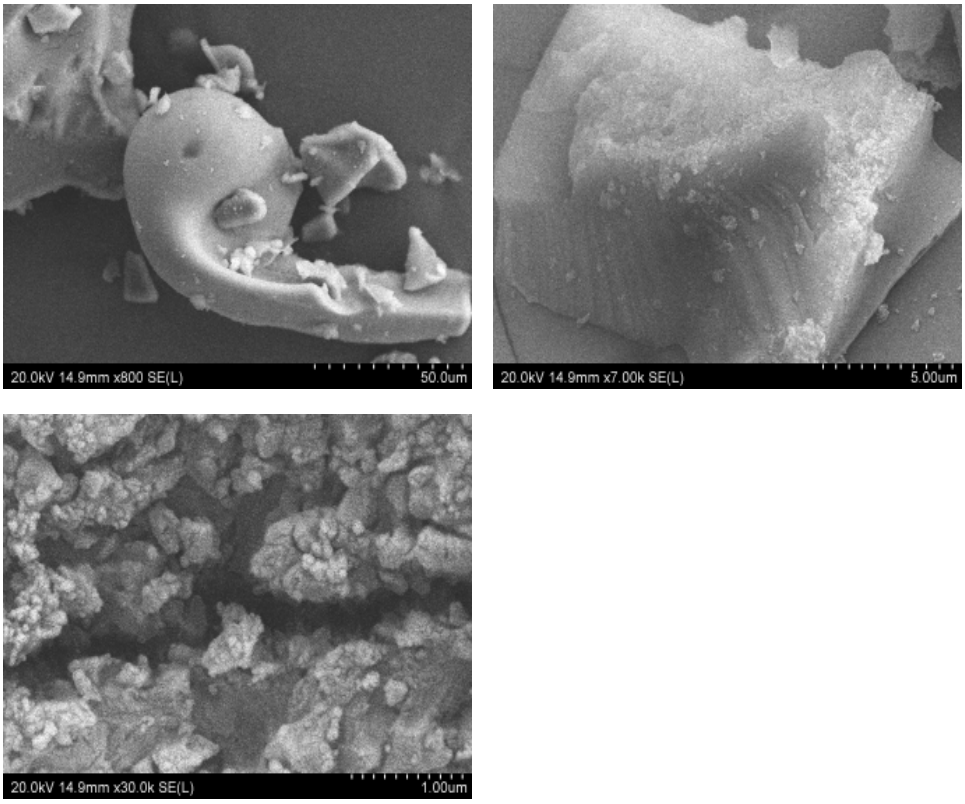

Figure 2.65. SEM photographs of SFA_3. Magnification (top left) x 800 (top right) x 7000 (bottom left) x 30,000.

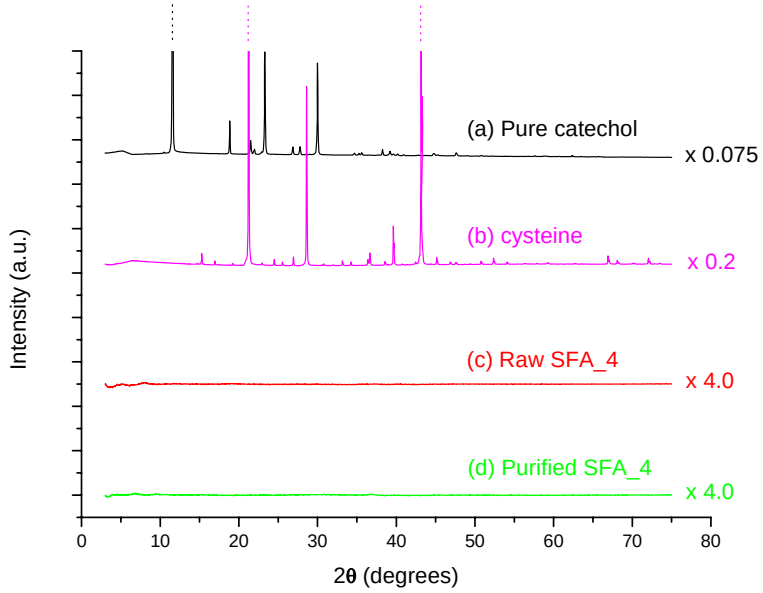

Figure 2.66. X-ray diffraction spectra of crystalline catechol (a), crystalline cysteine (b), raw SFA_4 prior to extraction (c), and purified (extracted) SFA_4.

4.4. ATR-FTIR spectroscopy

The ATR-FTIR spectrum of catechol has already been discussed in section *1.4.1* and will not be presented again.

4.4.1. Cysteine

Cysteine, a.k.a. 2-amino-3-thiol-propanoic acid ($NH_2CH(CH_2SH)COOH$), contains four different functional groups, including an aliphatic methylene $–CH_2–$ group, a carboxylic acid –COOH group, a primary amine $–NH_2$ group, and a thiol –SH group. The characteristic vibration bands of these four functional groups can be seen in the ATR-FTIR spectrum of pure cysteine recorded at 25ºC and 0.1 MPa and shown in Figure 2.67. These vibration bands are discussed separately below for each functional group.

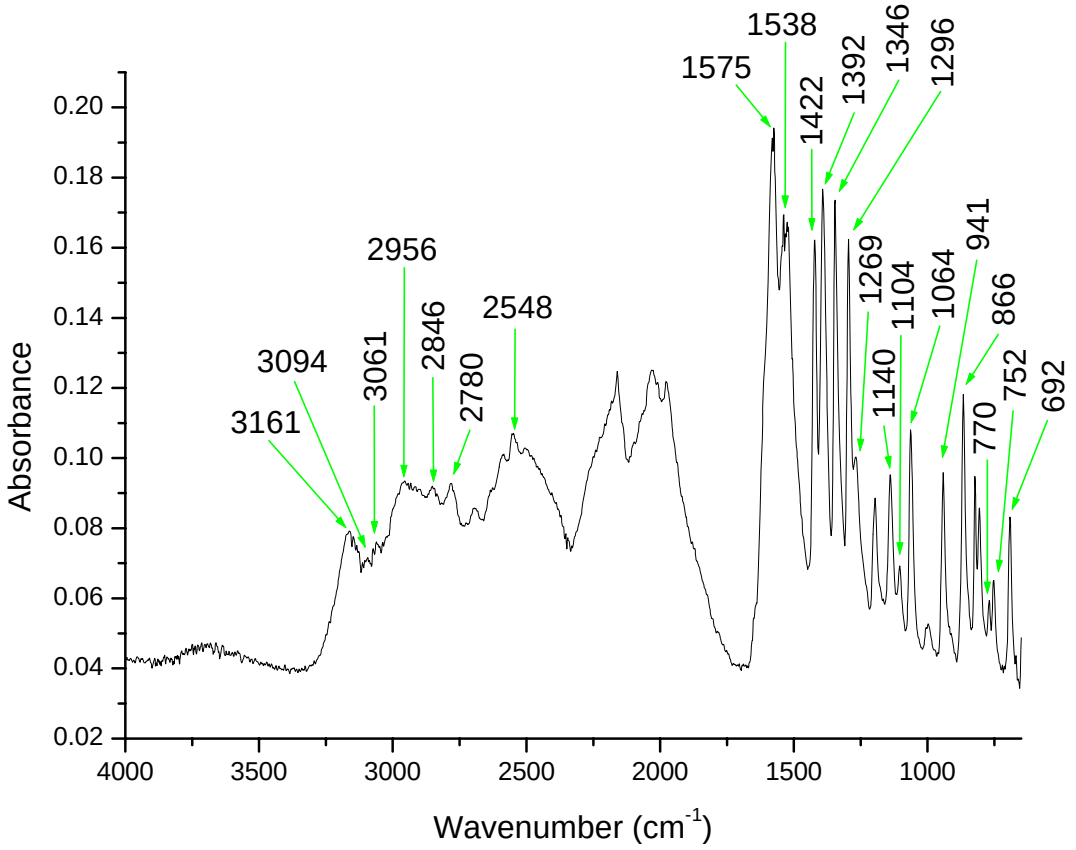

Figure 2.67. ATR-FTIR spectrum of pure L-cysteine ($NH_2CH(CH_2SH)COOH$): T = 25°C, P = 0.1 MPa.

✓ aliphatic $–CH_2–$ group

This group is characterized by three vibration modes:

- ❖ the stretching mode of C–H bonds which is characterized by a weak broadband in the range 3000 – 2400 cm^{-1}, with two $\nu_a CH_2$ and $\nu_s CH_2$ bands at 2956 cm^{-1} and 2780 cm^{-1}, respectively. The broadband in the range 2700 – 2400 cm^{-1} is assigned to the overtone of νC–H stretching modes.
- ❖ the stretching mode of C–C chains which appear in the region 1200 – 800 cm^{-1}. According to Silverstein et al. (1991), these νC–C bands are of little value for identification. They could overlap with vibrations of the amine group, including the $\delta_r NH_3^+$ rocking mode (1140 cm^{-1}, 866 cm^{-1}, and 692 cm^{-1}) and the νC–N stretching mode at 1064 cm^{-1}.
- ❖ the deformation mode of $–CH_2–$ groups, which raises three distinct bands originating from (Wojtkowiak and Chabanel, 1977)
  - a $\delta_t CH_2$ twisting mode at 1346 cm^{-1}
  - the $\delta_r CH_2$ rocking mode of the methylene group, with two distinct bands at 770 cm^{-1} and 752 cm^{-1}.

✓ carboxylic –COOH group

This group is characterized by four vibration modes:

- ❖ the stretching mode of O–H bonds, which corresponds to a weak broadband in the region 3000 – 2400 cm^{-1}. This broadband overlaps with three other stretching bands, which include a $\nu_a N–H$ band around 3000 cm^{-1}, a $\nu_a C–H$ near 2956 cm^{-1}, and a $\nu_s C–H$ around 2780 cm^{-1}.
- ❖ the bending mode of O–H bonds.
  - The $\delta_b O–H$ in-plane bending mode of the carboxylic group raises a distinct band at 1422 cm^{-1}. This band involves C-O-H interactions.
  - The $\delta_b O–H$ out-of-plane bending mode of this group is characterized by a distinct band at 941 cm^{-1}. This band overlaps with the $\delta_b S–H$ out-of-plane bending mode of the thiol group (see below).
- ❖ the stretching mode of the carboxylate anion COO^-, which is characterized by two distinct bands , one antisymmetric $\nu_a COO$ stretching band at 1575 cm^{-1} and one weak symmetric $\nu_s COO$ stretching band at 1392 cm^{-1}.
- ❖ the bending mode of C–O bonds, corresponding to two distinct bands at 1296 cm^{-1} and 1269 cm^{-1}.

✓ primary amine $–NH_2$ group

This group is characterized by three vibration modes

- ❖ the stretching mode of N–H bonds, which is coupled and characterized by two weak absorption bands near 3094 cm^{-1} and 3061 cm^{-1}.
- ❖ the bending mode of N – H bonds
  - the δ_sN–H scissoring mode is observed as a weak band around 1610 cm^{-1}.
  - the δ_bN–H bending mode is characterized by a distinct band at 1538 cm^{-1}.
  - the δ_rN–H rocking mode is represented by a distinct band at 1140 cm^{-1}.
  - the δ_wN–H wagging mode appears in two distinct bands at 866 cm^{-1} and 692 cm^{-1}.
- ❖ the stretching mode of C–N bonds. Two medium-to-weak distinct νC–N bands for the unconjugated C–N linkage in aliphatic primary amines appear at 1104 cm^{-1} and 1064 cm^{-1}. The latter overlaps with the νC–C stretching bands.

✓ thiol –SH group

This group is characterized by two vibration modes, including

- ❖ the stretching mode of S–H bonds which is characterized by one weak νS–H absorption band near 2548 cm^{-1}.
- ❖ the bending mode of S–H bonds which corresponds to a weak δ_bS–H band at 941 cm^{-1}. As mentioned above, this band overlaps with the δ_bO–H out-of-plane bending mode of the OH group of carboxylic acids.

4.4.2. Synthetic fulvic acid SFA_4

The ATR-FTIR spectra of the raw and purified (extracted) synthetic fulvic acids SFA_4 are presented in Figure 2.68. These spectra are again characterized by four groups of absorption bands which appear in the following wavenumber ranges: 3700 – 2350 cm^{-1}, 1800 – 1400 cm^{-1}, 1400 – 900 cm^{-1}, and 900 – 650 cm^{-1}.

- ✓ 3700 – 2350 cm^{-1}: this wavenumber range contains eight distinct bands, the first seven of which have already been described:
  - ❖ a $\nu_a NH_2$ antisymmetric stretching band of a primary amine $–NH_2$ group (3400 – 3380 cm^{-1})
  - ❖ a $\nu_s NH_2$ symmetric stretching band of a primary amine $–NH_2$ group (3344 – 3324 cm^{-1})
  - ❖ a νOH stretching band of an alcohol O–H functional group (3700 – 3300 cm^{-1})

- a νOH stretching band of the associated O–H group in a carboxylate functional group (3000 – 2500 cm^{-1})
- a νCH stretching band of an aromatic C–H bond (3075 – 3030 cm^{-1})
- ν_aCH_3 and ν_aCH_2 antisymmetric stretching bands of alkanes (2970 – 2915 cm^{-1})
- ν_sCH_3 and ν_sCH_2 symmetric stretching bands of alkanes (2880 – 2845 cm^{-1})
- a νSH stretching band of a thiol –SH group (2650 – 2550 cm^{-1})

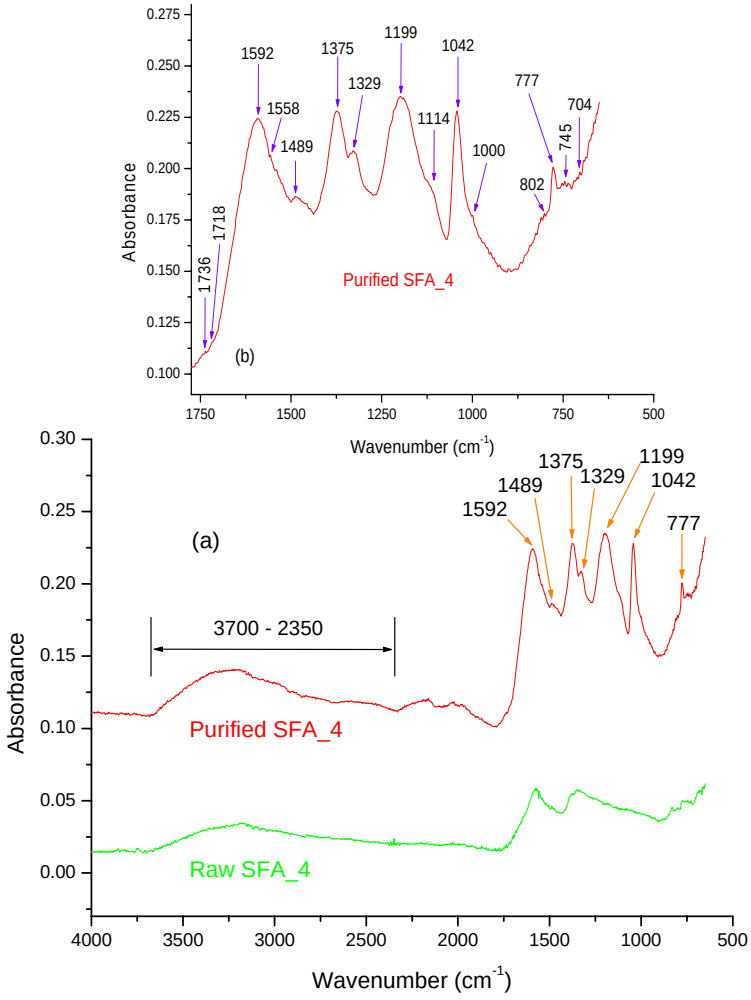

Figure 2.68. ATR-FTIR spectrum of raw and purified SFA_4. T = 25°C, P = 0.1 MPa. (a) complete spectrum; (b) enlargement of the lower wavenumber portion of the spectrum.

✓ 1800 – 1400 cm^{-1}: this wavenumber range is characterized by three absorption broadbands near 1592 cm^{-1}, 1558 cm^{-1}, and 1489 cm^{-1}. The first two of these broadbands are assigned to the antisymmetric stretching ν_aOCO^- of the carboxylate functional group in two different environments. Note that these two bands could also

correspond to the two vibration modes of aliphatic $–NH_2$ amine group, including the δ_sN–H scissoring mode (weakband around 1610 cm^{-1}) and the δ_bN–H bending mode (band near 1540 cm^{-1}). The small broadband near 1489 cm^{-1} characterizes the νC=C stretching mode of aromatic rings.

- ✓ 1400 – 900 cm^{-1}: this group of vibration bands includes
  - ❖ an intense broadband near 1375 cm^{-1} which is due to the $\nu_s OCO^-$ symmetric stretching of the carboxylate group
  - ❖ a distinct band at 1329 cm^{-1} corresponding to the stetching δCH_2 mode of the methylene group of the cysteinate ion
  - ❖ a very intense broadband in the region 1250 cm^{-1} – 1150 cm^{-1} with an absorption maximum at 1199 cm^{-1} and a shoulder near 1230 cm^{-1}. This broadband probably represents the sum of six different vibration modes (Wojtkowiak and Chabanel, 1977):
    - the νC–O stretching mode of the carboxylate group of cysteine (1210 cm^{-1} – 1320 cm^{-1})
    - the ν_aC–O–C antisymmetric stretching mode of an aromatic Ar–O–Ar ether (1270 cm^{-1} – 1230 cm^{-1})
    - the δC–H in-plane bending mode of aromatic rings (1225 cm^{-1} – 950 cm^{-1}) in different environments
    - the δ_rN–H rocking mode of the amine groups (band at 1140 cm^{-1})
    - the νC–O stretching mode of the alcohol groups (1200 cm^{-1} – 1000 cm^{-1})
    - the ν_sC–O–C symmetric stretching mode of ether (1150 cm^{-1} – 1100 cm^{-1})
  - ❖ one band near 1114 cm^{-1} and one intense and distinct band at 1042 cm^{-1} have been observed. Both of them could be assigned to the νC–N stretching mode of unconjugated C–N groups of aliphatic primary amines.
  - ❖ a broadband in the region 1150 cm^{-1} – 900 cm^{-1} could correspond to the sum of four different vibration modes, including
    - the δC–H in-plane bending mode of aromatic rings (1225 cm^{-1} – 950 cm^{-1}) in different environments
    - the νC–C stretching vibrations of the aliphatic groups in cysteine (1200 – 800 cm^{-1})
    - the δ_bO–H out-of-plane bending mode of the hydroxyl OH of the carboxylic group (distinct band near 940 cm^{-1})

- the δ_bS–H out-of-plane bending mode of the thiol –SH group (distinct band near 940 cm^{-1})

✓ 900 – 650 cm^{-1}: this group of vibration bands includes

❖ one major and distinct band at 777 cm^{-1} which characterizes the δC–H out-of-plane bending of C–H bonds of aromatic derivatives which have three substitutions at positions 1,2,3 (810 cm^{-1} – 750 cm^{-1})

❖ a minor broadband in the region 810 cm^{-1} – 800 cm^{-1} which can be assigned to the δC–H out-of-plane bending C–H bonds of aromatic derivatives with either three substitutions at positions 1,2,4 or four substitutions at positions 1,2,3,4

❖ a minor broadband in the region 745 cm^{-1} – 700 cm^{-1} corresponding to the δC–C out-of-plane bending of C=C bonds of aromatic derivatives having three substitutions at positions 1,2,3 and 1,2,4 (730 cm^{-1} – 685 cm^{-1}, Wojtkowiak and Chabanel, 1977).

4.5. UV-Visible absorption spectrophotometry

The UV-visible absorption spectra of the raw SFA_4 (0.022 $g \cdot L^{-1}$; pH = 10.13±0.01), purified SFA_4 (0.022 $g \cdot L^{-1}$; pH = 9.99±0.01), and catechol (0.022 $g \cdot L^{-1}$; pH = 10.48±0.01) are shown in Figure 2.69. The absorption spectrum of cysteine is not shown because this compound does not absorb in the wavelength range 250 – 800 nm. Catechol in solution at pH = 10.48±0.01 is characterized by an intense absorption band at 275 nm and a minor and broad absorption band with a maximum near 327 nm.

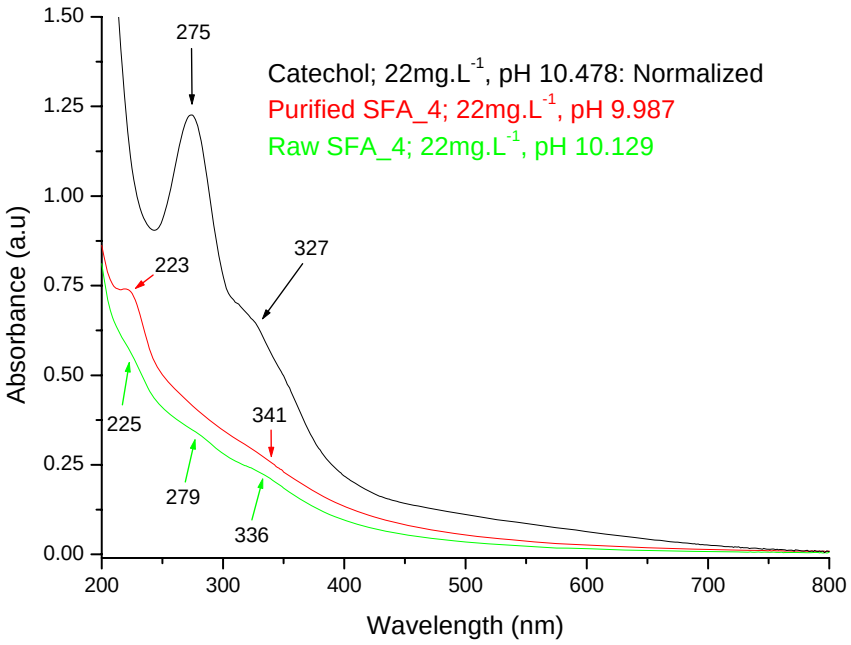

Figure 2.69. UV-Visible spectra of raw SFA_4 (green spectrum), purified SFA_4 (red spectrum), and catechol (black spectrum). Measurements were made with a 10 mm path length quartz cuvette.

The spectrum of the SFA_4 synthetic fulvic acid obtained after solvent extractions (red spectrum) differs from that of catechol (black spectrum) by the presence of two broadbands near 223 nm and 341 nm. The first broadband around 223 nm could result from two bands, including aromatic E_2 bands and conjugated K bands. The second broadband around 341 nm probably result from the hyperconjugation of π electrons or aromatic rings which are bonded to one another by two types of chemical bonds which are either carbon-carbon bonds between two aromatic rings (as in biphenyl structure) or ether bonds between two aromatic rings (as in diphenyl ether structure). The existence of these broadbands indicates that the SFA_4 mixture consists of high molecular weight compounds containing numerous atoms. In addition, the formation of SFA_4 from catechol and cysteine in basic solution (pH ~ 10) seems to be accompanied by a strong hypochromic shift in the ultraviolet region.

The effect of the concentration of purified SFA_4 on the absorption intensity at pH = 7.0 is shown in Figure 2.70 for two different concentrations of 0.022 $g \cdot L^{-1}$ and 0.044 $g \cdot L^{-1}$. It can be seen in this figure that the spectrum for the concentration of 0.044 $g \cdot L^{-1}$ differs from that for the concentration of 0.022 $g \cdot L^{-1}$ by the disappearence of the absorption band at 221 nm. Moreover, at 200 nm and 400 nm wavelengths, the absorption intensity is not multiplied

by a factor of 2 with increasing concentration of SFA_4 from 0.022 to 0.044 $g \cdot L^{-1}$. These differences may result from three causes:

- SFA_4 is a heterogeneous mixture of fulvic acids of various chemical compositions;
- in neutral solutions (pH ~ 7), the ratio of neutral to ionized SFA_4 compounds bearing thiol functional groups varies drastically, even with small pH variations. This is due to the fact that neutral pH at 25ºC differs by only 1.14 units from the second ionization constant of cysteine (pK_2 =8.14, which corresponds to the ionization of the thiol group). The difference between the pH values at which the two SFA_4 samples were analyzed is approximately 0.16 pH unit. Such a small difference could translate into a significant change of the neutral to ionized ratio of the individual compounds in the SFA_4 mixture, and a modification of the absorption spectrum. It should perhaps be recalled here that the ionization of a fulvic acid generally leads to a change in color and consequently a change in the UV-visible absorption spectrum.
- at pH ~ 7, which is close to the second ionization constant for the thiol group in cysteine (pK_2 =8.14), the effect of ionic strength becomes non negligible with respect to the stability of neutral and ionized SFA_4 compounds with thiol groups. The two SFA_4 samples analyzed in the present study were not analyzed at the same ionic strength. The difference in ionic strength between the two analyses may have resulted in a modification of the relative stabilities of some individual fulvic acids and therefore of their UV-visible absorption spectrum.

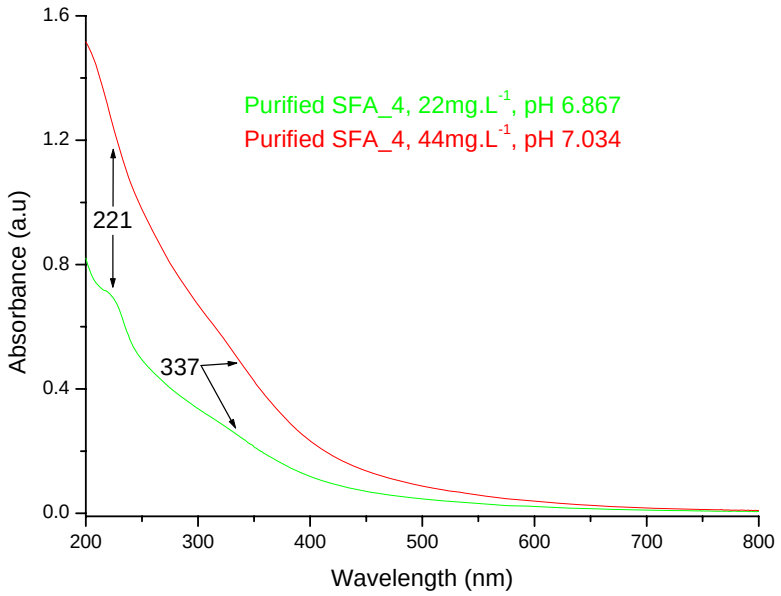

Figure 2.70. UV-Visible spectra of purified SFA_4 as a function of concentration at pH ~ 7. Measurements were made with a 10 mm path length quartz cuvette.

The effect of pH on the absorption intensity of purified SFA_4 is shown in Figure 2.71. It can be seen in this figure that increasing the pH of the solution from 6.87±0.01 to 9.99±0.01 again results in a slight hyperchromic effect (approximately +5%) of the absorption intensity without modifying the shape of the absorption spectrum. As suggested above, the hyperchromic effect observed in basic solution probably results from the ionization of abundant alcohol functional groups in the individual fulvic acids constituting the SFA_4 mixture. Ionization of these alcohol functional groups increases the number of nonbonded electrons on the oxygen atoms and of the $n \rightarrow \pi^*$ forbidden transitions under UV-visible excitation. As a result, the ionized alcohol species is colored and produces a hyperchromic shift.

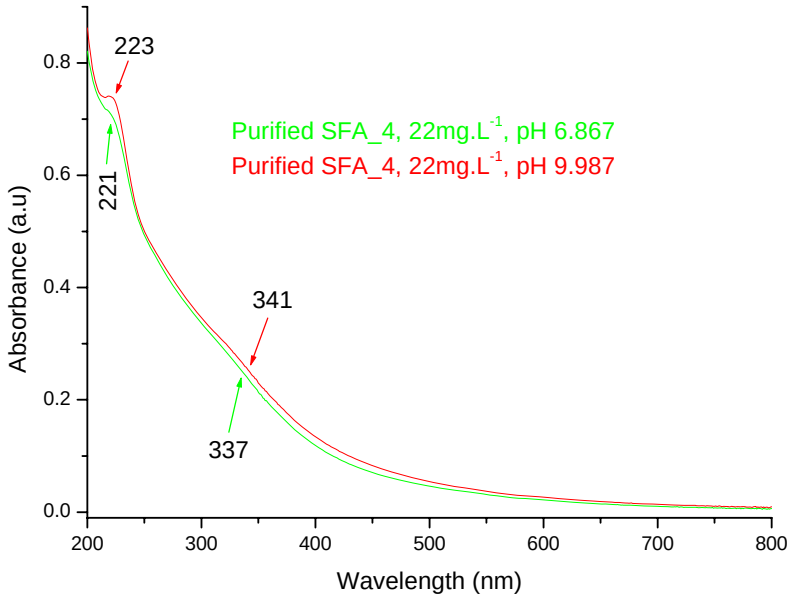

Figure 2.71. UV-Visible spectra of purified SFA_4 as a function of pH at a concentration of 0.022 g·L^{-1}. Measurements were made with a 10 mm path length quartz cuvette.

4.6. Electrospray ionization – mass spectrometry (ESI-MS)

A small amount of raw, lyophylized SFA_4 was dissolved in milli-Q water and analyzed by ESI-MS in both positive-ion (PI) and negative-ion (NI) modes. The purified SFA_4 has been analyzed by APCI-MS (see below). The ESI-MS spectra obtained in PI and NI modes are shown in Figure 2.72. It can be noted in this figure that the spectrum obtained in NI mode shows less intense peaks and appears to be noisy compared to the spectrum obtained in PI mode. Consequently, only the latter spectrum is discussed below.

Several peaks can be observed in the 0 – 1000 m/z range. These peaks are identified in Table 2.20 with their m/z values, with the exception of the peaks with m/z values lower than 100 and the peak with m/z equal to 185.06. No interpretation could be given for those peaks. Also listed in Table 2.20 are possible chemical formulas coinciding with (or rather approaching) the m/z values. The difference between the molecular weights and the m/z values is usually within 0.4 Da, and in some cases ~ 40 mDa. The chemical formulas were established by considering the possibility that Na^+ of H^+ ions or H_2O molecules could be attached to these fulvic acid ions. The Na^+ or H^+ ions and H_2O molecules are indicated in grey in Table 2.20, as are the molecular weights corresponding to the sum of the actual single fulvic acid molecules and their associated Na^+ or H^+ ions, or H_2O molecules. Tentative molecular structures corresponding to these chemical formulas and m/z ratios are shown in Figure 2.73. The Na atoms appearing in some of the structures result from the NaOH which is used to buffer the pH during the synthesis. The five molecular structures depicted in Figure 2.73 include two dimers, one trimer, one pentamer, and one heptamer of substituted aromatic rings. With the exception of structure (e), which corresponds to the heptamer, cysteine appears as an aliphatic part of the SFA_4 individual fulvic acids. The aromatic rings are linked to each other through aromatic ether bonds, while cysteine appears to be attached to these aromatic rings through its thiol functional group, resulting in the formation of C_{aro}–S–C_{ali} sulfide bonds. Note that there are other possibilities of linkages for cysteine than those shown in Figure 2.73. Possible reaction mechanisms leading to the formation of compounds with structures such as those shown in Figure 2.73 will be presented in the discussion to follow.

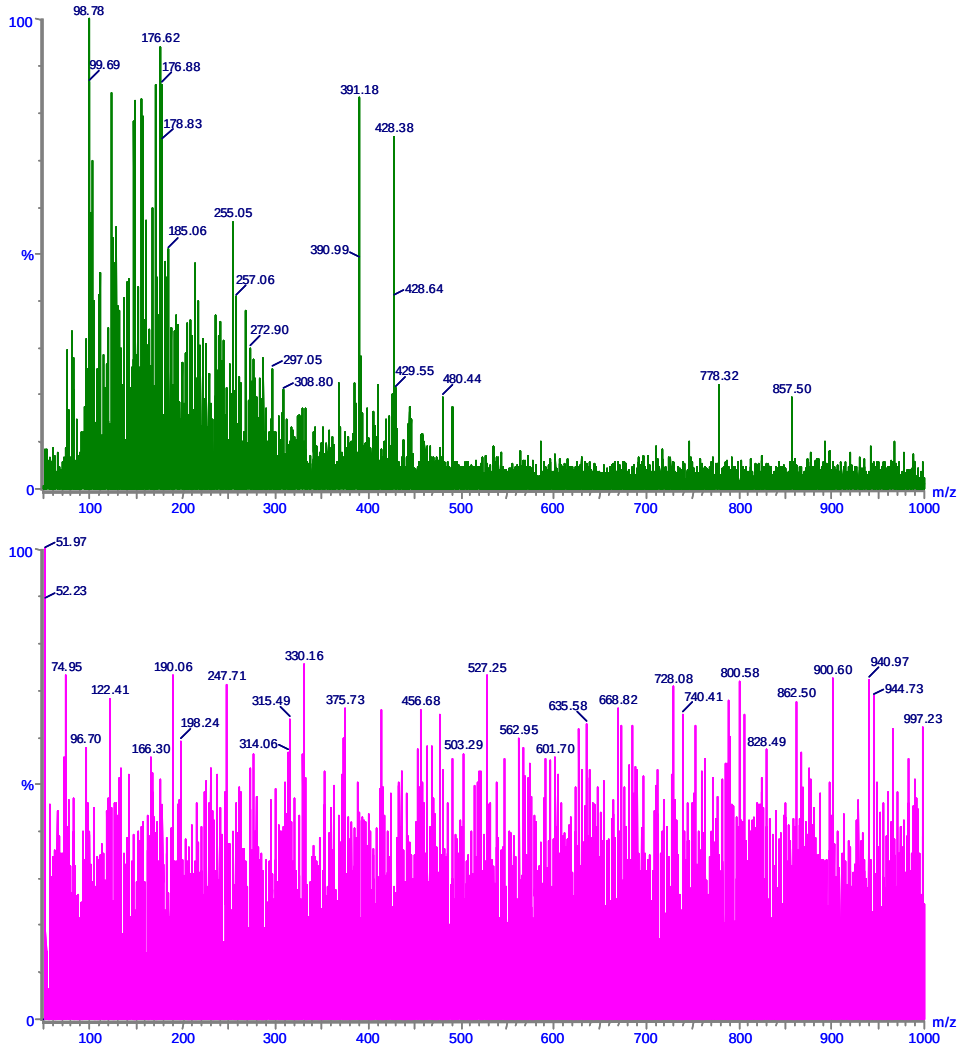

Figure 2.72. ESI-MS spectra of raw SFA_4 analyzed under both positive and negative modes (top and bottom, respectively).

Table 2.20. Summary of m/z ratios obtained in the ESI-MS analysis (PI mode) of the raw SFA_4, together with their corresponding molecular weights and possible chemical formulas for individual compounds in the SFA_4 mixture.

m/z	Chemical Formula	Molecular weight		Structures
176.62	$[C_6H_4O_4$ (+ 2 H_2O + H)$]^+$	154.12	(177.04)	Structure (b) in Fig. 2.8
255.05	$[C_{12}H_{10}O_4$ (+ 2 H_2O + H)$]^+$	218.06	(255.09)	Structure (f) in Fig. 2.16
391.99	$[C_{15}H_{15}O_6NS$ (+ 3 H_2O + H)$]^+$	337.06	(392.102)	Structure (a) in Fig. 2.73
428.38	$[C_{15}H_{14}NNaO_8S$ (+ H)$]^+$	391.03	(428.063)	Structure (b) in Fig. 2.73
480.44	$[C_{21}H_{19}NO_9S$ (+ H_2O)$]^+$	461.08	(480.096)	Structure (c) in Fig. 2.73
778.32	$[C_{33}H_{24}NNa_3O_{14}S$ (+ H_2O + H)$]^+$	759.06	(778.079)	Structure (d) in Fig. 2.73
857.50	$[C_{42}H_{28}O_{14}Na_2$ (+ 3 H_2O + H)$]^+$	802.13	(857.167)	Structure (e) in Fig. 2.73

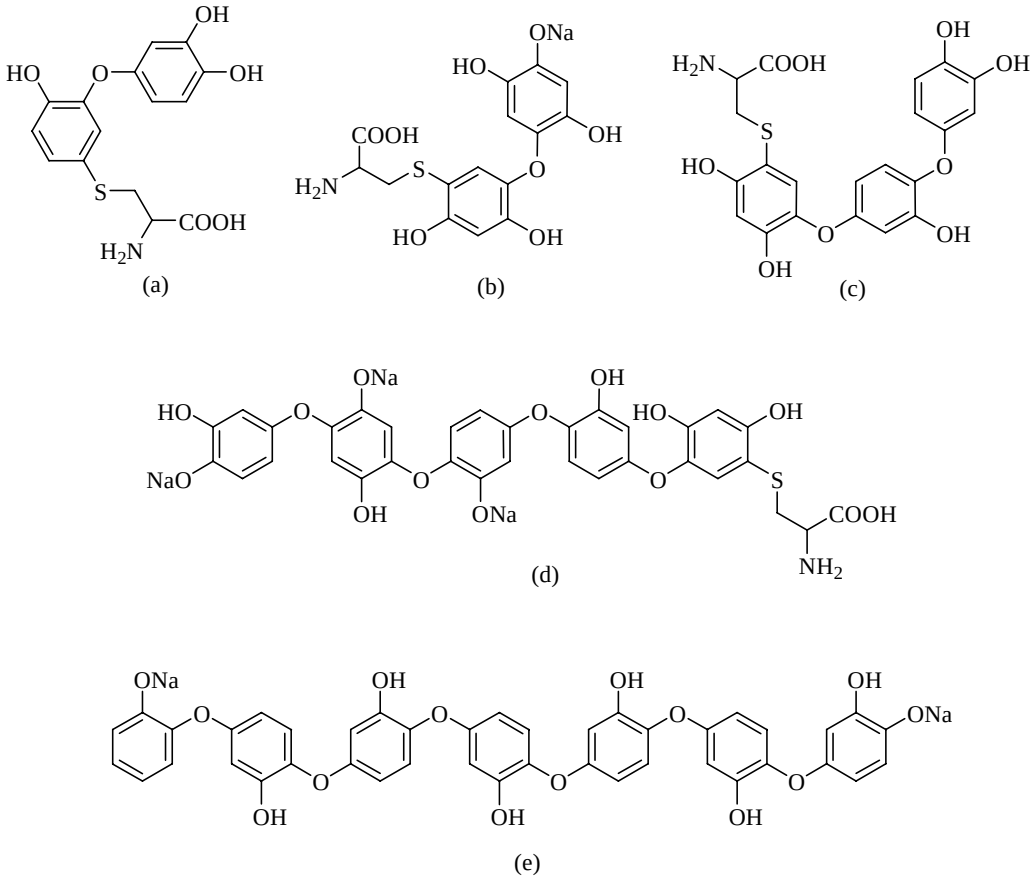

Figure 2.73. Possible molecular structures of individual fulvic acids in the raw SFA_4 mixture deduced from the ESI-MS analysis (positive ion mode).

4.7. Atmospheric pressure chemical ionization mass spectrometry

Despite the identification of several compounds, it appears that the SFA_4 did not ionize significantly during the ESI-MS analysis reported above. This may have been due

either to a low concentration of the compounds present in the SFA_4 mixture, or to the lack of separation before the analysis. This prompted us to further analyze both the raw and purified SFA_4 mixtures by atmospheric pressure chemical ionization mass spectrometry (APCI-MS), coupled to liquid chromatography and using tandem mass spectrometry (LC-APCI-MS-MS) in the case of the raw SFA_4. We found again this technique to give better results for the characterization of our SFA_4 mixtures. The protocols and results obtained for each of the samples are discussed separately below.

4.7.1. Analysis of raw SFA_4 by LC-APCI-MS-MS

The analysis of the raw SFA_4 mixture was performed by tandem mass spectrometry (MS/MS) after first separating the components of the mixture by liquid chromatography (LC) using a U3000 Dionex liquid chromatograph interfaced with a Bruker micro Q-ToF mass spectrometer. A saturated solution of raw SFA_4 was prepared by dissolving lyophilized solid SFA_4 in milli-Q water containing 0.2 % by volume of formic acid to favor ionization of the fulvic acid components during the analysis. The resulting solution was filtered through a 0.45 μm millex®-HA filter unit. The pH of the solution was lowered to pH ~ 5-8 using formic acid prior to injecting the sample on the LC column. The different parameters used in the LC-ACPI-MS-MS analysis of raw SFA_4 are the same as those given in Table 4, section 1.7.1.

The tandem mass spectrometry analysis was performed in an automatic mode. Peaks showing intensity higher than 5000 (in arbitrary units) were selected for the fragmentation in collision cells with the following parameters:

m/z	Isolation width	collision energy
300	8 Da	10 V
500	10 Da	15 V
1000	10 Da	20 V

The base peak chromatograms (BPC) shown in Figure 2.74 for SFA_4 are for retention times ranging between 0 and 30 minutes for the analysis carried out in positive-ion (PI) mode, and between 0 and 42 minutes for the analysis carried out in negative-ion (NI) mode. It can be deduced from these base peak chromatograms that elution was poor in the case of SFA_4 compared to the other three SFA. There are wide bumps between 5 – 21 and 39 – 41 minutes in the chromatogram under negative mode. Under positive mode, the chromatogram is characterized by poor separation above four minutes. Each peak probably corresponds to a series of compounds with similar elution times rather than a single compound.

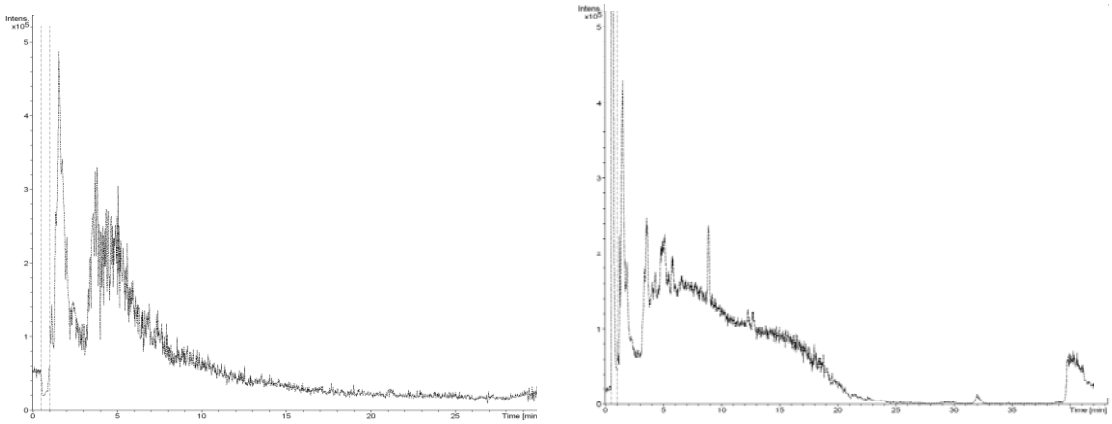

Figure 2.74. Base peak chromatograms (BPC) obtained in the LC-APCI-MS-MS of the raw SFA_4 mixture in positive-ion mode (left) and negative-ion mode (right).

The peak appearing after 1.0 minute of elution in Figure 2.74 (PI mode) correspond to clusters of sodium formate (HCOONa). Under PI mode, these clusters are represented by $[(HCOONa)_n + Na^+]$. The APCI-MS peaks with m/z values equal to 363, 431, 499, 567, 635, 703, 771, 839, 907 and 975 in Figure 2.75 correspond to clusters with n = 5, 6, 7, 8, 9, 10, 11, 12, 13 and 14, respectively.

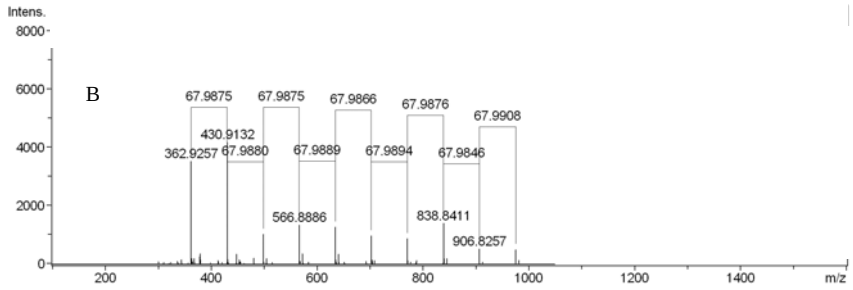

Figure 2.75. APCI-MS spectrum of the raw SFA_4 fraction eluted at 1.0 minute and analyzed in positive mode.

Selected retention times are listed in Table 2.21 along with the results of the mass spectrometry analysis. The selection of retention times was rendered necessary for clarity reasons in the discussion which is presented below. Also listed in Table 2.21 are possible chemical formulas and molecular weights corresponding to the m/z values. The difference between the molecular weights and m/z values is usually within 0.3 Da, and in some cases ~ 2.9 mDa. The mass spectra corresponding to retention times of 5.9 and 6.8 minutes (both positive ion mode) and 8.9 and 9.4 minutes (both negative ion mode) are shown in Figures 76 and 77 respectively. The molecular structures corresponding to the chemical formulas proposed in Table 2.21 are depicted in Figure 2.78.

Table 2.21. Summary of the LC retention times (RT) corresponding to the peaks in Figure 2.74 and of the m/z ratios obtained in the LC-APCI-MS-MS analysis (positive and negative modes) of the raw SFA_4 mixture, as well as of possible chemical formulas and corresponding molecular weights for individual fulvic acids in the raw SFA_4 mixture.

Peak number (Fig. 2.74)	RT (min)	m/z	Chemical formula	Molecular weight	Structures
Positive mode					
	5.9	423.8752	$[C_{15}H_{15}O_8NS + 3\ H_2O + H]^+$	424.091	Structure (a) in Fig. 2.78
		664.8565	$[C_{30}H_{18}O_{11}Na_4 + H_2O + H]^+$	665.062	Structure (h) in Fig. 2.14
		781.8640	$[C_{33}H_{23}O_{14}NSNa_4 + H]^+$	782.051	Structure (b) in Fig. 2.78
	6.8	320.9965	$[C_{12}H_7O_4Na_3 + 2\ H_2O + H]^+$	321.033	Structure (l) in Fig. 2.16
		388.9830	$[C_{18}H_{12}O_6Na_2 + H_2O + H]^+$	389.061	Structure (e) in Fig. 2.44
Negative mode					
	8.9	342.9815	$[C_{12}H_9O_6Na + 4\ H_2O - H]^-$	343.064	Structure (g) in Fig. 2.8
		403.0603	$[C_{18}H_{12}O_7Na_2 + H_2O - H]^-$	403.041	Structure (k) in Fig. 2.10
		469.0389	$[C_{18}H_{12}O_{10}Na_2 + 2\ H_2O - H]^-$	469.036	Structure (l) in Fig. 2.10
		513.0116	$[C_{18}H_{10}O_{10}Na_4 + 2\ H_2O - H]^-$	513.000	Structure (q) in Fig. 2.10
		580.9933	$[C_{30}H_{21}O_{10}Na + H_2O - H]^-$	581.106	Structure (o) in Fig. 2.44
		654.9355	$[C_{30}H_{20}O_{11}Na_2 + 3\ H_2O - H]^-$	655.104	Structure (g) in Fig. 2.14
		742.9824	$[C_{36}H_{24}O_{14}Na_2 + H_2O - H]^-$	743.099	Structure (c) in Fig. 2.78
		816.9203	$[C_{42}H_{28}O_{15}Na_2 - H]^-$	817.115	Structure (d) in Fig. 2.78
	8.9	387.9812	$[C_{15}H_{15}O_7NS + 2\ H_2O - H]^-$	388.070	Structure (e) in Fig. 2.78
		528.9845	$[C_{24}H_{16}O_9Na_2 + 2\ H_2O - H]^-$	529.072	Structure (r) in Fig. 2.10
		916.9116	$[C_{48}H_{34}O_{17} + 2\ H_2O - H]^-$	917.193	Structure (f) in Fig. 2.78
	9.4	322.9364	$[C_{12}H_9O_5Na + HCOONa - H]^-$	323.014	Structure (g) in Fig. 2.78
		451.3435	$[C_{18}H_{12}O_{10}Na_2 + H_2O - H]^-$	451.025	Structure (l) in Fig. 2.10
			$[C_{24}H_{18}O_8 + H_2O - H]^-$	451.103	Structure (m) in Fig. 2.10
		497.3454	$[C_{18}H_{10}O_{10}Na_4 + H_2O - H]^-$	497.005	Structure (q) in Fig. 2.10

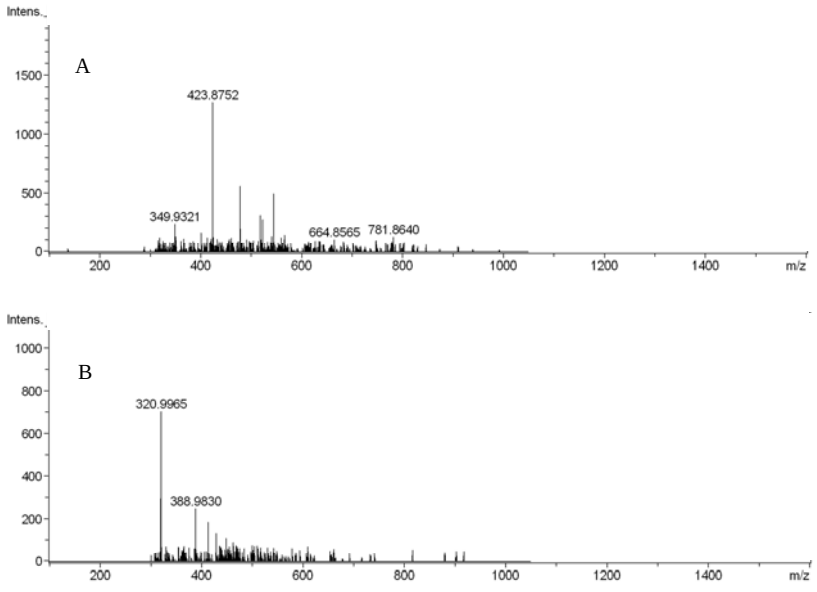

Figure 2.76. APCI-MS spectra of the raw SFA_4 fraction eluted at 5.9 minutes (A) and at 6.8 minutes (B), both analyzed in positive-ion mode.

In the analyses carried out in PI mode, at retention times of 5.9 and 6.8 minutes (Figure 2.76), five m/z values have been assigned to molecular structures shown in Figure 2.78. Structures (a) and (b) are the newly proposed structures while the other structures mentioned in Table 2.21 (but not shown in Figure 2.78) correspond to m/z values which have already been discussed in the previous sections. The m/z value equal to 350 observed under PI mode at a retention time of 5.9 minutes has not been assigned to any structure. In the case of the analyses carried out in NI modes, there appears to be similarities with the analyses carried out previously for SFA_1, SFA_2 and SFA_3 in relation to their retention times. SFA_1, SFA_2 and SFA_3 have elution at retention times equal to 8.9 minutes while SFA_4 has elution at 8.8 and 9.0 minutes. They all have m/z equal to 403 and 513 in common, though there are other m/z values that are common amongst each other but not necessarily common in all the four SFA. Several of the m/z values observed in the spectra appearing in Figure 2.77 have been assigned to the molecular structures shown in Figure 2.78. For the retention time equal to 8.9 minutes, two spectra (A and B) in Figure 2.77, while only one spectrum is shown for the retention time of 9.4 minutes. Most of m/z values observed in Figure 2.77 have already been interpreted and discussed in the preceding sections. A molecular structure could not be assigned for the m/z value equal to 230 for the retention time of 8.9 minutes under negative-ion mode analysis. Molecular structures (a), (b) and (e) in Figure 2.78 are characterized by both aromatic and aliphatic parts corresponding to polycatechol and cysteine subunits, respectively, while structures (c), (d), (f) and (g) do not contain the cysteine subunit. The structures shown in Figure 2.78 consist of highly substituted aromatic rings which are linked to each other mainly through aromatic ether (—O—) bonds, with in some cases C_{aro}—S—C_{ali} linkages. Even though C_{aro}-C_{aro} are not shown, it does not mean that fulvic acids with this particular linkage are not formed (see above). Possible reactions leading to the formation of the structures shown in Figure 2.78 will be presented in the discussion below.

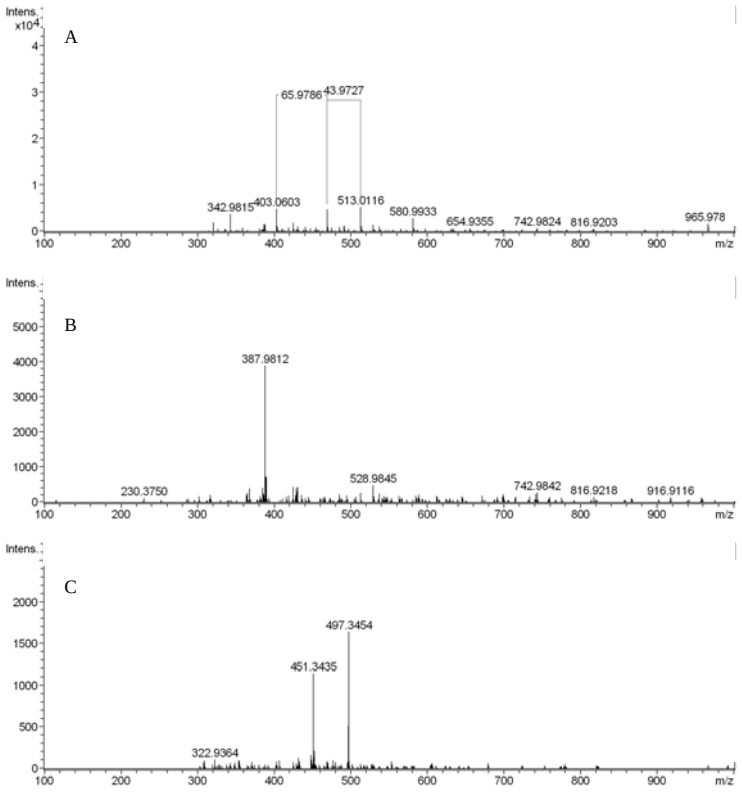

Figure 2.77. APCI-MS spectra of the raw SFA_4 fraction eluted at 8.9 minutes (both A and B) and a 9.4 minutes (C), all analyzed in negative-ion mode.

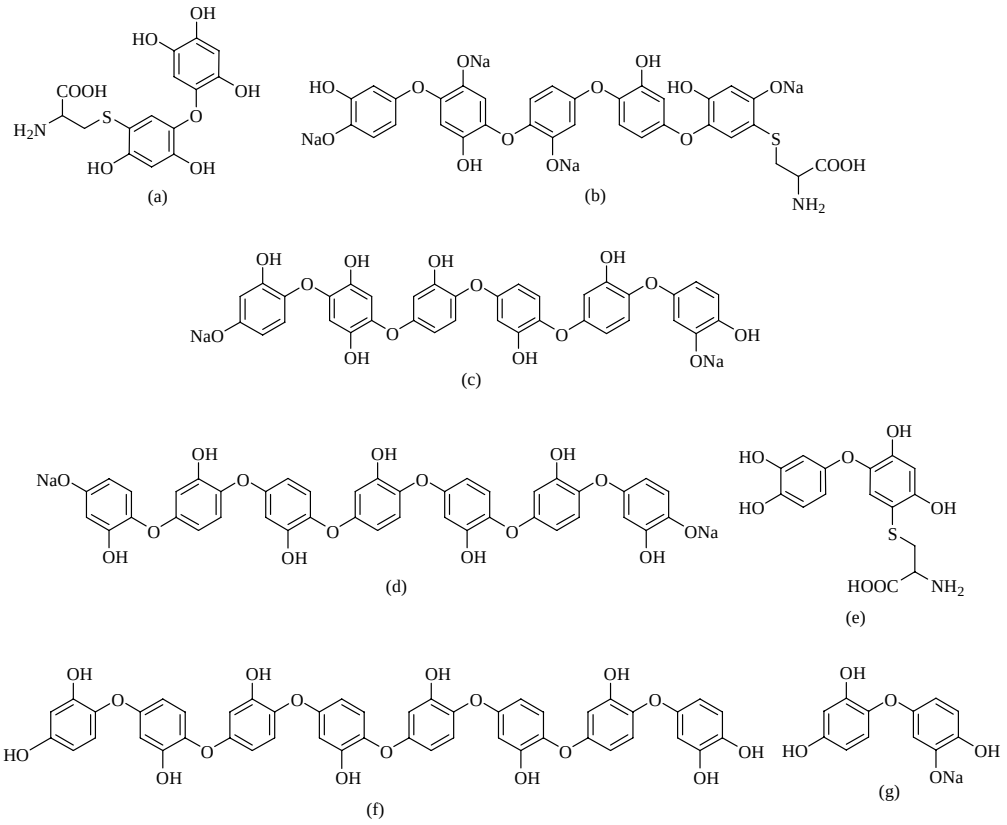

Figure 2.78. Possible molecular structures of individual fulvic acids in the raw SFA_4 mixture deduced from the LC-APCI-MS-MS analysis.

4.7.2. Analysis of purified SFA_4 by APCI-MS

A saturated solution of purified SFA_4 was prepared by dissolving lyophilized solid purified SFA_4 in milli-Q water. The resulting solution was filtered through a 0.45 μm millex®-HA filter unit. The pH of the solution was not adjusted prior to the APCI-MS analysis, which was performed in both positive-ion and negative-ion modes. The obtained spectra are shown in Figure 2.79. The m/z values equal to 97, 113 and 138 in spectrum A and 499 in spectrum C of this figure have not been assigned to any compound. The remaining m/z values in Figure 2.79 are listed in Table 2.22 along with possible corresponding chemical formulas. The molecular structures corresponding to these chemical formulas are either shown in Figure 2.80 or have already been proposed for the previous SFA. For example, the m/z values observed in spectrum A of Figure 2.79 corresponds to molecular structures that were earlier assigned to individual compounds in the purified SFA_1 mixture. Again, the stuctures proposed in Figure 2.80 are oligomers containing up to five highly substituted aromatic rings which are linked one to another through ether bonds, although the possibility of C_{aro}-C_{aro} linkages cannot be ruled out.

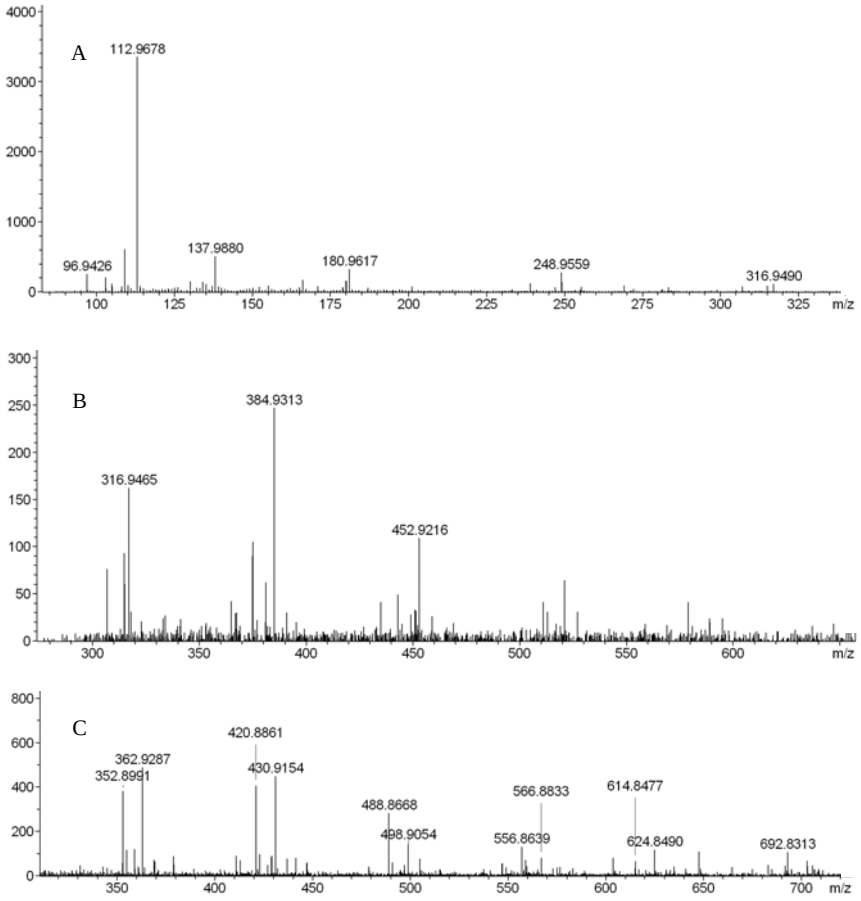

Figure 2.79. APCI-MS spectra of the purified SFA_4 mixture analyzed by APCI-MS in negative-ion mode (A and B) and positive-ion mode (C).

Table 2.22. Summary of the m/z ratios obtained in the APCI-MS analysis (positive and negative modes) of the purified SFA_4 mixture, as well as of possible chemical formulas and corresponding molecular weights for individual fulvic acids in the purified SFA_4 mixture.

m/z	Chemical formula	Molecular weight	Structures
Positive mode			
352.8991	$[C_{12}H_7O_6Na_3 + 2\ H_2O + H]^+$	353.023	Structure (a) in Fig. 2.80
362.9287	$[C_{18}H_{14}O_6 + 2\ H_2O + H]^+$	363.108	Structure (e) in Fig. 2.10
420.8861	$[C_{18}H_{12}O_8Na_2 + H_2O + H]^+$	421.051	Structure (b) in Fig. 2.80
430.9154	$[C_{18}H_{10}O_7Na_4 + H]^+$	431.010	Structure (b) in Fig. 2.64
488.8668	$[C_{24}H_{17}O_{10}Na + H]^+$	489.080	Structure (c) in Fig. 2.64
556.8639	$[C_{24}H_{14}O_9Na_4 + H_2O + H]^+$	557.041	Structure (d) in Fig. 2.64
566.8833	$[C_{24}H_{16}O_9Na_2 + 4\ H_2O + H]^+$	567.109	Structure (c) in Fig. 2.80
614.8477	$[C_{30}H_{21}O_{12}Na + H_2O + H]^+$	615.111	Structure (d) in Fig. 2.80
624.8490	$[C_{30}H_{19}O_{11}Na_3 + H]^+$	625.070	Structure (e) in Fig. 2.64
692.8313	$[C_{30}H_{20}O_{11}Na_2 + 5\ H_2O + H]^+$	693.141	Structure (g) in Fig. 2.14
Negative mode			
180.9617	$[C_6H_6O_2 + 4\ H_2O - H]^-$	181.071	Structure (a) in Fig.2. 14
248.9559	$[C_{12}H_{10}O_6 - H]^-$	249.040	Structure (f) in Fig. 2.8
316.9490	$[C_{12}H_7O_5Na_3 + H_2O - H]^-$	317.001	Structure (o) in Fig. 2.16
384.9313	$[C_{18}H_{12}O_7Na_2 - H]^-$	385.030	Structure (j) in Fig. 2.8
452.9216	$[C_{18}H_{13}O_7Na + 5\ H_2O - H]^-$	453.101	Structure (i) in Fig. 2.10

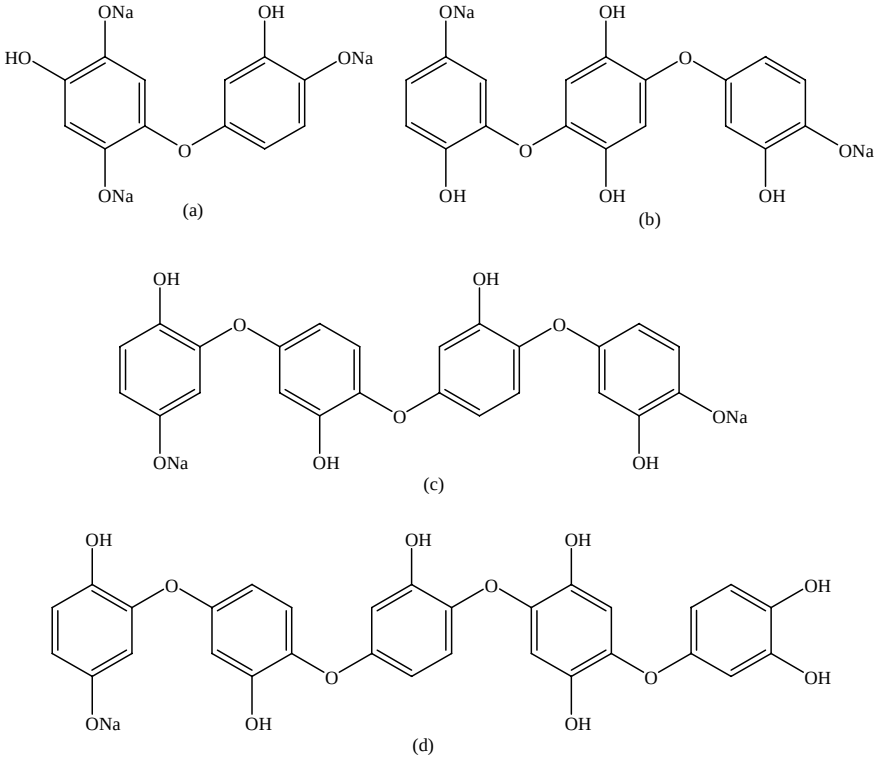

Figure 2.80. Possible molecular structures of individual fulvic acids in the purified SFA_4 mixture deduced from the APCI-MS analysis.

4.8. Discussion

From the results and observations summarized above concerning the nature of the products obtained by polymerization of catechol and cysteine, two reactions appear to be of major interest for explaining the obtention of these products from a reaction mechanism point of view. The first of these reactions, which is the *oxidative coupling* of catechol, has already been discussed in detail in section *1.8.1.* This oxidative coupling leads to the formation of catechol oligomers. The second one is actually similar to the first but represents this time the coupling between free radicals generated from catechol (see SFA_1 synthesis) and free radicals generated from cysteine. A free radical is generated from cysteine when cysteine reacts with a free radical of the system according to

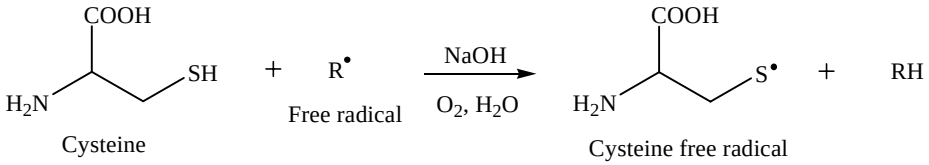

The generated cysteine free radical can then couple with any other free radical within the system leading to the formation of numerous compounds. An example out of the many possibilities of coupling between cysteine and a semiquinone free radical may be written as

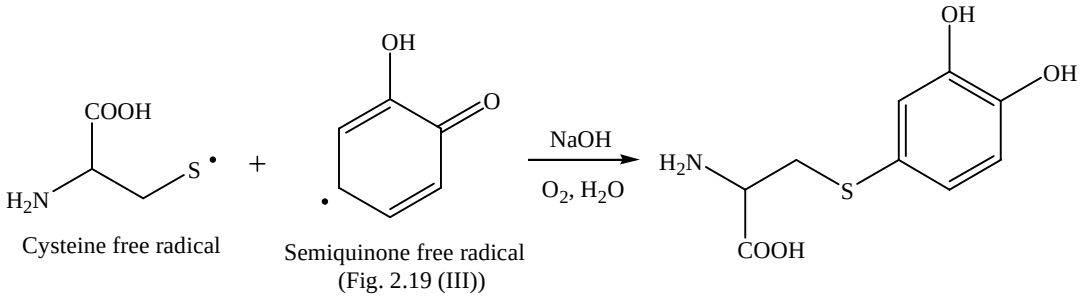

Note that it is possible to perform such couplings at different positions of the C atom on the aromatic ring.

As was seen under the discussion of SFA_1 (section *1.8.2*), quinone can undergo addition reactions with nucleophiles such as thiol. The addition reaction of quinone with cysteine is as shown

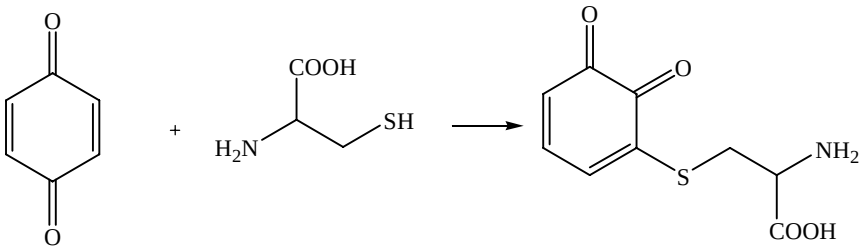

References

Aktaş N., Şahiner N., Kantoğlu Ö, Salih B., and Tanyolaç A. (2003) Biosynthesis and characterization of laccase catalyzed poly(catechol). *Journal of Polymers and the Environment* **11**, 123-128.

Dubey S., Singh D., and Misra R.A. (1998) Enzymatic synthesis and various properties of poly(catechol). *Enzyme and Microbial Technology* **23**, 432-437.

Eickhoff H., Jung G., and Rieker A. (2001) Oxidative phenol coupling – tyrosine dimers and libraries containing tyrosyl peptide dimers. *Tetrahedron* **57**, 353-364.

Fengel D. and Wegener G. (1983) Wood: Chemistry, Ultrastructure, Reactions I. *ISBN 3-11-008481-3* (de Gruyter), pp. 132-163. New York.

Fischer G., Cao X., Cox N., and Francis M. (2005) The FT-IR spectra of glycine and glycylglycine zwitterions isolated in alkali halide matrices. *Chemical Physics* **313**, 39-49.

Freudenberg K. (1965) Lignin: its constitution and formation from p-hydroxycinnamyl alcohols. *Science* **148**, 595-600.

Fujiwara M., Golovleva L.A., Saeki Y., Nozaki M. and Hayaishi O. (1975) Extradiol cleavage of 3-substituted catechols by an intradiol dioxygenase, pyrocatechase, from a Pseudomonad. *The journal of Biological Chemistry*. **250**, No. 13, 4848-4855.

Glasser W.G. (1980) Lignin. In *Pulp and Paper. Chemistry and Chemical Technology. Volume I* (ed. J.P. Casey), pp. 39-111 (3rd edition). Wiley-Interscience.

Gonçalves M., Guerreiro M.C., Oliveira L.C.A. and da Rocha C.L. (2008) Oxidation of organic compounds in wastewater from the humid processing of coffee berries. *Quim. Nova*, **31**, No. 7, 1636-1640.

Higuchi T. (1990) Lignin biochemistry: biosynthesis and biodegradation. *Wood Science and Technology* **24**, 23-63.

Jackson H. (1939) The oxidation of catechol and 1:2:4-trihydroxybenzene by polyphenol oxidase. *Biochemical Journal* **33**, 1452-1459.

Kobayashi S. and Higashimura H. (2003) Oxidative polymerization of phenols revisited. *Progress in Polymer Science* **28**, 1015-1048.

Lebedev A.V., Ivanova M.V., Timoshin A.A., and Ruuge E.K. (2007) Effect of group II metal cations on catecholate oxidation. *ChemPhysChem* **8**, 1863-1869.

Lim P.K., Cha J.A., and Patel C.P. (1983) Aerobic coupling of aqueous phenol catalyzed by cuprous chloride: Basis of a novel dephenolization scheme for phenolic wastewaters. *Industrial and Engineering Chemistry – Process Design and Development* **22**, 477-482.

Lin G., Reid G. and Bugg T.D.H. (2000) A biomimetic model reaction for the extradiol catechol dioxygenases. *Chem. Commun*. 1119-1120.

McNaught A.D. and Wilkinson A. (1997) *IUPAC Compendium of Chemical Terminology* (2nd ed.). Blackwell Science.

Parker F.S. (1971) *Applications of Infrared Spectroscopy in Biochemistry, Biology, and Medicine*. Hilger.

Perlinger J.A., Kalluri V.M., Venkatapathy R. and Angst W. (2002) Addition of hydrogen sulfide to juglone. *Environ. Sci. Technol.* **36**, 2663-2669.

Sánchez-Cortés S., Francioso O., García-Ramos J.V., Ciavatta C., and Gessa C. (2001) Catechol polymerization in the presence of silver surface. *Colloids and Surfaces. A: Physicochemical and Engineering Aspects* **176**, 177-184.

Silverstein R.M., Bassler G.C., and Morrill T.C. (1991) *Spectrometric Identification of Organic Compounds* (5th edition). Wiley.

Šmejkalová D., Piccolo A., and Spiteller M. (2006) Oligomerization of huic phenolic monomers by oxidative coupling under biomimetic catalysis. *Environmental Science and Technology* **40**, 6955-6962.

Sundaravel K., Dhanalakshmi T., Suresh E. and Palaniandavar M. (2008) Synthesis, structure, spectra and reactivity of iron(III) complexes of facially coordinating and sterically hindering 3N ligands as models for catechol dioxygenases. *Dalton Trans*., 7012-7025.

Thomson R.H. (1951) Studies in the juglone series. III. Addition reactions. *J. Org. Chem*. **16**, 1082-1090.

Uchimiya M. and Stone A.T. (2006) Aqueous oxidation of substituted dihydroxybenzenes by substituted benzoquinones. *Environ. Sci. Technol.* **40**, 3515-3521.

Uchimiya M. and Stone A.T. (2009) Reversible redox chemistry of quinones: Impact on biogeochemical cycles. *Chemosphere* **77**, 451-458.

Wojtkowiak B. and Chabanel M. (1977) *Spectrochimie Moléculaire*. Technique & Documentation.

CHAPTER 3. Uranyl(VI)-fulvate complexation

3.1. Objectives of the experiment and scientific background

Fulvic and Humic Acids play an important role in the mobility of dissolved metals and radionuclides in the environment due to their strong complexing ability. Therefore, knowledge of the extent of interactions between humic substances with metal ions, in particular radionuclides, such as uranium, is of vital importance in quantification and modelling of metals and radionuclides transport in the environment (lakes, rivers). The complexation of radionuclides, such as uranium, by fulvic (or humic) substances has been the subject of a large number of investigations (Mohan et al., 1982; Giesy et al., 1986; Munier-Lamy et al., 1986; Chen et al., 1988; Heitkamp and Wagener, 1990; Nagao and Nakashima, 1992; Turner et al., 1993; Czerwinski et al., 1994; Kim and Czerwinski, 1996; Pompe et al., 1996; Bubner et al., 1997; Denecke et al., 1997a, b; Zhang et al., 1997; Denecke et al., 1998; Nefedov et al., 1998; Schuster et al., 1998; Benes et al., 1999; Teterin et al., 1999a, b; Lenhart et al., 2000; Lubal et al., 2000; Marquardt, 2000; Pompe et al., 2000; Schmeide et al., 2000; Teterin et al., 2001a, b; Schmeide et al., 2003).

Meanwhile, due to high molecular weight, heterogeneous structure, multiple functional groups of fulvic (or humic) substances and experimental data in a large pH range (2-12), the nature and the stability fields of uranyl (VI) complexation sites in fulvic (or humic) substances is still poorly understood. Some earlier works have suggested that carboxylate groups are the only functional groups responsible for the complex formation of uranyl(VI) ion up to pH = 9 (Choppin et al., 1985; Lieser et al., 1991). Other authors have considered that further functional groups such as alcoholic (-OH) groups (Sarret et al., 1997; Korshin et al., 1998; Lubal et al., 2000) as well as amino ($-NH_2$) groups (Ephraim and Marinsky, 1990; Luster et al., 1996), could also contribute to complex uranyl(VI) ion. Formation constant values of some of the uranyl(VI) complexes with natural and synthetic humic acids have been determined using various measurement techniques: potentiometry (Munier-Lamy et al., 1986), ion exchange measurements (Czerwinski et al., 1997; Lenhart et al., 2000) and time-resolved laser-induced fluorescence spectroscopy (TRLFS) (Pompe et al., 1998). Published data have indicated the presence of uranyl(VI)-humate complexes in acidic solutions ($pH \leq 4$). However, the effect of ligands such as alcohol (-OH), amine ($-NH_2$), and thiol (-SH) on the uranyl(VI) – humate complex formation is still poorly known. Moreover, experimental data

on the uranyl(VI) – humate complexes in near neutral and basic aqueous solutions (pH = 4 – 14) appear to be not available.

With regards to the uranyl(VI) – fulvate or humate complexes structure, some recent works have reported that the X-ray absorption fine structure (EXAFS) spectroscopy have been used to determine structural details (n coordination number of OH^- bonded to U atom, U - OH and U - U bond lengths) of monouranyl(VI) hydrolyzed species $UO2(OH)_n^{2-n}$ (n = 1-4) (Clark et al., 1999; Wahlgren et al., 1999; Vallet et al., 2001; Testemale, 2003) as well as polyuranyl(VI) hydrolyzed complexes of the type $(UO_2)_p(OH)_q^{(2p-q)}$ (p = 2-3, q = 2-5) (Moll et al., 2000). In this connection, two studies (Denecke et al., 1997a; Schmeide et al., 2003) were devoted in measurements of structural parameters for the interaction of uranyl(VI) with both natural and synthetic humic acids using EXAFS. Two complexes have been suggested: the first one at pH 2 (Schmeide et al., 2003) and the second one at pH 4 (Denecke et al., 1997a). These authors have obtained similar results for both samples at pH 2 and 4, *i.e.* axial U-O distances of 1.77 - 1.78 ängstroms and five equatorial U-O bond lengths at 2.37-2.39 ängstroms. The humic acid carboxylate groups were assumed to be responsible for the complex formation with uranyl(VI) ion. They act predominantly as monodentate ligands when bound to the uranyl(VI) unit. Experimental EXAFS data on the uranyl(VI) – humate complexes in near neutral and basic aqueous solutions (pH = 4 – 14) appear not to be available. Also, there is lack of data concerning the identity of uranyl(VI) cation which is binded to fulvate or humate ligand. In this connection, UV-visible spectrometry appears to be a useful technique in the identification of the mono- or poly-uranyl(VI) cation which is binding to fulvate or humate ligands.

The study of the uranyl(VI)-fulvate complexes requires the knowledge of the solubility of uranium (VI) and its hydrolysed species in the ternary system UO_3-NaOH-H_2O. In acidic solution (pH <4), $UO_2(OH)_2.H_2O$ is the most stable solid phase. Due to its amphoterous character, its calculated solubility curve has one minimum ($U_{total} = 10^{-6}$ M) near neutral pH (= 7) and reaches two maxima in strong acid (pH <3) and strong base (pH >14) media, Figure 3.1. In near neutral and basic solution, uranium (VI) reacts with Na^+ cation to form insoluble alkaline uranate solid phase such as $Na_2U_2O_7$ and Na_2UO_4. Calculation of the solubility of the former solid phase produces a solubility curve with a minimum solubility ($U_{total} = 10^{-7}$ M) in the pH range (9-11) and two maxima in weak acid solution (pH < 6) and strong base (pH = 14), Figure 3.1. These results indicate that the solubility of uranium (VI) in non complexing aqueous solution containing Na^+ tends to the maximum in acidic solution

(pH < 4) and reaches the minimum ($U_{total} \approx 10^{-8}$ M) in basic medium (pH = 8-11). In strongly basic solution (pH >11), the uranium (VI) solubility slightly increases with increasing pH.

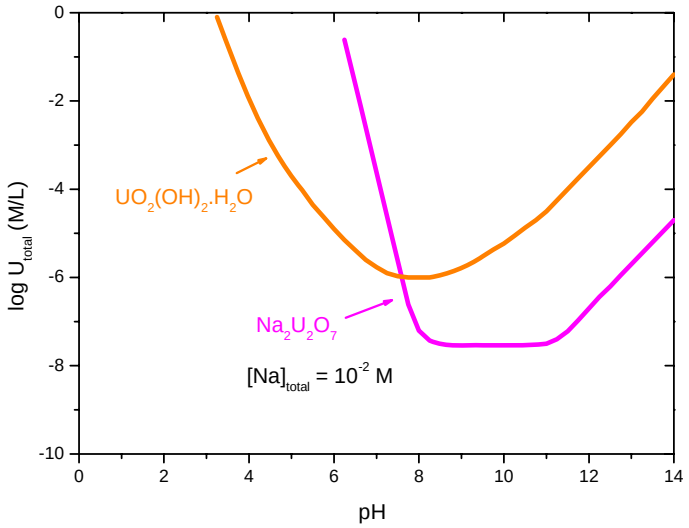

Figure 3.1. Solubility curves of $UO_2(OH)_2.H_2O$ (Schoepite) and $Na_2U_2O_7$ in H_2O containing Na_{total} = 10^{-2} M, as a function of pH at T = 25°C, P = 0.1MPa. Uranium (VI) solubility has been computed using published thermodynamic data on solid phases and aqueous uranyl(VI) hydrolyzed species (Grenthe et al., 1992, Guillaumont et al., 2003) by Nguyen-Trung (Unpublished ongoing research).

The corresponding aqueous uranyl(VI) ion in strongly acid solution (pH <3) is theoretically U^{6+}. This cation is highly unstable and spontaneously reacts with two oxygen anions to form the uranyl(VI) cation (UO_2^{2+}). According to Pearson (1966, 1968), UO_2^{2+} is a "hard" Lewis acid. Consequently, UO_2^{2+} prefers to associate with "hard" Lewis bases such as OH^-, F^-, Cl^-, CO_3^{2-}, SO_4^{2-}, PO_4^{3-}, $CH_3CO_2^-$, (R, Ar)O^- (R = alkyl, Ar = Aryl), (R, Ar)OH, NH_3, (R, Ar) NH_2. Among these Lewis bases, OH^- is the most abundant ligand in aqueous solution and reacts with UO_2^{2+} to form

- four mono-uranyl(VI) hydrolysed species: UO_2OH^+, $UO_2(OH)_2^o$ $UO_2(OH)_3^-$ and $UO_2(OH)_4^{2-}$
- five poly-uranyl(VI) hydrolysed species: $(UO_2)_2(OH)_2^{2+}$, $(UO_2)_3(OH)_5^+$, $(UO_2)_3(OH)_7^-$, $(UO_2)_3(OH)_8^{2-}$, and $(UO_2)_3(OH)_{10}^{4-}$ in the pH range 4 – 12 (Nguyen-Trung et al., 2000; Palmer and Nguyen-Trung, 1995).

Poly-uranyl(VI) hydrolysed species predominate in concentrated uranyl(VI) ($U_{total} > 10^{-4}$ M) solution. Palmer and Nguyen-Trung (1995) have reported that UO_2^{2+} in $5x10^{-3}$ M Uranyl(VI) solution forms in a non complexing aqueous solution, a succession of five species $(UO_2)_2(OH)_2^{2+}$ (pH = 3-4), $(UO_2)_3(OH)_5^+$ (pH = 4-5), $(UO_2)_3(OH)_7^-$ (pH > 5), $(UO_2)_3(OH)_8^{2-}$ (pH ≥ 11), and $(UO_2)_3(OH)_{10}^{4-}$ (pH > 11) with increasing pH from 2.5 to 11.5.

Concerning the complex formation with ligands other than OH^-, UO_2^{2+} forms two kinds of complexes:

1- Simple complexes of the type $(UO_2)(L)_n^{2-n}$ (L = inorganic or organic "hard" Lewis Base),

2- Mixed complexes corresponding to the general formula $(UO_2)_p(OH)_q(L)_r^{(2p-q-r)}$

The first type of complexes results from the interaction of the unhydrolysed UO_2^{2+} with inorganic or organic ligands. The second one is formed by the replacement of one or many OH^- by a corresponding number of L^- ligands. Thus, the presence of the uranyl(VI) mixed complex reveals competition between the abundant OH^- ligand in aqueous solution and a determined L^- ligand.

The UO_2^{2+} cation is yellow and has a characteristic absorption spectrum in both UV and visible region with distinct bands and a maximum absorption in visible region at 414 nm (Bell and Biggers, 1965, 1967, 1968). The hydrolysis of uranyl(VI) is characterized by a dramatic increase in the absorption and the formation of poly-uranyl(VI) hydrolyzed species results in the broadening or disappearance of individual absorption bands. All these characteristics make the UV-visible spectrometry suited for determining the structure of the uranyl(VI) complexes. Applied in the present study, the UV-visible spectroscopic measurements appear to be an effective way to determine the nature of uranyl (VI) ions forming complexes with fulvate ligands.

Figure 3.2 displays eight absorption spectra of uranyl(VI) hydrolysed species in $(CH_3)_4N\text{-}NO_3$ non-complexing solution containing 10^{-2} M uranyl(VI) ion as a function of pH (2.92 - 14.50) at T = 25°C, P = 0.1 MPa.

At pH = 2.92, the predominant species is UO_2^{2+}. Its absorption spectrum is characterised by low intense and distinct absorption bands. The maximum absorption in visible region is at 414 nm, Figure 3.2.

The increase of pH up to the value 3.85 corresponds to the first hydrolysis of UO_2^{2+} to give the dimer $(UO_2)_2(OH)_2^{2+}$. The absorption spectrum of this species is more intense than that of $(UO_2)_2(OH)_2^{2+}$ but its absorption bands are poorly defined. The maximum absorption in visible region is near 420 nm, Figure 3.2.

The second hydrolysis of UO_2^{2+} occurs at pH = 4.11 with the formation of the well known species $(UO_2)_3(OH)_5^+$. Broad absorption bands characterize this species. The maximum absorption near 420 cm^{-1} is two times more intense than that of $(UO_2)_2(OH)_2^{2+}$ (Figure 3.2).

The most intense absorption band (430 nm) was observed in basic solution (pH = 11.36) corresponding to the absorption of the species $(UO_2)_3(OH)_8^{2-}$.

In strongly basic solution, the increase of pH from 12.14 to 14.50 leads to a hypsohypochromic shift (blue shift and decrease of absorption intensity) of absorption bands. This is mainly due to the hydrolysis of the triuranyl(VI) species $(UO_2)_3(OH)_8^{2-}$ (high absorbance, red shift) to monouranyl(VI) species $(UO_2)(OH)_4^{2-}$ (pH = 13.68) and $(UO_2)(OH)_5^{3-}$ (pH = 14.50) (Clark et al., 1999, Moll et al., 2000) (low absorbance, blue shift).

The formation of uranyl(VI)-L complex results in a significant change in the shape of the absorption spectrum of uranyl(VI) hydrolysed species in the same pH value.

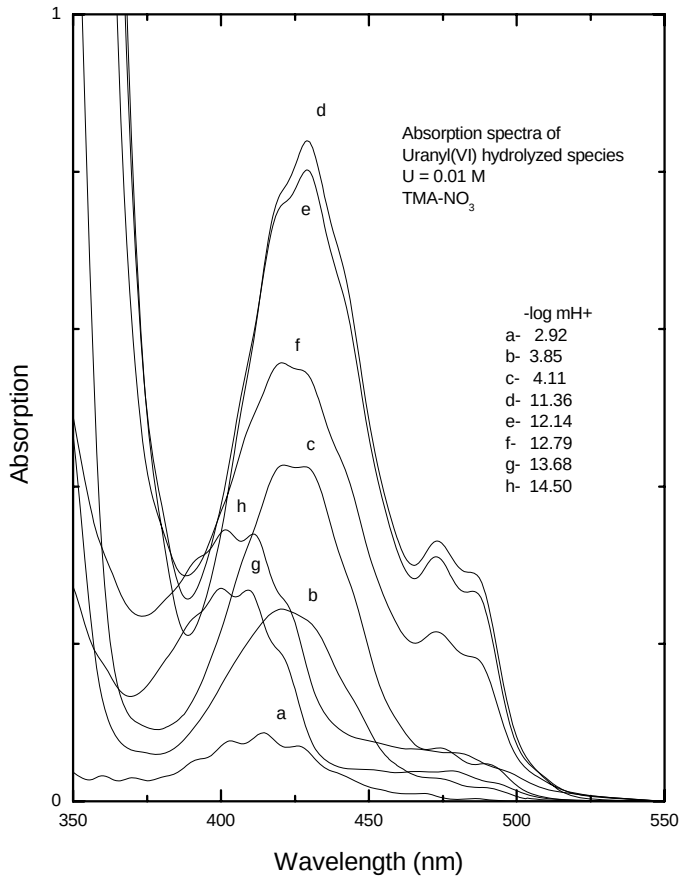

Figure 3.2. UV-visible absorption spectra of 0.01M Uranyl (VI) hydrolyzed species in $(CH_3)_4N\text{-}NO_3$ non-complexing medium, as a function of pH (2.9 - 14.5). Measurements were done using a 10 mm path length quartz cuvette at T = 25°C and 0.1 MPa, Nguyen-Trung (Unpublished ongoing research).

Based on the above mentioned characteristics of both uranyl(VI) ion and fulvate ligands, the objective of the present study is to bring a conclusive answer to two questions :

First question: Can the fulvate ligand form soluble complexes with uranyl (VI) over the whole pH range, in particular near neutral pH and basic solution?

Second question: Which species of uranyl (VI) can form soluble complexes with fulvate ligands?

In order to answer to these two questions, the scientific approach used in the present study consists to combine the uranyl(VI) - fulvate solubility data and the absorption spectra of uranyl(VI) solution containing soluble synthesized fulvic acid SFA_1 in a wide concentration range (2-11 mg/L) and a wide pH range (4-10) under atmospheric oxidation and at room temperature. Results obtained allow to identify the presence of uranyl(VI)-fulvate complexes.

3.2. Experimental section

Two stock solutions of 2.0×10^{-2} m $UO_2(ClO_4)_2$ and 88 $mg.L^{-1}$ SFA_1 have been prepared. The pH of each solution was adjusted using 1M NaOH or 1M $HClO_4$.

Table 3.1 shows the different pH and SFA_1 concentration values considered in the present study. The three types of solutions were then analysed using UV-visible spectroscopy.

Table 3.1. Different solutions studied at varying concentrations of SFA_1 at fixed concentration of uranyl(VI), 2.0 x 10^{-3} m at pH values 4, 7 and 10.

S. No	Uranyl(VI)	purified SFA_1	pH
1	2.0 x 10^{-3} M	2 mg.L^{-1}	4
	2.0 x 10^{-3} M	-	4
	-	2 mg.L^{-1}	4
2	2.0 x 10^{-3} M	2.75 mg.L^{-1}	4
	2.0 x 10^{-3} M	-	4
	-	2.75 mg.L^{-1}	4
3	2.0 x 10^{-3} M	4 mg.L^{-1}	4
	2.0 x 10^{-3} M	-	4
	-	4 mg.L^{-1}	4
4	2.0 x 10^{-3} M	5.5 mg.L^{-1}	4
	2.0 x 10^{-3} M	-	4
	-	5.5 mg.L^{-1}	4
5	2.0 x 10^{-3} M	11 mg.L^{-1}	4
	2.0 x 10^{-3} M	-	4
	-	11 mg.L^{-1}	4
6	2.0 x 10^{-3} M	2.75 mg.L^{-1}	7
	-	2.75 mg.L^{-1}	7
7	2.0 x 10^{-3} M	4 mg.L^{-1}	7
	-	4 mg.L^{-1}	7
8	2.0 x 10^{-3} M	5.5 mg.L^{-1}	7
	-	5.5 mg.L^{-1}	7
9	2.0 x 10^{-3} M	11 mg.L^{-1}	7
	-	11 mg.L^{-1}	7
10	2.0 x 10^{-3} M	2.75 mg.L^{-1}	10
	-	2.75 mg.L^{-1}	10
11	2.0 x 10^{-3} M	4 mg.L^{-1}	10
	-	4 mg.L^{-1}	10
12	2.0 x 10^{-3} M	5.5 mg.L^{-1}	10
	-	5.5 mg.L^{-1}	10
13	2.0 x 10^{-3} M	11 mg.L^{-1}	10
	-	11 mg.L^{-1}	10

3.2.1 Uranyl(VI)-SFA_1 systems at pH 4

Figure 3.3 displays six UV-visible absorption spectra (pH = 4), of 2.0 x 10^{-3} m uranyl(VI) solutions (pH = 4) containing five SFA_1 concentrations of (i) 2 mg/L, (ii) 2.75 mg/L, (iii) 4 mg/L, (iv) 5.5 mg/L, (v) 11 mg/L. The difference between a spectrum of the solution

containing the U(VI) – SFA_1 system and the one of the SFA_1 at the same pH value allows to obtain a spectrum characteristic of uranyl(VI) species, Figure 3.3. Table 3.2 shows a ratio of absorbance at 421 and 429 nm, as these values are the two maxima for the U(VI) cation in water and hence of significance for comparison. These ratios are of importance in determining the limit of uranyl(VI)-fulvate complex formation. It is evident from the ratios that the U(VI)-SFA_1 systems at SFA_1 concentration of 11 mg/L is a complex as its ratio is significantly different from that of U(VI) cation in water.

At pH ≈ 4, the comparison between this spectrum and the one of U(VI) hydrolysed species in water will provide information about the formation or not of a uranyl(VI)-fulvate complex, Figure 3.2. There seems to be different types of complexes as observed in Figure 3.4. At first sight, four types of complexes is noticeable, at SFA_1 concentrations of: (i) 2 mg/L, (ii) 2.75 and 4mg/L, (iii) 5.5 mg/L and (iv) 11 mg/L. Table 3.3 shows a ratio of absorbance at 418 and 428 nm.

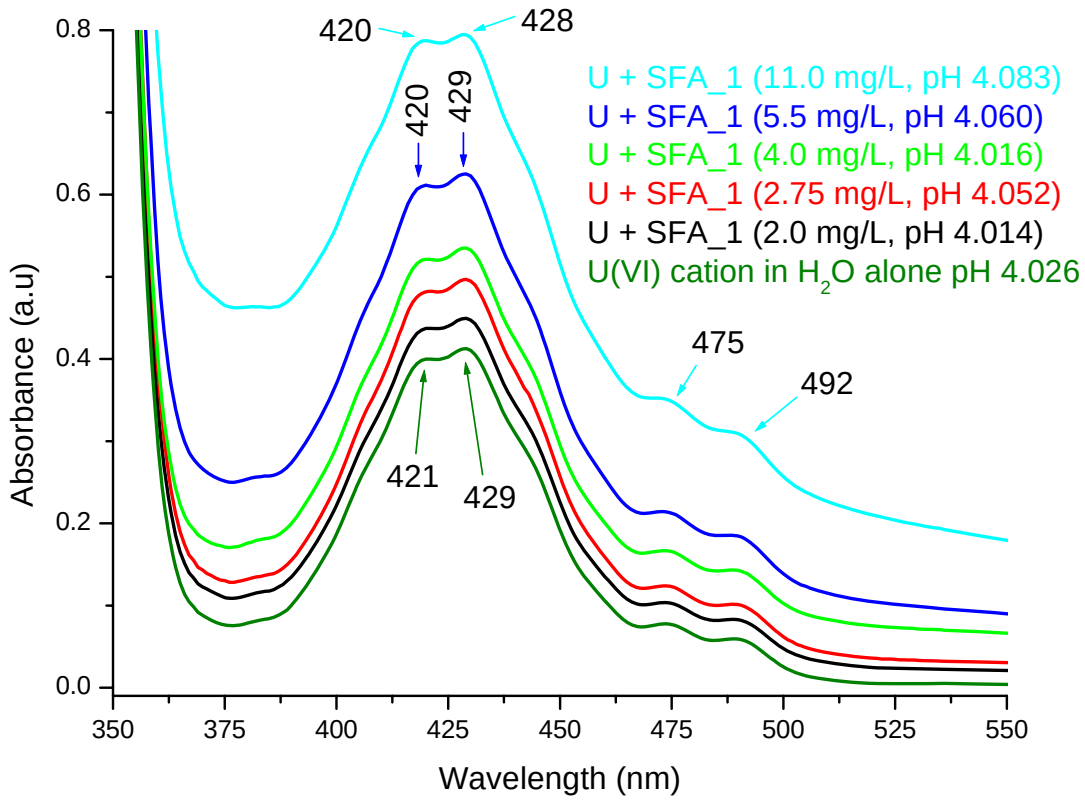

Figure 3.3. Six UV-visible spectra (after subtraction of SFA_1) of U(VI)-SFA_1 systems as a function of SFA_1 (purified) concentration: (i) 2 mg/L, (ii) 2.75 mg/L, (iii) 4 mg/L, (iv) 5.5 mg/L, (v) 11 mg/L and (vi) U(VI) cation in H_2O, all at pH 4. Measurements were done using a 50 mm path length quartz cuvette at T = 25°C and 0.1 MPa.

Table 3.2. Shows the ratio of the absorbance at 421 and 429 nm.

Sample	421 nm	429 nm	Absorbance Ratio (421 nm/ 429 nm)
U(VI) cation in water	0.4	0.413	0.968523002
Uranyl(VI) + SFA_1 (2 mg/L)	0.437	0.449	0.973273942
Uranyl(VI) + SFA_1 (2.75 mg/L)	0.482	0.497	0.969818913
Uranyl(VI) + SFA_1 (4 mg/L)	0.521	0.535	0.973831776
Uranyl(VI) + SFA_1 (5.5 mg/L)	0.611	0.625	0.9776
Uranyl(VI) + SFA_1 (11 mg/L)	0.786	0.795	0.988679245

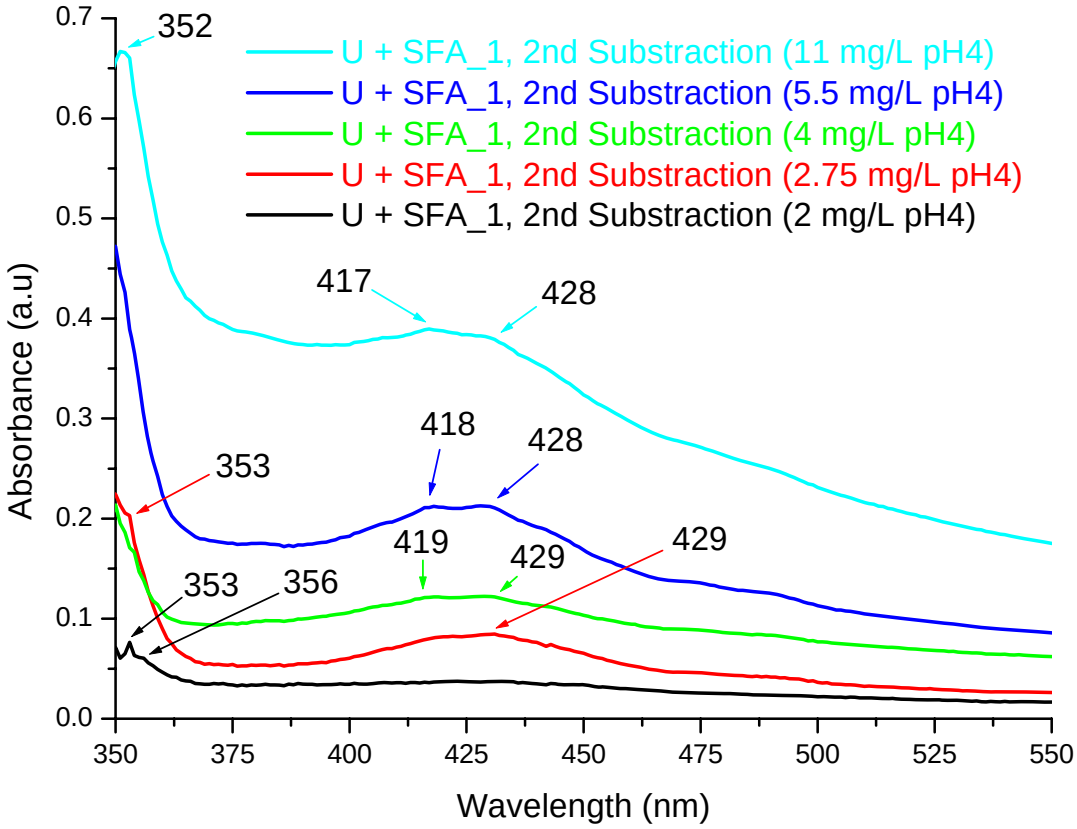

Figure 3.4. Five UV-visible spectra of complexes at different concentrations: (i) 2.0 mg/L, (ii) 2.75 mg/L, (iii) 4.0 mg/L, (iv) 5.5 mg/L, and (v) 11 mg/L. They are subtraction spectra (U(VI)-SFA_1 system - SFA_1 - U(VI) cation in H_2O). Measurements were done using a 50 mm path length quartz cuvette at T = 25°C and 0.1 MPa at T = 25°C and 0.1 MPa.

Table 3.3. Shows the ratio of the absorbance at 418 and 428 nm.

Sample	**418 nm**	**428 nm**	**Absorbance Ratio (418 nm/ 428 nm)**
Uranyl(VI) + SFA_1 (2 mg/L)	0.037	0.037	1
Uranyl(VI) + SFA_1 (2.75 mg/L)	0.081	0.084	0.96428571
Uranyl(VI) + SFA_1 (4 mg/L)	0.122	0.123	0.99186992
Uranyl(VI) + SFA_1 (5.5 mg/L)	0.212	0.213	0.99530516
Uranyl(VI) + SFA_1 (11 mg/L)	0.389	0.383	1.0156658

In order to determine the number of complexes formed in the SFA_1 concentration range of 2.0 – 11 mg/L, we have done subtraction of spectra at the different concentrations. The difference spectrum between the complexes at 11 mg/L and 2 mg/L clearly shows that the two are different complexes, while the one between complexes 11 mg/L and 5.5 mg/L seems not to be of any significant difference. The shapes of the different spectra between complexes at 11 mg/L and 2.75 mg/L and that of 11 mg/L and 4 mg/L are similar indicating that they are the same type of complex. In UV region, there are significant change in spectra as compared to that of U(VI) cation in water. For example, the complex at SFA_1 concentration of 2 mg/L is characterized by well defined bands at 353 and 356 nm, while the complex at 11 mg/L of SFA_1 is characterized by poorly defined band at 352 nm (Figure 3.5 below).

We conclude that at least two complexes have been formed in the interaction of SFA_1 (ligand) and uranyl(VI) ion. With regards to the chemical formula of uranyl(VI) complexes at pH = 4, it is well known that the predominant species is the trimer $(UO_2)_3(OH)_5^+$. This view is in agreement with the unpublished ongoing research work of Nguyen-Trung. Figure 3.2 shows the various uranyl(VI) hydrolyzed species. The absorption spectra observed for the complexes result from the coexistence of the major species $(UO_2)_3(OH)_5^+$ and a uranyl(VI)-fulvate complex. It should be emphasized that there are n-fulvate ligands in SFA_1 and hence there is formation of several complexes. What we observe in the spectra represents the sum of absorption spectra of an assemblage of uranyl(VI)-SFA_1 complexes. Due to the fact that the spectra of uranyl(VI)-fulvate differs slightly from that of uranyl(VI) hydrolysed species at the same pH value, uranyl(VI)-fulvate complexes could be considered as weak complexes or ion pairing. This is probably due to the low ionization of the SFA_1 in acidic solution (pH 4).

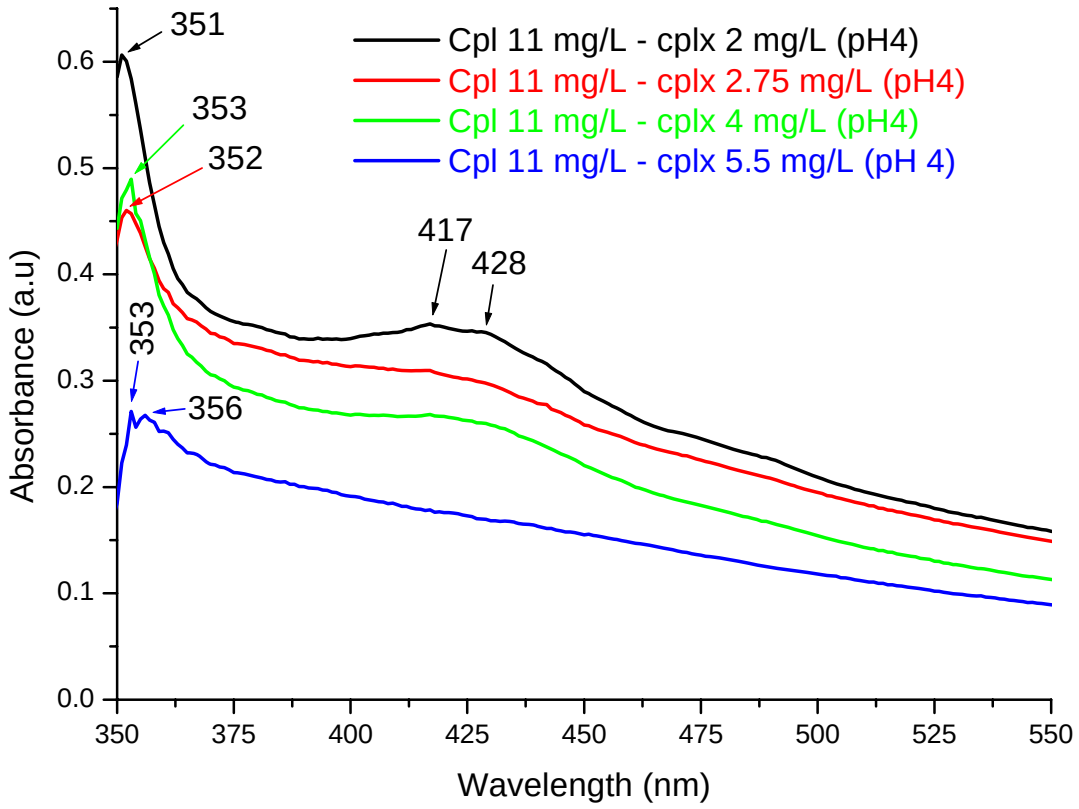

Figure 3.5. Four UV-visible spectra of complexes at different concentrations, they are subtraction spectra between complex at 11mg/L and the rest (i) 2.0 mg/L, (ii) 2.75 mg/L, (iii) 4.0 mg/L and (iv) 5.5 mg/L. Measurements were done using a 50 mm path length quartz cuvette at T = 25°C and 0.1 MPa.

3.2.2 Uranyl(VI)-SFA_1 systems at neutral pH (pH 7)

In neutral solution, the existence of a stable uranyl(VI)-fulvate complex indicates that the solubility of uranyl(VI) must be very important. It should be known that it is quite impossible to dissolve uranyl(VI) up to 10^{-3} M in a non-complexing aqueous solution. Indeed, uranium(VI) precipitates as schoepite ($UO_3.2H_2O$) and uranates ($Na_2U_2O_7.xH_2O$; $Na_2UO_4.yH_2O$) in a pH range 5 - 10. The solubility of schoepite and uranates in neutral solution is in the range 10^{-5} - $10^{-7.5}$ M. The following Figures 3.6 and 3.7 are for U(VI)-SFA_1 systems with varying concentration of purified SFA_1 (2.75, 4, 5.5 and 11 mg/L), constant concentration of uranyl(VI) (2 x 10^{-3} m) all at pH 7. In the present study, the presence of SFA_1 (2-11 mg/L) has allowed to dissolve 10^{-3} m uranyl(VI) at pH = 7, Figure 3.5. This result constitutes a strong argument that SFA_1 forms stable and very soluble complexes with uranyl(VI). Its absorption spectra are characterized by poorly defined bands in the range 370 - 500 nm with maxima at about 425 nm. The difference between these spectra and the ones of the SFA_1 at the same pH leads to a spectra representing only the uranyl(VI)-fulvate complexes (Figure 3.6). This result clearly proves that the uranyl(VI)-fulvate complexes

obtained in neutral pH are quite different from the ones formed in acidic medium (pH = 4). Unlike monouranyl(VI) ion, such as UO_2^{2+}, which is characterized by sharp and well defined absorption bands, the presence of poorly defined absorption bands in Figure 5 indicates that the comple(xes) formed at pH = 7 should be a polyuranyl(VI) - fulvate.

It is interesting to note that there is hyperchromic effect as the concentration of SFA_1 in the U(VI)-SFA_1 systems at pH 7 is increased, see Figure 3.5 below. The maxima exhibited by these systems (2.75, 4, 5.5 and 11 mg/L) are 427, 426, 426 and 425 nm respectively. It is evident that complexes were formed in all the systems studied at neutral pH. This is confirmed by the fact that uranyl(VI) was always maintained in solution despite the increase in SFA_1 concentration. The spectra of U(VI)-SFA_1 systems at neutral pH are characterized by a shoulder at about 478 nm as compared to well defined absorption bands (473 and 489 nm) observed for the systems studied at pH 4. As the concentration of the SFA_1 increases, the spectra loose their fineness in the above mentioned region.

In order to determine the number of complexes formed in the SFA_1 concentration range of 2.75 – 11 mg/L at the neutral pH, we have done subtraction of spectra at the different concentrations. The difference spectrum between the complexes at 11 mg/L and 2.75 mg/L clearly shows that the two are different complexes since the difference spectrum is characterized by poorly defined bands at about 386, 458 and 505 nm. The difference spectra between the complexes at 11 mg/L and 4 mg/L and 11 mg/L and 5.5 mg/L seems not to be of any significant difference. However, in the UV region for the former, it is characterized by well defined bands at 356 and 358 nm, while the latter is characterized by well defined band at 356 nm (Figure 3.6 below).

It should be noted that the studies undertaken at neutral pH is of importance as it actually reflects what happens in nature knowing that fulvic and humic acids are abundant in the environment.

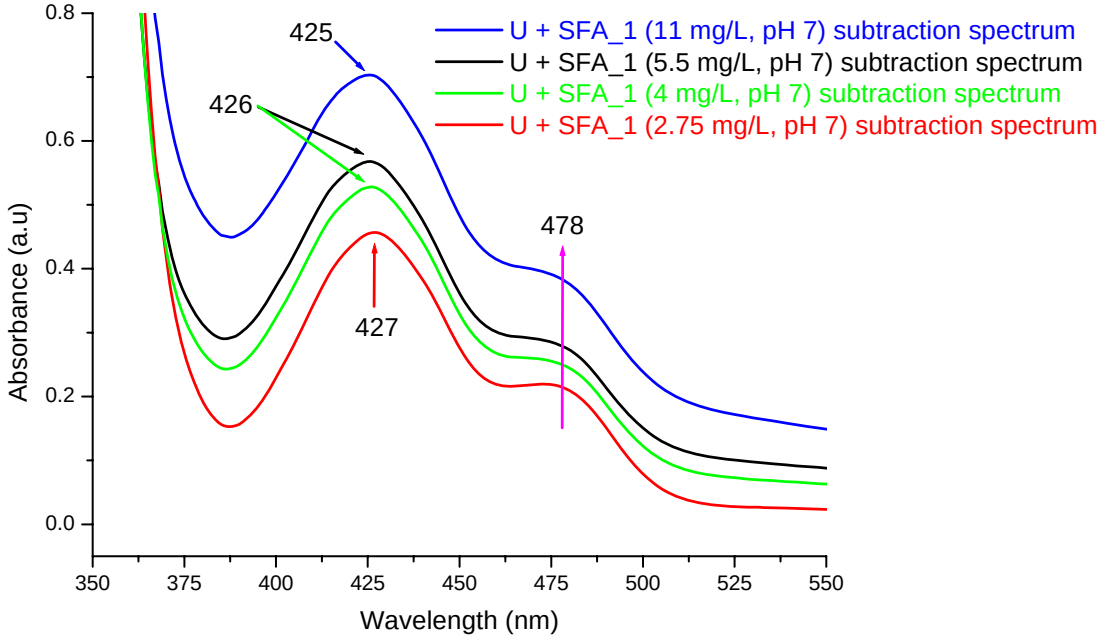

Figure 3.6. Four UV-visible spectra of complexes (after subtraction of SFA_1) at different concentrations of SFA_1 (i) 2.75 mg/L, (ii) 4.0 mg/L, (iii) 5.5 mg/L and (iv) 11 mg/L, all at neutral pH (pH 7). Measurements were done using a 50 mm path length quartz cuvette at T = 25°C and 0.1 MPa.

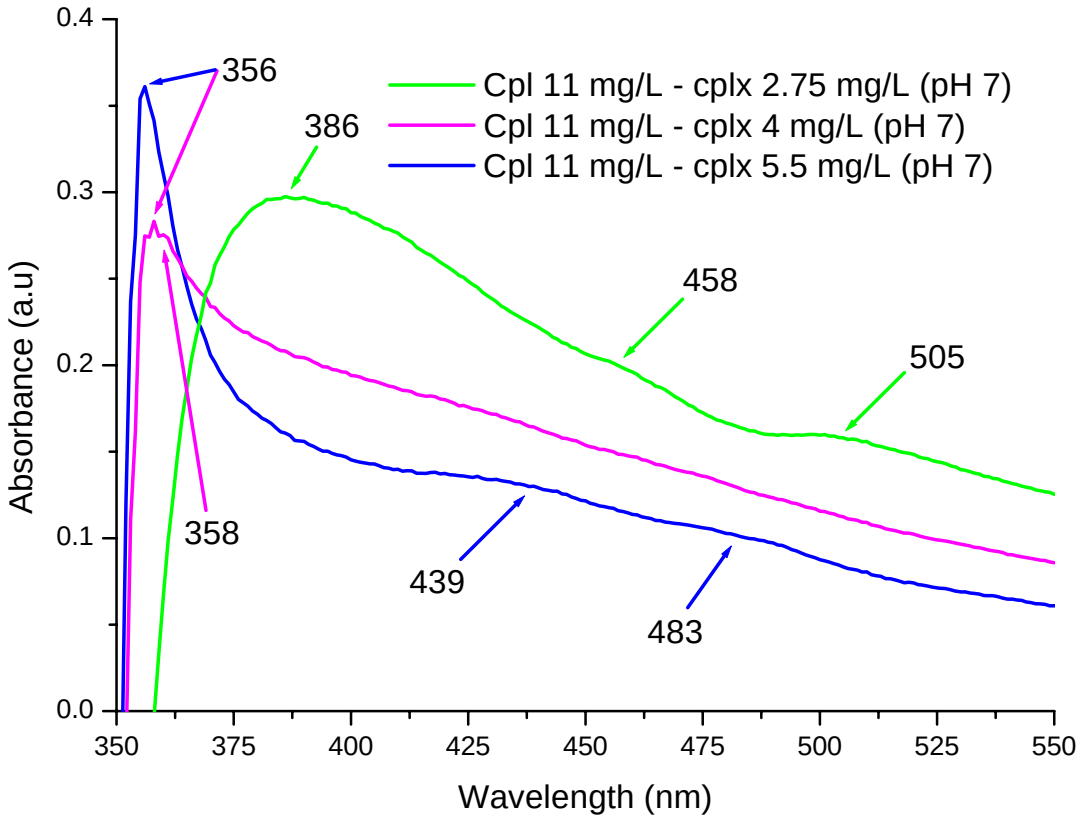

Figure 3.7. Four UV-visible subtraction spectra of complexes at different concentrations, they are subtraction spectra between complexes at 11 mg/L and the rest (i) 2.75 mg/L, (ii) 4.0 mg/L and (iii) 5.5 mg/L, all at neutral pH (pH 7). Measurements were done using a 50 mm path length quartz cuvette at T = 25°C and 0.1 MPa.

3.2.3 Uranyl(VI)-SFA_1 systems at basic pH (pH 10)

The following Figures 3.8 and 3.9 are for U(VI)-SFA_1 systems with varying concentration of purified SFA_1 (2.75, 4, 5.5 and 11 mg/L), constant concentration of uranyl(VI) (2×10^{-3} m) all at pH 10. There is hyperchromic effect as the concentration of SFA_1 in the U(VI)-SFA_1 systems at pH 10 is increased, see Figure 3.8 below. The maxima exhibited by these systems (2.75, 4, 5.5 and 11 mg/L) are 428, 427, 429 and 425 nm respectively. In comparison to the systems studied at neutral pH, the systems at basic pH are shifted to higher wavenumber. It is evident that soluble Uranyl(VI)-fulvate complexes were formed in all the systems studied at this basic pH. This is confirmed by the fact that uranyl(VI) was always maintained in solution despite the increase in SFA_1 concentration. The spectra of U(VI)-SFA_1 systems at the basic pH are characterized by a shoulder near 478 nm as compared to the well defined absorption bands (473 and 489 nm) observed for the systems studied at pH 4. There is close similarity in the shapes of the spectra studied at pH 10 and those at the neutral pH. As was observed at neutral pH, as the concentration of the SFA_1 increased, the spectra lost their fineness at about 478 nm.

In order to evaluate the number of soluble Uranyl(VI)-fulvate complexes formed in the SFA_1 concentration range of 2.75 – 11 mg/L at the pH 10, we have done subtraction of spectra at the different concentrations. The difference spectra between the complexes at 11 mg/L and 2.75 mg/L, 11 mg/L and 4 mg/L, and 11 mg/L and 5.5 mg/L, clearly shows that the three are different complexes since the difference spectra are all different. The first one is characterized by poorly defined bands at about 368 and 471 nm. The second one is characterized by a sharp absorption band at 353 nm and a wide band, poorly defined around 377 nm. The last one is characterized by wide bands at 399 and 467 nm (Figure 3.9 below).

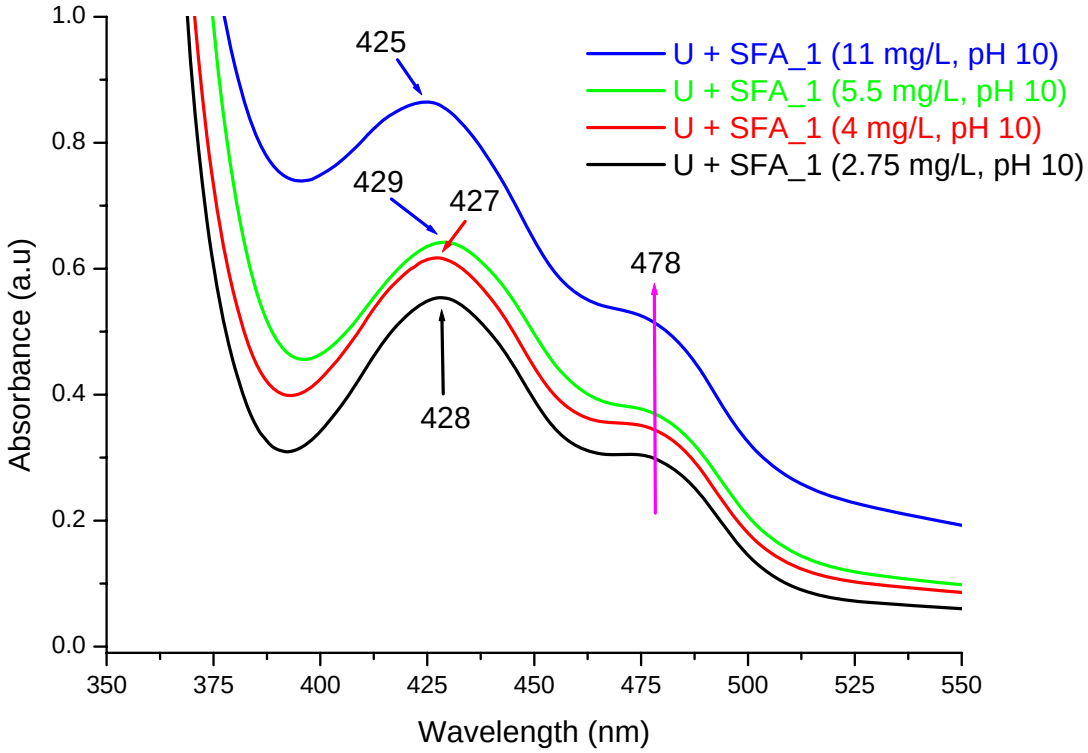

Figure 3.8. Four UV-visible spectra of U(VI)-SFA_1 systems as a function of SFA_1 (purified) concentration: (i) 2.75, (ii) 4, (iii) 5.5 and (iv) 11 mg/L, all at basic pH (pH 10). Measurements were done using a 50 mm path length quartz cuvette.

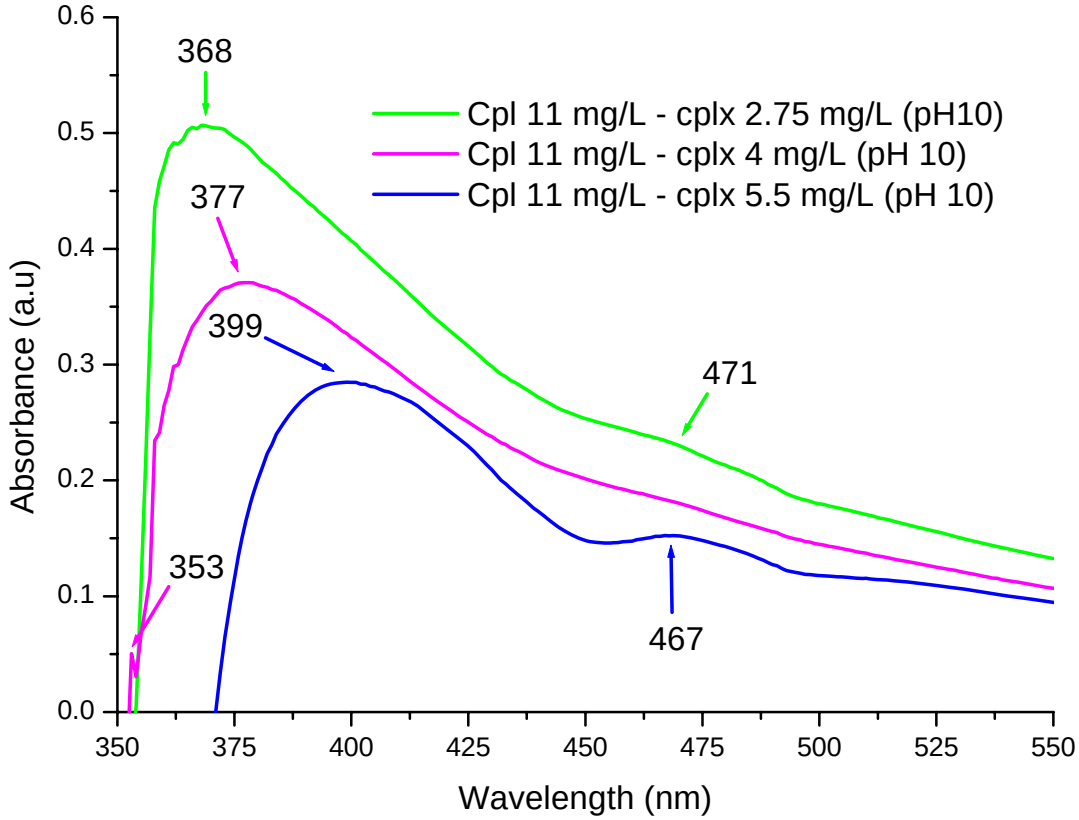

Figure 3.9. Four UV-visible spectra of complexes at different concentrations, they are subtraction spectra between complexes at 11 mg/L and the rest (i) 2.75 mg/L, (ii) 4.0 mg/L and (iii) 5.5 mg/L, all at pH 10. Measurements were done using a 50 mm path length quartz cuvette at T = 25°C and 0.1 MPa.

References

Bell J. T. and Biggers R. E. (1965) The absorption spectrum of the uranyl ion in perchlorate media. Part I. Mathematical resolution of the overlapping band structure and studies of the environmental effects. *J. Mol. Spectr.* **18** (3), 247-275.

Bell J. T. and Biggers R. E. (1967) The absorption spectrum of the uranyl ion in perchlorate media. Part II. The effects of hydrolysis on the resolved spectral bands. *J. Mol. Spectr.* **22** (1-4), 262-271.

Bell J. T. and Biggers R. E. (1968) . Absorption spectrum of the uranyl ion in perchlorate media Part III. Resolution of the ultraviolet band structure; some conclusions concerning the excited state of UO_2^{2+}. *J. Mol. Spectr.* **25** (3), 312-329.

Benes P., Czerwinski K. R. and Dolansky J. (1999) Effect of humic acid on the electrophoretic mobility of uranium(VI) in aqueous solutions. *Radiochim. Acta* **84** (2), 95-100.

Bubner M., Pompe S., Meyer M., Jander R., Schuster G. and Heise K. H. (1997) Synthesis of uranium(VI) and calcium complexes with carboxylic and humic acids. *Forschungszentrum Rossendorf e.V., [Bericht] FZR (1997)(FZR-180)*, 22-23.

Chen Y., Wu F., Zhang K. and Ren S. (1988) Effect of humic acids in solution on uranium solvent extraction. *Youkuangye* **7** (4), 15-23.

Choppin G.R., Allard B. (1985) Handbook on the Physics and Chemistry of the Actinides, Freeman A.J., Keller C. (Eds.), Elsevier, Amsterdam, p.407.

Clark, D.L., Conradson, S.D., Donohoe, R.J., Keogh, D.W., Morris, D.E., Palmer, P.D., Rodgers, R.D. and Tait, C.D. (1999) Chemical Speciation of the Uranyl Ion under Highly Alkaline Conditions. Synthesis, Structures, and Oxo Ligand Exchange Dynamics. *Inorg. Chem.* **38**, 1456-1466.

Czerwinski K.R., Buckau G., Scherbaum F. and Kim J.I. (1994) Complexation of the uranyl ion with aquatic humic acid. *Radiochim. Acta* **65** (2), 111-119.

Czerwinski K.R. and Kim J.I. (1997) Complexation of transuranic ions by humic substances: Application of laboratory results to the natural system. *Materials Research Society Symposium - Proceedings* **465**, 743-750.

Denecke M.A., Pompe S., Reich T., Moll H., Bubner M., Heise K.H., Nicolai R. and Nitsche H. (1997a) Measurements of the structural parameters for the interaction of uranium(VI) with natural and synthetic humic acids using EXAFS. *Radiochim. Acta* **79** (3), 151-159.

Denecke M.A., Reich T., Pompe S., Bubner M., Heise K.H., Nitsche H., Allen P.G., Bucher J.J., Edelstein N.M. and Shuh D.K. (1997b) Differentiating between monodentate and bidentate carboxylate ligands coordinated to uranyl ions using EXAFS. *J. Phys. IV 7 (C2, X-Ray Abs. Fine Struct.* **1**, 637-638.

Denecke M.A., Reich T., Pompe S., Bubner M., Heise K.H., Nitsche H., Allen P.G., Bucher J.J., Edelstein N.M., Shuh D.K. and Czerwinski K.R. (1998) EXAFS investigations of the interaction of humic acids and model compounds with uranyl cations in solid complexes. *Radiochim. Acta* **82**, 103-108.

Ephraim J.H., Marinsky J.A. (1990) Ultrafiltration as a technique for studying metal-humate interactions: studies with iron and copper. *Anal. Chim. Acta* **232**, 171-180.

Epstein J., Plapinger R.E., Michel H.O., Cable J.R., Stephani R.A., Hester R.J., Billington C., Jr., and List G.R. (1964) Reactions of isopropyl methylphosphonofluoridate with substituted phenols. I. *J. Amer. Chem. Soc*. **86**, 3075-3084.

Giesy J.P., Geiger R.A., Kevern N.R. and Alberts J.J. (1986) Uranyl ion (UO_2^{2+})-fulvate. *J. Env. Radioact.* **4** (1), 39-64.

Heitkamp D. and Wagener K. (1990) Kinetics of adsorption of uranium from seawater by humic acids. *Separ.Sci. Techn.* **25** (5), 535-46.

Kim J.I. Czerwinski K.R. (1996) Complexation of Metal Ions with Humic Acid: Metal Ion Charge Neutralization Model. *Radiochimica Acta* **73** (1), pp. 5-10.

Korshin G.V., Frenkel A.I., Stern E.A. and Korshin G.V. (1998) EXAFS Study of the Inner Shell Structure in Copper(II) Complexes with Humic Substances. *Environ. Sci. Technol.* **32**, 2699-2705.

Lenhart J.J., Cabaniss S.E., MacCarthy P. and Honeyman B.D. (2000) Uranium(VI) complexation with citric, humic and fulvic acids. *Radiochim. Acta* **88** (6), 345-353.

Lieser K.H., Hill R., Mühlenweg R.N, Singh T., Shu-De T. and Steinkoff T. (1991) Actinides in the environment. *J. Radioanal. Nucl. Chem.* **147** (1), 117-131.

Lubal P., Fetsch D., Siroky D., Lubalova M., Senkyr J. and Havel J. (2000) Potentiometric and spectroscopic study of uranyl complexation with humic acids. *Talanta* **51** (5), 977-991.

Luster J., Lloyd T. and Sposito T. (1996) Multi-wavelength molecular fluorescence spectrometry for quantitative characterization of copper(II) and aluminum(III) complexation by dissolved organic matter. *Environ. Sci. Technol.* **30**, 1565-74.

Marquardt C.S. (2000) Influence of Humic Acids on the Migration behaviour of radioactive and non-radioactive substances under conditions close to nature. Forschungszentrum

Karlsruhe. Technik und Umwelt Wissenschaftliche Berichte FZKA 6557. 235 p. (2000) uranium-rich organic material obtained from a South Texas lignite. *Fuel* **61** (9), 853-858.

Mohan M.S., Zingaro R.A., Macfarlane R.D. and Irgolic K.J. (1982) Characterization of a (2000) uranium-rich organic material obtained from a South Texas lignite. *Fuel* **61** (9), 853-858.

Moll, H., Reich, T. and Szabó, Z. (2000) The hydrolysis of dioxouranium (VI) investigated using EXAFS and ^{17}O-NMR. *Radiochim. Acta* **88**, 411-415.

Munier-Lamy C., Adrian P., Berthelin J. and Rouiller J. (1986) Comparison of binding abilities of fulvic and humic acids extracted from recent marine sediments with uranyl(2+) ion. *Org. Geochem.* **9** (6), 285-292.

Nagao S. and Nakashima S. (1992) Possible complexation of uranium with dissolved humic substances in pore water of marine sediments. *Sci. Total Env.* **117-118**, 439-47.

Nefedov V.I., Teterin Y.A., Lebedev A.M., Teterin A.Y., Dementjev A.P., Bubner M., Reich T., Pompe S., Heise K.H. and Nitsche H. (1998) Electron spectroscopy for chemical analysis investigation of the interaction of uranyl and calcium ions with humic acids. *Inorg. Chim. Acta* **273** (1,2), 234-237.

Nguyen-Trung C., Palmer D.A., Begun G.M., Peiffert C. and Mesmer R.E. (2000) Aqueous uranyl complexes 1. Raman spectroscopic study of the hydrolysis of uranyl(VI) in solutions of trifluoromethanesulfonic acid and/or tetramethylammonium hydroxide at 25°C and 0.1 MPa. *J. Sol. Chem.* **29** (2), 101-129.

Palmer, D.A. and Nguyen-Trung, C. (1995) Aqueous uranyl complexes. 3. Potentiometric measurements of the hydrolysis of uranyl(VI) ion at 25°C. Journal of Solution Chemistry **234**, No. 12, 1281-1291.

Pearson R.G. (1966) Acids and Bases. *Science* **151**, 172-177.

Pearson R.G. (1968) Hard and soft acids and bases: Part I. *J. Chem. Educat.* **45**, 581-587.

Pompe S., Bubner M., Denecke M.A., Reich T., Brachmann A., Geipel G., Nicolai R., Heise K.H. and Nitsche H. (1996) A comparison of natural humic acids with synthetic humic acid model substances: characterization and interaction with uranium(VI). *Radiochim. Acta* **74**, 135-140.

Pompe S., Brachmann A., Bubner M., Geipel G., Heise K. H., Bernhard G. and Nitsche H. (1998) Determination and comparison of uranyl complexation constants with natural and model humic acids. *Radiochim. Acta* **82**, 89-95.

Pompe S., Schmeide K., Bubner M., Geipel G., Heise K.H., Bernhard G. and Nitsche H. (2000) Investigation of humic acid complexation behavior with uranyl ions using modified synthetic and natural humic acids. *Radiochim. Acta* **88** (9-11), 553-558.

Ragnar M., Lindgren C.T., and Nilvebrant N.-O. (2000) pK_a-values of guaiacyl and syringyl phenols related to lignin. *J. Wood Chem. Technol.* **20**, 277-305.

Sarret G., Manceau J.L., Hazemann J.L., Gomez A. and Mench M. (1997) EXAFS study of the nature of zinc complexation sites in humic substances as a function of Zn concentration. *J. Phys. IV France*, **7** (2 Part 2), 799-802.

Serjeant E.P. and Dempsey B. (1979) *Ionization Constants of Organic Acids in Aqueous Solutions*. Pergamon, New York.

Schmeide K., Pompe S., Bubner M., Heise K.H, Bernhard G. and Nitsche H. (2000) Uranium(VI) sorption onto phyllite and selected minerals in the presence of humic acid. *Radiochimica* **88** (9-11), 723-728.

Schmeide K., Sachs S., Bubner M., Reich T., Heise K.H. and Bernhard G. (2003) Interaction of uranium(VI) with various modified and unmodified natural and synthetic humic substances studied by EXAFS and FTIR spectroscopy. *Inorganica Chimica Acta* **351**, 133-140.

Schuster G., Bubner M., Jander R., Pompe S., Heise K.H. and Nitsche H. (1998) Thermal analyses of iron and uranyl complexes with natural and synthetic humic acids. *Forschungszentrum Rossendorf e.V., [Bericht] FZR (1998), (FZR-218)*, 54-55.

Testemale D. PhD Thesis, UJF Grenoble (France), 2003, 156 p.

Teterin Y.A., Nefedov V.I., Teterin A.Y., Lebedev A.M., Ivanov K.E., Dement'ev A.P., Utkin I.O., Geipel G., Bubner M., Reich T., Pompe S., Heise K.H. and Nitche H. (1999a) Study of the interactions of UO_2^{2+} with calcite, diabase and humic acids by X-ray electron spectroscopy. *Poverkhnost* **2**, 79-82.

Teterin Y.A., Nefedov V.I., Teterin A.Y., Lebedev A.M., Dement'ev A.P., Utkin I.O., Bubner M., Reich T., Pompe S., Heise K.H. and Nitsche H. (1999b). Study of the interaction of the uranyl group UO_2^{2+} and Fe(III) with natural humic acid in aqueous solutions by x-ray photoelectron spectroscopy. *Zhurnal Neorganicheskoi Khimii* **44** (4), 593-597.

Teterin Y.A., Nefedov V.I., Nikitin A.S., Teterin A.Yu., Ivanov K.E., Maslakov K.I., Utkin I.O., Bubner M., Reich T., Pompe S., Heise K.H. and Nitsche H. (2001a) Interaction of uranyl UO_2^{2+} groups and Fe(III) ions with natural humic acid. *Inzhenernaya Fizika* **2**, 28-32.

Teterin Y.A., Nefedov V.I., Nikitin A.S., Teterin A.Y., Ivanov K.E., Maslakov K.I., Utkin I.O., Bubner M., Reich T., Pompe S., Heise K.H. and Nitsche H. (2001b) Interaction of UO_2^{2+} and Fe^{3+} ions with natural humic acid. *Zhurnal Neorganicheskoi Khimii* **46** (6), 990-995.

Turner C.E., Fishman N.S., Hatcher P.G. and Spiker E.C. (1993) Nature and role of organic matter in sandstone uranium deposits, Grants uranium region, New Mexico, USA. *Spec. Public. Soc. Geol. Appl. Min. Dep. (1993)* **9** *(Bitumens in Ore Deposits)*, 239-75.

Vallet V., Wahlgren U., Schimmelpfennig B., Moll H., Szabó Z. and Grenthe I. (2001) Solvent Effect on Uranium (VI) Fluoride and Hydroxide Complexes Studied by EXAFS and Quantum Chemistry. *Inorg. Chem*. **40**, 3516-3525.

Wahlgren U., Moll H., Grenthe I., Schimmelpfennig B., Maron L., Vallet V. and Gropen O. (1999) Structure of Uranium (VI) in Strong Alkaline Solutions. A Combined Theoretical and Experimental Investigation. *J. Phys. Chem. A* **103**, 8257-8264.

Zhang Y.J., Bryan N.D., Livens F.R. and Jones M.N. (1997) Selectivity in the complexation of actinides by humic substances. *Env. Pollut.* **96** (3), 361-367.

Conclusions et Perspectives

Cette étude a pour objectif d'apporter une réponse concluante à trois questions fondamentales :

1ère question : Est-ce qu'il est possible de synthétiser des composés organiques ayant une composition chimique proche de celles des acides humiques et/ou fulviques naturels, à partir de réactions chimiques entre des produits chimiques purs dans l'eau, dans des conditions ambiantes de température, de pression et d'oxydation ?

2ème question : Lors d'une synthèse expérimentale d'acides humiques et/ou fulviques en solution aqueuse, est ce qu'il est possible de déterminer le nombre d'acides humiques et/ou fulviques synthétisés, ainsi que leur masse moléculaire et formule chimique ?

3ème question: Est-ce qu'il est possible de quantifier l'effet du pH sur l'aptitude de l'anion fulvate et/ou humate à former des complexes aqueux avec des éléments toxiques tels que U, Cu présents dans les eaux naturelles?

De nombreuses études ont été consacrées à la synthèse des acides fulviques et/ou humiques à partir de composés chimiques purs, ainsi qu'à leur caractérisation. Cependant, la grande majorité de ces acides fulviques et/ou humiques ont été synthétisés dans des conditions fortement oxydantes (fO_2 = 0,1 MPa). Les données quantitatives sur le nombre d'acides fulviques et/ou humiques obtenus comme produits finaux au cours d'une expérience et leurs caractéristiques physico-chimiques sont quasi-inexistantes. Dans cette étude, la procédure scientifique développée a rendu possible la synthèse des acides fulviques (AFS) comme des produits résultant des interactions de composés chimiques purs dans quatre systèmes aqueux :

1- $C_6H_4(OH)_2$ (catéchol) – NaOH – H_2O

2- $C_6H_4(OH)_2$ (catéchol) – NaO_2CCH_3 (acétate de Na) – NaOH - H_2O

3- $C_6H_4(OH)_2$ (catéchol) – $NaO_2CCH_2(NH_2)$ (glycinate de Na) – NaOH - H_2O

4- $C_6H_4(OH)_2$ (catéchol) – $NaO_2CCH(NH_2)CH_2(SH)$ (cystéinate de Na) – NaOH - H_2O

à pH basique (pH = 10.0), dans des conditions ambiantes de température, de pression et d'oxydation. La cinétique de formation de ces acides fulviques synthétiques est lente (environ deux mois).

Pour la première fois, quatre différents types de AFS ayant un nombre déterminé de groupements fonctionnels (-OH, -COOH, R-O-R', $-NH_2$, -SH), ont été synthétisés à partir des quatre systèmes aqueux cités ci-dessus.

Cependant, les résultats obtenus ont montré que les interactions réalisées dans ces quatre systèmes aqueux ont généré un très grand nombre de produits finaux inconnus et soulève la deuxième question citée en haut.

Afin d'apporter une réponse correcte à la deuxième question, l'approche scientifique adoptée dans cette étude consiste à utiliser conjointement cinq techniques de mesures : (1) Diffractométrie des rayons X (DRX), (2) Spectrométrie infrarouge par transformée de Fourier en mode de réflexion totale atténuée FTIR-ATR, (3) Spectrométrie d'absorption UV-visible, (4) analyse quantitative des éléments C,O,H,N,S par pyrolyse et (5) la spectrométrie de masse en mode d'ionisation par nébulisation (ESI MS) et/ou en mode d'ionisation chimique sous pression atmosphérique (APCI MS), pour identifier les produits finaux en tant qu'acides fulviques synthétiques et déterminer leurs caractéristiques physico-chimiques (degré de cristallinité, nombre d'acides fulviques formés, groupements fonctionnels, masse moléculaire, formule chimique).

L'analyse diffractométrique à l'aide de la DRX a indiqué que tous les AFS produits dans les quatre systèmes aqueux sont amorphes. Ce résultat confirme la similitude des AFS obtenus dans cette étude avec le caractère amorphe des acides fulviques naturels.

La spectrométrie FTIR-ATR est un excellent moyen pour détecter la présence des principaux groupements fonctionnels majeurs qui pourraient être présents dans les acides fulviques naturels et synthétiques. En effet, la présence des bandes de vibrations caractéristiques des groupements alcool (-OH), carboxylate (-COOH) et éther (R-O-R', Ar-O-Ar' or R''-O-Ar'') ont été observés dans les deux premiers systèmes aqueux cités ci-dessus. Le groupement additionnel amine ($-NH_2$) a été observé dans le troisième système aqueux cité ci-dessus. Enfin, les AFS obtenus comme produits finaux dans le quatrième système aqueux cité ci-dessus contiennent probablement le plus grand nombre de groupements fonctionnels avec quatre groupements fonctionnels semblables à ceux obtenus dans les trois premiers systèmes plus le groupement thiol (-SH).

La spectrométrie d'absorption UV-visible a complété les données infra-rouge en fournissant deux caractéristiques sur les AFS. (1) Tous les spectres d'absorption des produits finaux montrent un déplacement bathohypochromique indiquant qu'ils sont constitués de molécules de grande taille lesquelles sont composées d'une succession de nombreux noyaux aromatiques. (2) la légère augmentation de l'intensité d'absorption du bruit de fond dans la région du visible (> 400 nm) montre qu'un grand nombre de différents types de AFS a été formé

Les résultats obtenus à partir de l'analyse élémentaire par pyrolyse ont montré que les trois éléments (C,O,H) ont été déterminées dans les produits finaux des deux premiers systèmes aqueux cités ci-dessus. L'élément additionnel N avec les élément C,O,H a été déterminé comme élément mineur dans le troisième système aqueux cité ci-dessus. La concentration de tous les cinq éléments (C,O,H,N,S) a été déterminée dans le quatrième système cité ci-dessus.

Le nombre *n* de molécules de AFS et leur rapport *m/z* ont été déterminés à l'aide de la spectrométrie de masse ESI-MS et/ou APCI-MS.

La combinaison des données qualitatives et quantitatives obtenues par les cinq techniques de mesures citées ci-dessus permet de déterminer pour la première fois et avec un degré de confiance élevé, le nombre de AFS formés dans chaque système et leur formule chimique. En se basant sur les données physico-chimiques et les conditions expérimentales de cette étude, un modèle de schéma réactionnel de formation des AFS dans les quatre systèmes aqueux cités ci-dessus est proposé. Le schéma réactionnel se compose de trois principales étapes :

1ère étape : Initiation

Cette étape est caractérisée par deux réactions

1-a : transformation d'une partie du catéchol initial en radicaux libres sous l'effet de l'oxydation modérée, selon la réaction (1-a)

$C_6H_4(OH)_2$ <==> $C_6H_3(OH)_2$• + H• (1-a)

1-b: Oxydation du catéchol en quinone (1-b)

$C_6H_4(OH)_2 + O_2$ <==> $C_6H_4(O)_2$ (1-b)

2ème étape: Propagation

Dans cette étape, trois types de réactions peuvent avoir lieu:

2-a: Formation d'une nouvelle molécule avec une masse moléculaire plus grande à partir de la réaction entre les radicaux libres des deux composés aromatiques selon les réactions (2-a)

$C_6H_3(OH)_2$• + $C_6H_3(OH)_2$• <==> $(OH)_2C_6H_3$-$C_6H_3(OH)_2$ (2-a)

2-b: Formation d'un éther aromatique à partir de deux molécules de catéchol selon la réaction de condensation (2-b)

$C_6H_4(OH)_2 + C_6H_4(OH)_2$ <==> $(OH)C_6H_4$-O-$C_6H_4(OH) + H_2O$ (2-b)

A son tour, cet éther aromatique peut aussi être transformé en radical libre et réagir avec un autre radical libre pour former une nouvelle molécule avec une masse moléculaire plus importante comme dans les réactions 2-a.

2-c: Formation des plusieurs composés à partir des réactions du glycine et cysteine avec catéchol ou quinone

2-c1: Réaction enre quinone et glycine:

$C_6H_4(O)_2 + NH_2CH_2COOH <==> C_6H_4(O)NCH_2COOH + H_2O$ (2-c1)

2-c2: Réaction entre radical libre du catéchol et le radical libre du cysteine:

$C_6H_3(OH)_2\bullet + HOOC(NH_2)CHCH_2S\bullet <==> C_6H_3(OH)_2SCH_2CH(NH_2)COOH$ (2-c2)

2-c3: Réaction entre quinone et cysteine:

$C_6H_4(O)_2 + HSCH_2CH(NH_2)COOH <==> C_6H_3(O)_2SCH_2CH(NH_2)COOH + H_2O$ (2-c3)

3ème étape: Terminaison

Les réactions dans cette étape sont semblables à celles de la précédente étape de propagation avec une caractéristique supplémentaire :

Tous les produits finaux dans l'étape de terminaison deviennent chimiquement inactifs. Ce phénomène résulte probablement de deux principales raisons :

1ère raison: les produits finaux ont atteint un niveau de stabilité maximale avec la valeur la plus négative de l'énergie libre de formation (ΔG_f)

2ème raison: les produits finaux ont une forme ayant un maximum d'encombrement stérique et une mobilité réduite excluant tout contact avec de nouveaux réactants (radicaux libres ou ions).

Il faut souligner que la liste de réactions présentées dans le schéma ci-dessus n'est pas exhaustive due au fait que les réactions de formation des AFS ne sont pas totalement comprises.

La présence des différents groupements fonctionnels (carboxylate, alcool, amine, thiol) dans les formules chimiques de divers AFS obtenus dans cette étude conduit à poser la troisième question mentionnée ci-dessus quant à la capacité de AFS de former des complexes aqueux solubles avec certains éléments toxiques en fonction du pH. Afin d'apporter une réponse concluante à la troisième question, une étude expérimentale de la formation de complexes uranyl(VI) – fulvate dans le système ternaire U(VI) – AFS_1 – H_2O a été développée en fonction de deux paramètres : pH (4.0 - 10.0) et concentration en ion Fulvate, à l'aide de la

spectroscopie d'absorption UV-visible. Les résultats obtenus ont montré que le ligand fulvate forme de nombreux complexes stables avec les ions U(VI) (2 x 10^{-3} mole).

Dans le domaine de pH compris entre 4 et 10, 2.75 mg/L de AFS_1 représente la limite inférieure pour la formation des complexes U(VI)-fulvate. Dans les solutions acides (pH = 4), l'accroissement de la teneur AFS_1 jusqu'à 11 mg/L conduit à la formation de deux types de complexes U(VI)-fulvate. En milieu neutre, la solubilité minimale de la schoepite ($UO_2(OH)_2.H_2O$) dans H_2O est comprise entre 10^{-5} M et 10^{-6} M. Pour la première fois, les résultats obtenus dans cette étude ont montré que la présence de 2.75 mg/L de AFS_1 est suffisante pour maintenir jusqu'à 2.10^{-3} m d'U(VI) à l'état soluble en solution neutre (pH = 7). Ce résultat prouve que AFS_1 est un puissant agent complexant capable de multiplier la solubilité de l'U (VI) par deux unités de logarithme décimal. L'accroissement de la concentration de AFS_1 de 2.75 à 11 mg/L conduit à la formation de quatre différents types de complexes U(VI)-fulvate. En solution basique (pH = 10), une forte solubilité de U(VI) (2.10^{-3} m) a été obtenue dans une solution contenant seulement 2.75 mg/L de AFS_1. La comparaison de ce résultat avec la faible solubilité de l'uranate de sodium Na-uranate (*e.g* $Na_2UO_4.nH_2O$) autour de 10^{-6} M permet de conclure que l'AFS_1 reste toujours un puissant agent complexant de l'ion U(VI) même en milieu basique. Les spectres d'absorption caractéristiques des complexes U(VI) – fulvate en fonction du pH et de la concentration en ion fulvate révèlent trois caractéristiques:

1- deux types de complexes U(VI)-fulvate ont été formés à pH 4, deux à pH 7 et trois à pH 10.

2- tous ces complexes U(VI)-fulvate sont différents les uns des autres. Cette différence est probablement due au fait que les cations U(VI) ont réagi avec de nombreux anions fulvates ayant des formules chimiques différentes.

3- la présence de larges bandes dans ces spectres d'absorption indiquent clairement que les complexes fulvates sont composés de cations polyuranyles (VI).

Sur la base des résultats obtenus dans cette étude, différentes voies de recherche peuvent être proposées :

- la détermination des "constantes d'ionisation conditionnelles (pKi)" des AFS à l'aide des titrations potentiométriques (cellule de concentration équipée d'électrode Ir/IrO_2) en fonction du pH (2-12) et de la température (5-100°C).

- la détermination des “constantes conditionnelles de formation de complexe (pK_f)” des complexes U(VI) - Fulvate à l’aide des titrations potentiométriques (cellule de concentration équipée d’électrode Ir/IrO_2) en fonction du pH (2-12) et de la température (5-100°C).
- étendre l’approche scientifique développée pour la formation de complexes U(VI) – Fulvate à d’autres éléments toxiques tels que Pb, Hg, Zn etc.

Conclusion and Perspectives

The objective of the present study is to provide a conclusive answer to three fundamental questions as follows:

1st question: Is it possible to reproduce organic compounds having chemical composition close to that of natural Fulvic and/or Humic Acid, using chemical reactions between pure organic chemicals and H_2O, under ambient conditions and atmospheric oxidation?

2nd question: In an experimental synthesis of Fulvic and/or Humic acids in aqueous solution, is it possible to determine the number of synthesized Fulvic and/or Humic acids as well as their molecular mass and their chemical formula?

3rd question: Is it possible to quantify the effect of the pH parameter on the ability of the fulvate and/or humate anion to form aqueous complex with toxic elements, *e.g* U, Cu in natural waters?

In the past, numerous experimental studies have been devoted to the synthesis of Fulvic and/or Humic acids using pure chemicals and to their characterization. Meanwhile, the great majority of those Fulvic and/or Humic acids have been synthesized under strongly oxidizing conditions (fO_2 = 0.1 MPa). Quantitative data on the number of synthesized Fulvic and/or Humic acids as final products in one experiment and their physico-chemical characteristics appear to be not available. In the present study, the scientific procedure developed has made possible the formation of synthetic fulvic acids (SFA) as final products of interactions of pure chemicals in four aqueous systems :

1- $C_6H_4(OH)_2$ (catechol) – NaOH – H_2O

2- $C_6H_4(OH)_2$ (catechol) – NaO_2CCH_3 (Na-acetate) – NaOH - H_2O

3- $C_6H_4(OH)_2$ (catechol) – $NaO_2CCH_2(NH_2)$ (Na-glycinate) – NaOH - H_2O

4- $C_6H_4(OH)_2$ (catechol) – $NaO_2CCH(NH_2)CH_2(SH)$ (Na-cysteinate) – NaOH - H_2O

at basic pH (pH = 10.0), under ambient conditions and atmospheric oxidation. The formation kinetics of those synthetic fulvic acids is slow (≈ 2 months).

For the first time, four different types of SFA containing a determined number of functional groups (-OH, -COOH, R-O-R', $-NH_2$, -SH), have been formed from the four aqueous systems cited above.

Meanwhile, results obtained have indicated that interactions in those four systems have provided a large number of unknown final products and raise the above cited second question.

In order to bring a right answer to the second question, the scientific approach adopted in the present study consists to use simultaneously five measurement techniques : (1) XRD, (2) ATR FTIR Spectrometry, (3) UV-visible Absorption Spectrometry, (4) Quantitative pyrolytic analysis of C,O,H,N,S elements and (5) Electrospray Ionization (ESI) and/or Atmospheric Pressure Chemical Ionization (APCI) Mass Spectrometry (MS), to identify final products as Synthetic Fulvic Acids and to determine their physico-chemical characteristics (crystalline degree, number, functional groups, molecular mass, chemical formula).

XRD measurements have indicated that all SFA produced in all four systems are amorphous. This result confirms the similitude of SFA in the present study with the amorphous character of the natural Fulvic Acid.

ATR FTIR Spectrometry is an excellent means to detect the presence of major functional groups which could be present in natural and synthesized Fulvic Acids. Indeed, the presence of characteristic vibration bands of alcohol (-OH), carboxylate (-COOH) and ether (R-O-R', Ar-O-Ar' or R''-O-Ar'') have been observed in the two first systems cited above. The additional amine ($-NH_2$) group was found in the above cited third system. Finally, the SFA obtained as final products in the above cited fourth system probably contain the largest number of functional groups with four functional groups similar to those in the three first systems plus the thiol (-SH) group.

UV-visible spectrometry has completed the IR data by providing two characteristics on the SFA. (1) All absorption spectra of final products show a bathohypochromic shift indicating that they are constituted of large size molecules which are composed of a succession of numerous aromatic rings. (2) The slight increase of the absorption intensity of the background in the visible wavelength region (> 400 nm) shows that a large number of different types of SFA have been formed.

Results obtained from the quantitative pyrolytic elemental analysis have indicated that three elements (C,O,H) have been determined in final products of the above cited two first systems. The additional N element with C,O,H elements was determined as a minor element in the above cited third system. The concentration of all five elements (C,O,H,N,S) have been determined in the above cited fourth system.

The *n* number of SFA molecules and their m/z ratio were determined using ESI-MS and/or APCI-MS measurements.

The combination of qualitative and quantitative data obtained from the above mentioned five measurement techniques allowed determining for the first time and with relative high degree of confidence, the number of SFA formed in each system and their chemical formula.

Based on the physico-chemical data and experimental conditions in the present study, a model of reaction scheme for the formation of SFA in the four above mentioned systems is suggested. The reaction scheme is composed of three principal steps:

1st step: Initiation

This step is characterized by two reactions

1-a: Transformation of part of initial catechol into free radicals due to moderate oxidation according to the reaction (1-a)

$C_6H_4(OH)_2$ <==> $C_6H_3(OH)_2$• + H• (1-a)

1-b: Oxidation of catechol into quinone (1-b)

$C_6H_4(OH)_2 + O_2$ <==> $C_6H_4(O)_2$ (1-b)

2nd step: Propagation

In this step, three types of reactions are expected to occur:

2-a: Formation of a new molecule with higher molecular mass resulting from a reaction between two aromatic compounds free radicals according to the reactions (2-a)

$C_6H_3(OH)_2$• + $C_6H_3(OH)_2$• <==> $(OH)_2C_6H_3$-$C_6H_3(OH)_2$ (2-a)

2-b: Formation of aromatic ether from two catechol molecules according to the condensation reaction (2-b)

$C_6H_4(OH)_2 + C_6H_4(OH)_2$ <==> $(OH)C_6H_4$-O-$C_6H_4(OH) + H_2O$ (2-b)

In its turn, this aromatic ether compound could also be transformed into free radical and reacts with another free radical to form a new molecule with higher molecular mass like 2-a reaction.

2-c: Formation of various compounds from the reactions of gycine and cysteine with catechol or quinones

2-c1: reaction between quinone and glycine:

$C_6H_4(O)_2 + NH_2CH_2COOH$ <==> $C_6H_4(O)NCH_2COOH + H_2O$ (2-c1)

2-c2: reaction between catechol free radical and cysteine free radical:

$C_6H_3(OH)_2$• + $HOOC(NH_2)CHCH_2S$• <==> $C_6H_3(OH)_2SCH_2CH(NH_2)COOH$ (2-c2)

2-c3: reaction between quinone and cysteine:

$C_6H_4(O)_2 + HSCH_2CH(NH_2)COOH$ <==> $C_6H_3(O)_2SCH_2CH(NH_2)COOH + H_2O$ (2-c3)

3rd step: Termination

Reactions in this step are similar to those of the previous propagation step with one additional characteristic:

All final products in the termination step become chemically inactive. This is probably due to two main reasons:

1st reason: Final products have reached the stability level with the most negative value of free energy of formation (ΔG_f)

2nd reason: Final products have reached a shape with a maximum of steric hindrance and limited mobility precluding all contact with new reactants (free radicals or ions).

Notice that the list of reactions presented in the above mentioned scheme is not exhaustive due to the fact the formation reactions of SFA are not totally understood.

The presence of numerous functional groups (carboxylate, alcohol, amine, thiol) in the chemical formula of various SFA obtained in the present study raises the above mentioned third question about the ability of SFA to form soluble aqueous complex with some toxic elements as a function of pH. In order to bring a right answer to the third question, an experimental study of the uranyl(VI) - fulvate complex formation in the ternary system U(VI) – SFA_1 – H_2O has been developed as a function of two parameters: pH (4.0 - 10.0) and [Fulvate ion], using the UV-visible absorption spectrometry. Results obtained for 2 x 10^{-3} molal U(VI) have indicated that fulvate ligand forms numerous stable complexes with U(VI) ions.

In the pH range 4-10, 2.75 mg/L of SFA_1 was the lower limit for the formation of U(VI)-fulvate complexes. In acidic solution (pH = 4), the addition up to 11 mg/L of SFA_1 led to the formation of two types of U(VI) fulvate complexes. In neutral medium, the minimum solubility of schoepite ($UO_2(OH)_2.H_2O$) is in the range 10^{-5} - 10^{-6} M. For the first time, results obtained in the present study have indicated that the presence of only 2.75 mg/L of SFA_1 is sufficient to maintain up to 2.10^{-3} m U(VI) soluble in neutral solution (pH = 7). This result clearly proves that SFA_1 is a strong complexing agent capable of multiplying the solubility of U(VI) by 2 decimal log units. The increasing concentration of SFA_1 from 2.75 to 11 mg/L led to formation of approximately four different types of U(VI)-fulvate complexes. In basic solution (pH = 10), high solubility of U(VI) (2.10^{-3} m) has also been obtained in a solution containing only 2.75 mg/L of SFA_1. The comparison of this result with the low solubility of Na-uranate (*e.g* $Na_2UO_4.nH_2O$) around 10^{-6} M allows to conclude that SFA_1 remains a strong complexing agent of U(VI) ion even in basic solution. Characteristic

absorption spectra of U(VI) – fulvate complexes as a function of pH and [fulvate ion] reveal three characteristics :

1- Two types of U(VI)-fulvate complexes have been formed at pH = 4, two at pH = 7 and three at pH = 10

2- All of these U(VI)-fulvate complexes are different from each other. This difference is probably due to the fact that U(VI) cations have reacted with numerous Fulvate anions having different chemical formula.

3- The presence of broadbands in those absorption spectra is a strong indication that fulvate complexes are composed of polyuranyl(VI) cations.

Based on the results obtained in the present study, different research paths could be suggested:

- the determination of “conditional ionization constant (pK_i)” of Synthetic Fulvic Acids using potentiometric titrations (concentration cell equipped with Ir/IrO_2 electrodes) as a function of pH (2-12) and temperature (5-100°C)
- the determination of “conditional complex formation constant (pK_f)” of U(VI) - Fulvate complexes using potentiometric titrations (concentration cell equipped with Ir/IrO_2 electrodes) as a function of pH (2-12) and temperature (5-100°C)
- extension of the scientific approach developed for the U(VI)-fulvate complex formation in the present study to other toxic elements such as Pb, Hg, Zn etc.

RÉSUMÉ

Des acides fulviques contenant éléments (1) C,H,O, (2) C,H,O,N et (3) C,H,O,N,S chimiques ont été synthétisés à partir de réactions dans quatre mélanges de composés chimiques purs : (1) $C_6H_4(OH)_2$ + NaOH, (2) $C_6H_4(OH)_2$ + CH_3COOH + NaOH, (3) $C_6H_4(OH)_2$ + NH_2CH_2COOH + NaOH et (4) $C_6H_4(OH)_2$ + $NH_2CH(CH_2SH)COOH$ + NaOH, à pH = 10,0, à l'abri de la lumière et dans des conditions expérimentales proches de celles de la nature (température ambiante, $f_{O_{2(g)}}$ et $f_{CO_{2(g)}}$ atmosphériques).

Des analyses qualitatives et semi-quantitatives des acides fulviques de synthèse (AFS) à l'aide d'une combinaison de techniques d'analyse en microscopie électronique, en spectrométrie moléculaire (FTIR-ATR, UV-visible, ESI-MS, APCI-MS) et en diffraction des rayons X ont permis d'obtenir les résultats suivants:

- les quatre mélanges réactionnels ont produit un nombre important d'acides fulviques individuels, dont les rapports m/z pouvant atteindre une valeur maximale de 943 et sont amorphes;
- les AFS comportent groupements fonctionnels: alcool, éther et carboxylate. L'introduction de composés tels que CH_3COOH, NH_2CH_2COOH et $NH_2CH(CH_2SH)COOH$ se traduit par d´acides fulviques contenant respectivement des groupements fonctionnels ester, amine et thiol.

Enfin, une étude systématique des interactions entre l´ion U(VI) et des ligands fulvate contenant trois éléments (C,H,O) en fonction du pH (4 – 10) a été développée à l'aide de la spectroscopie UV-visible. Deux types de complexes U(VI)-fulvate ont été formés à pH = 4 - 7 et trois types de complexes à pH = 10. La présence de bandes d'absorption larges montrent que des ions polyuranyle (VI) participent à ces complexes U(VI) - fulvate.

Mots clés: *acides fulviques, acides humiques, couplage oxidatif, radicaux libres, substances humiques.*

ABSTRACT

Fulvic acids containing chemical elements (1) C,H,O, (2) C,H,O,N and (3) C,H,O,N,S have been synthesized from reactions in four mixtures of pure chemical reactants: (1) $C_6H_4(OH)_2$ + NaOH, (2) $C_6H_4(OH)_2$ + CH_3COOH + NaOH, (3) $C_6H_4(OH)_2$ + NH_2CH_2COOH + NaOH and (4) $C_6H_4(OH)_2$ + $NH_2CH(CH_2SH)COOH$ + NaOH, at pH = 10.0, in the dark and under oxidative conditions close to those encountered in the nature (ambient temperature and atmospheric conditions, $f_{O_{2(g)}}$ and $f_{CO_{2(g)}}$).

Qualitative and semi-quantitative analysis of synthesized fulvic acids (SFA) using a combination of analytical techniques in electron microscopy, molecular spectrometry (ATR-FTIR, UV-visible, ESI-MS, APCI-MS), and X-ray diffraction have allowed to obtain the following results :

- all four reaction mixtures have produced a large number of individual fulvic acids, whose m/z ratios can be as high as 943 and are amorphous;
- the SFA contain functional groups: alcohol, ether and carboxylate. The addition of compounds such as CH_3COOH, NH_2CH_2COOH and $NH_2CH(CH_2SH)COOH$ led to fulvic acids containing respectively ester, amine and thiol functional groups.

Finally, a systematic study of the interactions between the U(VI) ion and fulvate ligands containing three elements (C,H,O) as a function of pH (4 – 10) has been developed using UV-visible spectroscopy. Two types of U(VI)-fulvate complexes have been identified in pH range 4 – 7 and three types of complexes at pH = 10. The presence of absorption broadbands indicates that polyuranyl (VI) ions are part of constituents of the U(VI) - fulvate complexes.

Key words: *free radicals, fulvic acids , humic acids, humic substances, oxidative coupling.*

UMR G2R 7566 – Géologie et Gestion des Ressources Minérales et Energétiques
BP239, Université Henry Poincaré, entrée 3B, 54506 Vandoeuvre-lès-Nancy, Cedex, France